U.S.NRC
United States Nuclear Regulatory Commission
Protecting People and the Environment

NUREG/CR-7280
ANL/EVS-20/8

Review of Radiation-Induced Concrete Degradation and Potential Implications for Structures Exposed to High Long-Term Radiation Levels in Nuclear Power Plants

Office of Nuclear Regulatory Research

AVAILABILITY OF REFERENCE MATERIALS IN NRC PUBLICATIONS

NRC Reference Material

As of November 1999, you may electronically access NUREG-series publications and other NRC records at the NRC's Library at www.nrc.gov/reading-rm.html. Publicly released records include, to name a few, NUREG-series publications; *Federal Register* notices; applicant, licensee, and vendor documents and correspondence; NRC correspondence and internal memoranda; bulletins and information notices; inspection and investigative reports; licensee event reports; and Commission papers and their attachments.

NRC publications in the NUREG series, NRC regulations, and Title 10, "Energy," in the *Code of Federal Regulations* may also be purchased from one of these two sources:

1. **The Superintendent of Documents**
   U.S. Government Publishing Office
   Washington, DC 20402-0001
   Internet: www.bookstore.gpo.gov
   Telephone: (202) 512-1800
   Fax: (202) 512-2104

2. **The National Technical Information Service**
   5301 Shawnee Road
   Alexandria, VA 22312-0002
   Internet: www.ntis.gov
   1-800-553-6847 or, locally, (703) 605-6000

A single copy of each NRC draft report for comment is available free, to the extent of supply, upon written request as follows:

Address: **U.S. Nuclear Regulatory Commission**
Office of Administration
Digital Communications and Administrative Services Branch
Washington, DC 20555-0001
E-mail: distribution.resource@nrc.gov
Facsimile: (301) 415-2289

Some publications in the NUREG series that are posted at the NRC's Web site address www.nrc.gov/reading-rm/doc-collections/nuregs are updated periodically and may differ from the last printed version. Although references to material found on a Web site bear the date the material was accessed, the material available on the date cited may subsequently be removed from the site.

Non-NRC Reference Material

Documents available from public and special technical libraries include all open literature items, such as books, journal articles, transactions, *Federal Register* notices, Federal and State legislation, and congressional reports. Such documents as theses, dissertations, foreign reports and translations, and non-NRC conference proceedings may be purchased from their sponsoring organization.

Copies of industry codes and standards used in a substantive manner in the NRC regulatory process are maintained at—

The NRC Technical Library
Two White Flint North
11545 Rockville Pike
Rockville, MD 20852-2738

These standards are available in the library for reference use by the public. Codes and standards are usually copyrighted and may be purchased from the originating organization or, if they are American National Standards, from—

American National Standards Institute
11 West 42nd Street
New York, NY 10036-8002
Internet: www.ansi.org
(212) 642-4900

Legally binding regulatory requirements are stated only in laws; NRC regulations; licenses, including technical specifications; or orders, not in NUREG-series publications. The views expressed in contractor prepared publications in this series are not necessarily those of the NRC.

The NUREG series comprises (1) technical and administrative reports and books prepared by the staff (NUREG–XXXX) or agency contractors (NUREG/CR–XXXX), (2) proceedings of conferences (NUREG/CP–XXXX), (3) reports resulting from international agreements (NUREG/IA–XXXX),(4) brochures (NUREG/BR–XXXX), and (5) compilations of legal decisions and orders of the Commission and the Atomic and Safety Licensing Boards and of Directors' decisions under Section 2.206 of the NRC's regulations (NUREG–0750).

U.S.NRC
United States Nuclear Regulatory Commission
Protecting People and the Environment

NUREG/CR-7280
ANL/EVS-20/8

Review of Radiation-Induced Concrete Degradation and Potential Implications for Structures Exposed to High Long-Term Radiation Levels in Nuclear Power Plants

Manuscript Completed: February 2020
Date Published: July 2021

Prepared by:

B. Biwer[1]
D. Ma[1]
Y. Xi[2]
Y. Jing[2]

Environmental Science Division[1]
Argonne National Laboratory
Lemont, IL 60439

Department of Civil, Environmental[2]
and Architectural Engineering,
University of Colorado
Boulder, CO 80309-0428

M. Sircar
Technical Lead, NRC Project Manager

Office of Nuclear Regulatory Research

ABSTRACT

The Expanded Material Degradation Assessment Report, NUREG/CR-7153 Vol. 4, *Aging of Concrete and Civil Structures*, identifies issues that are low-knowledge but high significance for concrete and concrete degradation related to the long-term operation of nuclear power plant (NPP) structures. Irradiation of reactor pressure vessel (RPV) concrete support structures emerged as the highest research priority, mainly because there was insufficient data to increase existing knowledge about the effects of irradiation on concrete mechanical properties. U.S. Nuclear Regulatory Commission (NRC) staff is conducting research activities to investigate this topic (see SECY-14-0016, January 31, 2014). This report reviews the state of knowledge related to radiation-induced degradation, estimated radiation levels, a limited survey of reactor support structures, and important design criteria. Collectively, this information provides a general framework for understanding the effects of irradiation on RPV concrete support structures.

This evaluation reviewed recently completed and ongoing license renewal-related research on the characterization of the degradation of irradiated concrete in NPP structures near the RPVs. A proper evaluation requires an understanding of (1) the effect of radiation on concrete (i.e., what degradation modes exist and which are the most important in a light-water reactor [LWR] environment), (2) the radiation levels concrete structures experience in the near-RPV environment, and (3) the functions those concrete structures must maintain over the course of an 80-year reactor lifetime.

The highest estimated neutron fluence level at the outer face of the RPV wall was found to be greater than 1×10^{19} n/cm^2 ($E > 0.1$ MeV) for all pressurized-water reactors (PWRs) and, with one exception, less than 1×10^{19} n/cm^2 for all boiling-water reactors (BWRs). These estimates are near or at the core mid-plane. The neutron fluence levels will rapidly decrease above the top and below the bottom of the core. There are indications that streaming effects could increase the fluence levels near RPV supports in these areas, but are not higher than the core mid-plane values.

Neutron fluence levels above 1×10^{19} n/cm^2 ($E > 0.1$ MeV) at the typical temperatures in LWR cavities (below 100°C) can significantly degrade concrete's physical and mechanical properties. The onset of noticeable degradation can appear at fluence levels above 1×10^{18} n/cm^2. However, there is insufficient evidence to change the currently adopted value of 1×10^{19} n/cm^2 as a damage threshold value for regulatory purposes. The contributing factors and degradation mechanisms are not well understood. There is strong, but not conclusive, experimental evidence that the primary effect is related to the disordering effect of neutrons on aggregate mineral structures, especially those with a covalent bond structure such as that found in siliceous aggregates with the quartz structure. Other issues are that aggregates are a mix of different mineral types that vary from plant to plant. The differential expansion of minerals within the aggregate may cause cracking.

Gamma dose levels above 1×10^8 Gy may result in the degradation of concrete properties, but there is no data directly related to isolated gamma irradiation of concrete in an air environment. The primary impact of gamma irradiation on concrete is water loss from the cement paste due to heating and radiolysis, which results in some shrinkage of the cement paste. The loss of water results in more open pore space within the cement paste, but this effect may be partially counteracted by gamma-induced carbonation of portlandite to calcite, where the calcite occupies slightly more volume than portlandite.

The synergistic effects of neutron and gamma radiation on concrete are not known at this time. Most of the reviewed neutron irradiation data were obtained using a nuclear reactor as a source which also produced gamma radiation. However, many tests did not track the corresponding gamma dose or qualify the neutron spectrum, and the relative values of neutron irradiation and gamma dose in the tests were not necessarily the same as those under commercial LWR operating conditions. In addition, little neutron- or gamma-only data under LWR conditions is available for comparison.

In addition, the extrapolation of experimental sample degradation to actual scale operating conditions still requires study. Radiation-induced volume expansion of the aggregate is considered to be one of the main contributors to the degradation. The aggregate expansion under structural confinement will create internal stress fields which may extend much further inside the bioshield, beyond the irradiated depth.

Other issues that remain to be investigated further are radiation rate effects and the lack of data on the effects of irradiation at the interfaces of steel and concrete, such as at anchorages and reinforcements.

The reactors that are more susceptible to concrete bioshield-support degradation are those in which the reactor supports sit on the concrete bioshield close to, and directly exposed to, the core radiation. The PWRs that rest on support skirts, neutron shield tanks, or pedestal (metal column) supports may not have any significant long-term concrete irradiation degradation issues because the distance from the core to the base of the reactor cavity is far enough to protect them and/or shielding is provided by a neutron shield tank. However, the effect of irradiation on concrete support structures near the core mid-plane requires evaluation, and the effect of irradiation on steel structures and components continues to be considered along with its impacts on concrete support structures.

This review indicates that all operating PWRs have the potential to generate neutron fluence levels in the reactor cavity that could result in concrete degradation before 80 years of operation. However, the extent of any potential degradation of concrete RPV supports cannot be quantified in a general manner because plant-specific, detailed design information of the RPV supports is necessary, knowledge of the radiation levels at plant-specific support locations is largely unknown, and the effect and extent of nuclear irradiation on the concrete supports in an LWR operating environment is not well understood and subject to uncertainty.

Although BWRs are expected to experience lower radiation levels than PWRs and are not likely to experience issues related to concrete irradiation-induced degradation, certain aspects of a given design may need to be addressed. Furthermore, there are NPPs that are operating under off-normal conditions in some cases and that are monitored as part of their aging management plans; these off-normal conditions could impact concrete irradiation degradation mechanisms. Thus, the impact of nuclear radiation on critical concrete support structures should be considered on a case-by-case basis as part of a Subsequent License Renewal application.

FOREWORD

The Office of Regulatory Research (RES) of the U.S. Nuclear Regulatory Commission (NRC) initiated research on the effects of irradiation on concrete structures to support subsequent license renewal activities for nuclear power plants in response to a 2015 user need request from the Office of Nuclear Reactor Regulation (NRR). In the Staff Requirements Memorandum SRM-SECY-014-0016, the Commission had directed the staff to keep the Commission informed regarding progress on concrete research activities, including the effects of irradiation on concrete. NUREG/CR 7153 Vol. 4, 'Expanded Materials Degradation Assessment (EMDA): Aging of Concrete and Civil Structures,' 2014, had identified irradiation-related concrete degradation as an area of low knowledge and high significance. Irradiation-related concrete degradation has been identified as a potential issue for two-loop and three-loop pressurized water reactors because they accumulate higher neutron fluence in the concrete around the RPV supports during long term operations.

Potential impacts of irradiation-related damage of concrete depend on several factors including the type of concrete, type of aggregates, level of irradiation, and design configurations of the RPV supports. Structures exposed to radiation are usually difficult to access for inspection which limits the options for monitoring and aging management. The RES research program addresses technical issues for which remaining uncertainties challenge applicants as well as staff guidance and reviews. The planned and undertaken research activities leverage the development of knowledge from domestic and international institutions through memoranda of understanding (MOUs) with the Electric Power Research Institute (EPRI) and the Department of Energy (DOE) and a bi-lateral agreement with the Nuclear Regulation Authority of Japan (NRAJ). To facilitate knowledge development, RES, DOE and EPRI have developed a joint research roadmap, which is frequently updated to help timely exchange of technical insights, resolution of issues, and avoidance of duplication of efforts.

The overall RES research program on irradiation-related concrete degradation involves confirmatory reviews of research on the subject performed within the US and abroad as well as independent research tasks to further knowledge aimed at clarifying regulatory guidance on technical issues facing challenging uncertainties. The research results will be used to enhance staff guidance for assessing the effects of concrete irradiation in structural safety evaluations for subsequent license renewal and to describe programs that licensees can use to manage the effects of concrete irradiation. The scope of the RES research activities on irradiation-related concrete degradation includes, in addition to the cooperative research activities, the following efforts:

1. Review of state of knowledge on radiation-induced concrete degradation and its implications on NPP structures at Argonne National Laboratory (ANL) as reported in this NUREG/CR (2016-2020)

2. Translation and review of the NRAJ report on the NRAJ-sponsored concrete irradiation testing (2018-2019)

3. Review and feedback on selected EPRI reports (2017-2018)

4. Verification of radiation transport methodology through the concrete biological shield at the Oak Ridge National Laboratory (ORNL) (2019-2020)

5. Development of numerical models to derive damaged concrete properties for use in finite element analysis frameworks at ANL and the University of Colorado (2019 – 2020)

6. Limited experimentation, modeling and numerical simulations of irradiated concrete including concrete-steel bonding and methodology for structural evaluation at ORNL (2019 – 2024)

7. In-house assessment of structural capacity (on-going)

8. Exploration of confirmatory harvesting opportunities to assess evidence of concrete damage and site-specific effects.

TABLE OF CONTENTS

LIST OF FIGURES

LIST OF TABLES

EXECUTIVE SUMMARY

The Expanded Material Degradation Assessment Report, NUREG/CR-7153 Vol. 4, *Aging of Concrete and Civil Structures*, identifies issues that are low-knowledge but high significance for concrete and concrete degradation related to the long-term operation of nuclear power plant (NPP) structures. Irradiation of reactor pressure vessel (RPV) concrete support structures emerged as the highest research priority, mainly because there was insufficient data to increase existing knowledge about the effects of irradiation on concrete mechanical properties. U.S. Nuclear Regulatory Commission (NRC) staff is conducting research activities to investigate this topic (see SECY-14-0016, January 31, 2014). This report reviews the state of knowledge related to radiation-induced degradation, estimated radiation levels, a limited survey of reactor support structures, and important design criteria. Collectively, this information provides a general framework for understanding the effects of irradiation on RPV concrete support structures.

This evaluation is designed to review recently completed and ongoing license renewal-related research on the characterization of the degradation of irradiated concrete in NPP structures near the RPVs. A proper evaluation requires an understanding of (1) the effect of radiation on concrete (what degradation modes exist and which are the most important in a light-water reactor [LWR] environment), (2) the radiation levels concrete structures experience in the near RPV environment, and (3) the functions those concrete structures must maintain over the course of an 80-year reactor lifetime.

ES.1 Effect of Radiation on Concrete

A collection of approximately 110 articles on neutron and gamma radiation damage to concrete and/or its components was reviewed, and information on study conditions and concrete performance was extracted for analysis. The effect of the water-to-cement ratio (w/c), aggregate, aggregate type, aggregate fraction, and temperature on concrete subjected to neutron and gamma irradiation was considered, focusing on the studies and data most relevant to the conditions in a commercial LWR.

The primary limitation of this review has been the lack of applicable data to address a number of variables, as discussed in Section 1.4. Even in some cases where data is available, there is a wide scatter in results due to uncertainties associated with the details of each experiment and the experimental measurements. In addition to the experimental variables considered (e.g., aggregate and cement paste types, temperature, aggregate fractions, and w/c), variables that influence results include the actual gamma and neutron radiation spectra used in irradiation experiments, sample preparation and curing procedures, sample size and shape, aggregate variation, and testing methods and equipment. These could differ across studies, even when measuring the same property.

ES.1.1 Neutron Radiation

Sections 3.1 and 4.1 cover the effect of neutron radiation on concrete and its components. These effects are summarized in Section 4.4.1.

No weight loss due to neutron irradiation was observed. At temperatures below 100°C, it is clear that neutrons have a much greater impact on aggregates than on cement paste because they cause disorder within the crystalline framework of an aggregate. The generally amorphous

nature of cement paste is affected to a much lesser extent. In particular, neutrons appear to disrupt covalent aggregate crystal structures (e.g., silicates with a quartz lattice) much more than ionic aggregate crystal structures (e.g., calcite). However, this appears to depend on the mineral crystal structure. For example, some silicates that do not have the quartz structure show little effect from neutron irradiation.

Disordering the aggregate crystal structure causes the aggregate's volume to expand. The relative onset of the quartz volume expansion under neutron irradiation also depends on temperature. Aggregate volume expansion appears to cause some reduction of the tensile strength and the elastic modulus of the aggregate. These impacts are noted at neutron fluence levels greater than 1×10^{19} n/cm^2. Observed degradation included calcareous aggregate and siliceous aggregates. Note that aggregates may be primarily calcareous or siliceous, but actual compositions are site-specific involving a mix of minerals. Since some crystal structures are more susceptible than others, differential expansion of the various minerals may lead to further cracking of the aggregate.

Irradiating concrete with neutrons can lead to significant degradation of its mechanical properties (compressive strength, tensile strength, and modulus of elasticity) at neutron fluence levels greater than 1×10^{19} n/cm^2 at temperatures less than 100°C. The reduction in compressive strength is due in part to the volume expansion of the aggregates, which results in a bonding mismatch with the cement paste. The volume expansion of the aggregate may also contribute to the reduction in tensile strength and the elastic modulus of the concrete. The effect of the w/c and aggregate fraction of the concrete on the mechanical properties of concrete under neutron irradiation shows no clear trends.

ES.1.2 Gamma Radiation

There is very limited data on the effects extended gamma irradiation has on concrete and its components. This is discussed in Sections 3.2 and 4.2 and summarized in Section 4.4.2.

Cement paste and concrete experience weight loss due to the gamma radiolysis of water in the cement paste pores. Cement paste also shows shrinkage due to water loss, but the limited data on concrete shrinkage is inconclusive. Exposing Portland cement to higher radiation resulted in the partial disappearance of the original hydrated minerals and the loss of chemically bound water after a dose of 1.3×10^8 Gy. The loss of water and partial disappearance of the original hydrated materials may result in more open pore space within the cement paste but this may be partially counteracted by gamma-induced carbonation of portlandite to calcite, where the calcite occupies slightly more volume than portlandite. A slight increase in the compressive strength of concrete with a dose of 2×10^8 Gy was observed with an increase in carbonate formation.

Heating caused by gamma irradiation can also cause water loss and shrinkage of cement paste. The very limited data show that there is no apparent change in aggregate and concrete volume under gamma irradiation. Some experiments show a potential for concrete properties to degrade at doses greater than 1×10^8 Gy, but these experiments were not consistent with the conditions found in an LWR cavity. There are also no data on how the w/c and aggregate fraction of the concrete affect the mechanical properties of concrete under gamma irradiation.

The effect of gamma irradiation on the important properties of concrete are indeterminate. The data on compressive strength and the modulus of elasticity include neutron irradiation that could be responsible for the relative decreases observed in concrete with increasing gamma dose. The mechanical properties of cement paste do not appear to change significantly with gamma

irradiation, despite the weight loss experienced by cement paste due to radiolysis. The concurrent formation of calcium carbonate may account for this behavior. Data for gamma doses approaching 10^9 Gy and beyond without companion neutron radiation are needed to address this uncertainty.

ES.2 Radiation Levels near Concrete Support Structures

The highest radiation levels outside of the RPV are in the reactor cavity around the belt-line region. For extended exposure periods, concrete support structures in this area are more susceptible to potential radiation damage. Many reactor designs include concrete support functions in close proximity to the highest radiation areas. As detailed in Section 5, boiling-water reactor (BWR) and pressurized-water reactor (PWR) support designs were reviewed in conjunction with estimated cumulative radiation exposures in the reactor cavity after 80 years of operation for all commercial NPPs to provide a general understanding of the problem.

ES.2.1 RPV Support Designs

All BWRs share a similar design for the configuration of the bioshield around the RPV. The RPV rests on a metal vessel support skirt, which is an integral part of the BWR RPV, on top of a concrete reactor pedestal. The cylindrical concrete bioshield also rests on the reactor pedestal, surrounding the core area of the RPV. The bioshield is a self-supporting structure and may be anchored at the top to the containment structure to maintain horizontal stability of the bioshield. In turn, horizontal stabilizers at the top of the bioshield may provide horizontal support for the upper end of the RPV and allow for thermal expansion and contraction of the RPV in some designs.

Six general RPV support system designs are used for PWRs. Four support types rest on the bioshield itself, which provides structural support for the RPV. The two remaining types of support system—skirt and column designs—rest on the concrete basemat, upon which the bioshield also sits. The skirt design is similar to that used for BWRs; the column support design has the RPV supported on the tops of steel columns, the bottoms of which are anchored on the basemat. The columns either support a ring girder that encircles the RPV under the inlet and outlet nozzles or are attached to supports under the inlet and/or outlet nozzles. Lateral support of the columns could include anchoring or embedment of the columns in the biological shield.

ES.2.2 Radiation Levels in the Reactor Cavity

The neutron radiation levels at critical concrete structure boundaries in the vicinity of the RPV have not been directly monitored in the past, although some ex-vessel neutron dosimetry has been conducted in the core belt-line region. Concrete degradation, as a result of neutron irradiation, is considered primarily due to interactions with fast neutrons (E > 0.1 MeV), as discussed in Section 3.1. For this review, through a series of steps, data obtained for neutron radiation for E > 1.0 MeV at the inner RPV wall is converted to an estimated fluence (E > 0.1 MeV) in the vicinity of concrete support structures in the reactor cavity. In each step of the calculation, there are variabilities and uncertainties that cannot be totally quantified at present without further confirmatory research and plant-specific information. Thus, the method used in this review is a rough approximation that is intended to produce reasonable results, but may not be conservative.

The highest estimated neutron fluence level at the outer face of the RPV wall was found to be greater than 1×10^{19} n/cm^2 (E > 0.1 MeV) for all PWRs, and, with one exception, less than

1×10^{19} n/cm^2 for all BWRs. These estimates are near or at the core mid-plane. The neutron fluence levels will rapidly decrease above the top and below the bottom of the core. There are indications that streaming effects could increase the fluence levels near RPV supports in these areas, but not higher than the core mid-plane values.

Few data are available on the expected gamma flux at the outer wall of a commercial RPV and in the reactor cavity. Estimated maximum doses at the outer RPV wall for two- and three-loop PWRs are on the order of 1×10^{10} rad (1×10^8 Gy) and 4×10^9 rad (4×10^7 Gy), respectively, for a hypothetical 80-year reactor life of 80 years (72 EFPY). Because the radiation damage threshold for concrete is considered by some to be around 10^{10} rad (10^8 Gy), there is the possibility for some gamma radiation damage by the end of a PWR's lifetime.

ES.3 Design Criteria, Degradation, and Modeling

Given the potential degradation characteristics of concrete after irradiation, a methodology is needed to determine whether a specific concrete structure will meet its design criteria, which includes the performance of its safety functions, over an extended period of operation in a specific radiation environment. Because of the complexity of the interactions within the concrete itself (e.g., cement paste-aggregate; irradiation effects; temperature and humidity effects), the subsequent change in radiation transport in the concrete over time, and interactions of the concrete with embedded reinforcement and anchorages, a better understanding of how microscale interactions translate into macroscale performance is needed to better understand and eventually quantify structural performance in a long-term radiation environment. Structural performance is necessarily plant-specific and depends on the structural design details and loads. Maximum potential loads on an RPV support structure can include those loads resulting from postulated accident conditions such as a loss-of-coolant accident in combination with a safe shutdown earthquake.

As discussed in Section 6, the combination of those loads and the resulting horizontal and vertical loadings could result in forces in multiple directions that would be counteracted by complex interactions of the concrete, including degraded concrete, with its metal reinforcement and anchorages as well as other RPV support interfaces. It is necessary to understand how the radiation-induced degradation affects the load carrying mechanisms and their continued ability to resist the applied forces. Improved understanding of how microscale interactions translate into macroscale performance will provide a better understanding and address uncertainties in the quantification of the effects of the concrete irradiation on the load-carrying ability of the RPV support structures and, therefore, on their structural performance in a long-term radiation environment.

Data on radiation-induced concrete degradation from operating experience is limited by the inaccessible nature of the affected structures. Efforts to obtain suitable concrete samples from decommissioned plants has been unsuccessful to date. Thus, appropriate concrete samples are not available for large-scale testing. Current research is based on small-scale testing due to space limitations in the test reactors, which also have higher temperature gradients than commercial reactors, and modeling techniques to characterize the degradation and its implications. By collecting the latest available data on irradiated concrete, this review provides a foundation for future work in estimating macroscale performance based on microscale events. The currently available models are valid only from the centimeter scale (the so-called representative volume element) down to the micrometer scale. These models need to be further developed in two directions in order to be used in structural analysis for concrete structures in NPPs.

One of these directions is to assess the effects of nuclear irradiation on the nanostructure of C-S-H and on the expansion of aggregates. Current models depend on experimental results summarized by several empirical equations for C-S-H and for aggregates. What happens in C-S-H and aggregates under nuclear irradiation should be further studied and characterized.

The other direction is to extend the multiscale models up to the meter level (the macro-structural level), because the degradation of concrete materials needs to be reflected in the structural analysis, which is the ultimate goal of the multiscale analysis. To this end, the multiscale models should be integrated with commercial finite-element software, or their results appropriately accounted for in the modeling with that software, so engineers can use the available software as a platform to examine the structural effects of nuclear irradiation.

ES.4 Recommendations and Conclusion

Neutron fluence levels above 1×10^{19} n/cm^2 ($E > 0.1$ MeV) at the typical temperatures in LWR reactor cavities (below 100°C) can significantly degrade concrete's physical and mechanical properties. The onset of noticeable degradation can appear at fluence levels above 1×10^{18} n/cm^2. However, there is insufficient evidence to change the currently adopted value of 1×10^{19} n/cm^2 as a damage threshold value for regulatory purposes. The contributing factors and degradation mechanisms are not well understood. There is strong, but not conclusive, experimental evidence that the primary effect is related to the disordering effect of neutrons on aggregate mineral structure, especially those with a covalent bond structure such as that found in siliceous aggregates with quartz structure. Other issues are that aggregates are a mix of different mineral types and vary from plant to plant. The differential expansion of minerals within the aggregate may cause cracking.

Gamma dose levels above 1×10^8 Gy may result in the degradation of concrete properties, but there is no data directly related to isolated gamma irradiation of concrete in an air environment. The primary impact of gamma irradiation on concrete is water loss from the cement paste due to heating and radiolysis, which results in some shrinkage of the cement paste. The loss of water results in more open pore space within the cement paste, but this effect may be partially counteracted by gamma-induced carbonation of portlandite to calcite, where the calcite occupies slightly more volume than portlandite.

The synergistic effects of neutron and gamma radiation on concrete are not known at this time. Most of the reviewed neutron irradiation data were obtained using a nuclear reactor as a source which also produced gamma radiation. However, many tests did not track the corresponding gamma dose or qualify the neutron spectrum, and the relative values of neutron irradiation and gamma dose in the tests were not necessarily the same as those under commercial LWR operating conditions. In addition, little neutron- or gamma-only data under LWR conditions is available for comparison.

The synergistic effects of nuclear radiation and heat are also not well characterized. At temperatures below 100°C, thermal effects can solely lead to some degradation in mechanical properties. Higher temperatures correlate with a shift in the apparent onset of quartz volume expansion under neutron irradiation to higher neutron fluence values.

Issues that remain to be explored include those related to degradation depth, steel reactor cavity liners, and bonding between steel embedments and concrete. The neutron and gamma radiation are attenuated as they pass into the bioshield or other concrete support structure. At some depth, the radiation levels will be below those that cause degradation that could affect

support functions. In addition, even if the degradation is limited to a short distance from the face of the inner bioshield wall, it can lead to the development of internal stress and strain fields within the bioshield that extend much further. For NPPs with a steel cavity liner, the liner could constrain concrete expansion due to neutron irradiation at the bioshield surface, resulting in additional stress and strain fields in the concrete. The liner would also have an effect on the relative amounts of water present in the concrete by limiting movement of water and its byproducts due to heating and radiolysis caused by gamma radiation. Steel embedments such as rebar and anchorages are used throughout the bioshield and RPV supports and are essential elements of the RPV support structures. Effects of irradiation degradation of concrete support structures could be exacerbated by potential effects of the concrete degradation on the rebar-concrete bond.

The reactors that are more susceptible to concrete bioshield support degradation are those where the reactor supports sit on the concrete bioshield close to, and directly exposed to, the core radiation. The PWRs that rest on support skirts, neutron shield tanks, or pedestal (metal column) supports may not have any significant long-term concrete irradiation degradation issues because the distance from the core to the base of the reactor cavity is far enough to protect them and/or shielding is provided by a neutron shield tank. However, the effect of irradiation on concrete support structures near the core mid-plane requires evaluation, and the effect of irradiation on steel structures and components continues to be considered along with its impacts on concrete support structures.

This review indicates that all operating PWRs have the potential to generate neutron fluence levels in the reactor cavity that could result in concrete degradation before 80 years of operation. However, the extent of any potential degradation of concrete RPV supports cannot be quantified in a general manner because plant-specific, detailed design information of the RPV supports is necessary, knowledge of the radiation levels at plant-specific support locations is largely unknown, and the effect and extent of nuclear irradiation on the concrete supports in an LWR operating environment is not well understood and subject to uncertainty.

Although BWRs are expected to experience lower radiation levels than PWRs and are not likely to experience issues related to concrete irradiation-induced degradation, certain aspects of a given design may need to be addressed. Furthermore, there are NPPs that are operating under off-normal conditions in some cases, that are monitored as part of their aging management plans; these off-normal conditions could impact concrete irradiation degradation mechanisms. Thus, the impact of nuclear radiation on critical concrete support structures should be considered on a case-by-case basis as part of a subsequent license renewal application.

ACKNOWLEDGMENTS

The work described in this report was sponsored by the U.S. Nuclear Regulatory Commission (NRC), Office of Nuclear Regulatory Research (RES). The authors would like to thank Madhumita Sircar for her capable guidance as the NRC project manager. Her breadth of knowledge on the subject of irradiated concrete and helpful comments were invaluable to the success of this report. A number of NRC staff contributed constructive comments on draft versions of this report. Among those, special thanks are in order to Andrew Prinaris, Jinsuo Nie, and Jose Pires for their enthusiasm and insightful observations.

ABBREVIATIONS AND ACRONYMS

ACI	American Concrete Institute
ASME	American Society of Mechanical Engineers
ASR	alkali-silica reaction
BWR	boiling-water reactor
CLB	current licensing basis
DLF	dynamic load factor
DOE	U.S. Department of Energy
DSC	differential scanning calorimetry
EFPY	effective full-power year
FDM	finite difference method
FEM	finite element method
FSAR	Final Safety Analysis Report
LOCA	loss-of-coolant accident
LRA	license renewal application
LWR	light-water reactor
NPP	nuclear power plant
NRC	Nuclear Regulatory Commission
OBE	operating basis earthquake
PWR	pressurized-water reactor
RH	relative humidity
RPV	reactor pressure vessel
RVE	representative volume element
SLR	subsequent license renewal
SSE	safe shutdown earthquake
TG	thermogravimetry
w/c	water-to-cement ratio

1 INTRODUCTION

1.1 Background

As a fundamental building material, concrete is one of the primary structural materials used in the construction of commercial nuclear power plants (NPPs). It is used in such applications as building foundations, reactor containment, shielding, and for support of the reactor pressure vessel (RPV).

The degradation of concrete over time at NPPs has been well studied in most areas and depends on its environment [1]. Concrete degradation mechanisms include alteration/erosion, chemical attack, thermal exposure, fatigue, cement-aggregate reactions, freeze/thaw cycles, irradiation, leaching, volume changes, external loads, fire damage, steam impingement, and settlement. Until recently, aging management of concrete degradation due to irradiation had not been addressed in aging management programs at U.S. NPPs [2, 3].

Concrete has been used for radiation shielding for decades. A mix of cement and various aggregates, concrete provides protection from both gamma and neutron radiation generated in a nuclear reactor. In conjunction with its radiation resistance and protection, concrete's relatively low cost and its structural properties have led to its extensive use in the vicinity of the RPV. Earlier work showed that the physical properties of concrete remain relatively unaffected by a fast neutron fluence below approximately 1×10^{19} neutrons/cm^2 [4, 5]. However, a number of studies involved conditions (e.g., temperature and humidity) that are non-representative of the environment of concrete structures exposed to the highest radiation levels at an NPP [6, 7]. In addition, gamma radiation is responsible for other aging mechanisms that must be considered [8, 9]. Thus, there is some uncertainty related to the longer-term performance of structural concrete in a high-radiation environment. Further information can be found in William et al. [10].

1.2 Subsequent License Renewal

NPPs were originally designed and licensed for 40 years of operation. Since then, most plants have undergone license renewal to extend plant operation to 60 years; the few remaining NPPs may do the same. The NRC has embarked on the subsequent license renewal (SLR) process of reviewing license applications that would extend those reactors' operating licenses for an additional 20 years (80 years total) if approved. Research data indicate that radiation causes degradation of concrete's physical and mechanical properties.

When evaluating the reduction of strength and mechanical properties of concrete due to radiation, "fluence limits of 1×10^{19} neutrons/cm^2 neutron radiation and 1×10^8 Gy (1×10^{10} rad) gamma dose are considered conservative radiation exposure levels beyond which concrete material properties may begin to degrade markedly" [3]. In addition, a neutron energy cutoff level of $E > 0.1$ MeV was suggested for the fluence limit [3]. Further research is ongoing to evaluate the safety performance of the RPV support structures.

Technical issues related to concrete degradation due to irradiation are one area where evaluation is necessary for power reactor operation beyond 60 years. The highest fast neutron fluence ($E > 0.1$ MeV) estimated in this study at the outside wall of a commercial U.S. NPP RPV after 80 years of operation is about 7.5×10^{19} neutrons/cm^2 (8.0×10^{18} neutrons/cm^2 for $E > 1.0$ MeV). Thus, operation of some NPPs over a period of 80 years could result in higher

fluence levels than originally anticipated. This might impair the intended support functions of concrete structures in the vicinity of the RPV.

1.3 Objective and Scope

The objective of this evaluation is to conduct a confirmatory review of recently completed and ongoing SLR-related research on the degradation of irradiated concrete material in NPP structures close to RPVs. Our intention is to assess and evaluate the suitability and sufficiency of the research to establish radiation levels that would not require subsequent evaluation of structural significance and plant-specific irradiation-related aging management programs.

To reconsider established radiation levels that would not require subsequent evaluation for an SLR [3], an understanding of both the degradation of concrete by radiation and the overall configuration (structure/geometry and operating environment) of the NPPs is required. Irradiation impacts on concrete depend, in part, on the concrete variability (e.g., aggregate type, texture, cement types, and water content) and radiation energy, intensity, and duration (flux and fluence). The review considers preliminary estimates for concrete radiation damage already provided by the U.S. Department of Energy's (DOE's) light water reactor sustainability research [11, 12], as well as research done by other domestic and international programs. The combined effects of various processes (e.g., neutron and gamma irradiation, temperature, and humidity) are considered.

A compilation of the different reactor types, their structural configuration and layouts, concrete variability, and operating environments (neutron and gamma irradiation levels, temperature, humidity) is part of this evaluation. The compilation of the irradiation environments includes a determination of the neutron fluence and gamma dose estimates in the vicinity of RPVs for operation up to 80 years, as well as a discussion of the associated uncertainties for the concrete structures of interest. In combination with the review of information on the radiation effects on concrete and its functions, an attempt was made to identify radiation levels that would not require subsequent evaluation of structural significance. The radiation effects on concrete components and any embedded steel include both structural (strength, stiffness, and the concrete-steel bond for both structural reinforcement and anchoring elements) and shielding properties. However, the present study is only concerned with the potential effects on concrete's structure.

As a baseline, Chapter 2 of this report briefly summarizes concrete composition, non-radiation processes that contribute to its degradation, and the general type of concrete used in the construction of U.S. NPPs. How gamma and neutron radiation interact with concrete is discussed in Chapter 3. Chapter 4 covers the impacts of irradiation on concrete properties. Discussions on the designs of concrete RPV support structures and estimates of the potential radiation levels in reactor cavities appear in Chapter 5. Examples of potential accident loads on concrete support structures and the need for estimating and extending nano- and microscale impacts from irradiation degradation to the macroscale for structural analysis are provided in Chapter 6. Chapter 7 covers plant-specific considerations related to concrete support configurations and potential radiation levels. Conclusions are summarized in Chapter 8.

1.4 Study Limitations

The analysis and conclusions presented in this review are limited by the complexity of the problem and the corresponding research in this area to date. The primary limitation of this review has been the lack of applicable data to address the influence of a number of variables.

Even in cases where data is available, there is often a wide scatter in the plotted results due to both uncertainties associated with experimental measurements and uncertainties related to the details of each experiment. Acknowledging these limitations will give the reader a better appreciation of the available data's relevance to the degradation of concrete in general and in a light-water reactor (LWR) in particular.

1.4.1 Variability and Uncertainty

In addition to the experimental variables considered, such as aggregate and cement paste types, temperature, aggregate fractions, and water-to-cement ratio (w/c), variables that influence results include: (a) the actual gamma and neutron radiation energy distributions used in irradiation experiments, (b) sample preparation and curing procedures, (c) sample size and shape, (d) aggregate type, and (e) testing methods and equipment that could differ across studies when measuring the same property.

The neutron fluence values reported in different studies on concrete or its components were based on different neutron energy levels. Some values correspond to reported energies >1 MeV, while others do not even provide the information. Thus, the effects reported for the same material and neutron fluence levels could have different results in different studies. The best way to ensure the consistency of the neutron energy level for all the tests is to obtain the neutron energy spectrum during each test. Unfortunately, only a few studies provide this information.

The various fabrication procedures and pretreatments can cause inconsistencies of the reference properties of samples across studies. For instance, some cement paste and concrete specimens were cured for several months and others were aged for more than 1 year. Some samples were preheated to different temperatures before testing, and some were only cured at ambient temperature.

The samples tested in the various studies varied in shape; most samples were cylinders or cubes, in sizes ranging from several millimeters up to 400 mm. The size and geometry of these samples may influence property tests. They limited the types of tests conducted, as well as the size and shapes of aggregates in concrete samples, which in turn limits their applicability to real-world conditions.

A number of studies tested mortar samples in place of concrete samples. Mortar is composed of cement, fine aggregate, and water (no coarse aggregate). This practice enabled the testing of smaller samples in reactors with limited sample space, but could affect the outcome of property tests, as mentioned in the previous paragraph.

The range of aggregates considered in testing was quite broad. Due to the limited number of data points, it is difficult to delineate or eliminate the effect of aggregate type. Behavior within a particular rock group could vary considerably, because the mineral/chemical compositions of aggregates could be quite different, even if they share the same name. Many studies did not provide detailed information about the chemical compositions of the aggregates.

Testing methodology and equipment for some properties could also differ between studies. For example, the values of tensile strength in the figures could represent either splitting tensile strength or flexural strength. However, because relative values are used, the effects of testing methods should not be very significant.

1.4.2 Relevant Data

This review is concerned with the potential degradation of concrete support structures in an LWR radiation environment. Consequently, the data of interest is related to the concrete used to construct existing NPPs and how it ages in an indoor environment at a temperature of about 65°C (150°F) in gamma and neutron radiation fields due to uranium fission.

Concrete is primarily a two-component system with aggregate bound in a cement paste matrix. Ordinary Portland cement, typically with a w/c of about 0.45, was the type used in U.S. commercial NPP construction. The aggregates used at each NPP were typically obtained from nearby quarries, which resulted in a range of aggregate types being used.

Experimental data from irradiation (neutron and/or gamma) studies of any type of concrete or its cement and aggregate components is scarce. Thus, this review includes data from experiments where some parameters may not have been within the envelope defined by LWR operations (e.g., temperatures less than or greater than 65°C [150°F]). Such results could represent potential off-normal operating conditions or have the potential to provide insight into various aspects of radiation effects. For example, very few comprehensive studies examined irradiation effects on the mechanical properties of concrete and its cement paste and aggregate components separately to elucidate potential degradation mechanisms. One of these studies involved a temperature well above LWR conditions and cement and aggregate types not used in U.S. NPPs; however, some degradation mechanisms could still be relevant. As another example, the w/c at most NPPs was originally around 0.45. Over time (decades), that value will likely exhibit a gradient from the surface of the bioshield into the bulk material and be plant-specific, changing due to relative humidity (RH) conditions, the temperature in the reactor cavity, the presence of a reactor cavity liner (if used in the NPP design), and potential off-normal conditions (e.g., water leaks or elevated temperatures). In the end, collective studies may show trends that pass into the envelope defined by LWR operations or show similar mechanisms or effects.

1.4.3 Complete Datasets

Most studies do not have complete sets of data. To properly analyze the radiation impacts on concrete, it is necessary to understand the effects on concrete itself and its components (cement and aggregates). However, most studies are not comprehensive; they do not separately test the three primary mechanical properties (the elastic modulus and the compressive and tensile strengths) of the concrete and/or do not separately test its cement matrix and the aggregates used.

2 CONCRETE

Concrete is a two-phase composite material with aggregates as inclusions in a cement paste as a matrix. The two phases have different transport, thermal, hygro, and mechanical properties, and thus respond differently to temperature change, moisture fluctuation, and nuclear irradiation. The aggregates in concrete expand with increasing temperature and prolonged nuclear irradiation. Cement paste may expand if the thermal expansion is dominant and may shrink if the moisture loss is dominant.

The combined effect of the deformation mechanisms of the two phases depends on many factors such as heating/cooling rate, wetting/drying rate, irradiation intensity, aging and exposure periods, and composition of the concrete. For example, the thermal incompatibility between the two phases causes a very large mismatch in the deformation between aggregates and cement paste; this results in micro-cracks in the interface transition zone around aggregates. Subsequent and simultaneous heating and drying (especially under an accidental condition), irradiation, and loading may cause coalescence of such cracks to form discrete large cracks. This, in turn, can lead to fracture and spalling of concrete and other degradation of concrete structures, including the potential loss of bonding to metal embedments. This chapter provides a brief description of concrete and its components in a non-irradiation environment.

2.1 Cement Paste

Cement paste is a porous material formed by the hydration reactions between Portland cement and water. It is composed of several hydration products of Portland cement: calcium hydroxide (CH) particles, which are needle- or plate-shaped crystals; calcium silicate hydrate ($C_3H_2S_3$, or simplified as C-S-H), which has a nonstoichiometric amorphous structure; ettringite ($C_6AS_3H_{32}$) particles, which are needle-shaped crystals formed with a large volume expansion. There are also other minor chemical compounds, water, and pores in the cement paste.

Calcium hydroxide and ettringite are crystalline materials, but C-S-H is not. The atomic structure of C-S-H is important because C-S-H binds all of the concrete components together and produces the strength of the concrete. Based on adsorption/desorption test data for cement paste, the internal structure of C-S-H has been estimated as layered structures with plate-like solid layers or randomly shaped flexible layers (see Figure 2-1).

There are several types of water in cement paste, which is very important for the durability of concrete. The following types of water are found in concrete paste: (1) Chemically combined water, the water consumed during hydration reactions, which becomes part of the solid components; the loss of chemically combined water under high temperature is called dehydration, and is associated with major strength reduction of cement paste and concrete. (2) Capillary water, the water in capillary pores, which is evaporable during air drying; the loss of capillary water is the primary reason of drying shrinkage. Capillary water is also referred to as free water. (3) Interlayer water between the solid layers of C-S-H. This interlayer water is not evaporable under regular air drying, but is mobile under very low RH and/or vacuum drying. The loss of interlayer water may cause excessive drying shrinkage.

The amount of water used in the cement paste is characterized by the w/c. A high w/c creates a different elemental composition in the concrete (i.e., a higher content of O and H in the concrete). Light elements like H attenuate neutrons more effectively than other elements in the concrete, which reduces overall damage to the concrete. The value found at most NPPs is

typically about 0.45 per ACI 318 [13]. This value achieves the desired compressive strength, and it allows the paste to remain workable when the water and cement are mixed. However, for durability, the w/c may be lower.

2.1.1 Thermal Effects

Temperature rise could potentially occur in the reactor cavity and is associated with nuclear irradiation. Therefore, changes in the properties of cement paste under elevated temperatures (greater than room temperature) should be assessed. There are two possible damage mechanisms in cement paste under high temperature conditions: phase transformation and spalling damage. Explosive spalling can occur at a very high heating rate that could only occur under potential NPP accident conditions. Concrete spalling can also occur under other degradation mechanisms, most notably in reinforced concrete or with other embedded metals where corrosion products build up at the metal-concrete interface, exerting outward pressure. Spalling may also occur due to chemical attack, due to compressive stresses in concrete, or from the vaporization of moisture (expansion) in the cover concrete. We will only consider phase transformations in this section; these data will be used later to analyze the test data from concrete under nuclear irradiation.

The primary effect of heating in the temperature range experienced by concrete in a NPP reactor cavity is loss of capillary water, which results in drying shrinkage. The hardened cement paste, through the loss of chemically combined (bound) water, will only become dehydrated when the temperature is higher than the regular operating temperature of 65°C (150°F). Initially, elevated temperatures drive out the capillary water in pores and accelerate the diffusion of water in cement paste. At the regular operation temperature, chemically bound water is not affected by temperature. However, as temperatures rise above this level, chemically bound water eventually will begin to be lost before all of the capillary water is gone. Given sufficient time at slightly higher temperatures, by about 105°C, all of the capillary water will be driven out [14]. All of the hydration products, such as C-S-H, decompose under high temperatures. The decomposition processes of the hydration products at various temperature ranges are listed in Table 2-1 [15].

On heating ordinary Portland cement up to 100°C, ettringite had disappeared by 90°C with an increase in portlandite and calcite formation due to their precipitation caused by the loss of free and chemically bonded water, as well as contributions of Ca^{+2} from the ettringite [16]. At temperatures up to 200°C, hardened cement paste exhibits a small volume expansion, and contracts at higher temperature [17].

The chemical reactions for the decomposition processes can be described as follows:

Decomposition of C-S-H: $3.4CaO \cdot 2SiO_2 \cdot 3H_2O \rightarrow 3.4CaO \cdot 2SiO_2 + 3H_2O \uparrow$ (2-1)

Decomposition of CH: $Ca(OH)_2 \rightarrow CaO + H_2O \uparrow$ (2-2)

The formation of $CaCO_3$is due to the accelerated carbonation reaction of CH:

$$Ca(OH)_2 + CO_2 + H_2O \rightarrow CaCO_3 + 2H_2O \quad (2\text{-}3)$$

Then, $CaCO_3$ decomposes at high temperatures as shown in Table 2-1.

The new phases formed during the phase transformations have densities, strengths, and stiffnesses that differ from those of the original phases in the cement paste. For example, cracks and voids form in cement paste along with the decomposition of CH.

a)

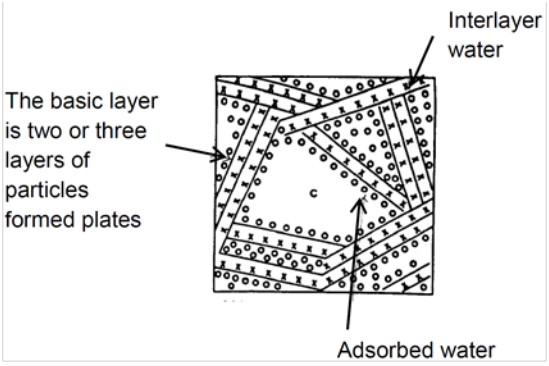

Mindess and Young (1981)

b)

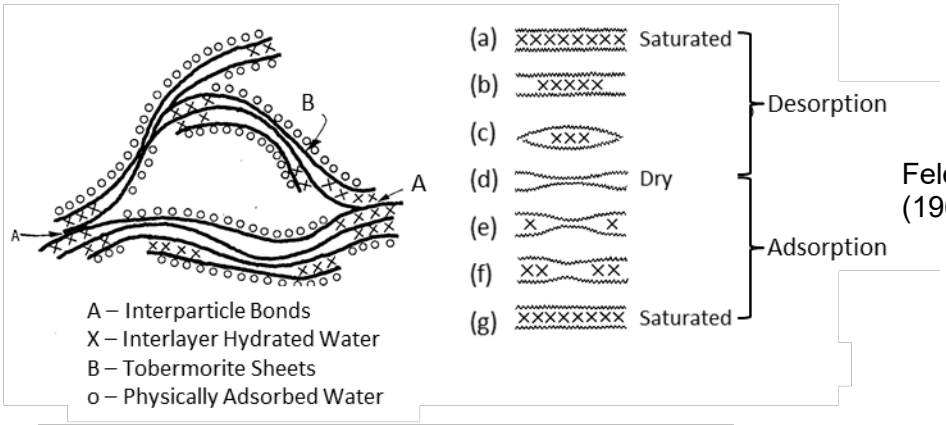

Feldman and Sereda (1968)

c)

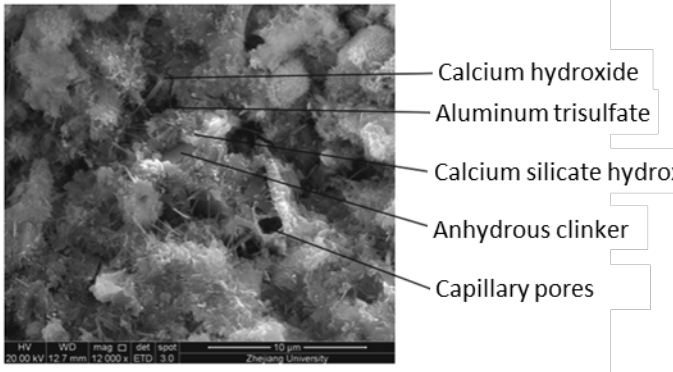

Chen et al. (2014)

Figure 2-1 (a, b) Proposed Internal Layer Structures and (c) Scanning Electron Image of Hardened Cement Paste (Sources: (a) [18] Figure 4-6(a) from *Concrete*, Mindess, S., & Young, J. F. (1981) Prentice-Hall, NJ. reprinted by permission from the American Concrete Institute; (b) [19] Reprinted by permission from Springer Nature *Matériaux et constructions*, "A model for hydrated Portland cement paste as deduced from sorption-length change and mechanical properties," R. F. Feldman and P.J. Sereda, 1968; (c) [20] Republished with permission of ICE Publishing from *Magazine of Concrete Research*, 68(22), "A nano-model for micromechanics-based elasticity prediction of hardened cement paste." J. Chen et al., 2014; permission conveyed through Copyright Clearance Center, Inc.)

Table 2-1 Decomposition of Cement Paste at Various Temperature Ranges

Temperature Range (°C)	Transformation or Decomposition Reaction	Heat of Reaction or Transformation (kJ/kg)	Heat of Reaction or Transformation (MJ/m^3 concrete)	Mass of Reaction (kg/m^3 concrete)
30–120	Desorption or evaporation of physically adsorbed water	Heat of evaporation of water: 2,258	290	130 kg water
30–300	Gel destruction: 1. stage of dehydration	Heat of hydration: 250	<20	<78 kg hardened cement paste
120–600	Release of chemically adsorbed or zeolithically bonded water	Heat of evaporation of water >2,258	>135	60 kg water
450–550	Decomposition of portlandite $Ca(OH)_2 \rightarrow CaO + H_2O$	1,000	<40	<40 kg CaO
570	Transformation of quartz α → β SiO_2	5.9	8.8 1.2	1,500 kg quartz 200 kg quartz
600–700	Decomposition of CSH-phases; formation of β-C2S	Heat of hydration: 500	<120	<240 kg hardened cement paste
600–900	Only calcite: dissociation of calcite	Heat of decomposition: 1,637	2,360	1,500 kg limestone $CaCO_3$-content approx. 90%
1,100–1,200	Melting of concrete, formation of glassy material	Melting heat: 500–1,000	quartzitic: 1,575 calcitic: 1,125	2,100 kg concrete 1,500 kg concrete

Source: [15]

2.1.2 Carbonation

Over the last 40 years, the corrosion of reinforcing steel has become one of the most important problems surrounding the durability of concrete structures. The initiation of steel corrosion has many possible influential factors. One of them is the carbonation reaction [21, 22]. Not only can rust formation associated with steel corrosion reduce the cross-sectional area of the steel, but the strength of cementitious materials is also reduced due to the volume expansion associated with the rust formation. Usually, the steel in cementitious material is protected by a thin layer of oxide that forms on the steel surface due to the highly alkaline environment of the pore solution. The hydration reactions of cement drastically increase the pH of the pore solution from 7 to about 13. This increase is the result of the generation of calcium hydroxide during the hydration process [23-26].

Carbonation reactions can change the behavior of cement paste from several aspects. The general carbonation reactions can be expressed as [27]:

$$CO_2 + H_2O \leftrightarrow H_2CO_3 \leftrightarrow H^+ + HCO_3^- \leftrightarrow 2H^+ + CO_3^{2-} \quad (2\text{-}4)$$

$$Ca(OH)_2 + 2H^+ + CO_3^{2-} \rightarrow CaCO_3 + 2H_2O \quad (2\text{-}5)$$

$$Ca(OH)_2 + H^+ + HCO_3^- \rightarrow CaCO_3 + 2H_2O \quad (2\text{-}6)$$

$$C - S - H + 2H^+ + CO_3^{2-} \rightarrow CaCO_3 + SiO_xOH_x \quad (2\text{-}7)$$

$$C - S - H + H^+ + HCO_3^- \rightarrow CaCO_3 + SiO_xOH_x \quad (2\text{-}8)$$

$$CO_2 + H_2O + CaCO_3 \leftrightarrow Ca^{2+} + 2HCO_3^- \quad (2\text{-}9)$$

$$2H^+ + CaCO_3 \leftrightarrow CO_2 + Ca^{2+} + H_2O \quad (2\text{-}10)$$

The CO_2 first dissolves in water to form carbonic acid and its dissociation products (hydrogen, carbonate, and bicarbonate ions) as shown in Equation (2-4) [27]. In the next steps, Equations (2-5) to (2-8), the acid reacts with the calcium hydroxide first to generate the calcium carbonate. Then the calcium silicate hydrate (C-S-H) gel (the main product of the hydration reaction of Portland cement) reacts with the acid to produce the amorphous silica gel and calcium carbonate.

The calcium carbonate is very stiff and can increase the overall strength of the cement paste, but it can also decrease the tensile strength and the modulus of elasticity. The generation of the amorphous silica and calcium carbonate decreases the permeability as they precipitate in the open pores. The process usually ends at this stage in regular Portland cement concrete in aboveground structures where the moisture level is low. If the cement paste is in contact with liquid water or the moisture content is high, which is a common environmental condition underground, the reaction process will continue (Equations (2-9) and (2-10)).

Because the pH of the pore solution drops as the calcium hydroxide and alkali phases are depleted in the reactions up through Equation (2-8), bicarbonate (HCO_3^-) becomes thermodynamically favored over carbonate (CO_3^{2-}) in a wetter environment [27]. At the end of the process in this case, the calcium carbonate content will decrease with a rise in dissolved calcium, and the strength of the cement paste will decrease as well. This demonstrates that, for normal Portland cement concrete in NPPs whose moisture content is very low, carbonation could have both positive and negative effects on concrete durability: carbonation reactions reduce pH value and destroy the passive oxide film on the surface of steel which can initiate the

corrosion of reinforcing steel, but it can also densify the concrete and reduce its porosity and permeability.

Based on previous research, the rate of the carbonation reaction is very important [28, 29]. Several other influential factors were considered: RH, temperature, w/c, types of cement used, CO_2 content of the atmosphere, and so on [30]. For example, with increasing temperature, the rate of the carbonation reaction increases. Equation (2-11) is an empirical equation developed based on available test results:

$$\delta = AT + F_T, \tag{2-11}$$

where δ is the carbonation depth (mm), T is the temperature (°C), A is the influential factor of temperature to carbonation depth (mm/°C), and F_T is a constant (mm). The carbonation reaction involves water, and the reaction cannot proceed if the internal RH is lower than 50%. Between RH levels of 50% and 75%, the reaction rate varies. At higher humidity levels, the reaction rate can reach the maximum. However, the diffusion of CO_2 in concrete (the supply of CO_2) is slower at high internal RH.

The w/c is very influential among the mix design parameters of concrete. With a higher w/c, the rate of carbonation reaction is higher; this effect is because the porosity of concrete is higher with a higher w/c.

The initial CO_2 content in the air is an important environmental parameter. Equation (2-12) is an empirical equation developed for evaluating the carbonation depth (x), taking into account the CO_2 content in the air and other influential parameters:

$$x = \left(\sqrt{\frac{2D}{a}(c_1 - c_2)}\right)\sqrt{t} = A\sqrt{t}, \tag{2-12}$$

where x is the carbonation depth (m), D is the diffusion coefficient of CO_2 in concrete (m^2/s), a is the necessary amount of CO_2 for the carbonation of the alkaline components (g/m^3), c_1 is the CO_2 concentration of the surrounding air (g/m^3), c_2 is the CO_2 concentration at the carbonation front (g/m^3), t is the time (s), and A is the carbonation constant [31, 32].

In addition, many researchers have started to conduct accelerated experimental studies to analyze changes in the chemical composition of concrete by using thermogravimetry (TG) and/or differential scanning calorimetry (DSC) analysis [33, 34]. Using TG and DSC, researchers can follow the loss in sample mass as a function of increasing temperature (TG) and measure the heat flow into or from the sample as the temperature increases (DSC). This combination of methods provides key thermodynamic data to aid in determining the chemical reactions that are taking place.

2.1.3 Alkali-Silica Reaction (ASR)

An ASR is a deleterious chemical reaction between the alkali hydroxide in Portland cement and certain siliceous rocks and minerals present in aggregates, such as chalcedony and opal [35]. ASR was first reported by Stanton [36] in 1940. The product of ASR, referred to as ASR gel, expands with time. The pressure the expansive ASR gel imposes on the surrounding matrix causes many cracks in the concrete. This reduces the stiffness and strength of unconfined concrete and may affect the stability and safety of structures [37].

ASR is a chemical reaction between amorphous or poorly crystalline silica present in a reactive aggregate and the alkali and hydroxyl ions in the pore solution of concrete [38]. The ASR process is complex and includes several phases. The process can be summarized in two main steps [39-41], as shown in Figure 2-2 and Equations (2-13), (2-14), and (2-15). The aggregate siloxane networks are attacked by hydroxyl ions in the first step to generate alkali silicate and silicic acid. In these equations, R^+ denotes a metal ion, such as a sodium or calcium ion (Na^+, Ca^{2+}) (Equation (2-13)). Then the silicic acid reacts with more hydroxyl ions to produce the alkali-silica gel (Equation (2-14)). The alkali-silica gel absorbs free water, either from the internal moisture in the concrete or from the outside environment, in the second step where *n* is the hydration number in Equation (2-15). Through the absorption of water, the ASR products swell and induce cracking in aggregates and in the cement paste around them, resulting in the deterioration of concrete [42, 43]:

$$\equiv Si\text{-}O\text{-}Si \equiv + R^+ + OH^- \rightarrow \equiv Si\text{-}O\text{-}R + H\text{-}O\text{-}Si \equiv, \quad (2\text{-}13)$$

$$\equiv Si\text{-}O\text{-}H + R^+ + OH^- \rightarrow \equiv Si\text{-}O\text{-}R + H_2O, \quad (2\text{-}14)$$

$$\equiv Si\text{-}O\text{-}R + nH_2O \rightarrow \equiv Si\text{-}O^-\text{-}(H_2O)_n + R^+ \quad (2\text{-}15)$$

There are several factors that may influence the rate of ASR expansion, and they can be divided into three groups. The first group is cement properties, especially the alkali content of cement. The second group is the aggregate properties such as mineralogy and aggregate size. The last group is the environmental conditions such as temperature and moisture.

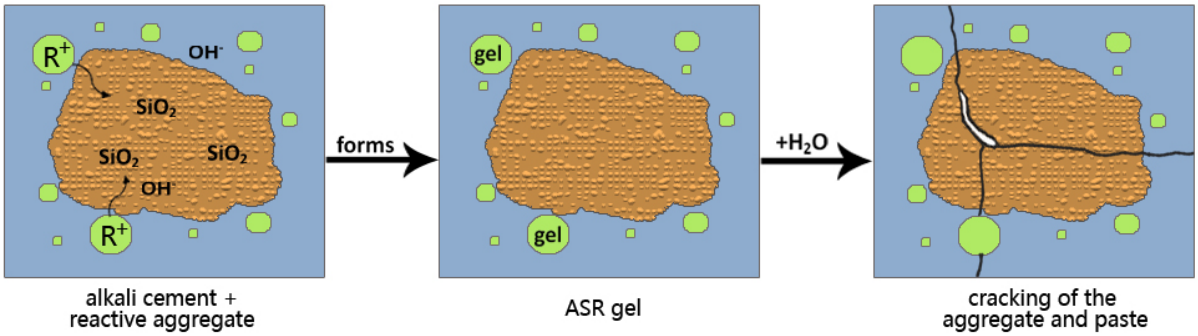

Figure 2-2 ASR Process

Almost all of the alkali in concrete comes from Portland cement. It has been proven that the higher the content of alkali in the Portland cement, the more powerful the ASR that takes place. Past research shows that water-soluble alkalis occupy around 45% to 80% of the total alkali content in Portland cement [36]. We considered 0.6% of the equivalent alkali content (the equivalent alkali content in Portland cement is expressed as $\%Na_2O + 0.658 \times \%K_2O$, by ASTM C150) as a dividing value for the alkalis in Portland cement. Portland cement with an equivalent alkali content higher than 0.6% is a high-alkali cement.

For aggregates, there are two main parameters which can dramatically affect the ASR: the type of aggregate and the aggregate size. The potentially susceptible types of aggregate that can cause ASR are the porous and non-crystalline forms of silica and silicates, such as volcanic glass and opal. The size of the aggregate particles matters because the rate of ASR depends on the surface area of reactive aggregates. Some researchers [44, 45] report that the expansion

may be larger when the aggregate size is smaller, which corresponds to a larger surface area given a fixed volume of aggregate. However, some studies found that there is a pessimum size for reactive aggregate, where the ASR affected concrete can reach the maximum expansion. The pessimum size is about 37.5 μm for certain types of reactive aggregates [46-49]. Previous studies showed that the critical RH is 80% at 23°C [50]. The temperature is also very important during the ASR; a higher temperature can accelerate the expansion rate [51].

2.2 Aggregates

For normal weight concrete, there are two common aggregate groups by mineralogical composition: (1) siliceous aggregates such as quartzite, gravel, granite, and flint; and (2) calcareous aggregates such as limestone, dolomite, and anorthosite. Under nuclear irradiation, the atomic structure of some aggregates can be converted from a crystalline structure to a distorted amorphous structure with a decrease in specific gravity and an increase in volume [5]. It is generally understood that siliceous aggregates, for example, quartzite, expand under intensive neutron irradiation (as discussed in Section 3.1.3.1), expand under high alkali and moist environments (the so-called alkali-silica reaction), and experience a phase transformation at approximately T = 570°C.

Figure 2-3 shows the responses of unirradiated concrete with different aggregates at elevated temperatures. The combined effect of the deformation mechanisms of concrete depends on many factors, such as heating rate, holding period, and composition of the concrete. At the range of service temperature (T < 65ºC), the difference between the thermal strains shown in Figure 2-3 is not large. As temperature increases, the difference becomes larger, so the thermal response of concrete shares the same trend as the response to neutron irradiation.

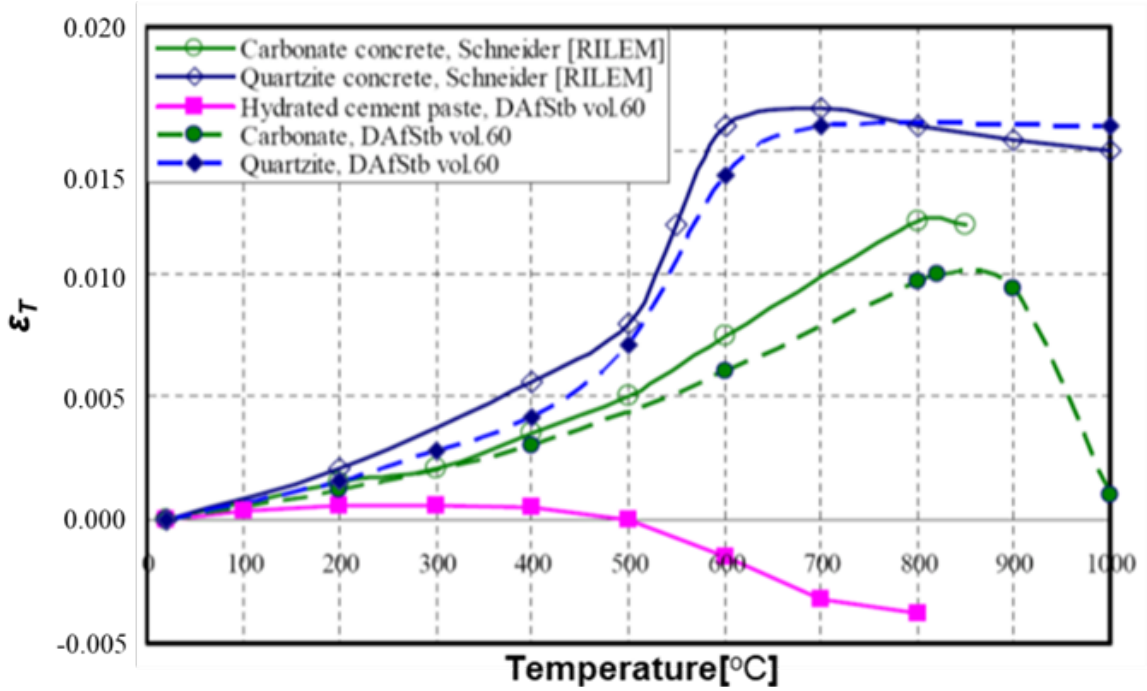

Figure 2-3 Thermal Strain (ε_T) for Different Concretes, Aggregates, and Hydrated Cement Paste (Source: [52])

Aggregates can also be classified by size as fine or coarse. The dividing size is 4.75 mm, which is the size of the opening of a No. 4 sieve for concrete structures in the U.S. construction industry. The aggregate size is important because, with a fixed volume fraction of aggregate, a smaller size of aggregate particles corresponds to a higher surface area, which can accelerate chemical reactions between the aggregate and the chemicals in surrounding cement paste.

2.3 Bioshield Concrete

The composition of the concrete in the bioshields at commercial NPPs followed the appropriate recommendations at the time of their construction. Hardened cement paste, fine aggregate, coarse aggregate, and water are the primary constituents of concrete for both nuclear and non-nuclear structures. Concrete strength is affected by many factors, such as quality of raw materials, w/c, coarse/fine aggregate ratio, aggregate/cement ratio, compaction of concrete, temperature, RH, and curing of concrete. Reducing the w/c increases the concrete strength but reduces the concrete workability. Aggregate quality, size, shape, texture, and strength are additional factors that determine the strength of concrete. The presence of salts (chlorides and sulphates), silt, and clay also reduces the strength of concrete. Section 2.3.1 provides an overview of the concrete guidelines and specifications used for the construction of NPPs in the United States. A review of available information on the composition of concrete at existing NPPs is provided in Section 2.3.2.

2.3.1 Codes, Standards, and Guidelines

The codes of the American Concrete Institute (ACI) 318 series, ACI 349 series, and the American Society of Mechanical Engineers (ASME) Code Section III, Division 2 (Code for Concrete Containments) are the three main design codes used in the design and construction of U.S. nuclear concrete structures. The designs of older plants were mainly based on ACI 318 (Building Code Requirement for Reinforced Concrete) such as ACI 318-63 and ACI 318-71, the versions published in 1963 and 1971, respectively.

Applicable codes, standards, and guidance documents are listed in the NPP design documents, and a summary may be found in respective updated safety analysis reports. The applicable code should be considered when evaluating the effects of radiation-related degradation.

Appendix A lists some of the industry specifications for concrete, cement, aggregates, and water related to concrete structures at NPPs.

2.3.2 Bioshield Concrete Composition

There is only limited information from a few NPPs on the actual composition of the concrete they used. In most cases, the materials used were what was locally available [53]. The available information for some existing and past NPPs is summarized in Table 2-2. Some information can also be extracted from the design specifications. Table 2-3 provides the design specifications for a sample of NPPs, as provided in their Final Safety Analysis Reports.

At present, the focus is on determining the predominant nature of the aggregate used in bioshield construction for the reactors considered to be susceptible to concrete degradation associated with irradiation. The primary concern is the higher propensity of damage to siliceous aggregates, with more covalent type bonding, from neutron irradiation as compared to more calcareous aggregates, with more ionic type bonding. The cement used for most plants conforms to ASTM C150, Type II (Type II Portland cement), as shown in Tables 2-2 and 2-3.

Table 2-2 Concrete Aggregate and Cement Types for Some U.S. NPPs

Reactor	Aggregate Type	Cement	Location	Ref.
Bellefonte[a]	Calcareous		Hollywood, AL	[53]
Columbia	Siliceous		Richland, WA	[53]
Enrico Fermi 2	Calcareous		Monroe, MI	[53]
Hartsville[b]	Calcareous		Hartsville, TN	[53]
Humbolt Bay[c]	Siliceous		Eureka, CA	[53]
Oconee	Calcareous (Gaffney marble)	ASTM C 150, Type II	Seneca, SC	[54]
Palo Verde	Siliceous	ASTM C 150-74, Type II	Wintersburg, AZ	[53]
Pathfinder[d]	Siliceous		Sioux Falls, SD	[53]
Rancho Seco[d]	Siliceous		Herald, CA	[53]
Susquehanna	Calcareous		Salem Township, Luzerne County, PA	[53]
Turkey Point	Calcareous; Maule Pennsuco limestone (Miami Oolite) aggregate	ASTM C-150-64 Florida Type II cement	Homestead, FL	[53], [55]
Waterford	Siliceous		Killona, LA	[53]
Wolf Creek	Calcareous, limestone		Burlington, KS	[53]

[a] Not yet licensed.

[b] Cancelled, never completed.

[c] Shut down.

[d] Shut down/decommissioned.

Table 2-3 Concrete Design Specifications for Selected U.S. NPPs[a]

Reactor	Concrete	Aggregate	Cement	Water	Air	Fly Ash
Beaver Valley 2 **[56]**	ACI – 211.1-70, 214-65, 301-72, 304-73, 305-77, 306-72, 309-72, 318-71, 347-68 ASTM – C31, C39	ASTM C33	ASTM C150, Type II	ASTM C109-73, C151-74, C191-71, D512-67	ACI – 301 ASTM C233-73 & C260-73	ASTM C311 & C618
North Anna **[57]**	ACI – 301-66, 306-66, 318-63, 347-63, 605-59, 614-59	ASTM C33	ASTM C 150, Type II	ASTM D512, D1888		
Oconee **[54]**	ACI – 301, 315, 318-63, 347, 605, 613, 614	ASTM – C33 & C40, C87, C88, C117, C127, C128, C131, C136, C142, C227, C289	ASTM C150 & C114			
Palo Verde **[58]**	ACI – 318-71	ASTM C33 & C40-73, C88-73, C117-69, C123-69, C131-69, C136-71, C142-71, C235-68, C289-71, C295-65, D75-71	ASTM C150-74, Type II	ASTM C109-73, C151, C191-74		
Seabrook **[59]**	ACI – 224R, 301, 304, 306, 318-71, 349.1R-07	ASTM C33	ASTM C 150, Type II			

[a] Specification titles are provided in Appendix A.

With the exception of some early experimental reactors, as noted in Evans et al. [53] and later by Esselman and Bruck [12], the aggregates used in NPP construction are most likely obtained locally to minimize transportation costs. Therefore, where documentation is not available, a good indication of what types of aggregates (primarily siliceous vs calcareous) may have been used in a NPP's construction is the type of aggregate present in the local area. Although the specific quarries used during NPP construction may not still be operating (decades later), similar operations in the same types of rock formations are expected to be present in support of local present-day construction. For example, a search for aggregate quarries in the Palo Verde and Wolf Creek areas found that siliceous aggregates are currently produced in the Palo Verde area and calcareous aggregates are currently produced in the Wolf Creek area. These findings agree with the types of aggregate identified for these NPPs in Table 2-2. Thus, for those commercial reactors identified as potentially having greater concrete radiation damage, the type of aggregate used (calcareous versus siliceous) can be determined by analyzing samples obtained from an unirradiated portion of the bioshield or relevant support structure, if documented concrete compositions are not available. If it is not feasible to obtain such samples, a first-order approximation would be to generate an estimate based on past or present-day quarry activities in the local area.

Siliceous aggregate properties could also be used, if a bounding analysis would be appropriate. However, minerals in the natural world are not pure compounds. A calcareous mineral deposit could have a predominant percentage range of calcium/magnesium compounds with inclusions of silicates and other compounds. For example, the calcareous aggregate used at Turkey Point (see Table 2-2) was found to have a calcium content of 29.4% and a silicon content of 8.5% [53]. Similarly, a siliceous mineral deposit could have a predominant percentage of silicate compounds with lesser amounts of other compounds, including those with calcium or magnesium. For example, the siliceous aggregate used at Waterford (see Table 2-2) was found to have a silicon content of 32.4% and a calcium content of 12.0% [53]. Thus, a rigorous assessment of irradiation impacts on aggregates in concrete requires knowledge of the actual mineral composition of the aggregate—which is unknown in most cases. However, as mentioned above, it may be possible to perform a detailed examination of a concrete sample from an unirradiated portion of the bioshield. Section 3.1.3.1 covers some information on the effects of the relative amounts of quartz in aggregate.

3 INTERACTION OF RADIATION WITH CONCRETE

Nuclear reactors emit various types of radiation. Concrete in the vicinity of the RPV is mainly affected by two of them, namely neutron and gamma-ray radiation. These two types of radiation interact differently with matter. This chapter discusses the fundamental mechanisms through which each type of radiation interacts with concrete and its components. Potential alteration of the physical structure and chemical makeup of concrete and its components is covered.

3.1 Neutron Radiation

Neutrons are a product of, and necessary contributor to, the nuclear fission reaction employed in commercial nuclear power reactors. Most neutrons begin as *fast* neutrons (E > 0.1 MeV), as shown in Figure 3-1. This distribution is modified as neutrons pass through internal reactor components, out through the RPV wall, and into the reactor cavity. A summary of the fundamental mechanisms through which neutrons interact with matter is given in Section 3.1.1. Sections 3.1.2, 3.1.3, and 3.1.4 discuss our understanding of how neutron radiation affects cement paste, aggregates, and concrete, respectively, found in the reactor cavity. Estimated neutron radiation levels in the reactor cavities of commercial boiling-water reactors (BWRs) and pressurized-water reactors (PWRs) are discussed in Section 5.2.1.

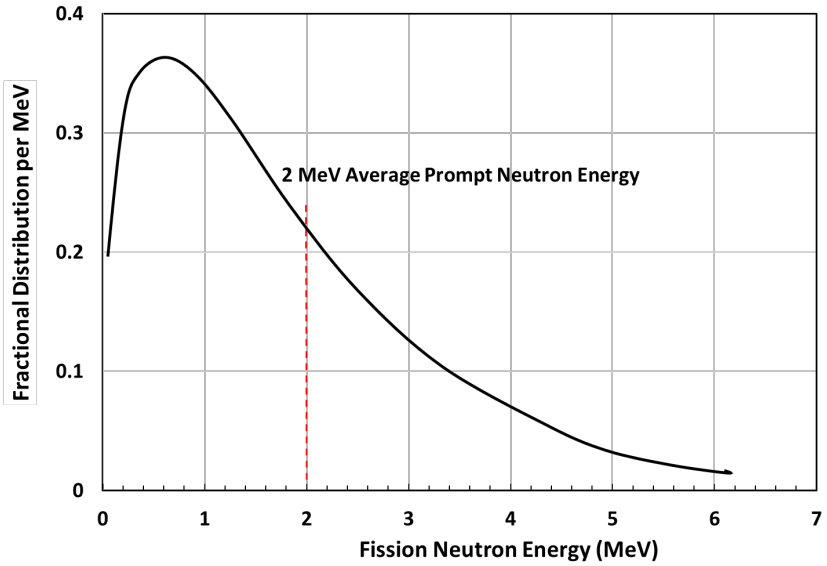

Figure 3-1 Neutron Energy Distribution Associated with Uranium Fission (data from NRC [60])

3.1.1 Interaction with Matter

Neutrons are subatomic particles, and in combination with protons, they constitute the nuclei of atoms. The nucleus of an atom consists of Z protons, where Z is referred to as the atomic number, and N neutrons, where N is referred to as the neutron number. A neutron has essentially the same size and mass as a proton and is a neutral particle (it has no electrical charge).

Neutron interactions with matter can be classified in two general categories: absorption and scattering. In absorption, the incident neutron is absorbed into the target nucleus to form what is commonly considered to be a compound nucleus in an excited state. This excited state relaxes through (1) the emission of a particle (i.e., a neutron, proton, or alpha particle), (2) the emission of a gamma-ray photon (known as gamma-ray capture), or (3) the breakup into two somewhat equivalent parts (i.e., fission) [61].

Two types of scattering are possible—elastic and inelastic—as depicted in Figure 3-2. Elastic scattering can also be broken down into two types. Potential elastic scattering is analogous to the collision of two billiard balls, where some of the kinetic energy of the incident neutron is transferred to the target nuclei and the overall energy is conserved [62]. In this case, the neutron and target nucleus do not touch; instead, they interact through short-range nuclear force without any electrostatic (Coulomb) influences because the neutron does not carry an electric charge. However, a neutron does have a magnetic moment that can give rise to scattering associated with magnetic materials [63]. This interaction of the neutron is with the electronic moment—the unpaired spins among the outer electronic cloud—of a nucleus. Such interactions are minimal in a material such as concrete.

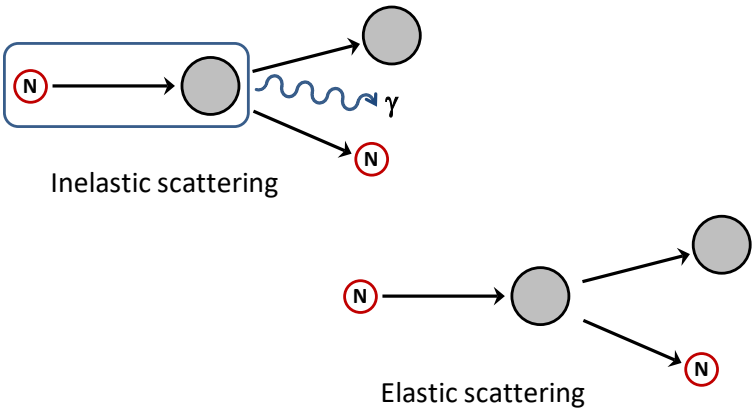

Figure 3-2 Neutron Interactions with Matter

Resonance (or compound) elastic scattering involves the absorption of the incident neutron by the target nucleus to form a compound nucleus, followed by the emission of a neutron. This second type of elastic scattering is much less common than potential elastic scattering because it is highly dependent on resonances with the energy levels of the target nucleus, which will vary with *Z* and *N*.

Inelastic scattering is similar to absorption and resonance elastic scattering in that the incident neutron interacts with the target nucleus to form an intermediate compound nucleus. The compound nucleus then emits a neutron with lower kinetic energy than the incident neutron. The compound nucleus is then in a lower excited state and finally emits gamma-ray(s) to reach a stable (ground) state.

Neutron radiation is attenuated through collisions with atomic nuclei as the neutrons pass through matter and are relatively immune to local charging effects. The result of a collision between a neutron and a nucleus is dependent, in part, on the kinetic energy of the neutron. Neutron energies have been characterized into a number of different categories and/or energy ranges dependent on the application. There is no one standard definition. Some of the more common terms are listed in Table 3-1. Other classification schemes used have fewer energy ranges. One example is that from Hilsdorf et al. [4] where:

- Thermal neutrons Energy < 1eV
- Epithermal neutrons 1 eV < Energy < 0.1 MeV
- Fast neutrons Energy > 0.1 MeV

The current work follows the example of Hilsdorf et al. [4], who collapsed their three energy ranges to two; neutrons with energies up to 0.1 MeV are characterized as thermal neutrons, and neutrons with energies greater than 0.1 MeV are characterized as fast neutrons. SLR guidance also uses 0.1 MeV as the lower-end cutoff energy for damaging neutron flux [3]. However, the works cited in this report do not always base their definitions of fast versus thermal neutrons on the same cutoff energy level (0.1 MeV). For example, some studies consider fast neutrons to have E > 1.0 MeV.

The attenuation of a neutron beam through collisions in a material such as concrete results in a loss of kinetic energy that either directly or indirectly translates into vibrational/thermal energy (heat generation). The amount of heat generation depends on the relative overall energy levels of the initial and final products associated with a given collision mechanism.

3.1.2 Cement Paste

The general overall structure of cement paste is an amorphous matrix with small crystallite inclusions, as discussed in Section 2.1. Within this matrix, water molecules are chemically bound, found in capillaries, or found between the C-S-H layers. The amorphous nature of the cement paste and its water content are the principal features of cement paste that are responsible for its end state after interacting with neutron radiation.

Table 3-1 Classification of Neutrons

Type	Energy	Comments
Thermal	~0.025 eV	Neutrons that are in thermal equilibrium with their surroundings. The Maxwell-Boltzmann equation is used to describe such a distribution. At room temperature, energies are approximately 0.025 eV.
Epithermal	0.025–0.4 eV	Generally the transition region between thermal and slow neutrons with energies up to approximately 1 eV.
Cadmium	0.4–0.6 eV	Neutrons that are strongly absorbed by cadmium, <0.6 eV.
Epicadmium	0.6–1 eV	Neutrons which are not strongly absorbed by cadmium, >0.6 eV.
Slow	1–10 eV	Neutrons of energy slightly greater than thermal, <1–10 eV (sometimes up to 1 keV).
Resonance	10–300 eV	Usually refers to neutrons that are strongly captured in the resonance of U-238 and of a few commonly used detectors (indium, gold, etc.).
Intermediate	300 eV–1 MeV	Neutrons that are between slow and fast.
Fast	1–20 MeV	Generally neutrons with energies in the range of about 0.1 to 10–20 MeV. This energy range dominates the energy spectrum produced by fission sources such as nuclear reactors.
Relativistic	>20 MeV	Generated by cosmic rays in the atmosphere.

Sources: [62, 64]

3.1.2.1 Dimension Change

Neutron bombardment can alter the position of individual target nuclei in the cement paste, but that interaction does not change the original amorphous nature of the cement paste. However, neutron irradiation may lead to water loss due to (1) a high hydrogen cross-section (likelihood of interaction between an incident neutron and a target nucleus), (2) potential small temperature increases due to neutron attenuation, and (3) radiolysis due to secondary gamma-ray formation. Thus, the overall impact is expected to be one of dimensional shrinkage, as shown in Figure 3-3. Note that the experiments by Dubrovskii et al. [65], which included gamma irradiation along with the neutron irradiation, demonstrated that the primary cause of the shrinkage was the exposure temperature, not the radiation exposure. In more recent experiments, Maruyama et al. [66] confirmed some shrinkage of cement paste due to irradiation, although low levels of gamma radiation were also present during the experiments.

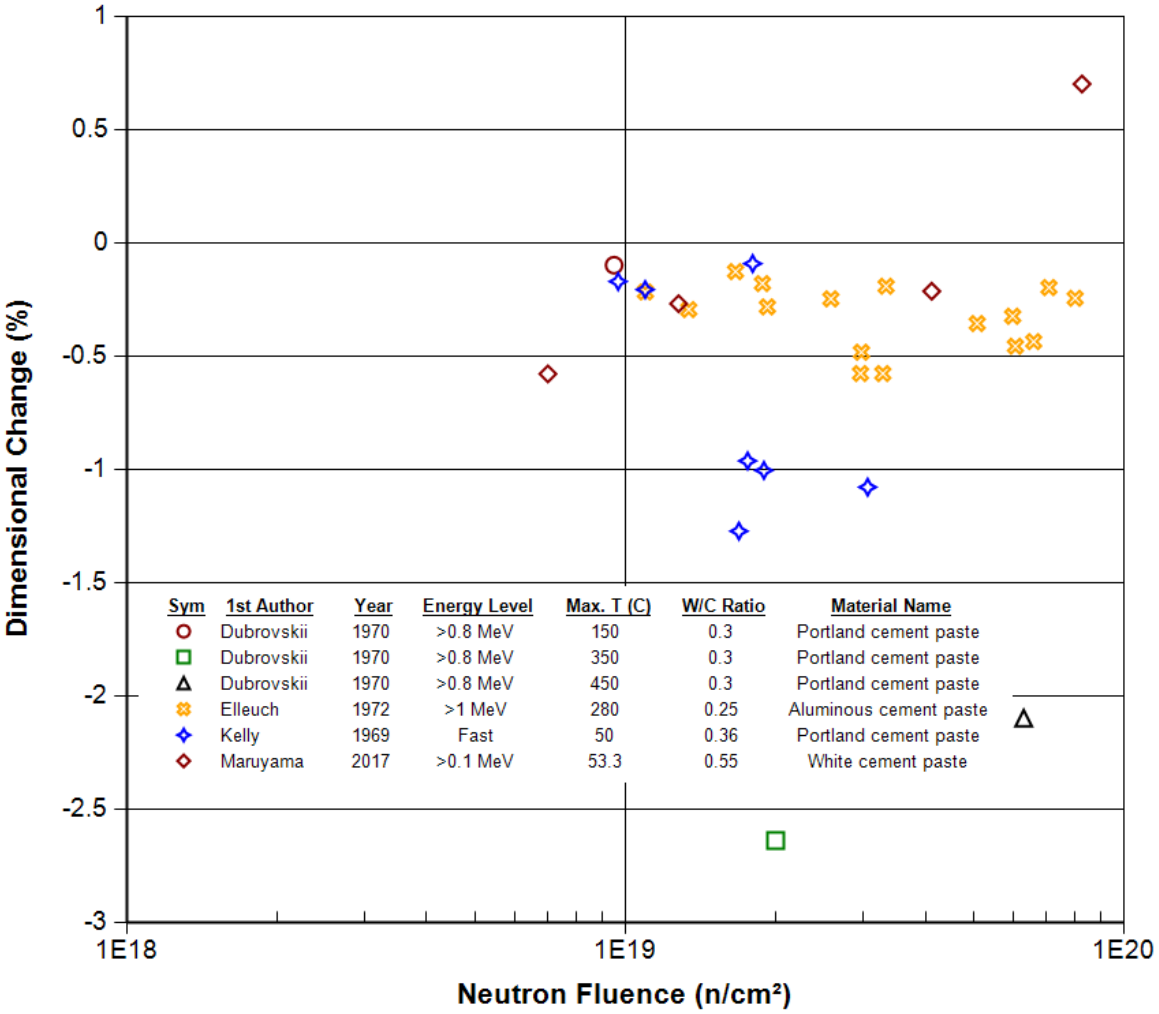

Figure 3-3 Dimensional Change of Cement Paste Induced by Neutron Irradiation

3.1.2.2 Weight Loss

Figure 3-4 shows the weight loss due to irradiation for cement paste. The weight loss for hardened cement paste was about 10% or less. There is no clear trend for the effect of neutron radiation on weight loss of hardened cement paste. The sample weight losses observed by Alexander [67] were all within the range experienced by temperature control samples. Kelly et al. [68] noted that the weight losses in their experiments may have been due to a drying effect caused by the helium carrier gas used to collect any gases given off during neutron irradiation. Two samples in Maruyama et al.'s experiments [66] (included in Figure 3-4) actually experienced weight gain during irradiation that was attributed to condensation or flooding occurring within the sample capsules. Weight loss is mainly due to dehydration of the cement paste, which also leads to shrinkage, as discussed in the previous section.

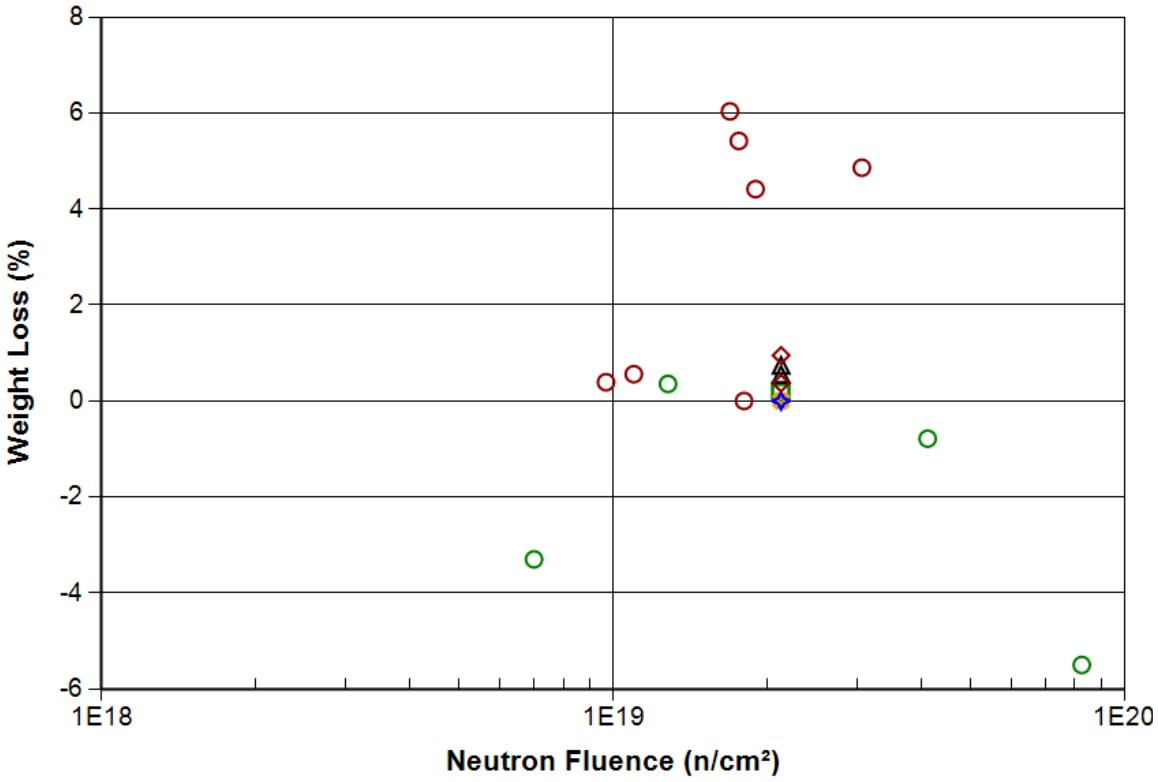

Sym	1st Author	Year	Energy Level	Max. T (C)	W/C Ratio	Material Name
○	Kelly	1969	Fast	50	0.36	Portland cement paste
□	Alexander	1963	Thermal	100	N/A	Portland cement paste
△	Alexander	1963	Thermal	100	N/A	High-alumina cement paste
⊠	Alexander	1963	Thermal	100	N/A	Low-heat-slag cement paste
◇	Alexander	1963	Thermal	100	N/A	Supersulphate cement
◇	Alexander	1963	Thermal	100	N/A	Pulverised fuel ash paste
○	Maruyama	2017	>0.1 MeV	53.3	0.55	White cement paste

Figure 3-4 Weight Loss of Cement Paste Induced by Neutron Irradiation (see text for discussion on sample data from Maruyama et al. [66])

3.1.3 Aggregates

3.1.3.1 Dimension Change

Dimensional changes in siliceous aggregates are much more pronounced than in calcareous aggregates caused by fast neutrons because of their primarily covalent bond nature as opposed to the ionic bonding which is prevalent in calcareous aggregates (e.g., calcite [$CaCO_3$]) [69]. Neutron irradiation studies on quartz (a predominant form of crystalline SiO_2), the primary constituent in many siliceous aggregates, show significant expansion of samples that are subjected to fast neutron fluence in excess of 1×10^{19} n/cm^2 [70-72], as shown in Figure 3-5. The dimensional change of unirradiated quartz is also temperature dependent [72]. It manifests in the shift in dimensional change with neutron fluence as a function of temperature in Figure 3-5. Wittels [71] also showed that dimensional changes in quartz is structure dependent, because a more compact crystalline form of silica, the rare mineral coesite, was observed to be stable after being subjected to neutron fluence levels that completely disorder quartz.

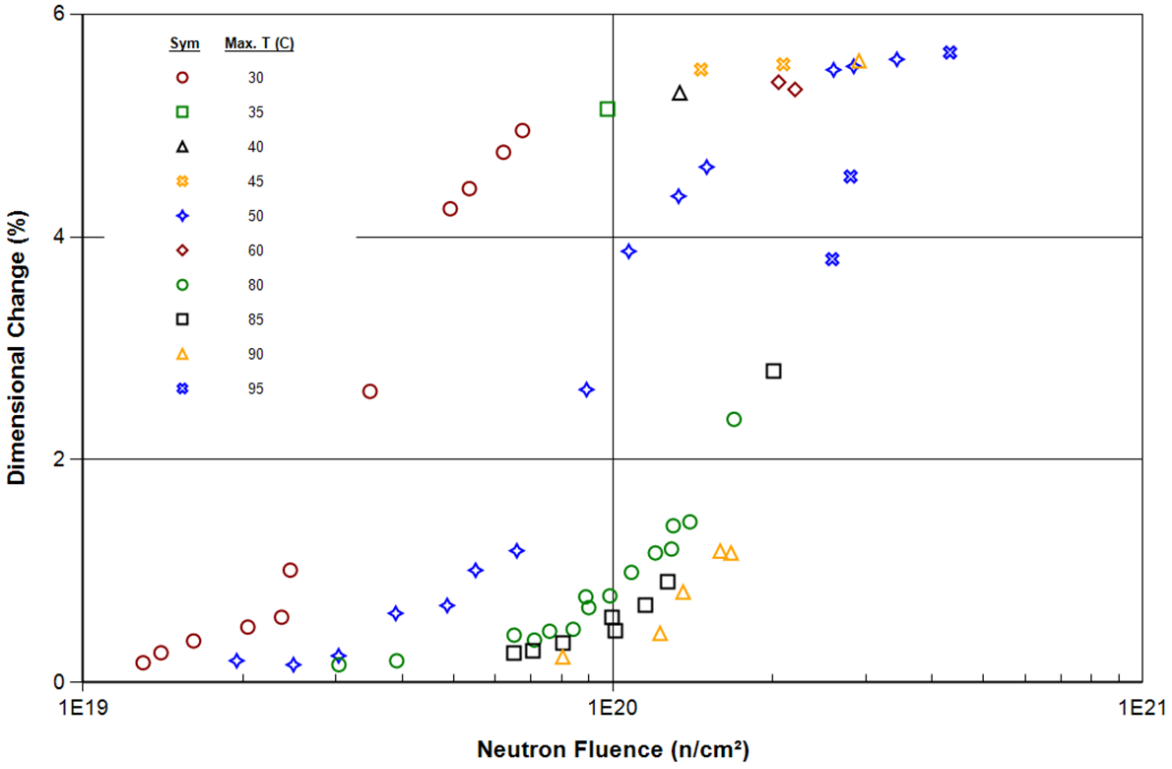

Figure 3-5 Dimensional Change of Quartz with Fast Neutron Irradiation ($E > 0.01$ MeV) (Source: [72])

Figure 3-6 shows the dimensional changes of other aggregates. Aggregates such as the thermally altered tuff and felsic sandstone investigated by Maruyama et al. [66] show the largest changes. These aggregates have large quartz contents: approximately 92% for the thermally altered tuff and on the order of 40% for the felsic sandstone, which also contained other silicate materials. Maruyama et al.'s work also drew a correlation between the degree of expansion and the quartz content of the aggregate for a given neutron exposure.

Figure 3-7 shows an expanded view of dimensional changes in aggregates that omits the data from Maruyama et al. Silicate aggregates such as flint (a cryptocrystalline[1] form of quartz) and the dolerites displayed an increase in dimension with neutron fluence to a lesser degree [68]. Serpentine, a mineral that contains a number of related silicates, expanded somewhat with neutron fluence [73] at temperatures above 200°C, whereas temperature-control samples showed no change. Dubrovskii et al. [65] investigated the dimensional change of hematite ore at different temperatures and observed some increase in size after neutron irradiation. Hematite has more of an ionic structure, but the ore in question had a silica content of about 7% [65].

Kelly et al. [68] observed some expansion for calcareous aggregates such as limestone. However, Maruyama et al. [66] did not observe any expansion of limestone samples when irradiated with neutrons, as shown in Figure 3-6.

1 Cryptocrystalline refers to a form composed of microscopic crystals. Such a configuration would not have exactly the same properties as a macroscopic crystal. In this case, expansion under neutron irradiation would not be expected to be as significant as it is for larger crystals.

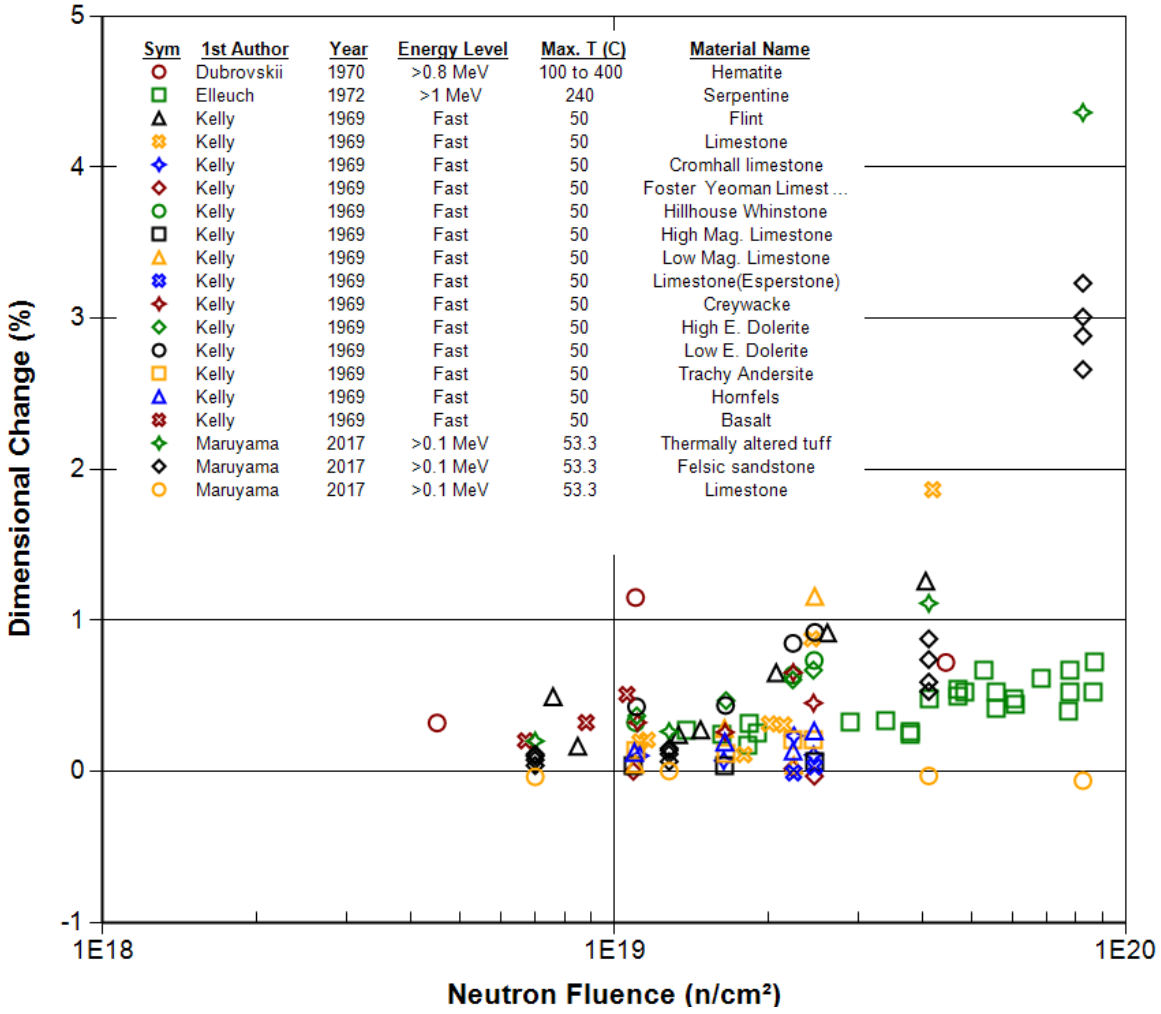

Figure 3-6 Dimensional Change of Aggregates with Fast Neutron Irradiation

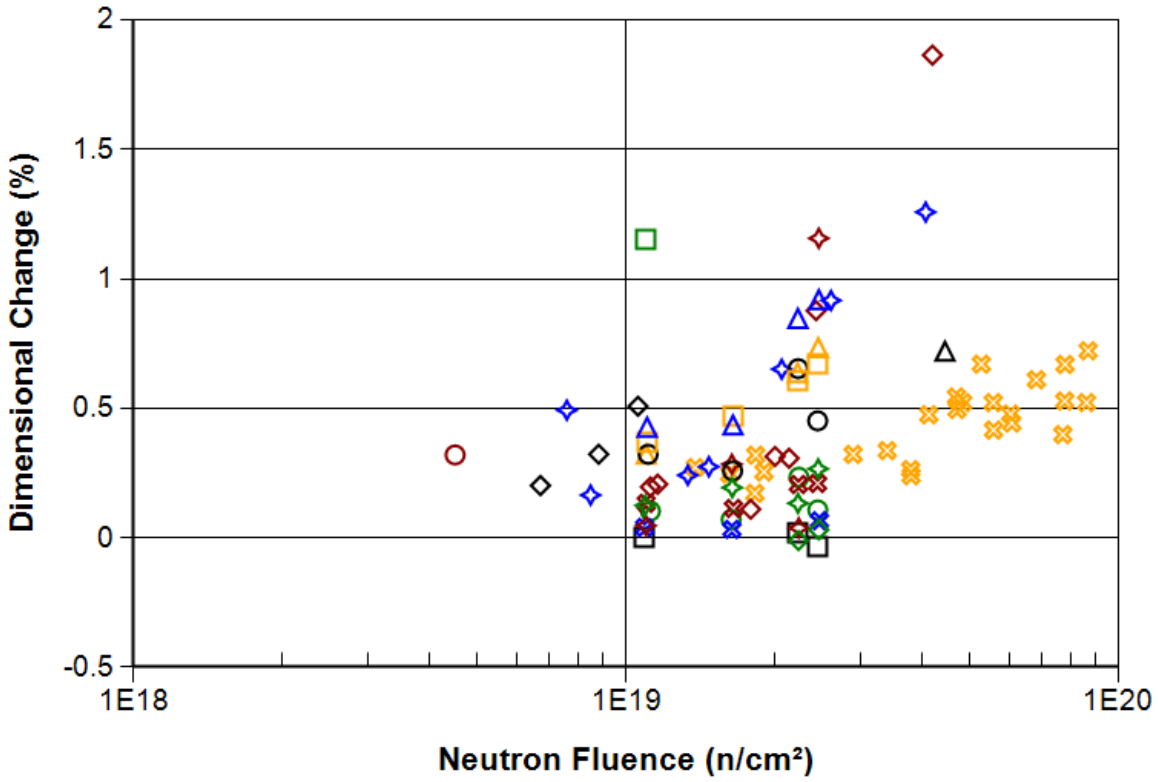

Sym	1st Author	Year	Energy Level	Max. T (C)	Material Name
○	Dubrovskii	1970	>0.8 MeV	100	Hematite
□	Dubrovskii	1970	>0.8 MeV	150	Hematite
△	Dubrovskii	1970	>0.8 MeV	400	Hematite
✕	Elleuch	1972	>1 MeV	240	Serpentine
✦	Kelly	1969	Fast	50	Flint
◇	Kelly	1969	Fast	50	Limestone
○	Kelly	1969	Fast	50	Cromhall limestone
□	Kelly	1969	Fast	50	Foster Yeoman Limestone
△	Kelly	1969	Fast	50	Hillhouse Whinstone
✕	Kelly	1969	Fast	50	High Mag. Limestone
✦	Kelly	1969	Fast	50	Low Mag. Limestone
◇	Kelly	1969	Fast	50	Limestone(Esperstone)
○	Kelly	1969	Fast	50	Creywacke
□	Kelly	1969	Fast	50	High E. Dolerite
△	Kelly	1969	Fast	50	Low E. Dolerite
✕	Kelly	1969	Fast	50	Trachy Andersite
✦	Kelly	1969	Fast	50	Hornfels
◇	Kelly	1969	Fast	50	Basalt

Figure 3-7 Dimensional Change of Aggregates Less Influenced by Neutron Irradiation

3.1.3.2 Weight Loss

No significant weight loss was observed for aggregates. No change in weight was observed for serpentine (Elleuch et al. [73]). Felsic sandstone showed changes within ±0.2% up to a fast neutron fluence of 8.25×10^{19} n/cm^2 (Maruyama et al.[66]).

3.1.4 Concrete

Concrete is an admixture of cement, fine and coarse aggregate, and water, as described in Section 2.3. However, in testing irradiated concrete specimens, mortar—which is made of cement, fine aggregate, and water (no coarse aggregate)—was often used because of sample size limitations. This substitution introduces uncertainty into the evaluation of such results, as discussed in Section 1.4.1.

3.1.4.1 Dimension Change

On average, concrete exhibits an overall increase in volume when irradiated by fast neutrons, as shown in Figures 3-8 ($T < 100°C$) and 3-9 ($T \geq 100°C$). Whereas the cement paste in concrete decreases slightly in volume, the increase in volume for concrete is driven by aggregate expansion, which in turn disrupts the aggregate–cement bonding. As was the case for aggregate expansion, the extent of concrete expansion appears to be correlated with the silicate content of the aggregate [66]. We expect that the silicate content in these aggregates is in crystalline quartz form, because vitreous (amorphous) silica is relatively unaffected by neutron bombardment at 25°C and is subject to slight compaction [70].

For those high-temperature samples (up to approximately 350°C) with an observed dimensional change of about 6% or higher (Dubrovskii et al. [74]), as seen in Figure 3-9, the change was attributed solely to the neutron irradiation because the high-temperature control samples showed no change in dimension. For the samples with sandstone aggregates, the data from Dubrovskii et al. [74] show a clear trend of expansion with increasing neutron fluence ($E > 0.8$ MeV) in Figure 3-9. Based on the reported neutron energy distribution in Dubrovskii et al. [74], this trend could be shifted by a factor of about 3.4 higher, if converted to neutron fluences where $E > 0.1$ MeV. This is just one example where there could be significant uncertainties when comparing studies where the neutron fluence energies are not the same and/or are not well characterized.

3.1.4.2 Weight Loss

Figure 3-10 shows the weight loss due to irradiation for concrete and mortar. The weight loss for concrete and mortar is generally less than 5%. As with the hardened cement paste, the effect of neutron radiation on weight loss of concrete exhibits no clear trend. Temperature control samples (not shown in the graph) exhibit the same variation in weight loss as irradiated samples. There are no obvious differences between the temperature control groups and the irradiated groups. Any weight loss is mainly due to dehydration of the cement paste (type identified in Figure 3-10 for each dataset) in concrete under high temperatures.

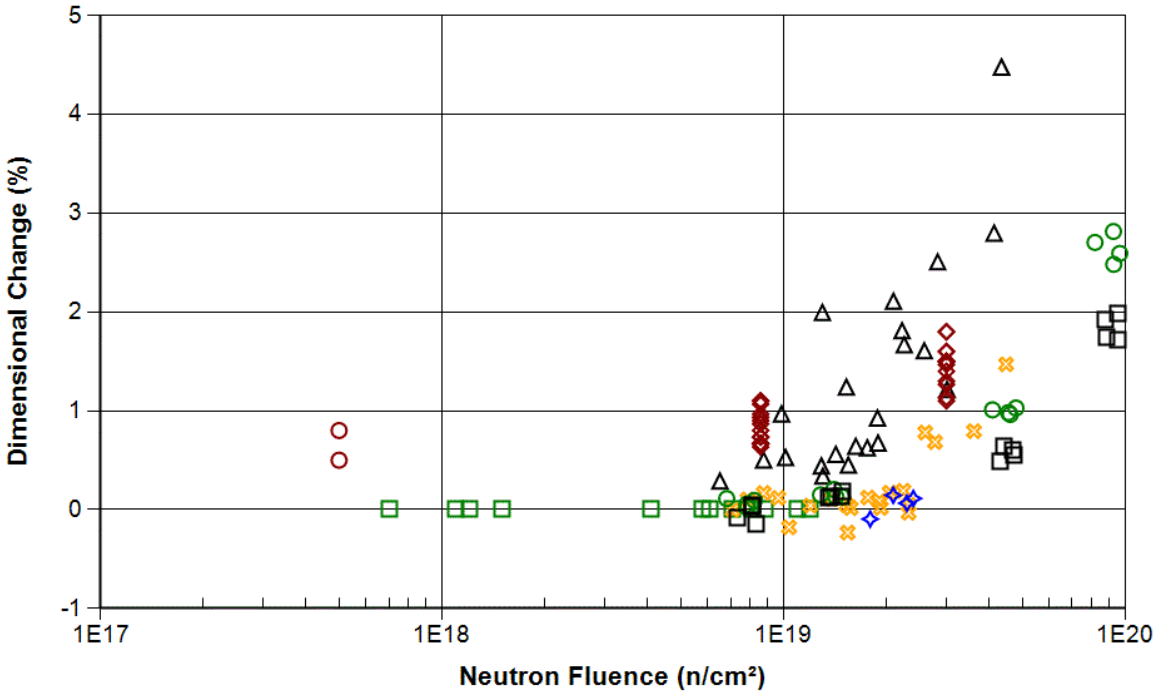

Sym	1st Author	Year	Energy Level	Max. T (C)	Ag. Frac.	W/C Ratio	Aggregate	Cement Type
○	Dubrovskii	1967	>0.8 MeV	50	0.76	0.5	Sandstone, Riversand(quartz)	Portland cement
□	Fujiwara	2009	>0.1 MeV	50 to 56	0.79	0.55	Gravel, Sand	Cement
△	Kelly	1969	Fast	50	0.67	0.36	Flint	Portland cement
✕	Kelly	1969	Fast	50	0.67	0.36	Limestone	Portland cement
✦	Kelly	1969	Fast	50	N/A	N/A	Light weight rock, Sand	Portland cement
◇	Pedersen	1971	Fast	80	0.68	0.4	Quartz	Portland cement
○	Maruyama	2017	>0.1 MeV	66 to 73	0.77	0.5	Thermally altered tuff, Sandstone	high early-strength ordinary Portland cement
□	Maruyama	2017	>0.1 MeV	66 to 73	0.77	0.5	Felsic sandstone, Sandstone	high early-strength ordinary Portland cement

Figure 3-8 Dimensional Change of Concrete and Mortar Induced by Neutron Irradiation (T < 100°C)

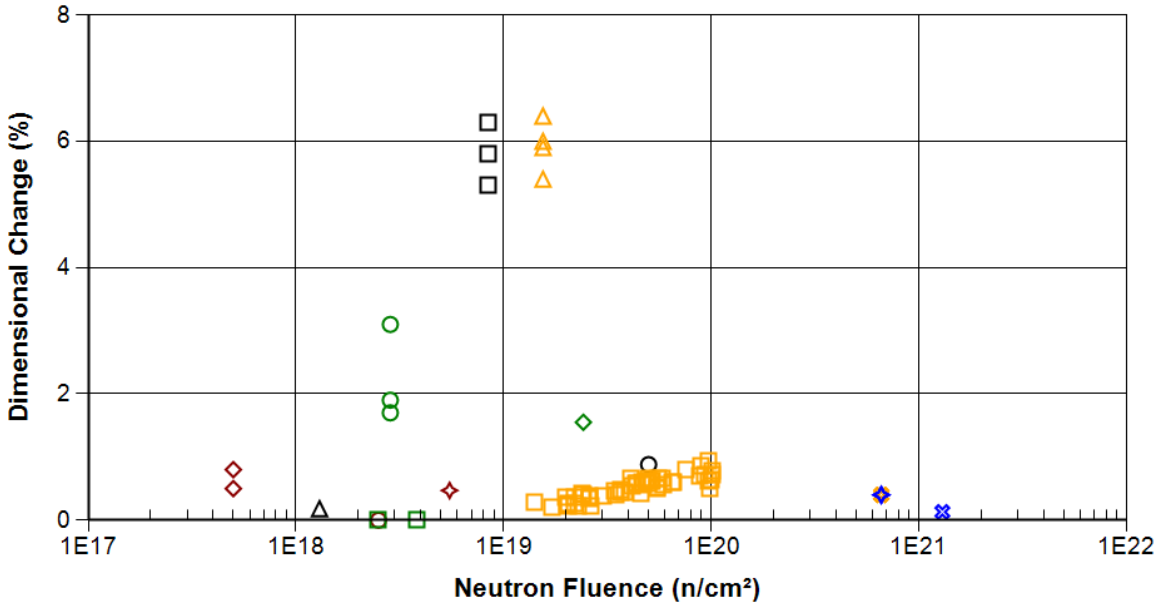

Sym	1st Author	Year	Energy Level	Max. T (C)	Ag. Frac.	W/C Ratio	Aggregate	Cement Type
○	Cristiani	1971	Fast	100	0.67	0.5	Limestone	Portland cement
□	Cristiani	1971	Fast	125	0.67	0.5	Limestone	Portland cement
△	Dickeman	1951	Thermal	120	N/A	N/A		
⊠	Dubrovskii	1966	>0.7 MeV	550	N/A	N/A	Chromite	Portland cement
✦	Dubrovskii	1966	>0.7 MeV	550	N/A	N/A	Chromite	Liquid glass
◇	Dubrovskii	1967	>0.8 MeV	50	0.76	0.5	Sandstone, Riversand(quartz)	Portland cement
○	Dubrovskii	1967	>0.8 MeV	150	0.76	0.5	Sandstone, Riversand(quartz)	Portland cement
□	Dubrovskii	1967	>0.8 MeV	275	0.76	0.5	Sandstone, Riversand(quartz)	Portland cement
△	Dubrovskii	1967	>0.8 MeV	350	0.76	0.5	Sandstone, Riversand(quartz)	Portland cement
⊠	Dubrovskii	1968	>0.01 MeV	350	N/A	N/A	Serpentine	Portland cement
✦	Dubrovskii	1970	>0.8 MeV	100	0.8	1.01	Hematite	Portland cement
◇	Dubrovskii	1970	>0.8 MeV	200	0.8	1.01	Hematite	Portland cement
○	Dubrovskii	1970	>0.8 MeV	400	0.8	1.01	Hematite	Portland cement
□	Elleuch	1972	>1 MeV	240	0.74	0.38	Serpentine	Aluminous cement

Figure 3-9 Dimensional Change of Concrete and Mortar Induced by Neutron Irradiation ($T \geq 100°C$)

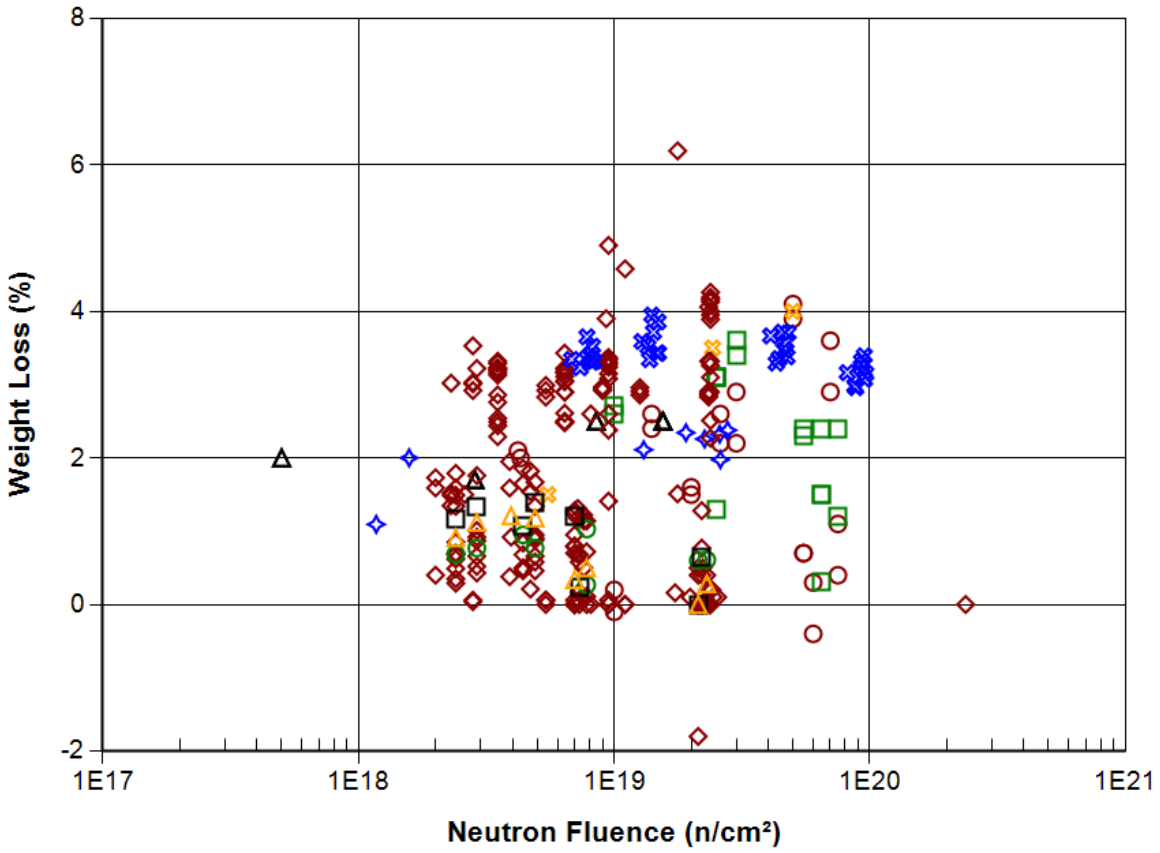

Sym	1st Author	Year	Energy Level	Max. T (C)	Ag. Frac.	W/C Ratio	Cement Component
○	Batten	1960	Thermal	50	0.67 to 0.84	0.45 to 0.5	Portland cement
□	Batten	1960	Thermal	50	0.84	0.5	Aluminous cement
△	Dubrovskii	1967	>0.8 MeV	50 to 350	0.76	0.5	Portland cement
✕	Dubrovskii	1970	>0.8 MeV	100 to 400	0.8	1.01	Portland cement
✦	Kelly	1969	Fast	50	0.67	0.36	Portland cement
◇	Alexander	1963	Thermal, Fast	20 to 100	N/A	N/A	Portland cement
○	Alexander	1963	Thermal	100	N/A	N/A	High-alumina cement
□	Alexander	1963	Thermal	100	N/A	N/A	Low-heat-slag cement
△	Alexander	1963	Thermal	100	N/A	N/A	Supersulphate cement
✕	Maruyama	2017	>0.1 MeV	66 to 73	0.77	0.5	high early-strength ordinary Portland cement

Figure 3-10 Weight Loss of Concrete and Mortar Induced by Neutron Irradiation

3.2 Gamma Radiation

By definition, gamma-rays are photons that originate from nuclear transitions. Thus, gamma radiation is high-energy electromagnetic radiation with photon energies typically above 100 keV. At these energies, their wavelengths are less than 10 picometers, which is on the atomic scale, resulting in strong interactions with matter. These energies are also well above the ionization threshold of inner-shell electrons. Section 3.2.1 provides a summary of the fundamental mechanisms through which gamma-rays interact with matter. Sections 3.2.2, 3.2.3, and 3.2.4 describe our understanding of how gamma radiation impacts cement paste, aggregates, and concrete, respectively, in the reactor cavity.

3.2.1 Interaction with Matter

As shown in Figure 3-11, gamma radiation interacts with matter through three primary mechanisms [75], each involving the ejection of an electron:

- Photoelectric effect—A gamma-ray is absorbed, and an electron is subsequently ejected; the sum of the binding energy of the ejected electron and its subsequent kinetic energy equals the energy of the incoming gamma-ray. In general, the probability of photoelectric absorption decreases with increasing photon energy. Relative to atomic weight, the probability (or cross-section, the probability of interaction) of photoelectric absorption is roughly proportional to Z^n/E_γ^m where Z is the atomic number, E_γ is the energy of the incident gamma-ray, n varies from 4 to 5, and m varies from 3 to 4 [75-77]. This relationship helps to explain the preferred use of higher Z materials (better absorption) such as depleted uranium in gamma shielding applications.

- Compton scattering—A gamma-ray is inelastically scattered (deflected) by interaction with an electron which is ejected. The deflected photon's energy is reduced (i.e., decreased frequency, increased wavelength) by the amount of the original binding energy of and the kinetic energy associated with the ejected electron. Because the cross-section of scattering increases with electron density, the probability for scattering increases linearly with Z.

- Pair production—An incoming photon interacts with the strong electromagnetic field surrounding the nucleus of an atom, undergoes a change of state (creation of matter from energy), and is transformed into a matter–anti-matter pair (electron and positron being the most common manifestation). In this case, the incoming photon energy must be greater than 1.022 MeV, because the rest mass of an electron or positron is equivalent to 0.511 MeV (using $E = mc^2$). The cross-section of pair production increases with energy and is approximately proportional to Z^2 once the 1.022-MeV threshold energy is met [76].

Other interactions of gamma radiation with matter include coherent (Bragg or Rayleigh) scattering, photodisintegration, and nuclear resonance scattering [75, 76]. However, these latter interactions are minor compared to the three primary mechanisms.

Figure 3-12 shows which of the three mechanisms predominates as a function of energy and atomic number. The left line in the figure denotes where the photoelectric cross-section equals that for Compton scattering, and the right line denotes where the Compton scattering cross-section equals that for pair production. As discussed above, the photoelectric effect is more prevalent at lower energies, decreasing with energy; Compton scattering occurs over all energy ranges with higher probability for larger Z values; and pair production becomes significant quickly after the 1.022-MeV threshold is exceeded.

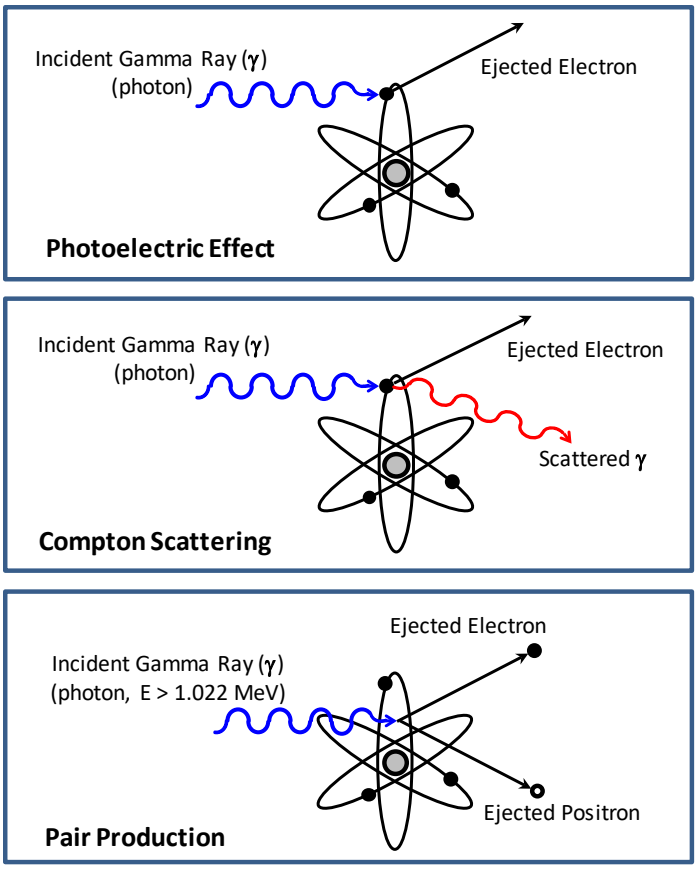

Figure 3-11 Gamma-Ray Interactions with Matter

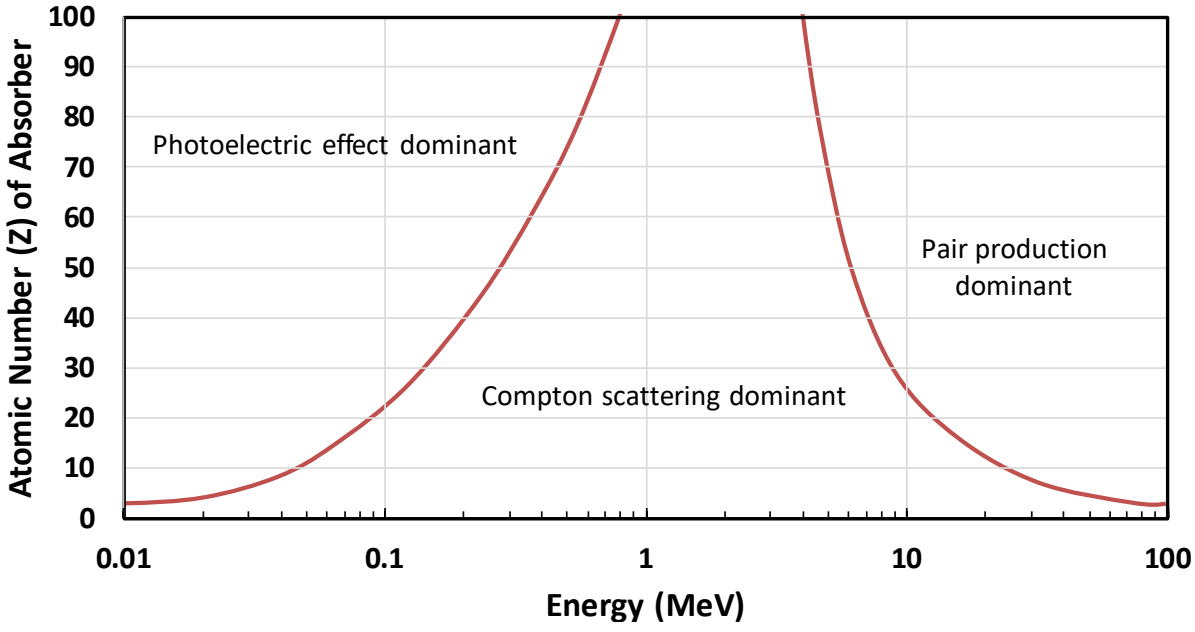

Figure 3-12 Relative Importance of the Three Major Interactions of Gamma Radiation with Matter (adapted from Evans [78])

In all cases, electrons are ejected and their kinetic energy absorbed by the surrounding system. Typically, a K-shell electron is ejected from an atom by an incident gamma-ray [78] through either the photoelectric effect or Compton scattering, leaving the atom in an excited state. Subsequent relaxation of the atom results in the transition of an L-shell electron to fill the K-shell vacancy, which in turn results in the emission of an x-ray photon (x-ray fluorescence) (primarily in heavier elements, >90% for $Z > 60$ and <10% for $Z < 17$) or an Auger electron (primarily in light elements) [78]. An x-ray or Auger electron can go on to eject an electron in a lower-energy shell with similar results. Overall, the initial ejected electron and additional ejected electron due to x-ray fluorescence or as an Auger electron go on to collide with other electrons in the surrounding material which in turn are ejected (secondary electrons). This process continues until the kinetic energies of the secondary electrons are below the ionization energies of the surrounding material. In solids, such as concrete, the majority of the x-rays and ejected and secondary electrons generated due to incident gamma-rays are retained in the material, leading to the generation of heat as the kinetic energies of the electrons dissipate through collisions and subsequent vibrational relaxation of the affected compounds.

For molecular compounds, the ejection of an electron or electrons and subsequent relaxation could lead to dissociation (radiolysis, breakup of a molecular bond) if the energy level of the excited state is greater than the bond energy. Covalent compounds are more likely to be affected than ionic compounds because the ejection of an electron in a shared covalent bond could readily lead to dissociation of the bond, whereas ionic compounds are held together by electrostatic attraction and the ejection of one electron from one of the ions is less likely to affect the overall crystalline lattice.

3.2.2 Cement Paste

The materials in cement paste that are most susceptible to gamma irradiation would be its covalent-bonded components, water and C-S-H. Ionization from gamma-rays can break covalent bonds, through mechanisms such as the radiolysis of water and the potential breaking of bonds within the C-S-H structure. Because the C-S-H layers are responsible for binding the other cement components together, as well as incorporating aggregates to form concrete, an understanding of the C-S-H framework and its dissociation products in a gamma irradiation environment is critical to estimate long-term degradation effects.

3.2.2.1 Radiolysis of Water

One focus pertaining to the gamma irradiation of concrete has been the investigation of the radiolysis of water in the cement paste. For Portland cement samples, Mockel and Koster [79] found that hydrogen generation was roughly linear with gamma dose up to a total dose of 1×10^6 Gy, using dose rates of about 3,000 to 5,000 Gy/h. The samples were sealed under vacuum before irradiation and no generated oxygen was observed. Mockel and Koster also found that the hydrogen yield remained linear with dose with w/c between 0.2 and 0.6, although hydrogen yields were higher for higher w/c, with about a 30% increase between a w/c of 0.2 and one of 0.6. Bar-Nes et al. [80] reported similar findings, with a roughly linear correspondence between hydrogen generation and gamma dose for Portland cement samples irradiated up to 1×10^7 Gy at 1,440 Gy/h. They also observed the formation of micro-cracks attributed to the radiolysis reaction and noted a higher release of hydrogen for a w/c of 0.6 rather than 0.3, but the difference was about a factor of 2 or more. The samples irradiated by Bar-Nes et al. also produced slightly less oxygen than the stoichiometric ratio of 1:2 for oxygen to hydrogen.

Gamma radiolysis work by Bibler and Orebaugh [81] on a mixture of Portland cement and gypsum-perlite plaster showed that the initial rate of hydrogen production was proportional to dose rate, with higher dose rates producing more hydrogen. In addition, the G value (number of molecules produced per 100 eV of energy absorbed) was independent of the dose rate over the range investigated (890 to 2.8×10^5 Gy/h). In these experiments, oxygen in the air in the sealed containers was partially consumed. Similar results were observed for a w/c of 0.29 to 0.77.

More recent work by Kontani et al. [8] also showed that hydrogen generation from Portland cement paste is linear with a gamma dose rate between 1 and 10 kGy/h. Increased hydrogen generation rates are related to increased gamma dose rates and increased w/c. The G value for hydrogen generation remained the same for all dose rates employed, as previously observed [81]. No appreciable differences were observed for tests conducted at different temperatures (20, 40, or 60°C). Test results based on samples dried at a temperature of 120°C versus 40°C indicate that free pore water hydrolyzed while only minor amounts of the chemically bound water in the cement were affected [8].

The tests conducted by Maruyama et al. [66] also showed that the hydrogen generation rate of white cement paste increases with the gamma dose rate ranging from 0.9 to 7.1 kGy/h. The total water production does not appear to change for the same gamma dose when using different dose rates. In all cases, hydrogen generation decreases with time, following the decrease in the cement water content. Higher radiation exposures of Portland cement resulted in the partial disappearance of the original hydrated minerals and the loss of chemically bound water after a dose of 1.3×10^8 Gy [82].

Bar-Nes et al. [80] and Vodák et al. [83] suggest that the formation of micro-cracks in cement paste is associated with the radiolysis of water. Later experiments by Lowinska-Kluge and Piszora [82], used microscopic investigation to show that increased gamma doses result in progressively greater micro-crack formation in Portland cement. Such cracking was evident at gamma doses on the order of 10^8 Gy. The cement samples were irradiated in a chamber maintained at 20°C. Mobasher et al. [84] also observed micro-crack formation in cement samples composed of a mixture of Portland cement and blast furnace slag exposed to a gamma dose of 4.66×10^6 Gy over a period of 256 hr. The cement samples reached a temperature of approximately 50°C due to radiation heating.

As observed, a range of gamma dose rates (up to 2.8×10^5 Gy/h) are used across the studies reviewed in this section. All studies that involved dose rate effects agree that the hydrogen generation rate increases with and is proportional to the gamma dose rate. Maruyama et al.'s work [66] indicates that the gamma dose rate does not seem to affect the amount of evaporable water released from cement paste.

3.2.2.2 Compositional Changes

Evidence of calcite (calcium carbonate, $CaCO_3$) formation at the expense of portlandite ($Ca(OH)_2$) has emerged from experiments involving gamma irradiation (up to a dose of 1.6 MGy) of Portland cement samples [83] as a follow-up to previous work with similar results [9]. These changes were observed at the surface of the samples as well as at the center of the samples. Maruyama et al. [66] observed the formation of three different forms of calcium carbonate (aragonite, calcite, and vaterite) when cement paste was irradiated up to 2×10^8 Gy, also at the expense of portlandite. In other work, it was shown that the degree of calcite formation (carbonation) paralleled the radiolysis of water in the cement paste [80]. The formation of calcite is discussed further in Section 4.3.2.

3.2.3 Aggregates

As discussed in Section 2.2, aggregates are typically classified in one of two categories: (1) siliceous aggregates such as quartzite, gravel, granite, and flint, which are primarily covalently bonded (the Si-O bond); and (2) calcareous aggregates such as limestone, dolomite, and anorthosite, which are primarily ionically bonded (the $Ca\text{-}CO_3$ bond). The Si-O bonds in alpha quartz have been reported to be significantly disrupted at gamma doses $>1 \times 10^{12}$ Gy [85]. On the other hand, ionic bonding is least disrupted by gamma irradiation, and no significant changes in the calcium carbonate structure have yet been reported. A slight dimensional increase was evident in the gamma-ray irradiation test Maruyama et al. [66] performed on aggregates, except limestone, but volume changes were considered by the authors to be "unremarkable."

3.2.4 Concrete

3.2.4.1 Weight Loss

Concrete experiences weight loss when exposed to gamma irradiation due to radiolysis (water loss). Figure 3-13 shows the effect of gamma irradiation on the weight loss of concrete and mortar. Note that the experiments performed by Dubrovskii et al. [65, 74] also involved neutron irradiation. One can see that the weight loss of concrete and mortar starts to increase sharply when the gamma dose is above 10^8 Gy.

3.2.4.2 Dimension Change

The effect of gamma irradiation on the dimensional change of concrete and mortar is shown in Figure 3-14. The dimensional change of concrete and mortar starts to increase sharply when the gamma dose is above 10^8 Gy, which is similar to the trend shown in Figure 3-13 for weight loss. However, this observation was obtained based on the data points collected under both neutron and gamma irradiation. If the specimens are exposed to only gamma irradiation, no dimensional change is observed based on the test data collected so far (the data from Kelly et al. [68]), although those test data are very limited. Note that a decrease in volume due to water loss is partly offset by the formation of micro-cracks and the subsequent bonding mismatch with the aggregate.

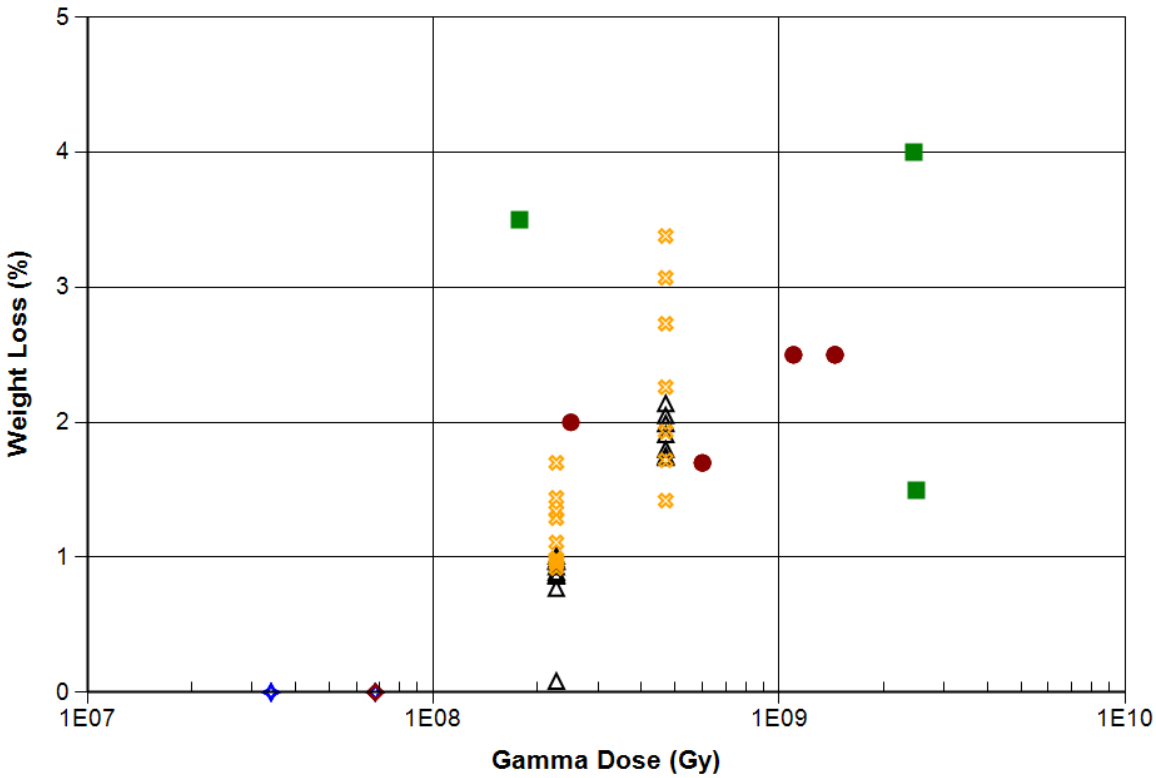

Sym	1st Author	Year	Energy Level	Max. T (C)	Ag. Frac.	W/C Ratio	Aggregate	Cement Type
●	Dubrovskii	1967	>0.8 MeV	50 to 350	0.76	0.5	Sandstone, Riversand(quartz)	Portland cement
■	Dubrovskii	1970	>0.8 MeV	100 to 400	0.8	1.01	Hematite	Portland cement
△	Kelly	1969	N/A	20	0.67	0.36	Flint	Portland cement
✖	Kelly	1969	N/A	20	0.67	0.36	Limestone	Portland cement
◇	Alexander	1963	N/A	100	N/A	N/A	Heston sand	Portland cement
◇	Alexander	1963	N/A	100	N/A	N/A	Heston gravel	Portland cement

Figure 3-13 Weight Loss as a Function of Gamma Dose for Concrete and Mortar Using Ordinary Portland Cement (neutron energy level indicated if neutron radiation present; solid symbol denotes presence of both gamma and neutron radiation)

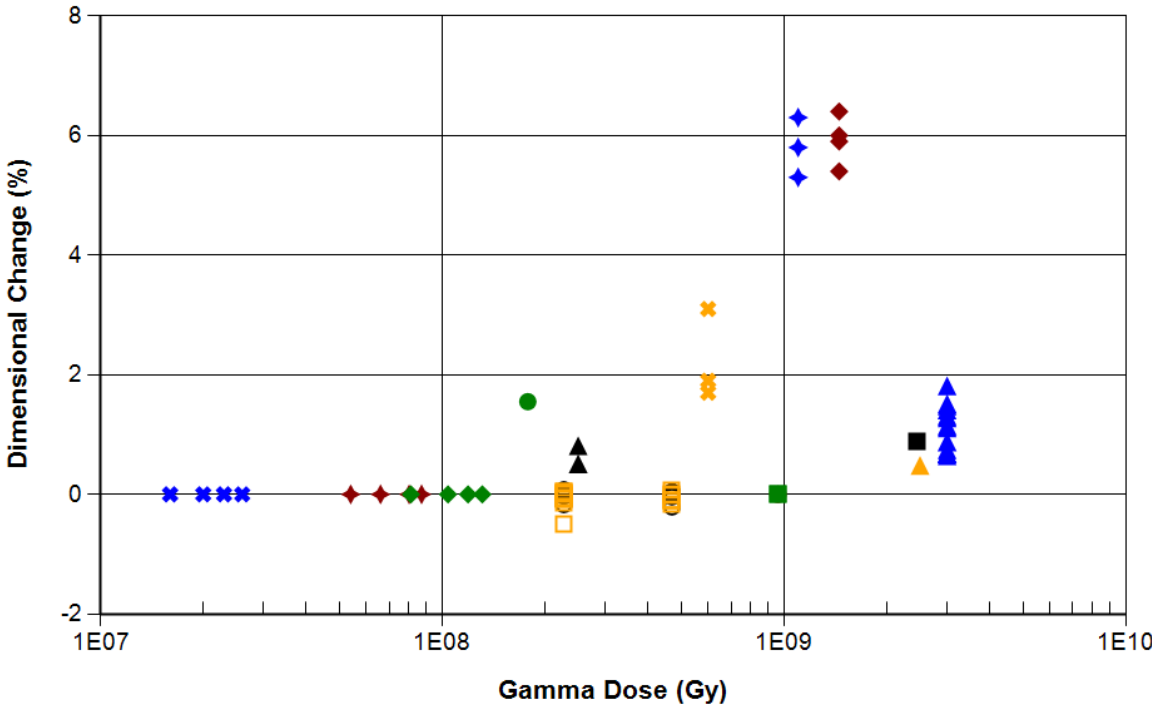

Sym	1st Author	Year	Energy Level	Max. T (C)	Ag. Frac.	W/C Ratio	Aggregate	Cement Type
●	Cristiani	1971	Fast	100	0.67	0.5	Limestone	Portland cement
■	Cristiani	1971	Fast	125	0.67	0.5	Limestone	Portland cement
▲	Dubrovskii	1967	>0.8 MeV	50	0.76	0.5	Sandstone, Riversand(quartz)	Portland cement
✖	Dubrovskii	1967	>0.8 MeV	150	0.76	0.5	Sandstone, Riversand(quartz)	Portland cement
✦	Dubrovskii	1967	>0.8 MeV	275	0.76	0.5	Sandstone, Riversand(quartz)	Portland cement
◆	Dubrovskii	1967	>0.8 MeV	350	0.76	0.5	Sandstone, Riversand(quartz)	Portland cement
●	Dubrovskii	1970	>0.8 MeV	200	0.8	1.01	Hematite	Portland cement
■	Dubrovskii	1970	>0.8 MeV	400	0.8	1.01	Hematite	Portland cement
▲	Dubrovskii	1970	>0.8 MeV	100	0.8	1.01	Hematite	Portland cement
✖	Fujiwara	2009	>0.1 MeV	56.2	0.79	0.55	Gravel, Sand	Cement
◆	Fujiwara	2009	>0.1 MeV	50.1	0.79	0.55	Gravel, Sand	Cement
◆	Fujiwara	2009	>0.1 MeV	50.9	0.79	0.55	Gravel, Sand	Cement
○	Kelly	1969	N/A	20	0.67	0.36	Flint	Portland cement
□	Kelly	1969	N/A	20	0.67	0.36	Limestone	Portland cement
▲	Pedersen	1971	Fast	80	0.68	0.4	Quartz	Portland cement

Figure 3-14 Dimensional Change as a Function of Gamma Dose and Neutron Fluence for Concrete and Mortar (neutron energy level indicated if neutron radiation present; solid symbol denotes presence of both gamma and neutron radiation)

4 EFFECTS OF RADIATION ON CONCRETE

The effect of radiation on the structure and chemical constituents of concrete is dependent on the radiation type and its energy, as well as the composition of the concrete, as discussed in Chapter 3. This chapter explores how these changes in concrete affect its ability to maintain the structural properties necessary to continue safely supporting RPVs.

We acquired a collection of approximately 110 articles on radiation damage to concrete and/or its components. The citations for these documents are presented in Appendix B. Information on study conditions and concrete performance was extracted for review. Efforts in this area focused on identifying those data most relevant to the conditions present in a commercial LWR. A key issue at this point is to separate impacts due solely to neutron irradiation, gamma irradiation, temperature, or variations in concrete composition, as well as any synergistic effects. These findings are presented in Section 4.1. Once basic trends are understood, more reliable material models can be developed and used to predict the physical properties of concrete as it ages. Some observations from past review articles are summarized below.

A critical neutron radiation value of 1×10^{19} n/cm^2 was first suggested by Hilsdorf et al. [4] based on the data available at the time. Fujiwara et al. [6] analyzed the test data collected and highlighted some issues (see Figure 4-1). Additional discussion on the issues appears in William et al. [10].

- During irradiation, the temperatures in some of the specimens reached 100°C or higher (approximately 140–550°C). As discussed earlier, phase transformations occur under high temperatures in cement paste, and thus the strength reduction could be induced by the elevated temperatures more than by the radiation.

- The sizes of some specimens (mortar) were very small (some were as small as 8–15 mm). This did not properly characterize the compressive strength of concrete, because no coarse aggregates were in the specimens. The response of the coarse aggregate is very important for the properties of concrete under irradiation.

- Some specimens were tested for bending strength, but not for compressive strength. There is a significant difference between the two testing methods.

Then, Field et al. [69] collected more test data with a better partitioning scheme. The compressive strength test data of concrete were partitioned according to types of aggregate, testing temperature, and mix designs. The collection of test data is shown in Figure 4-2. As shown, the neutron spectrum and specimen temperature vary between experiments. Siliceous concrete is depicted with red symbols, calcareous with blue, and miscellaneous concretes with green. Filled symbols indicate experiments conducted above 100°C; open symbols indicate experiments conducted below 100°C. Mix design can be determined by cross-referencing with Table 3 in the paper [69]. A decrease in compressive strength above 2×10^{19} n/cm^2 was suggested by Field et al. [69].

Because the expansion of aggregate under irradiation is important, the capacity of cement paste to accommodate the expansion of aggregate is equally important. In a case where cement paste can hold high volume expansion of aggregate without severe damage, the concrete will be fine for a longer term of operation. The properties of cement paste, such as stiffness and

fracture resistance, depend on the mix design, especially the w/c. Therefore, the mix design parameters of concrete are an important category of input parameters in our review.

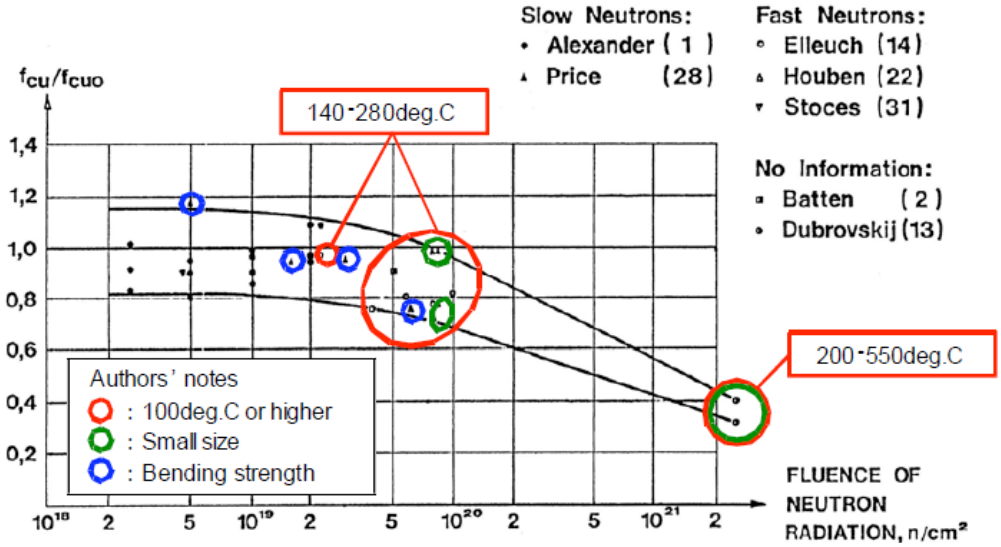

Figure 4-1 Problems in the Test Data Collected by Hilsdorf et al. [4] on the Compressive Strength of Concrete (as Identified by Fujiwara et al. [6])

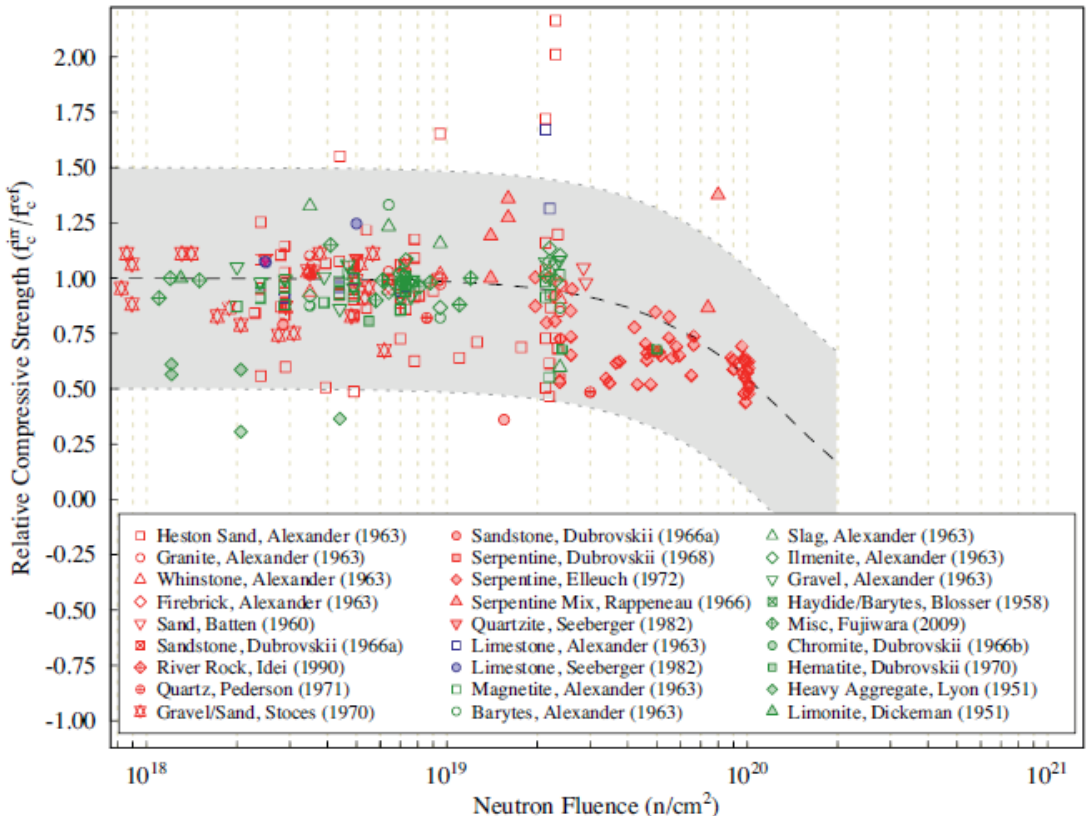

Figure 4-2 Relative Compressive Strength of Concrete and Mortar Specimens vs. Neutron Fluence in the Range of 1 × 10^{18} n/cm² to 1 × 10^{21} n/cm² [69]

The properties of concrete are affected by both neutron and gamma irradiation. Sections 4.1 and 4.2 present analyses of studies involving neutron and gamma irradiation, respectively. However, all experiments involving neutrons were carried out in nuclear reactors, so gamma radiation was also present. Thus, a totally clear delineation between neutron and gamma irradiation impacts is subject to interpretation. In other words, is an effect/impact due solely to gamma radiation, neutron radiation, or some combination of both? Very few studies have been conducted using gamma irradiation only (e.g., ^{60}Co). As a result, some data with both neutron fluence and gamma-ray dose are used in both neutron irradiation effects analysis and gamma irradiation effects analysis.

4.1 Neutron Irradiation Impacts

The effects of neutron radiation on the mechanical properties of cementitious material were reviewed based on the collected test data. The mechanical properties included compressive strength, tensile strength, and the modulus of elasticity. These mechanical properties are examined from several different perspectives where the effects of the temperature, the w/c, and the aggregate content are considered in conjunction with neutron fluence ($>1 \times 10^{18}$ n/cm^2).

4.1.1 Compressive Strength

Figure 4-3a shows the significant reduction of the compressive strength of concrete and mortar by neutron irradiation and potential thermal effects, which is consistent with the general trends shown in the literature. Figure 4-3b shows the data collected at temperatures less than 100°C, and thermal-only data is reviewed in Section 4.3.1 to better distinguish between neutron irradiation, temperature, and combined/synergistic effects. In addition, all experiments were carried out in nuclear reactors, so gamma radiation was also present. In the figure, normalized compressive strength was used, so the value of 1.0 means that there is no strength reduction. As shown in the figure, with increasing neutron fluence, the normalized strength decreased to 0.4, which is 40% of the original value.

On the other hand, there are no general trends for significant reductions of compressive strength of cement paste and aggregate, which are shown in Figure 4-4 for cement paste and in Figure 4-5 for aggregate. Different types of cement were used for the concrete and mortar specimens, including slag cement, aluminous cement, and regular Portland cement. For aggregates, only serpentine was studied. In that case, test conditions were at 240°C, well above those expected in an LWR reactor cavity [73]. Thus, no specific conclusions can be derived from these results, as discussed below.

For cement paste in Figure 4-4, the scattering of test data is very large, and there may be a reduction in the compressive strength depending on the type of cement, but it is not as significant as shown in Figure 4-3 for concrete. The test data on the compressive strength of aggregates shown in Figure 4-5 are from one experimental study of serpentine specimens (Elleuch et al. [73]). This study used a high aluminous cement that is a good candidate for use in high-temperature applications and exhibits good chemical resistance in conjunction with serpentine. Because serpentine is a hydrous aggregate that retains its chemically bound water up to a temperature of about 500°C, it is very good at neutron radiation shielding and a good candidate for use in NPPs [86]. The scattering of test data in Figure 4-5 is also very large. There is no obvious decrease in strength. In fact, at the lowest neutron fluence levels shown in Figure 4-5, there is a slight increase in the compressive strength. This increase is thought to occur because both neutron radiation and high temperature (in this case, the environmental temperature is 150–240°C) result in the expansion of the minerals in the aggregate, which may

increase the compactness of the components and thus lead to a potential increase in compressive strength.

(a) all temperatures

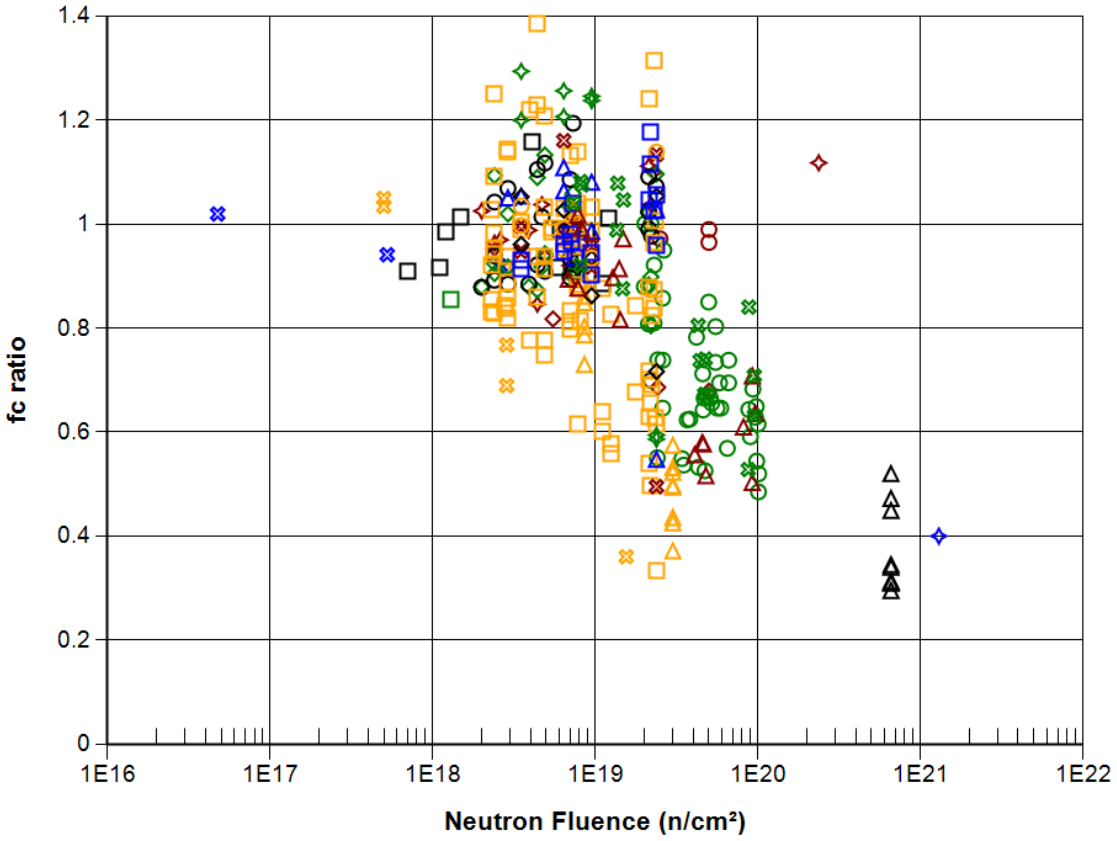

Sym	1st Author	Year	Energy Level	Max. T (C)	Ag. Frac.	W/C Ratio	Aggregate	Cement Type
○	Batten	1960	Thermal	50	0.67 to 0.84	0.45 to 0.5	Riversand	2 cement types
□	Dickeman	1951	Thermal	120	N/A	N/A		
△	Dubrovskii	1966	>0.7 MeV	550	N/A	N/A	Chromite	2 cement types
✖	Dubrovskii	1967	>0.8 MeV	50 to 350	0.76	0.5	Sandstone, Riversand(quartz)	Portland cement
✦	Dubrovskii	1968	>0.01 MeV	350	N/A	N/A	Serpentine	Portland cement
◇	Dubrovskii	1970	>0.8 MeV	100 to 400	0.8	1.01	Hematite	Portland cement
○	Elleuch	1972	>1 MeV	240	0.74	0.38	Serpentine	Aluminous cement
□	Fujiwara	2009	>0.1 MeV	50 to 56	0.79	0.55	Gravel, Sand	Cement
△	Pedersen	1971	Fast	80	0.68	0.4	Quartz	Portland cement
✖	Stoces	1970	>1 MeV	80	0.73	0.35	Crushed stone, Sand-gravel mix	"Iochkov" cement PC 350
✦	Alexander	1963	Thermal	100	N/A	N/A	Heston gravel	Portland cement
◇	Alexander	1963	Thermal	100	N/A	N/A	Limestone	Portland cement
○	Alexander	1963	Thermal	100	N/A	N/A	Magnetite	Portland cement
□	Alexander	1963	Fast, Thermal	20 to 100	N/A	N/A	Heston sand	4 cement types
△	Alexander	1963	Thermal	100	N/A	N/A	Granite	Portland cement
✖	Alexander	1963	Thermal	100	N/A	N/A	Barytes	Portland cement
✦	Alexander	1963	Thermal	100	N/A	N/A	Slag	Portland cement
◇	Alexander	1963	Thermal	100	N/A	N/A	Whinstone	Portland cement
○	Alexander	1963	Thermal	100	N/A	N/A	Crushed Firebrick	Portland cement
□	Alexander	1963	Thermal	100	N/A	N/A	Ilmenite	Portland cement
△	Maruyama	2017	>0.1 MeV	66 to 73	0.77	0.5	Thermally altered tuff, Sandstone	high early-strength ordinary Portland cement
✖	Maruyama	2017	>0.1 MeV	66 to 73	0.77	0.5	Felsic sandstone, Sandstone	high early-strength ordinary Portland cement

Figure 4-3 Relative Compressive Strength of Concrete and Mortar as a Function of Neutron Fluence

(b) temperatures < 100°C

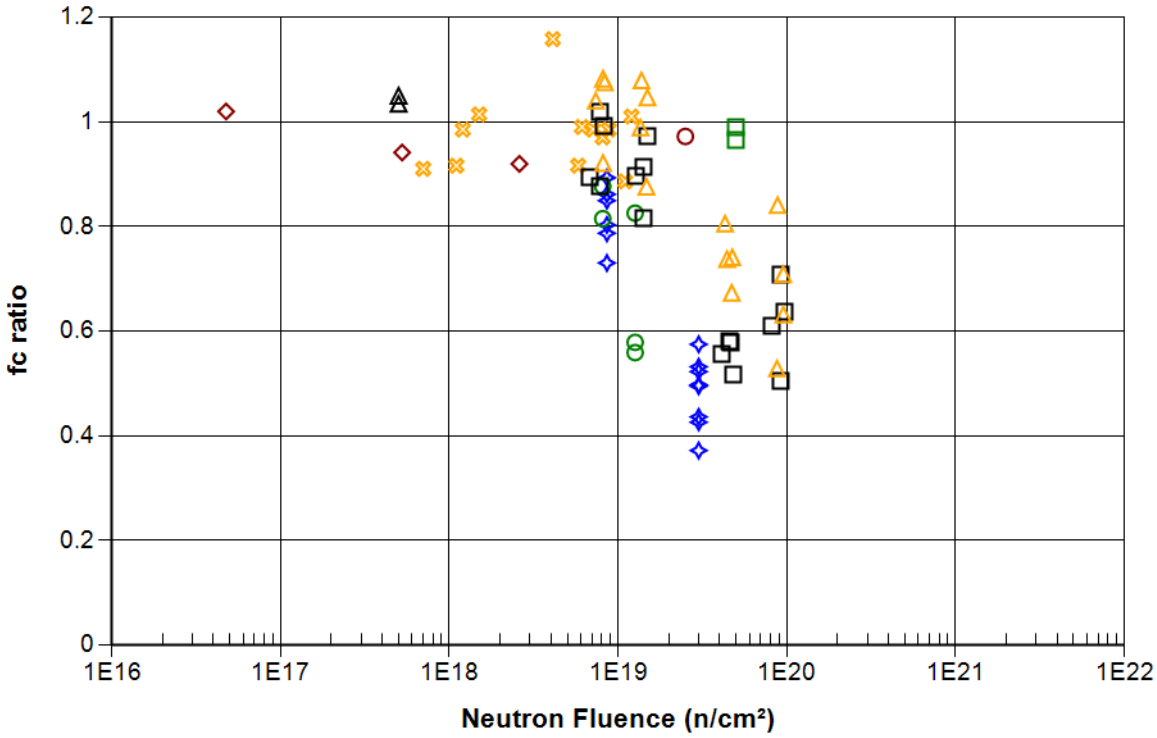

Sym	1st Author	Year	Energy Level	Max. T (C)	Ag. Frac.	W/C Ratio	Aggregate	Cement Type
○	Batten	1960	Thermal	50	0.84	0.5	Riversand	Aluminous cement
□	Batten	1960	Thermal	50	0.67	0.45	Riversand	Portland cement
△	Dubrovskii	1967	>0.8 MeV	50	0.76	0.5	Sandstone, Riversand(quartz)	Portland cement
⊠	Fujiwara	2009	>0.1 MeV	50 to 56	0.79	0.55	Gravel, Sand	Cement
◇	Pedersen	1971	Fast	80	0.68	0.4	Quartz	Portland cement
◇	Stoces	1970	>1 MeV	80	0.73	0.35	Crushed stone, Sand-gravel mix	"lochkov" cement PC 350
○	Alexander	1963	Thermal	20	N/A	N/A	Heston sand	Portland cement
□	Maruyama	2017	>0.1 MeV	66 to 73	0.77	0.5	Thermally altered tuff, Sandstone	high early-strength ordinary Portland cement
△	Maruyama	2017	>0.1 MeV	66 to 73	0.77	0.5	Felsic sandstone, Sandstone	high early-strength ordinary Portland cement

Figure 4-3 Relative Compressive Strength of Concrete and Mortar as a Function of Neutron Fluence (cont.)

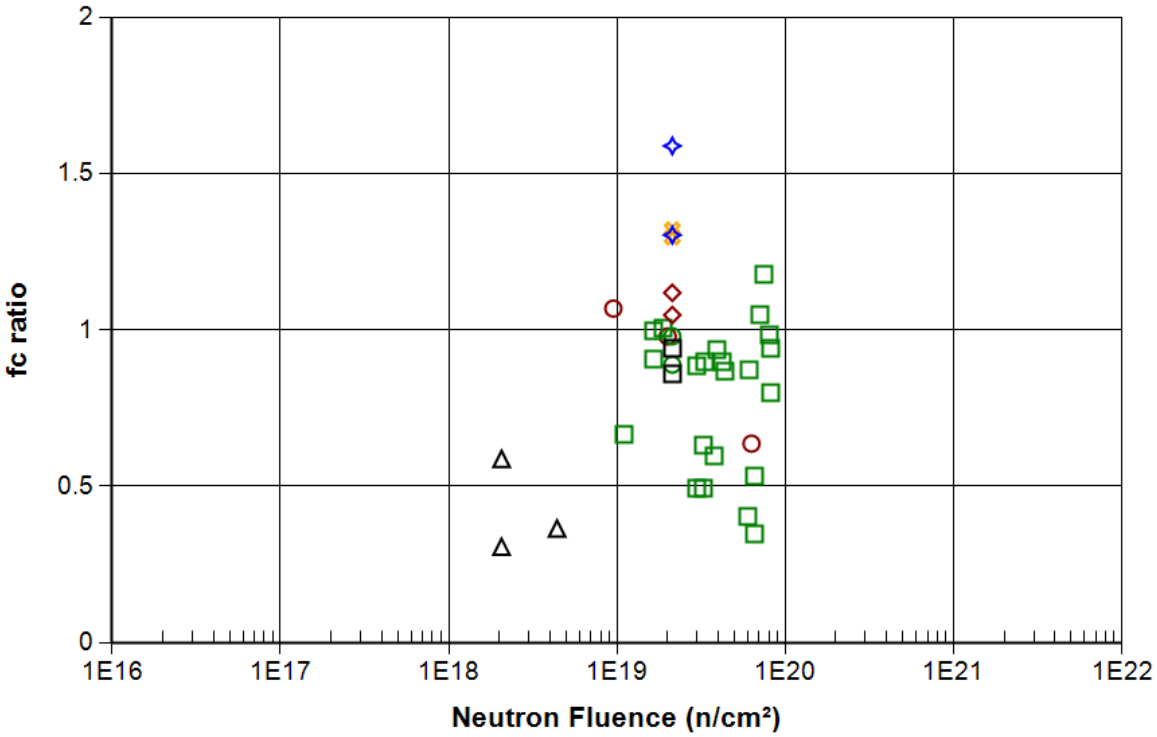

Sym	1st Author	Year	Max. T (C)	W/C Ratio	Material Name
○	Dubrovskii	1970	150 to 450	0.3	Portland cement paste
□	Elleuch	1972	280	0.25	Aluminous cement paste
△	Lyon	1950	N/A	N/A	Magnesium oxychloride cement paste
✕	Alexander	1963	100	N/A	Portland cement paste
✦	Alexander	1963	100	N/A	High-alumina cement paste
◇	Alexander	1963	100	N/A	Low-heat-slag cement paste
○	Alexander	1963	100	N/A	Supersulphate cement
□	Alexander	1963	100	N/A	Pulverised fuel ash paste

Figure 4-4 Potential Reduction of the Compressive Strength of Cement Paste by Neutron Irradiation

Because concrete can be considered a composite material with the aggregate as inclusions and cement paste as matrix, the general trends shown in Figures 4-3 through 4-5 suggest that the strength reduction of concrete may not be due to the strength degradation of its components, but to the increased volumetric mismatches between the two constituent phases during long-term neutron irradiation. However, the onset of significant dimensional change in quartz as a function of neutron fluence was shown to be temperature dependent between 30°C and 100°C, as shown in Figure 3-5. Thus, temperature also seems to have some indirect influence, via neutron-induced dimensional changes, on concrete strength degradation. Further data on the compressive strength changes for concrete and individually for its cement paste and aggregate components is needed because the trends suggested in Figures 4-3 through 4-5 are based on only one common set of experiments [73] that were conducted around 240°C, well outside the expected operating temperature in an LWR reactor cavity. The effect of temperature is discussed further in Section 4.3.1.

The volumetric mismatch appears to be the key factor that results in the degradation of the compressive strength. This result is different from the conventional long-term durability problems of concrete. For example, during a sulfate attack, the mechanical properties of aggregate remain intact and those of cement paste decrease, resulting in the degradation of concrete. Therefore, to evaluate the effect of neutron irradiation on concrete, the volumetric properties of the aggregate and the cement paste—such as the coefficient of thermal expansion and the coefficient of drying shrinkage—are very important. Furthermore, the volumetric properties depend on the type and amount of aggregate and the w/c used in the concrete, which are discussed below.

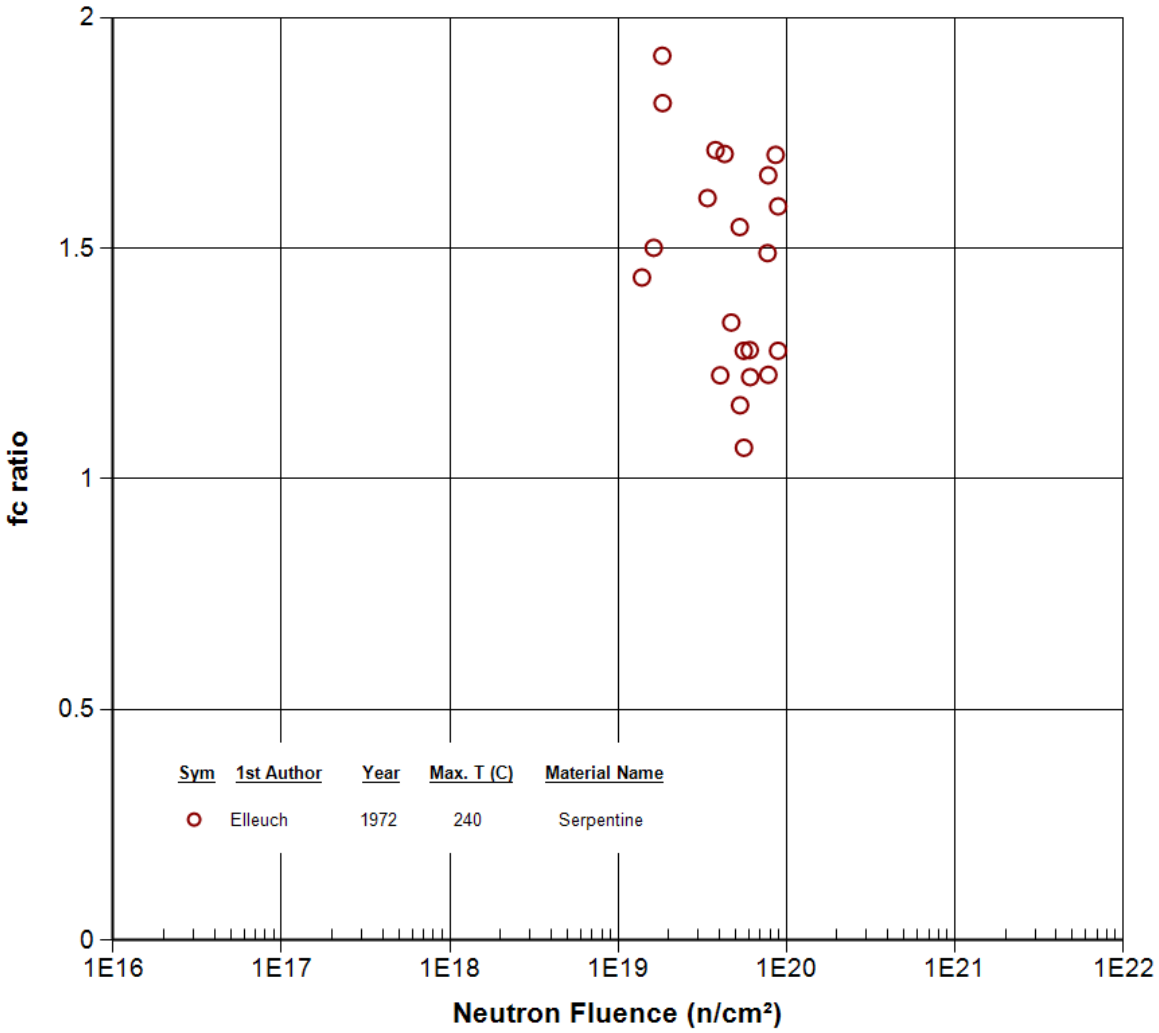

Figure 4-5 No Significant Reduction of the Compressive Strength of Serpentine at 240°C by Neutron Irradiation (*E* > 1 MeV)

4.1.1.1 Water-to-Cement Ratio (w/c)

The w/c is one of the most important among all concrete mix design parameters and is typically about 0.45 for NPPs per ACI 318 and ACI 349. The effect of w/c on compressive strength of irradiated concrete is shown in Figure 4-6. The effect of w/c may be explained through the

consideration of several mechanisms, some of which have both a positive and a negative impact: (1) A low w/c results in a low porosity in cement paste. The low porosity helps to increase the bond between cement paste and aggregate, which is a positive effect. (2) On the other hand, the less porous cement paste reduces the cement paste's ability to accommodate the volume expansion of aggregate, which is a negative effect. (3) A high w/c leads to higher water content in cement paste, and thus higher neutron resistance of the concrete, which is a positive effect. (4) A high w/c leads to a higher porosity of the cement paste, which increases the cement paste's ability to accommodate the volume expansion of aggregate, which is also a positive effect. The total effect of w/c is the combined effect of these mechanisms with different impacts, and one or two of the mechanisms may play dominant roles.

From Figure 4-6, one can see that with increasing w/c, the relative compressive strength tends to increase in general. However, Portland cement was not used in all cases, so the differences observed could be due to different cement compositions that are not known at this time. If the compositions are similar, it appears that the increasing porosity (increasing w/c) better accommodates the aggregate expansion due to neutron irradiation (mechanism 4), and, if pore water is still present, the additional water reduces the local neutron fluence (mechanism 3).

The spread in relative compressive strength values for each set of concrete samples at a given w/c is due, in part, to experimental variability, but also to the neutron fluence. The lower values were obtained at higher neutron fluences, as is evident when comparing Figure 4-6 with Figures 4-3a and 4-3b. Scatter in the plots was reduced by only considering data obtained at neutron fluences greater than 1×10^{18} n/cm^2. However, the different neutron energy cutoffs among the studies considered also contributes to the experimental variability and cannot be quantified because the neutron energy distributions from each study are not available.

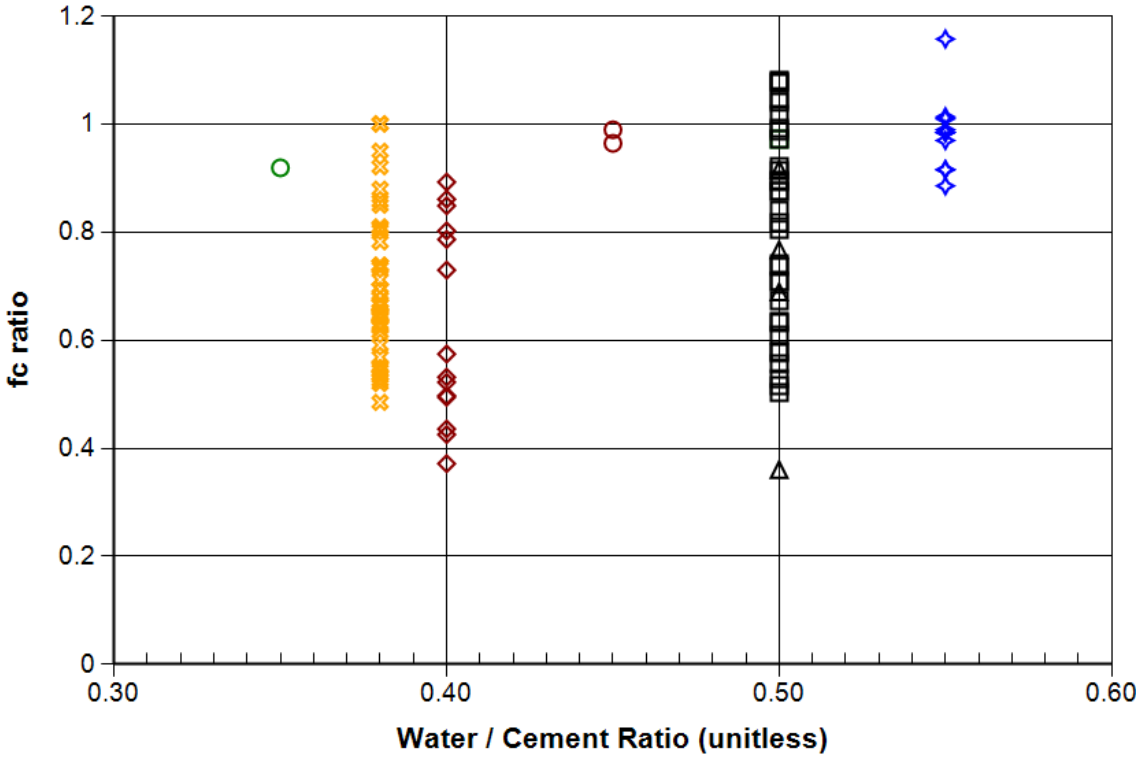

Sym	1st Author	Year	Energy Level	Max. T (C)	Ag. Frac.	Aggregate	Cement Type
○	Batten	1960	Thermal	50	0.67	Riversand	Portland cement
□	Batten	1960	Thermal	50	0.84	Riversand	Aluminous cement
△	Dubrovskii	1967	>0.8 MeV	150 to 350	0.76	Sandstone, Riversand(quartz)	Portland cement
✕	Elleuch	1972	>1 MeV	240	0.74	Serpentine	Aluminous cement
✧	Fujiwara	2009	>0.1 MeV	50 to 56	0.79	Gravel, Sand	Cement
◇	Pedersen	1971	Fast	80	0.68	Quartz	Portland cement
○	Stoces	1970	>1 MeV	80	0.73	Crushed stone, Sand-gravel mix	"Iochkov" cement PC 350
□	Maruyama	2017	>0.1 MeV	66 to 73	0.77	2 aggregate types	high early-strength ordinary Portland cement

Figure 4-6 Effect of the w/c on the Normalized Compressive Strength of Concrete and Mortar (neutron fluence > 1 × 10^{18} n/cm^2)

4.1.1.2 Aggregate Content

Figure 4-7 shows the compressive strength reduction of high-level neutron irradiated concrete samples. Note that the strength reduction is higher when the aggregate weight fraction is lower. The same effect was also noted in NUREG/CR-6900 [87]. As discussed in Section 4.1.1, the compressive strength of aggregates does not appear to be significantly affected by neutron irradiation. Thus, if the aggregate fraction is the only variable considered, a higher aggregate fraction may lead to less reduction of concrete compressive strength after neutron irradiation. In addition, the volumetric mismatch between aggregate and cement paste induced by neutron radiation may be changed by varying the aggregate content, but the overall damage mechanism needs further study.

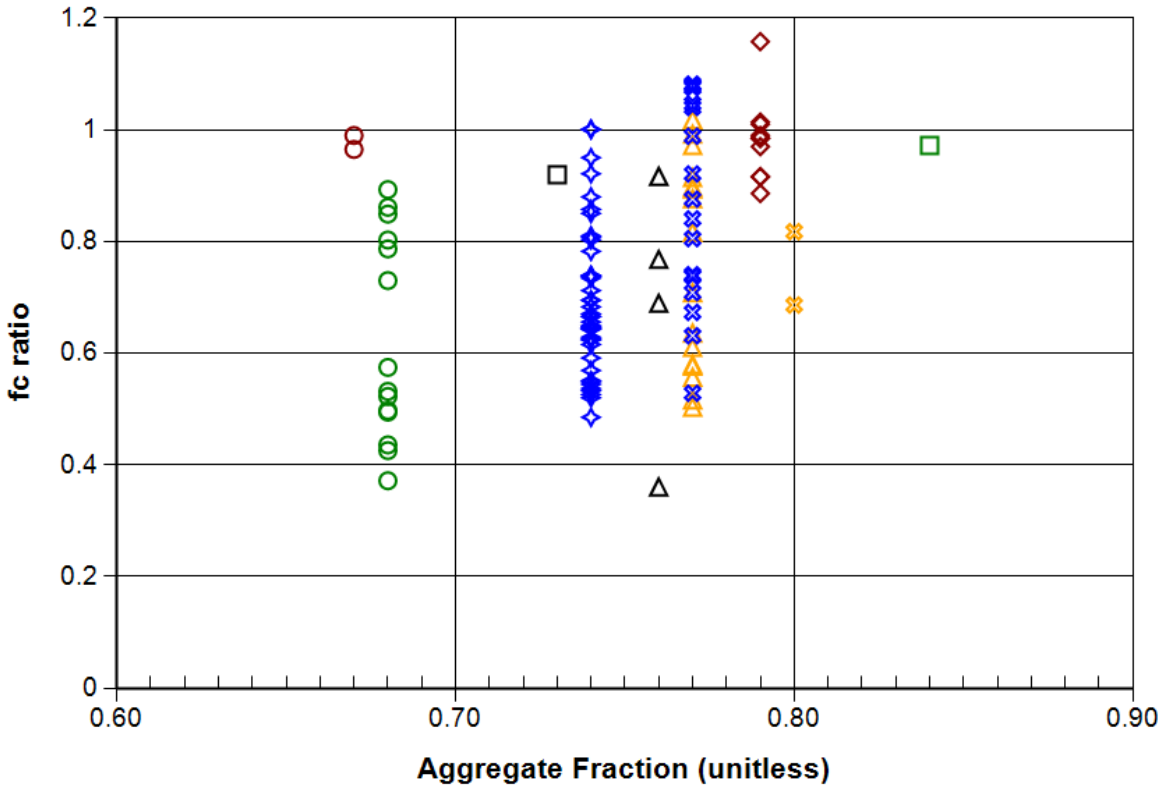

Sym	1st Author	Year	Energy Level	Max. T (C)	W/C Ratio	Aggregate	Cement Type
○	Batten	1960	Thermal	50	0.45	Riversand	Portland cement
□	Batten	1960	Thermal	50	0.5	Riversand	Aluminous cement
△	Dubrovskii	1967	>0.8 MeV	150 to 350	0.5	Sandstone, Riversand(quartz)	Portland cement
✖	Dubrovskii	1970	>0.8 MeV	100 to 200	1.01	Hematite	Portland cement
✦	Elleuch	1972	>1 MeV	240	0.38	Serpentine	Aluminous cement
◇	Fujiwara	2009	>0.1 MeV	50 to 56	0.55	Gravel, Sand	Cement
○	Pedersen	1971	Fast	80	0.4	Quartz	Portland cement
□	Stoces	1970	>1 MeV	80	0.35	Crushed stone, Sand-gravel mix	"Iochkov" cement PC 350
△	Maruyama	2017	>0.1 MeV	66 to 73	0.5	Thermally altered tuff, Sandstone	high early-strength ordinary Portland cement
✖	Maruyama	2017	>0.1 MeV	66 to 73	0.5	Felsic sandstone, Sandstone	high early-strength ordinary Portland cement

Figure 4-7 Effect of Aggregate Fraction on the Compressive Strength of Concrete and Mortar (neutron fluence > 1 × 10^{18} n/cm^2)

4.1.2 Tensile Strength

Figure 4-8 shows a significant reduction of tensile strength of concrete and mortar by neutron irradiation, for (a) all experiments and (b) experiments conducted at temperatures less than 100°C, which is consistent with the general trends in the literature. In the figure, the normalized tensile strength was used. As shown in Figure 4-8b, as the neutron level increased, the normalized strength decreased to 0.2, which is 20% of the original value.

Similar to the compressive strength results, the tensile strength of neutron irradiated cement paste may be relatively unaffected, as shown in Figure 4-9. Kelly et al. [68] did not observe any reduction in tensile strength of ordinary Portland cement with neutron irradiation. Although the

results for the aluminous cement obtained by Elleuch et al. [73] show a significant reduction in the tensile strength of samples, this can be attributed to thermal effects because the results were determined to be insignificant relative to the results for the temperature control samples that were maintained under the same temperature profile as the neutron irradiated samples [73]. Thermal effects on concrete and its components are discussed further in Section 4.3.1.

Unlike compressive strength, there is a clear trend for the significant reduction of tensile strength of aggregates, as shown in Figure 4-10. In this case, Elleuch et al.'s study of serpentine [73] found that the tensile strength of neutron-irradiated samples was about 50% less than the temperature-control samples, indicating that both temperature and irradiation effects contribute to the decrease.

As shown in Figures 4-9 and 4-10, the available data for tensile strength of pure cement paste and aggregate are very limited and any interpretation is tentative. As mentioned earlier, concrete is a composite material with the aggregate as inclusions and the cement paste as the matrix. The general trends shown in Figures 4-8 through 4-10 suggest that the tensile strength reduction of concrete is due to additional cracks in the cement paste caused by the volumetric mismatch between the two constituent phases during the long-term neutron irradiation. This behavior is consistent with the tensile failure of unirradiated concrete that usually results from the formation and propagation of cracks in the cement paste and the interfaces surrounding aggregates. However, the strength degradation of the aggregate may have some effect on the tensile strength of the irradiated concrete as well, since any volumetric expansion of the aggregate could result in both intra- and inter-granular cracking within and between the mineral grains, respectively, that compose the aggregate.

4.1.2.1 Water-to-Cement Ratio (w/c)

Figure 4-11 shows the effect of the w/c on tensile strength. The general trend appears to be different from that in Figure 4-6 for compressive strength. As mentioned in the previous section, the reduction of tensile strength in concrete under neutron radiation appears to be due to the strength degradation of aggregates and the volume mismatch between the cement paste and aggregates.

Figure 4-11 shows that, with increasing w/c, the relative tensile strength generally increases first and then decreases. These two behaviors can be explained by the different mechanisms discussed in Section 4.1.1.1 (for compressive strength). The increasing section in Figure 4-11 means that the negative effect due to low porosity (a reduced capability of cement paste pore space to accommodate aggregate volume expansion) is decreasing. However, at some point, the benefit of higher porosity becomes outweighed by its disadvantage, the weaker bond strength between the cement paste and aggregate.

Another consideration is the type of cement paste used in the experiments. The greatest reduction in concrete tensile strength was reported for concretes that used aluminous cement, rather than Portland cement, as seen in Figure 4-11. In addition, Elleuch et al. [73] reported that the tensile strengths for their neutron-irradiated samples approached those for temperature-control samples as the neutron fluence (time at temperature) increased. This indicates that the effect is more temperature dependent, as observed for the cement paste and discussed in Section 4.1.2. Thus, there are no clear trends in the limited data on the effect of the w/c on neutron-irradiated concrete tensile strength.

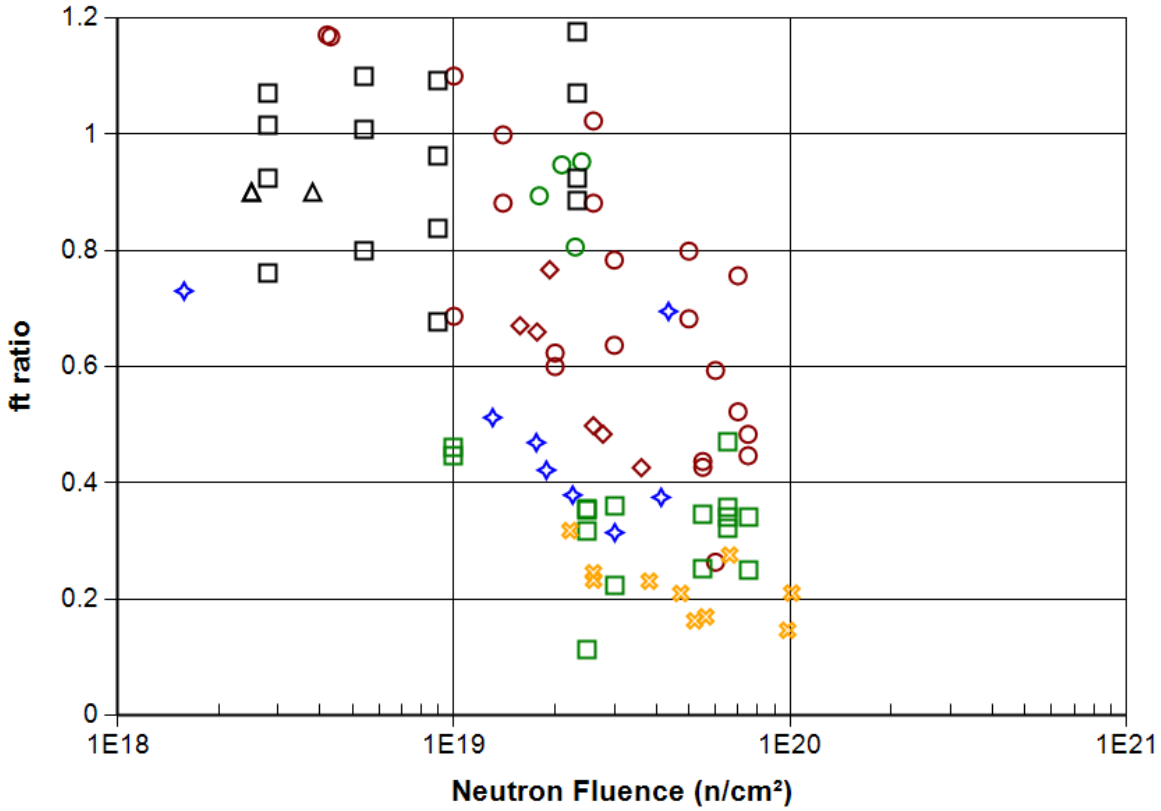

Sym	1st Author	Year	Energy Level	Max. T (C)	Ag. Frac.	W/C Ratio	Aggregate	Cement Type
○	Batten	1960	Thermal	50	0.67 to 0.84	0.45 to 0.5	Riversand	Portland cement
□	Batten	1960	Thermal	50	0.84	0.5	Riversand	Aluminous cement
△	Cristiani	1971	Fast	100 to 125	0.67	0.5	Limestone	Portland cement
✕	Elleuch	1972	>1 MeV	240	0.74	0.38	Serpentine	Aluminous cement
✧	Kelly	1969	Fast	50	0.67	0.36	Flint	Portland cement
◇	Kelly	1969	Fast	50	0.67	0.36	Limestone	Portland cement
○	Kelly	1969	Fast	50	N/A	N/A	Light weight rock, Sand	Portland cement
□	Alexander	1963	Thermal	100	N/A	N/A	Heston sand	Portland cement

Figure 4-8a Relative Tensile Strength Reduction of Concrete and Mortar as a Function of Neutron Fluence (all temperatures)

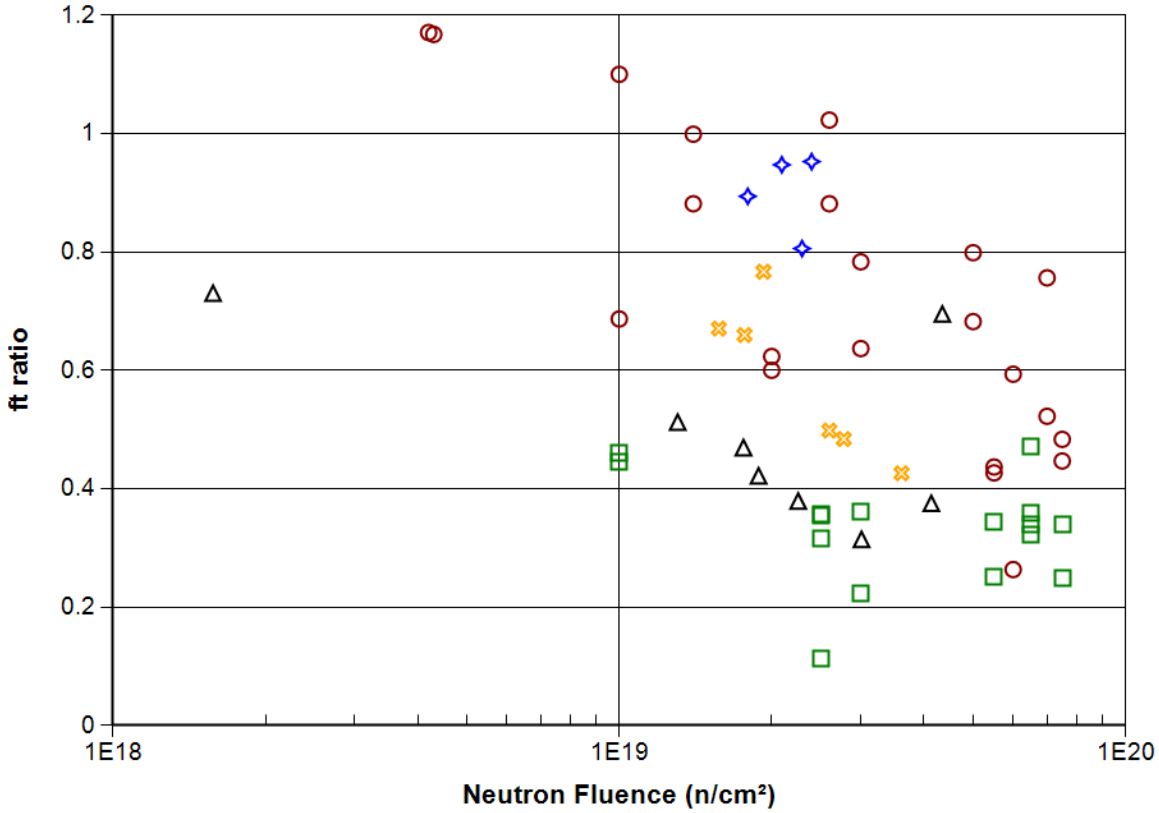

Sym	1st Author	Year	Energy Level	Max. T (C)	Ag. Frac.	W/C Ratio	Aggregate	Cement Type
○	Batten	1960	Thermal	50	0.67 to 0.84	0.45 to 0.5	Riversand	Portland cement
□	Batten	1960	Thermal	50	0.84	0.5	Riversand	Aluminous cement
△	Kelly	1969	Fast	50	0.67	0.36	Flint	Portland cement
✖	Kelly	1969	Fast	50	0.67	0.36	Limestone	Portland cement
✧	Kelly	1969	Fast	50	N/A	N/A	Light weight rock, Sand	Portland cement

Figure 4-8b Relative Tensile Strength Reduction of Concrete and Mortar as a Function of Neutron Fluence (T < 100°C)

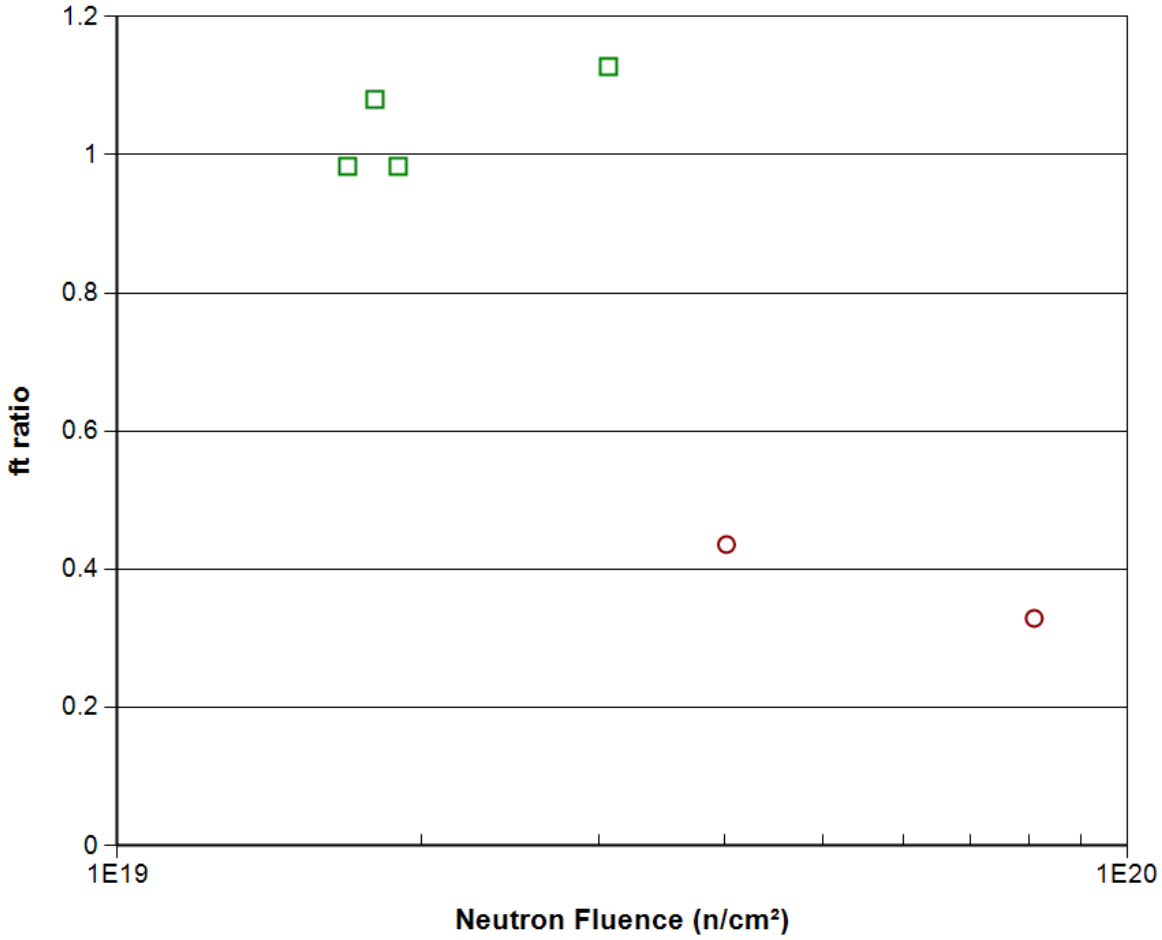

Sym	1st Author	Year	Energy Level	Max. T (C)	W/C Ratio	Material Name
○	Elleuch	1972	>1 MeV	280	0.25	Aluminous cement paste
□	Kelly	1969	Fast	50	0.36	Portland cement paste

Figure 4-9 Tensile Strength Reduction of Cement Paste by Neutron Irradiation (note: no significant difference was seen between irradiated samples and temperature-control samples in Elleuch et al. [73])

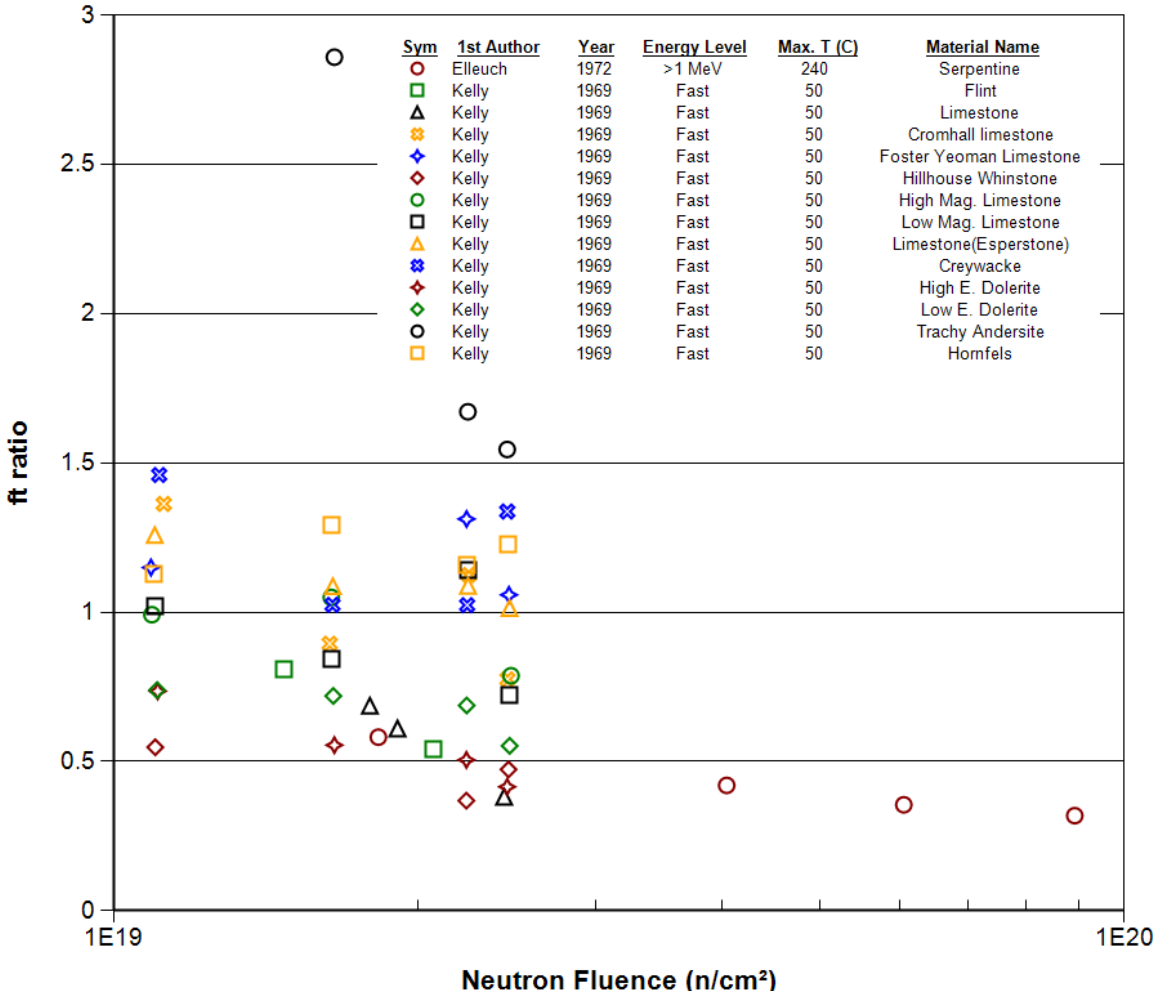

Figure 4-10 Tensile Strength Reduction of Aggregates by Neutron Irradiation

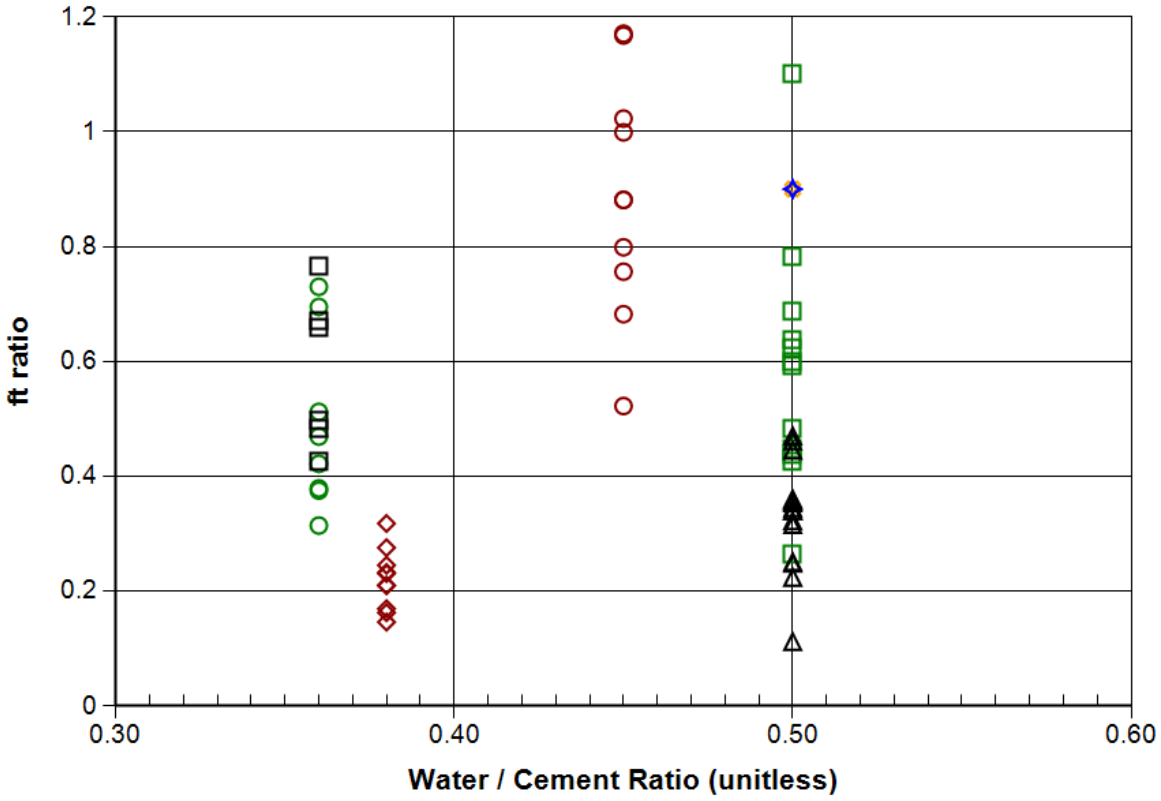

Sym	1st Author	Year	Energy Level	Max. T (C)	Ag. Frac.	Aggregate	Cement Type
○	Batten	1960	Thermal	50	0.67	Riversand	Portland cement
□	Batten	1960	Thermal	50	0.84	Riversand	Portland cement
△	Batten	1960	Thermal	50	0.84	Riversand	Aluminous cement
⊠	Cristiani	1971	Fast	100	0.67	Limestone	Portland cement
◆	Cristiani	1971	Fast	125	0.67	Limestone	Portland cement
◇	Elleuch	1972	>1 MeV	240	0.74	Serpentine	Aluminous cement
○	Kelly	1969	Fast	50	0.67	Flint	Portland cement
□	Kelly	1969	Fast	50	0.67	Limestone	Portland cement

Figure 4-11 Effect of w/c on the Tensile Strength of Concrete and Mortar (neutron fluence > 1 × 10^{18} n/cm^2)

4.1.2.2 Aggregate Content

Figure 4-12 shows the effect of aggregate fraction on tensile strength of concrete and mortar. It appears that when there is more aggregate in the concrete, the tensile strength reduction is higher. Again, note that the tensile strength reduction in the data from Elleuch et al. [73] is partially due to thermal effects, as discussed in Section 4.1.2. The trend in Figure 4-12 may occur because the tensile strength of aggregate is reduced by the neutron irradiation (see Figure 4-10). Thus, when there is more distressed aggregate in the composite, the effective tensile strength of the composite (the irradiated concrete) is lower. However, no microscopic evaluations of the test samples were conducted to determine whether failure was along the cement paste interface and/or through the aggregate (intergranular vs. transgranular). In addition, at higher coarse aggregate fractions, the likelihood of very thin regions of cement paste between aggregates or even voids between aggregates becomes more important, leading to weaker bonding as a starting point.

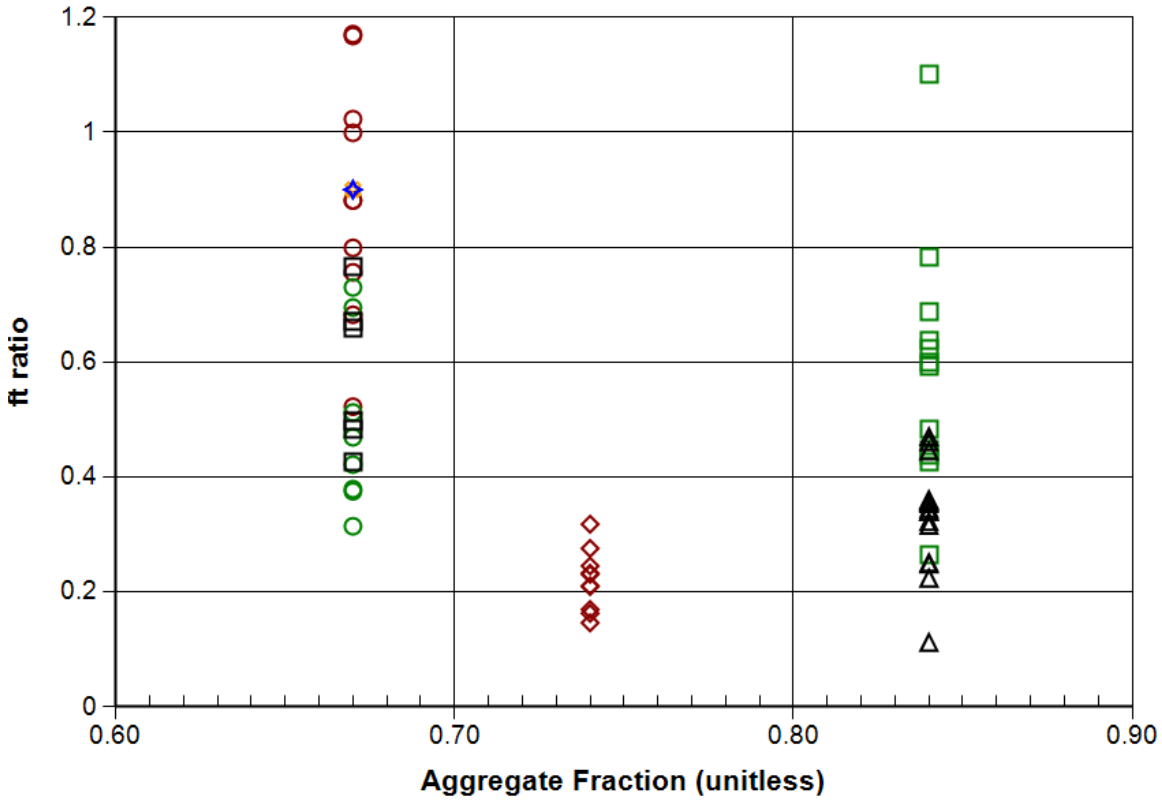

Sym	1st Author	Year	Energy Level	Max. T (C)	W/C Ratio	Aggregate	Cement Type
○	Batten	1960	Thermal	50	0.45	Riversand	Portland cement
□	Batten	1960	Thermal	50	0.5	Riversand	Portland cement
△	Batten	1960	Thermal	50	0.5	Riversand	Aluminous cement
✕	Cristiani	1971	Fast	100	0.5	Limestone	Portland cement
✦	Cristiani	1971	Fast	125	0.5	Limestone	Portland cement
◇	Elleuch	1972	>1 MeV	240	0.38	Serpentine	Aluminous cement
○	Kelly	1969	Fast	50	0.36	Flint	Portland cement
□	Kelly	1969	Fast	50	0.36	Limestone	Portland cement

Figure 4-12 Effect of Aggregate Fraction on the Tensile Strength of Concrete and Mortar (neutron fluence > 1 × 10^{18} n/cm^2)

4.1.3 Modulus of Elasticity

The effect of neutron irradiation on the modulus of elasticity, *E*, of concrete and mortar, cement paste, and aggregate are shown in Figures 4-13 through 4-15. The test data reveal general trends: there is a significant reduction of the elastic modulus of concrete and mortar by neutron irradiation; there may be no or little reduction of the elastic modulus of cement paste by neutron irradiation; and there is a significant reduction of the elastic modulus of aggregates by neutron irradiation. Therefore, the reduction of concrete stiffness as indicated by the reduction of *E* may be mainly due to the reduction of *E* of the aggregate and damage induced by the volumetric mismatch between aggregate and cement paste, as described in Section 4.1.1 for compressive strength. The reduction in *E* may also be due to temperature and to some contribution from neutron irradiation, as discussed in Section 4.3.1.4. However, as shown in Figure 4-13b, there is a significant reduction (up to 70% of the original value) in *E* of concrete due to neutron irradiation at LWR temperatures.

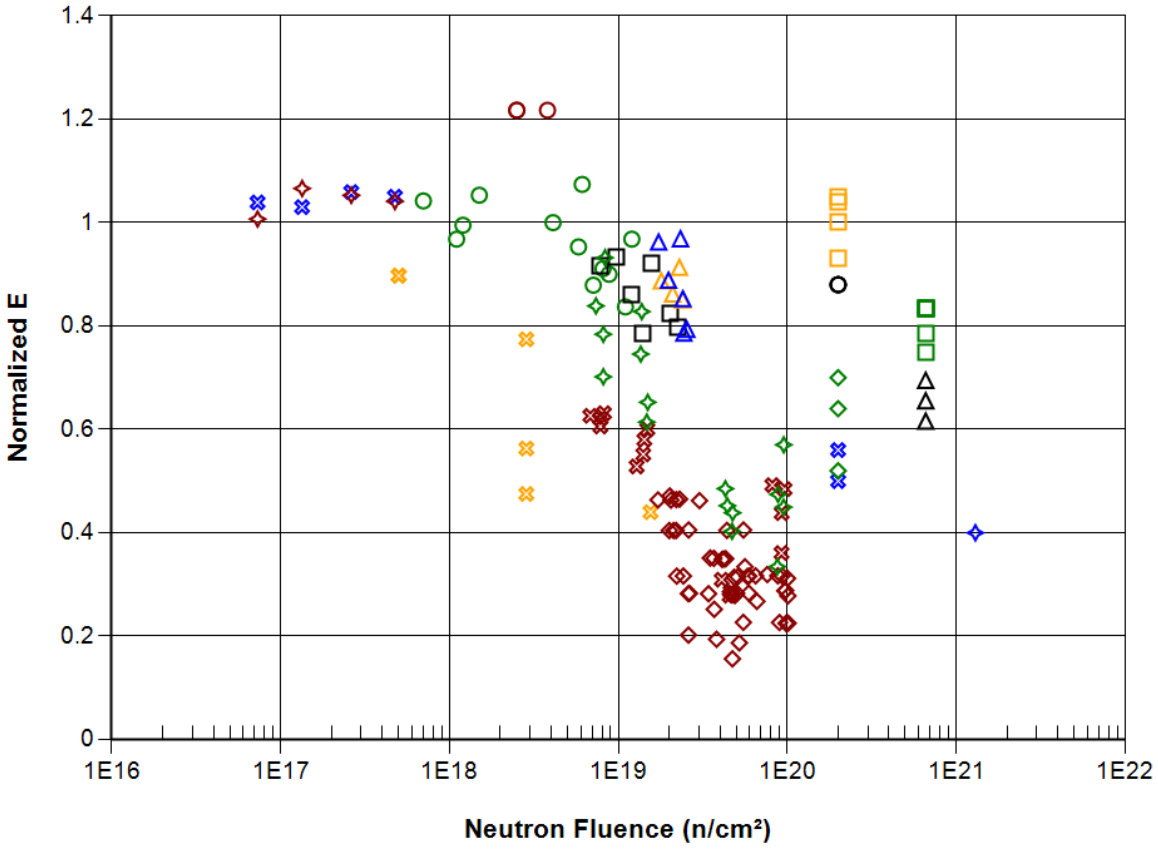

Sym	1st Author	Year	Energy Level	Max. T (C)	Ag. Frac.	W/C Ratio	Aggregate	Cement Type
○	Cristiani	1971	Fast	100 to 125	0.67	0.5	Limestone	Portland cement
□	Dubrovskii	1966	>0.7 MeV	550	N/A	N/A	Chromite	Portland cement
△	Dubrovskii	1966	>0.7 MeV	550	N/A	N/A	Chromite	Liquid glass
✖	Dubrovskii	1967	>0.8 MeV	50 to 350	0.76	0.5	Sandstone, Riversand(quartz)	Portland cement
✦	Dubrovskii	1968	>0.01 MeV	350	N/A	N/A	Serpentine	Portland cement
◇	Elleuch	1972	>1 MeV	240	0.74	0.38	Serpentine	Aluminous cement
○	Fujiwara	2009	>0.1 MeV	50 to 56	0.79	0.55	Gravel, Sand	Cement
□	Kelly	1969	Fast	50	0.67	0.36	Limestone	Portland cement
△	Kelly	1969	Fast	50	N/A	N/A	Light weight rock, Sand	Portland cement
✖	Van der Schaaf	1967	Fast	60 to 200	N/A	N/A	Barite	Portland cement
◇	Van der Schaaf	1967	Fast	60	N/A	0.45	Sand	Portland cement
◇	Van der Schaaf	1967	Fast	200	N/A	0.5	Barite	Blastfurnace slag cement
○	Van der Schaaf	1967	Fast	200	N/A	0.5	Magnetite	Portland cement
□	Van der Schaaf	1967	Fast	200	N/A	1	Sintered shale	Portland cement
△	Alexander	1963	Thermal	100	N/A	N/A	Heston gravel	Portland cement
✖	Maruyama	2017	>0.1 MeV	66 to 73	0.77	0.5	Thermally altered tuff, Sandstone	high early-strength ordinary Portland cement
✦	Maruyama	2017	>0.1 MeV	66 to 73	0.77	0.5	Felsic sandstone, Sandstone	high early-strength ordinary Portland cement

Figure 4-13a Relative Reduction of the Elastic Modulus of Concrete and Mortar as a Function of Neutron Fluence (all temperatures)

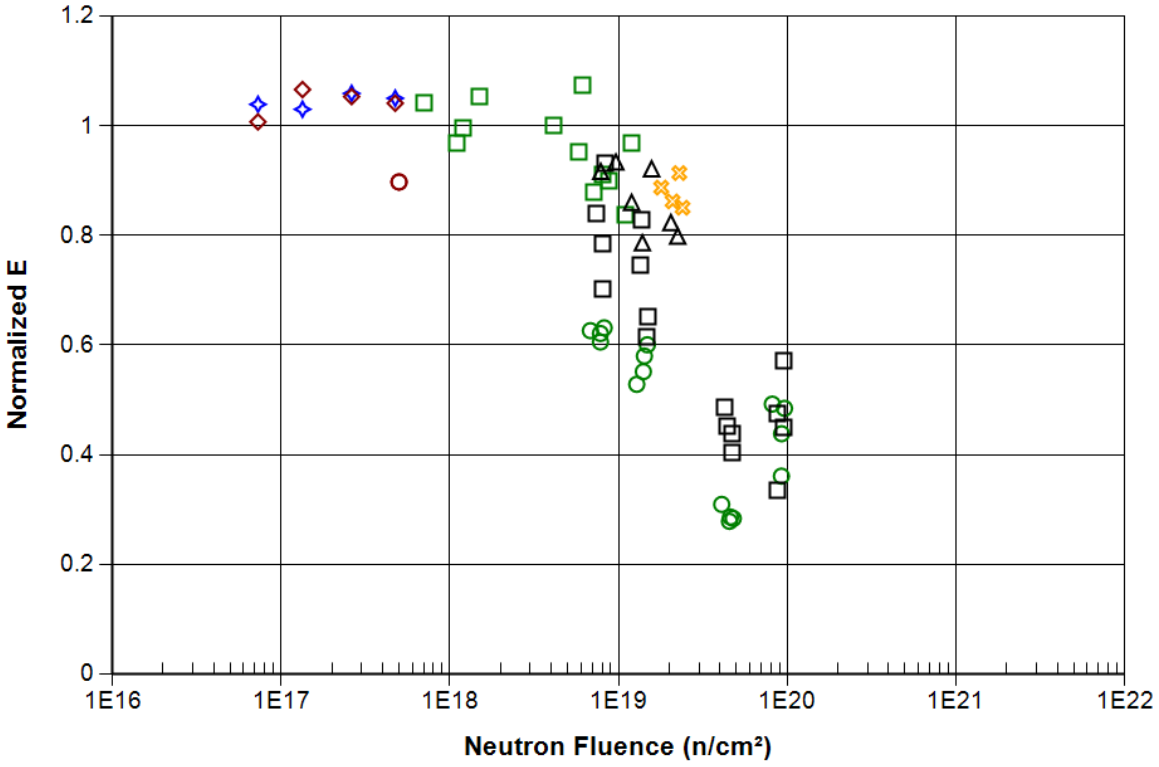

Sym	1st Author	Year	Energy Level	Max. T (C)	Ag. Frac.	W/C Ratio	Aggregate	Cement Type
○	Dubrovskii	1967	>0.8 MeV	50	0.76	0.5	Sandstone, Riversand(quartz)	Portland cement
□	Fujiwara	2009	>0.1 MeV	50 to 56	0.79	0.55	Gravel, Sand	Cement
△	Kelly	1969	Fast	50	0.67	0.36	Limestone	Portland cement
✕	Kelly	1969	Fast	50	N/A	N/A	Light weight rock, Sand	Portland cement
✦	Van der Schaaf	1967	Fast	60	N/A	N/A	Barite	Portland cement
◇	Van der Schaaf	1967	Fast	60	N/A	0.45	Sand	Portland cement
○	Maruyama	2017	>0.1 MeV	66 to 73	0.77	0.5	Thermally altered tuff, Sandstone	high early-strength ordinary Portland cement
□	Maruyama	2017	>0.1 MeV	66 to 73	0.77	0.5	Felsic sandstone, Sandstone	high early-strength ordinary Portland cement

Figure 4-13b Relative Reduction of the Elastic Modulus of Concrete and Mortar as a Function of Neutron Fluence (T < 100°C)

For the aluminous cement paste studied by Elleuch et al. [73], the reported reduction in E with neutron fluence (see Figure 4-14) was similar to the temperature-control samples. Thus, there may be little effect, if any, on E for cement paste, since Kelly et al. [88] did not observe a noticeable difference.

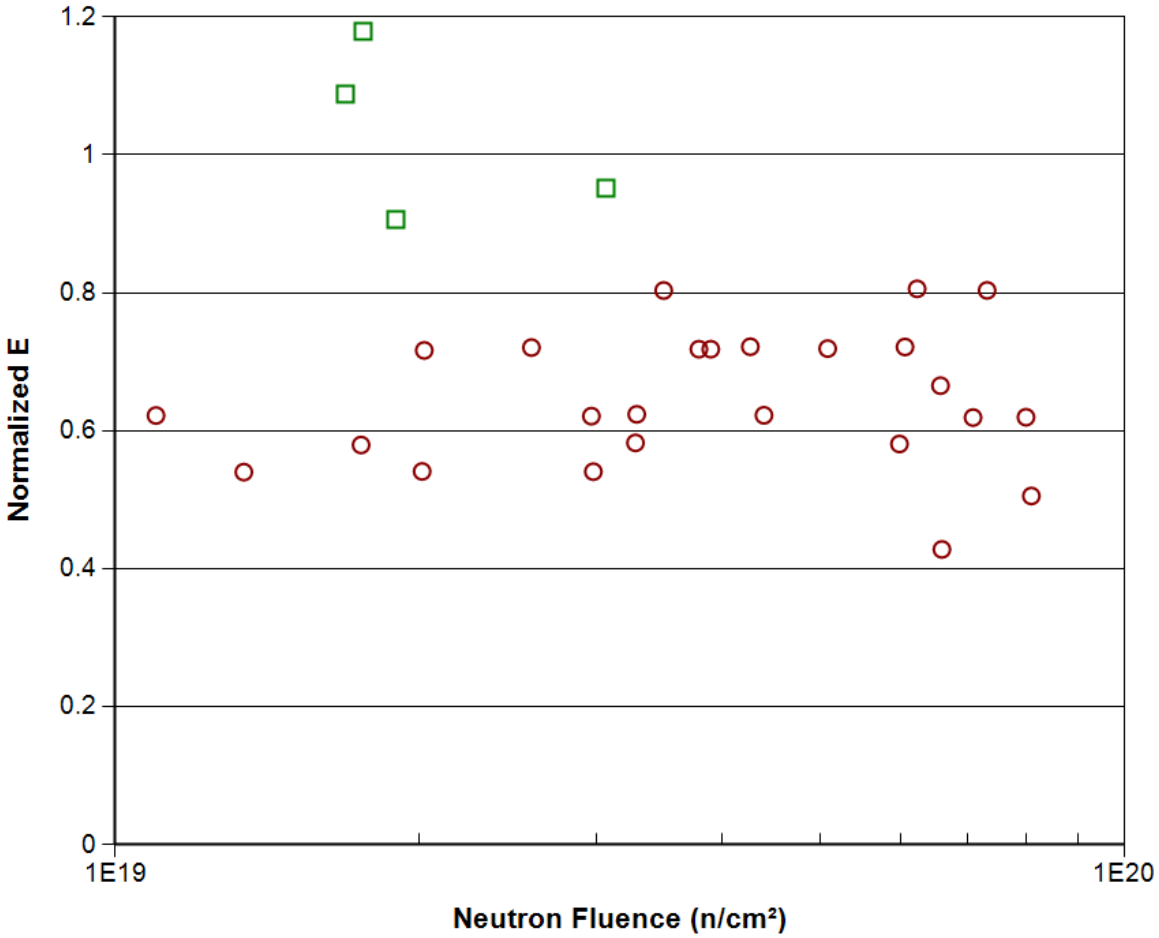

Sym	1st Author	Year	Energy Level	Max. T (C)	W/C Ratio	Material Name
○	Elleuch	1972	>1 MeV	280	0.25	Aluminous cement paste
□	Kelly	1969	Fast	50	0.36	Portland cement paste

Figure 4-14 Relative Elastic Modulus of Cement Paste after Neutron Irradiation (note: no significant difference was seen between irradiated samples and temperature-control samples in Elleuch et al. [73])

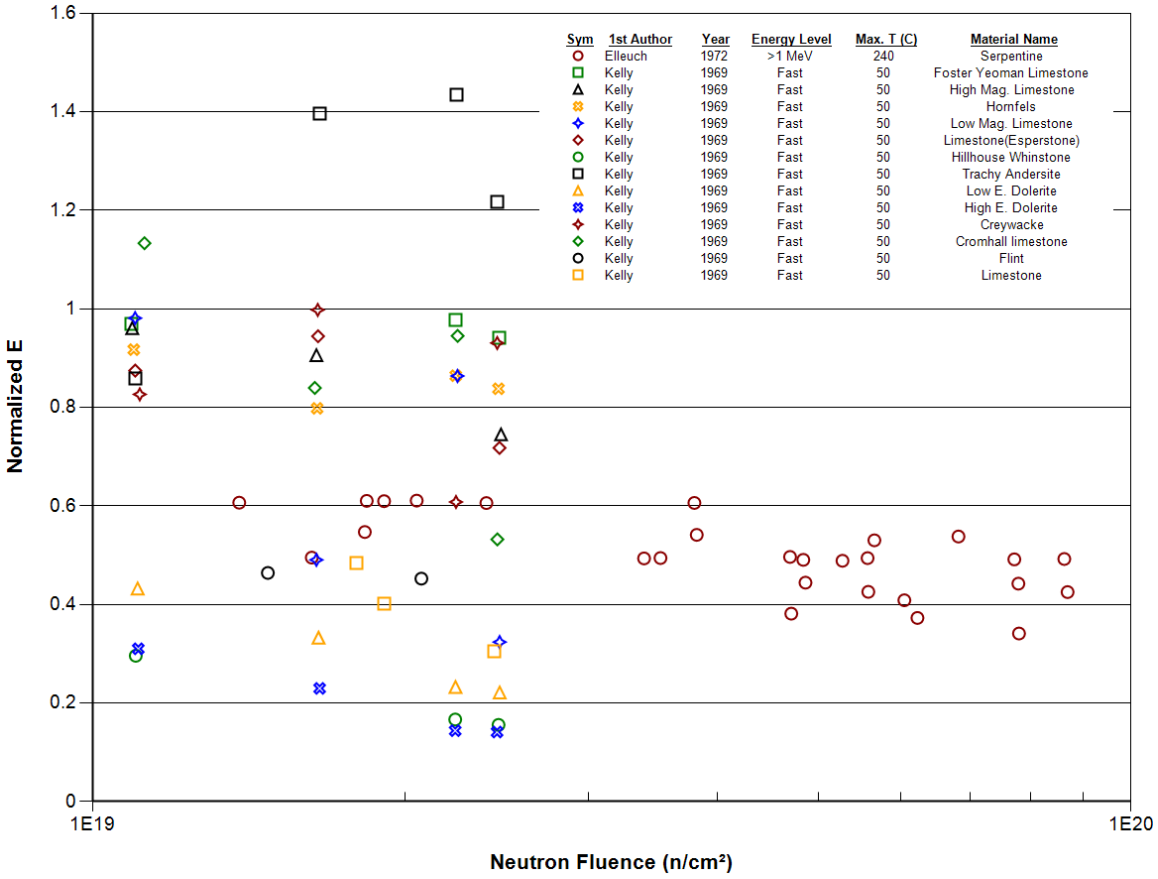

Figure 4-15 Relative Elastic Modulus of Aggregates after Neutron Irradiation

4.1.3.1 Water-to-Cement Ratio (w/c)

Concrete design parameters are important. The effect of the w/c is very consistent. A lower w/c appears to lead to a higher reduction of *E*, as shown in Figure 4-16. This is because a lower w/c results in a more densified concrete framework where it is more difficult to accommodate the volume change of aggregate, and thus results in more damage to the concrete. On the other hand, those data showing a reduction of *E* are from experiments with elevated temperatures that could also be responsible for some reduction in *E*. Elleuch et al. [73] mentioned that the elastic modulus was lower for the irradiated samples compared to the control samples at their elevated temperature, but did not specify whether any reduction in elasticity was due to the elevated temperature itself. Van der Schaaf [89] tested a wide range of specimens with varying sample sizes, compositions, and w/c. He referred to the sintered shale concrete (with a w/c of 1) as an insulating concrete. We are not aware of any U.S. NPPs that use sintered shale.

4.1.3.2 Aggregate Content

Figure 4-17 shows the effect of the aggregate weight fraction on *E*. The trend is similar to the one for the effect of aggregate weight fraction on compressive strength. With increasing aggregate weight fraction, as in the figure, the reduction increases and then decreases. The effect is quite significant, reaching about 80% reduction at the aggregate weight fraction of 74%, and then reversing back to the original value at the aggregate weight fraction of 79%. The

reason for this trend is not apparent. The effect of aggregate content on the modulus of elasticity of concrete cannot be well determined because the 80% reduction at 74% aggregate weight fraction could also be due to the high experimental temperature (up to 240°C). However, Elleuch et al. [73] noted that both concrete and aggregate sample tests revealed a decrease in the elastic modulus for the irradiated samples with respect to the temperature-control samples. More test data and improved modeling are required to reach any conclusion.

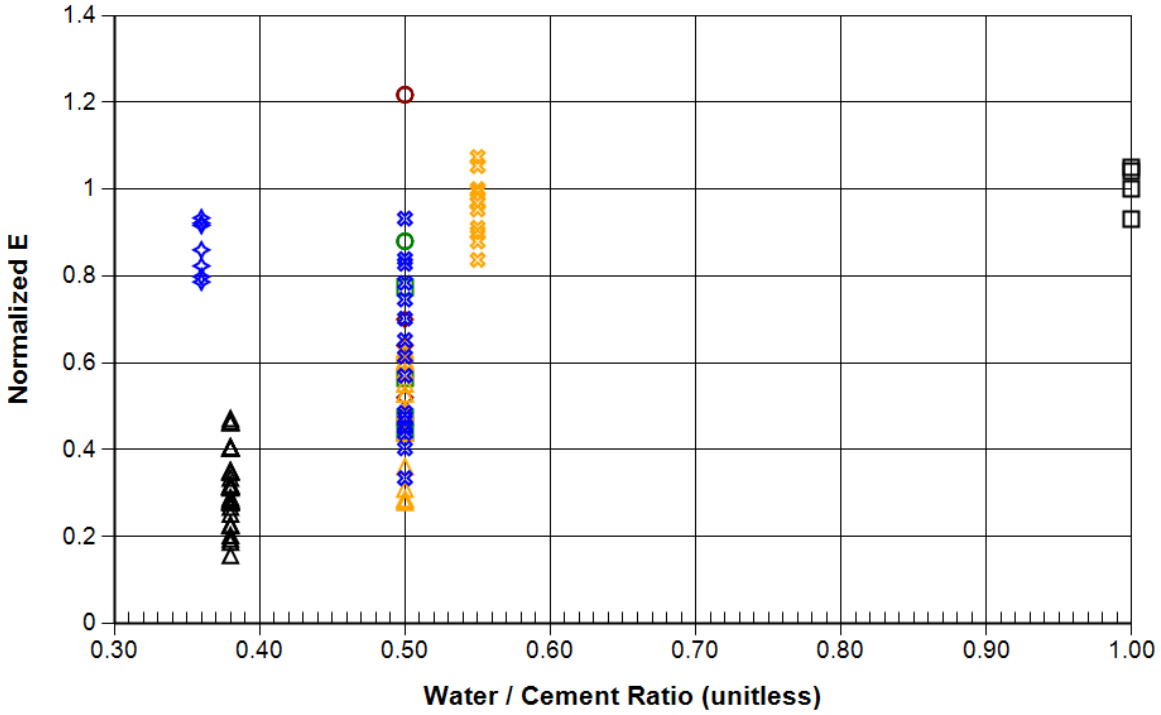

Sym	1st Author	Year	Energy Level	Max. T (C)	Ag. Frac.	W/C Ratio	Aggregate	Cement Type
○	Cristiani	1971	Fast	100 to 125	0.67	0.5	Limestone	Portland cement
□	Dubrovskii	1967	>0.8 MeV	150 to 350	0.76	0.5	Sandstone, Riversand(quartz)	Portland cement
△	Elleuch	1972	>1 MeV	240	0.74	0.38	Serpentine	Aluminous cement
✕	Fujiwara	2009	>0.1 MeV	50 to 56	0.79	0.55	Gravel, Sand	Cement
◇	Kelly	1969	Fast	50	0.67	0.36	Limestone	Portland cement
◇	Van der Schaaf	1967	Fast	200	N/A	0.5	Barite	Blastfurnace slag cement
○	Van der Schaaf	1967	Fast	200	N/A	0.5	Magnetite	Portland cement
□	Van der Schaaf	1967	Fast	200	N/A	1	Sintered shale	Portland cement
△	Maruyama	2017	>0.1 MeV	66 to 73	0.77	0.5	Thermally altered tuff, Sandstone	high early-strength ordinary Portland cement
✕	Maruyama	2017	>0.1 MeV	66 to 73	0.77	0.5	Felsic sandstone, Sandstone	high early-strength ordinary Portland cement

Figure 4-16 Effect of w/c on the Elastic Modulus of Concrete and Mortar (neutron fluence > 1 × 10^{18} n/cm^2)

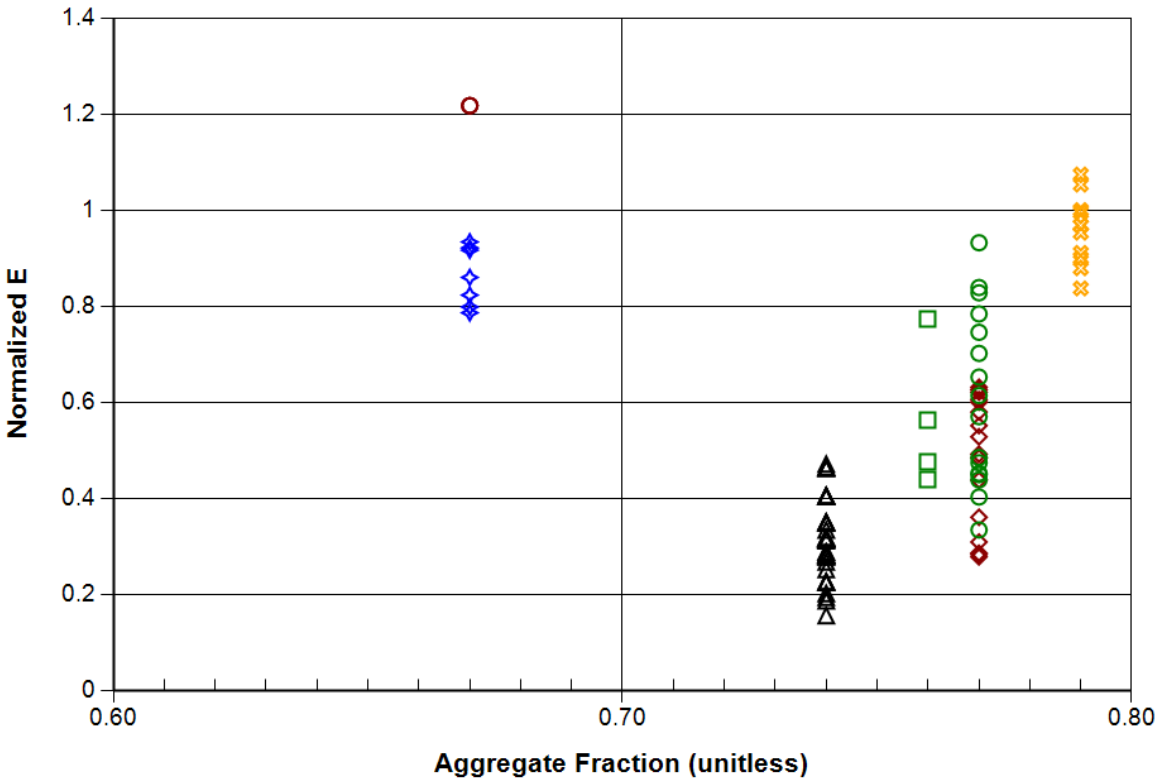

Sym	1st Author	Year	Energy Level	Max. T (C)	Ag. Frac.	W/C Ratio	Aggregate	Cement Type
○	Cristiani	1971	Fast	100 to 125	0.67	0.5	Limestone	Portland cement
□	Dubrovskii	1967	>0.8 MeV	150 to 350	0.76	0.5	Sandstone, Riversand(quartz)	Portland cement
△	Elleuch	1972	>1 MeV	240	0.74	0.38	Serpentine	Aluminous cement
⊠	Fujiwara	2009	>0.1 MeV	50 to 56	0.79	0.55	Gravel, Sand	Cement
✦	Kelly	1969	Fast	50	0.67	0.36	Limestone	Portland cement
◇	Maruyama	2017	>0.1 MeV	66 to 73	0.77	0.5	Thermally altered tuff, Sandstone	high early-strength ordinary Portland cement
○	Maruyama	2017	>0.1 MeV	66 to 73	0.77	0.5	Felsic sandstone, Sandstone	high early-strength ordinary Portland cement

Figure 4-17 Effect of Aggregate Fraction on the Elastic Modulus of Concrete and Mortar (neutron fluence > 1 × 10^{18} n/cm^2)

4.2 Gamma Irradiation Impacts

Limited studies are available on the gamma irradiation of concrete and its components. Much of this available information involves simultaneous neutron irradiation (i.e., tests conducted with a nuclear reactor as the radiation source, as presented in Section 4.1).

4.2.1 Compressive Strength

Figure 4-18 shows the effects of gamma-rays on the normalized compressive strength of concrete and mortar. Note that the compressive strength of concrete and mortar may start to decrease when the gamma dose is above 10^8 Gy. However, tests by Sommers [90], the only higher gamma dose experiments without the presence of neutron radiation, were conducted with the concrete samples underwater. Therefore, it is unclear whether similar results would be obtained in an air environment. Consistent with these results was the investigation of Kitsutaka and Matsuzawa [91] where they indicated that no apparent effect on the compressive strength

was found for concrete using ordinary Portland cement irradiated up to a gamma dose of 1.3×10^7 Gy. Maruyama et al. [66] observed a slight increase of compressive strength under gamma irradiation, for both concrete and cement paste, up to a dose of 2×10^8 Gy, which was attributed, in part, to gamma-induced carbonation. X-ray diffraction analysis showed the formation of three different crystalline forms of calcium carbonate ($CaCO_3$): aragonite, vaterite, and calcite [66]. They also observed little change in the compressive strength of aggregate up to a dose of 1×10^8 Gy.

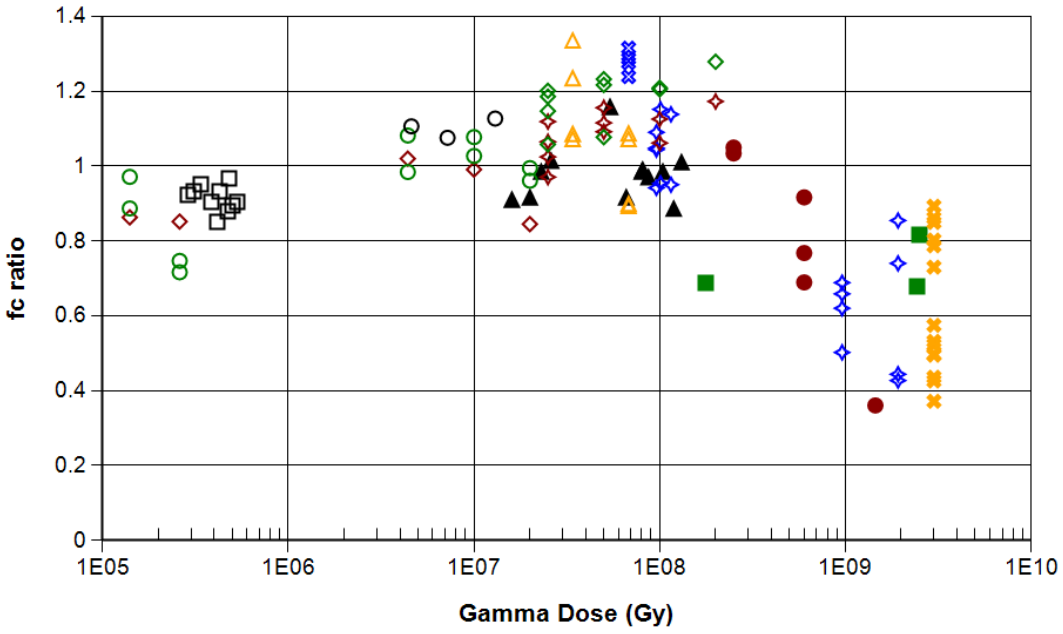

Sym	1st Author	Year	Energy Level	Max. T (C)	Ag. Frac.	W/C Ratio	Aggregate	Cement Type
●	Dubrovskii	1967	>0.8 MeV	50 to 350	0.76	0.5	Sandstone, Riversand(quartz)	Portland cement
■	Dubrovskii	1970	>0.8 MeV	100 to 400	0.8	1.01	Hematite	Portland cement
▲	Fujiwara	2009	>0.1 MeV	50 to 56	0.79	0.55	Gravel, Sand	Cement
✖	Pedersen	1971	Fast	80	0.68	0.4	Quartz	Portland cement
✦	Sommers	1969	N/A	24	0.8	0.46	Aggregate, Sand	Portland cement
◇	Soo	2001	N/A	10	0.65	0.485	Standard Ottawa sand	Portland cement(Type I)
○	Soo	2001	N/A	10	0.65 to 0.66	0.4 to 0.485	Standard Ottawa sand	Portland cement(Type V)
□	Sopko	2004	N/A	N/A	0.7	0.43	Siliceous gravel	Portland cement(CEM I 42,5R Mokra)
△	Alexander	1963	N/A	100	N/A	N/A	Heston sand	Portland cement
✖	Alexander	1963	N/A	100	N/A	N/A	Heston gravel	Portland cement
◆	Maruyama	2017	N/A	45	0.77	0.5	Thermally altered tuff, Sandstone	high early-strength ordinary Portland cement
◇	Maruyama	2017	N/A	45	0.77	0.5	Felsic sandstone, Sandstone	high early-strength ordinary Portland cement
○	Kitsutaka	2010	N/A	17	0.76	0.5	Crushed stone, Pit sand and crushed sand	ordinary Portland cement

Figure 4-18 Gamma Dose vs. Normalized fc' of Concrete and Mortar (neutron energy level indicated if neutron radiation present; solid symbol denotes presence of both gamma and neutron radiation)

Soo and Milian [92, 93] found a decrease in the compressive strength of Portland cement with time (independent of gamma irradiation rate) with total doses less than 1×10^7 Gy. There was some speculation that curing time had a role in the effects recorded [92].

Figure 4-19 shows the effect of aggregate weight fraction on normalized compressive strength of concrete and mortar under gamma irradiation. The effect of aggregate weight fraction does not appear to be significant relative to the gamma dose when considering those samples only exposed to gamma radiation. The results from the samples exposed to concurrent neutron radiation suggest that neutron effects dominate any gamma effects, as shown by the increase in impact with a reduction in aggregate fraction seen in Figure 4-7.

Figure 4-20 shows the effect of the w/c on the normalized compressive strength of concrete and mortar under gamma irradiation. The effect of w/c does not appear to be significant based on existing data.

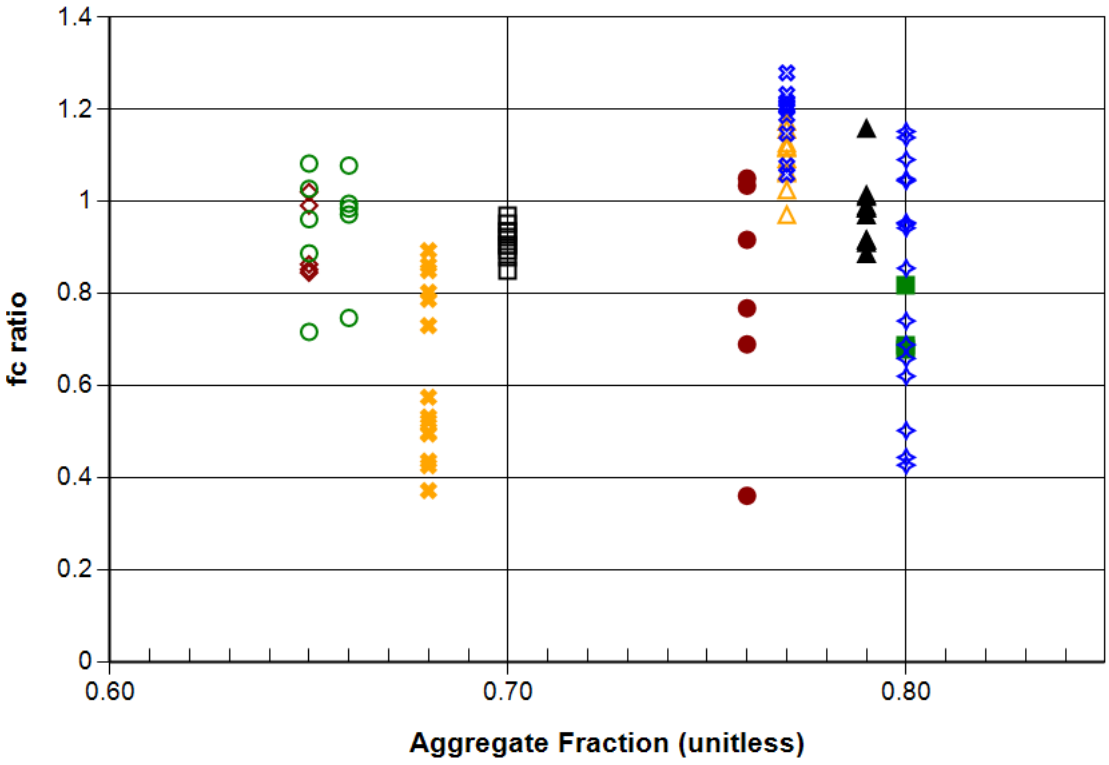

Sym	1st Author	Year	Energy Level	Max. T (C)	W/C Ratio	Aggregate	Cement Type
●	Dubrovskii	1967	>0.8 MeV	50 to 350	0.5	Sandstone, Riversand(quartz)	Portland cement
■	Dubrovskii	1970	>0.8 MeV	100 to 400	1.01	Hematite	Portland cement
▲	Fujiwara	2009	>0.1 MeV	50 to 56	0.55	Gravel, Sand	Cement
✖	Pedersen	1971	Fast	80	0.4	Quartz	Portland cement
✦	Sommers	1969	N/A	24	0.46	Aggregate, Sand	Portland cement
◇	Soo	1989	N/A	10	0.485	Standard Ottawa sand	Portland cement(Type I)
○	Soo	1989	N/A	10	0.4 to 0.485	Standard Ottawa sand	Portland cement(Type V)
□	Sopko	2004	N/A	N/A	0.43	Siliceous gravel	Portland cement(CEM I 42,5R Mokra)
△	Maruyama	2017	N/A	45	0.5	Thermally altered tuff, Sandstone	high early-strength ordinary Portland cement
✖	Maruyama	2017	N/A	45	0.5	Felsic sandstone, Sandstone	high early-strength ordinary Portland cement

Figure 4-19 Aggregate Fraction vs. Normalized fc' of Concrete and Mortar under Gamma Irradiation (neutron energy level indicated if neutron radiation present; solid symbol denotes presence of both gamma and neutron radiation)

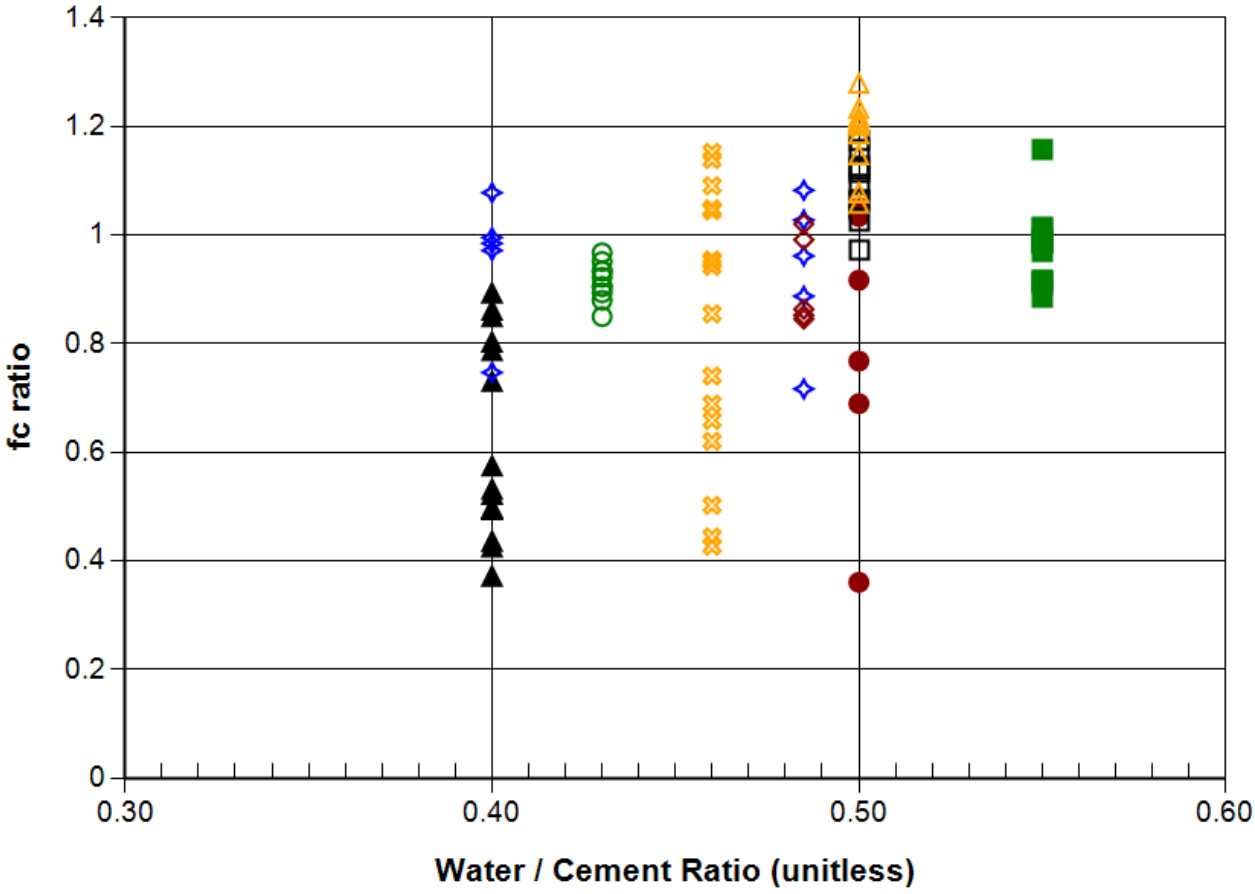

Sym	1st Author	Year	Energy Level	Max. T (C)	Ag. Frac.	Aggregate	Cement Type
●	Dubrovskii	1967	>0.8 MeV	50 to 350	0.76	Sandstone, Riversand(quartz)	Portland cement
■	Fujiwara	2009	>0.1 MeV	50 to 56	0.79	Gravel, Sand	Cement
▲	Pedersen	1971	Fast	80	0.68	Quartz	Portland cement
⊠	Sommers	1969	N/A	24	0.8	Aggregate, Sand	Portland cement
◈	Soo	1989	N/A	10	0.65 to 0.66	Standard Ottawa sand	Portland cement(Type V)
◇	Soo	1989	N/A	10	0.65	Standard Ottawa sand	Portland cement(Type I)
○	Sopko	2004	N/A	N/A	0.7	Siliceous gravel	Portland cement(CEM I 42,5R Mokra)
□	Maruyama	2017	N/A	45	0.77	Thermally altered tuff, Sandstone	high early-strength ordinary Portland cement
△	Maruyama	2017	N/A	45	0.77	Felsic sandstone, Sandstone	high early-strength ordinary Portland cement

Figure 4-20 W/c vs. Normalized fc' of Concrete and Mortar under Gamma Irradiation (neutron energy level indicated if neutron radiation present; solid symbol denotes presence of both gamma and neutron radiation)

4.2.2 Tensile Strength

Figure 4-21 shows the effect of gamma-rays on the normalized tensile strength of concrete and mortar. The effect of gamma-rays does not appear to be significant based on existing data.

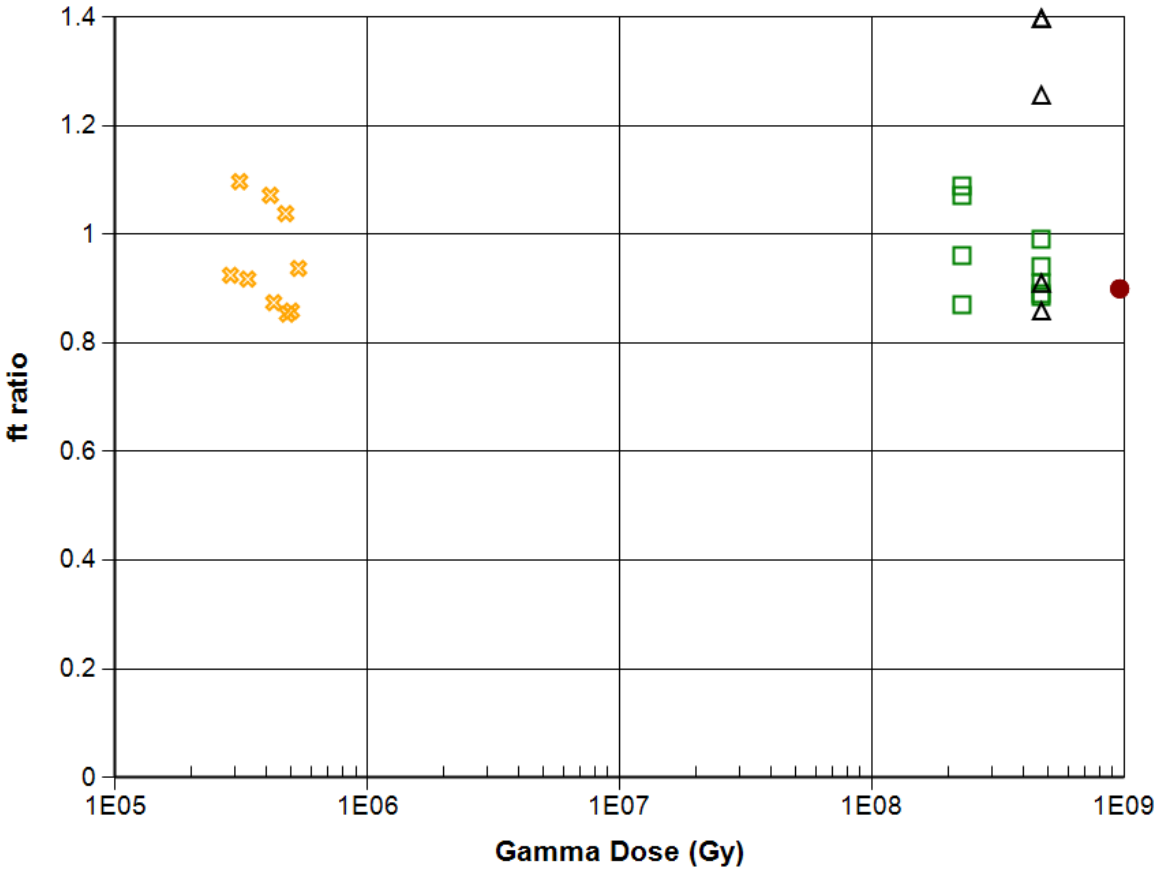

Sym	1st Author	Year	Energy Level	Max. T (C)	Ag. Frac.	W/C Ratio	Aggregate	Cement Type
●	Cristiani	1971	Fast	100 to 125	0.67	0.5	Limestone	Portland cement
□	Kelly	1969	N/A	20	0.67	0.36	Limestone	Portland cement
△	Kelly	1969	N/A	20	0.67	0.36	Flint	Portland cement
⊠	Sopko	2004	N/A	N/A	0.7	0.43	Siliceous gravel	Portland cement(CEM I 42,5R Mokra)

Figure 4-21 Gamma Dose vs. Normalized Tensile Strength of Concrete and Mortar (neutron energy level indicated if neutron radiation present; solid symbol denotes presence of both gamma and neutron radiation)

4.2.3 Modulus of Elasticity

Figure 4-22 shows the effects of gamma-rays on the normalized modulus of elasticity of concrete and mortar. Note that the normalized modulus of elasticity of concrete and mortar starts to decrease when the gamma dose is above 10^8 Gy, which is similar to the trend for the normalized compressive strength. However, this trend is defined by experiments that included neutron irradiation, and the results from Maruyama et al. [66] up to a dose of 2×10^8 Gy show that Young's modulus was unchanged by gamma irradiation.

The effect of aggregate weight fraction and w/c on the modulus of elasticity under gamma irradiation do not appear to be significant. Figure 4-23 shows the effect of aggregate weight fraction on the normalized modulus of elasticity of concrete and mortar. Figure 4-24 shows the effect of the w/c on the normalized modulus of elasticity of concrete and mortar.

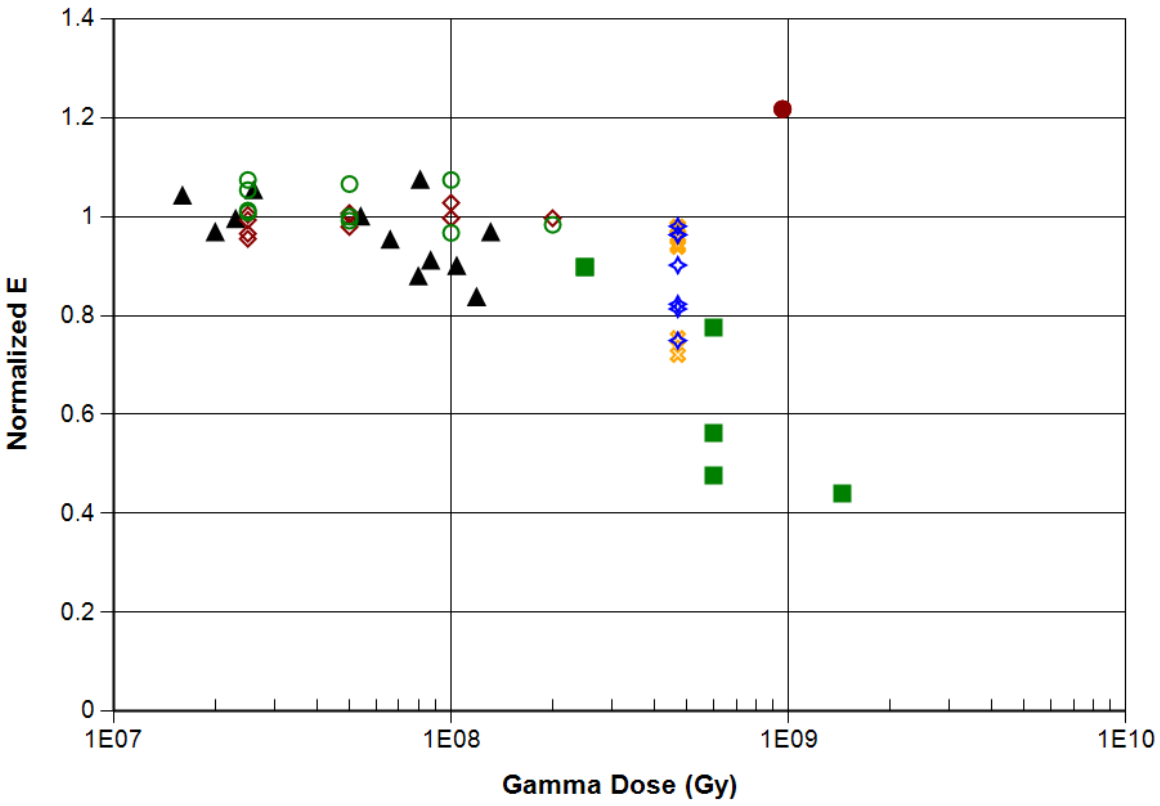

Sym	1st Author	Year	Energy Level	Max. T (C)	Ag. Frac.	W/C Ratio	Aggregate	Cement Type
●	Cristiani	1971	Fast	100 to 125	0.67	0.5	Limestone	Portland cement
■	Dubrovskii	1967	>0.8 MeV	50 to 350	0.76	0.5	Sandstone, Riversand(quartz)	Portland cement
▲	Fujiwara	2009	>0.1 MeV	50 to 56	0.79	0.55	Gravel, Sand	Cement
⊠	Kelly	1969	N/A	20	0.67	0.36	Flint	Portland cement
◈	Kelly	1969	N/A	20	0.67	0.36	Limestone	Portland cement
◇	Maruyama	2017	N/A	45	0.77	0.5	Thermally altered tuff, Sandstone	high early-strength ordinary Portland cement
○	Maruyama	2017	N/A	45	0.77	0.5	Felsic sandstone, Sandstone	high early-strength ordinary Portland cement

Figure 4-22 Gamma Dose vs. Normalized Modulus of Elasticity of Concrete and Mortar (neutron energy level indicated if neutron radiation present; solid symbol denotes presence of both gamma and neutron radiation)

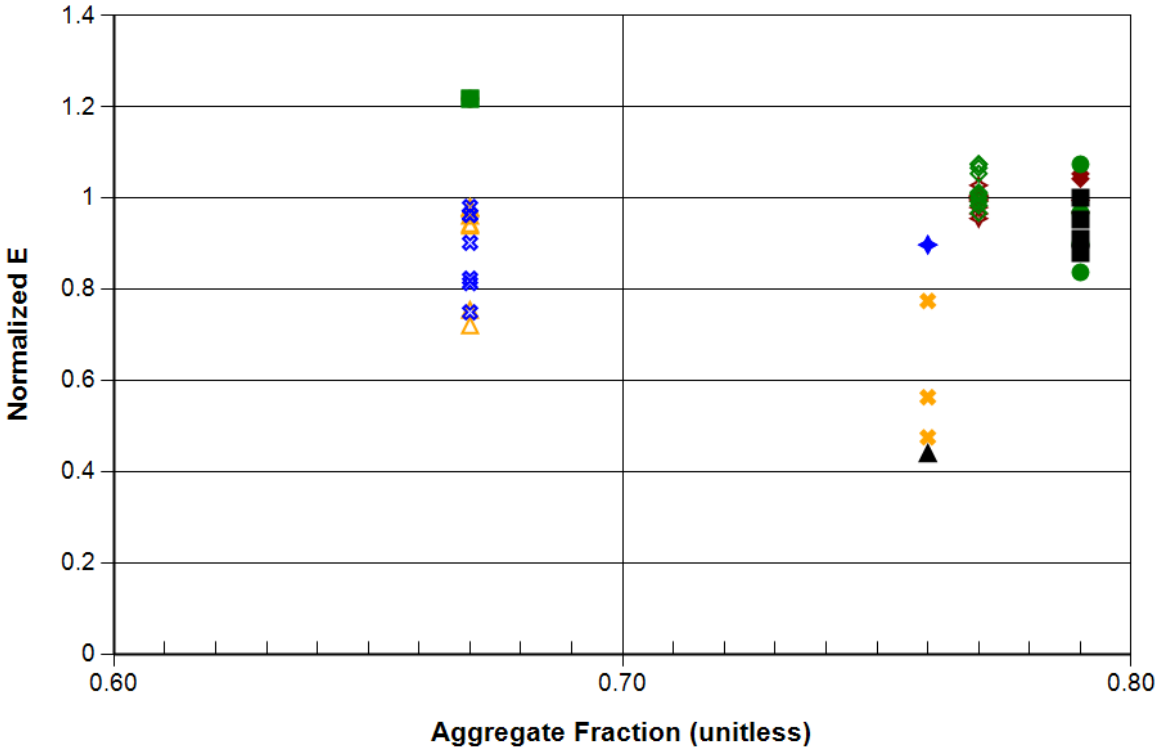

Sym	1st Author	Year	Energy Level	Max. T (C)	W/C Ratio	Aggregate	Cement Type
●	Cristiani	1971	Fast	100	0.5	Limestone	Portland cement
■	Cristiani	1971	Fast	125	0.5	Limestone	Portland cement
▲	Dubrovskii	1967	>0.8 MeV	350	0.5	Sandstone, Riversand(quartz)	Portland cement
✖	Dubrovskii	1967	>0.8 MeV	150	0.5	Sandstone, Riversand(quartz)	Portland cement
✦	Dubrovskii	1967	>0.8 MeV	50	0.5	Sandstone, Riversand(quartz)	Portland cement
◆	Fujiwara	2009	>0.1 MeV	56.2	0.55	Gravel, Sand	Cement
●	Fujiwara	2009	>0.1 MeV	50.9	0.55	Gravel, Sand	Cement
■	Fujiwara	2009	>0.1 MeV	50.1	0.55	Gravel, Sand	Cement
△	Kelly	1969	N/A	20	0.36	Flint	Portland cement
✖	Kelly	1969	N/A	20	0.36	Limestone	Portland cement
◆	Maruyama	2017	N/A	45	0.5	Thermally altered tuff, Sandstone	high early-strength ordinary Portland cement
◇	Maruyama	2017	N/A	45	0.5	Felsic sandstone, Sandstone	high early-strength ordinary Portland cement

Figure 4-23 Aggregate Fraction vs. Normalized *E* of Concrete and Mortar under Gamma Irradiation (neutron energy level indicated if neutron radiation present; solid symbol denotes presence of both gamma and neutron radiation)

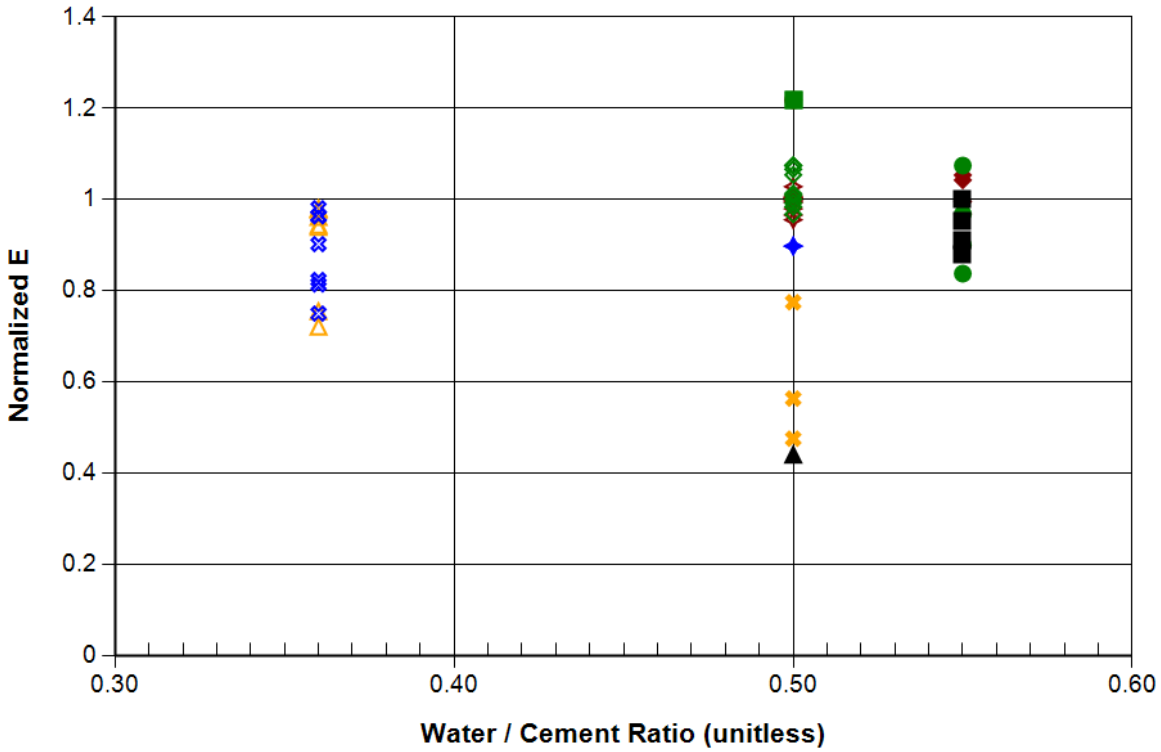

Sym	1st Author	Year	Energy Level	Max. T (C)	Ag. Frac.	Aggregate	Cement Type
●	Cristiani	1971	Fast	100	0.67	Limestone	Portland cement
■	Cristiani	1971	Fast	125	0.67	Limestone	Portland cement
▲	Dubrovskii	1967	>0.8 MeV	350	0.76	Sandstone, Riversand(quartz)	Portland cement
✱	Dubrovskii	1967	>0.8 MeV	150	0.76	Sandstone, Riversand(quartz)	Portland cement
✦	Dubrovskii	1967	>0.8 MeV	50	0.76	Sandstone, Riversand(quartz)	Portland cement
◆	Fujiwara	2009	>0.1 MeV	56.2	0.79	Gravel, Sand	Cement
●	Fujiwara	2009	>0.1 MeV	50.9	0.79	Gravel, Sand	Cement
■	Fujiwara	2009	>0.1 MeV	50.1	0.79	Gravel, Sand	Cement
△	Kelly	1969	N/A	20	0.67	Flint	Portland cement
✖	Kelly	1969	N/A	20	0.67	Limestone	Portland cement
✧	Maruyama	2017	N/A	45	0.77	Thermally altered tuff, Sandstone	high early-strength ordinary Portland cement
◇	Maruyama	2017	N/A	45	0.77	Felsic sandstone, Sandstone	high early-strength ordinary Portland cement

Figure 4-24 W/c vs. Normalized *E* of Concrete and Mortar under Gamma Irradiation (neutron energy level indicated if neutron radiation present; solid symbol denotes presence of both gamma and neutron radiation)

4.2.4 Summary

The effects of gamma irradiation on the important properties of concrete and mortar are indeterminate. Data on compressive strength and the modulus of elasticity include neutron irradiation that could be responsible for the relative decreases observed in concrete with increasing gamma dose. The mechanical properties of cement paste do not appear to change significantly with gamma irradiation, despite the weight loss and micro-crack formation cement paste experiences due to radiolysis. The concurrent formation of calcium carbonate may account for this behavior. Additional data are needed for gamma doses approaching 10^9 Gy and beyond without companion neutron radiation. The limited data and uncertainties (see

Section 1.4) are not sufficient to draw any definite conclusions on the impact gamma irradiation has on concrete, or any synergistic impacts with neutron radiation or temperature.

4.3 Synergistic Effects

4.3.1 Thermal Impacts

4.3.1.1 Unirradiated Concrete

In 2010, Naus [14] published a comprehensive review of concrete subjected to elevated temperatures. In the temperature range from room temperature to 200°C, a dip in the compressive strength is observed with a minimum just below 100°C, as reported by Blundell et al. [94] and shown in Figure 4-25. The same behavior of the tensile strength, slightly shifted to lower temperatures (Figure 4-26), was also reported, but the relative tensile strength does not recover to the same extent as the compressive strength before decreasing at higher temperatures. Naus [14] indicated that the compressive strength decrease between about 20°C and 120°C "is attributable to thermal swelling of the physically bound water that causes disjoint pressures. From 120°C to about 300°C, there is a regain of compressive strength that is generally attributed to greater van der Waal's forces as a result of the cement gel layers moving closer to each other during heating."

A review of the literature suggests that these relative strength versus temperature characteristics are generally independent of the type of cement, aggregate size, heating rate, and the w/c [14]. William et al. [52] noted that the type of aggregate has an influence that tends to disappear at temperatures above 200°C.

As shown in Figure 4-27, a similar dip in the relative bond strength of concrete with mild steel reinforcement (rebar) between room temperature and 100°C was indicated by Sullivan [95] as summarized by Naus [14]. Thus, an operating temperature of 65°C in the reactor cavity falls in the range where concrete performance is degraded by 10 to 20% or more without accounting for radiation impacts. However, there is not enough data on irradiated samples at this time to draw any comparisons.

In a later study, Komonen and Penttala [96] investigated the properties of normal Portland cement (w/c = 0.32) subject to temperatures from 20 to 1,000°C. They observed a similar dip in compressive strength in the range of 50 to 120°C, with a minimum near 100°C, recovering by about 200°C. In this case, the minimum for the cement paste is shifted to slightly higher temperatures than that for observed for concrete, as discussed above. The decrease in compressive strength was attributed to larger pore radii due to water evaporation at the attainment of 50°C, with a clear coarsening of the pore structure by 100°C; the coarsening was potentially caused by the decrystallization of ettringite [96].

Rani and Santhanam [97] studied the effect of temperatures under 100°C on a concrete mix composed of ordinary Portland cement with river sand as a fine aggregate and crushed granite as the coarse aggregate. In contrast to the previously reported results, the compressive strengths of concrete samples heated at temperatures of 65°C, 75°C, and 90°C were found to approach the same slightly elevated value compared to the control sample after a test period of 540 days. This could be due to the confining effect of the partially saturated pores in cement paste, as explained in the study. However, they observed a decrease in the modulus of elasticity for samples held at all three temperatures.

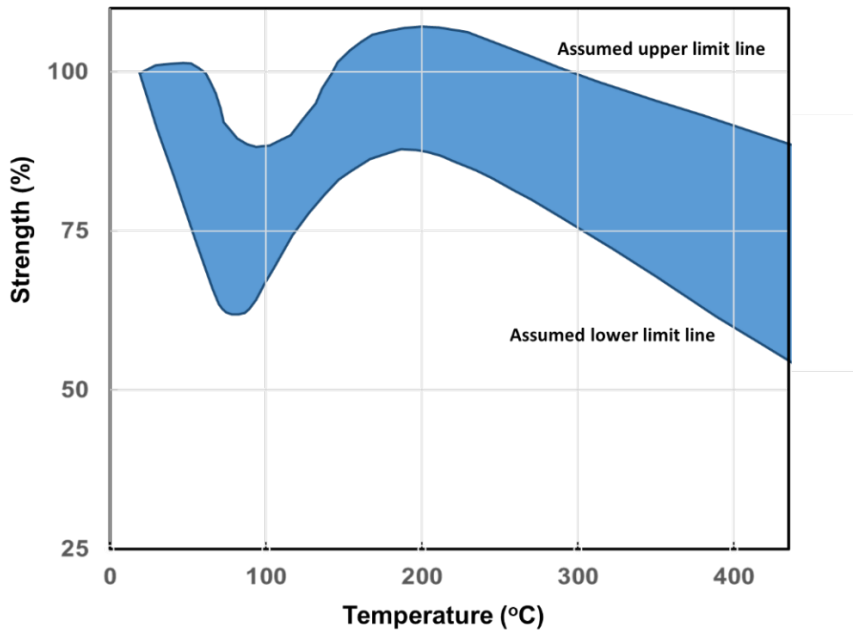

Figure 4-25 Comparison of the Effect of Elevated Temperature on the Compressive Strength of Concretes Fabricated Using Different Types of Conventional Aggregate Materials (Data from Blundell et al. [94] as referenced in Naus [14])

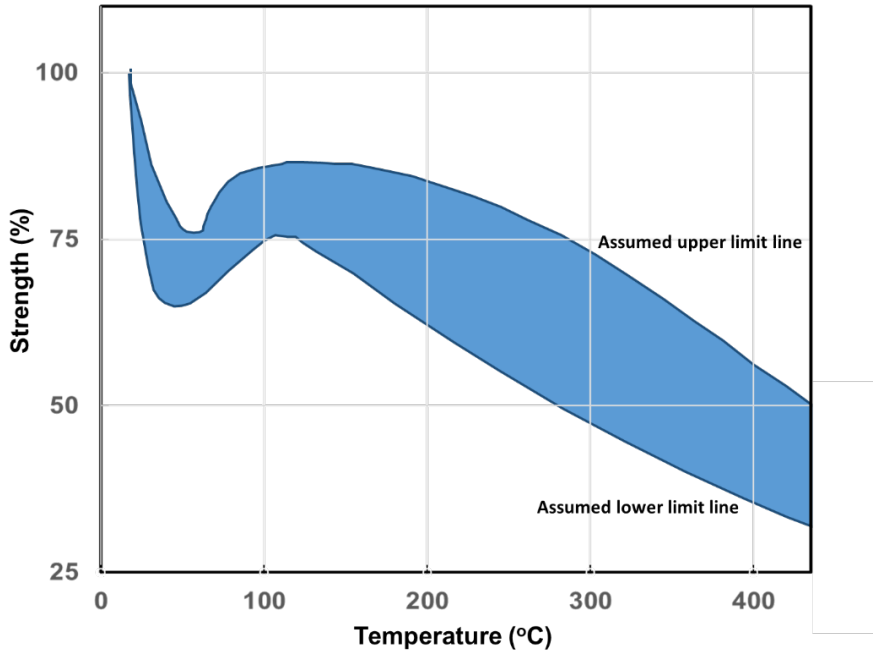

Figure 4-26 Comparison of the Effect of Elevated Temperature on the Tensile Strength of Concretes Fabricated Using Different Types of Conventional Aggregate Materials (Data from Blundell et al. [94] as referenced in Naus [14])

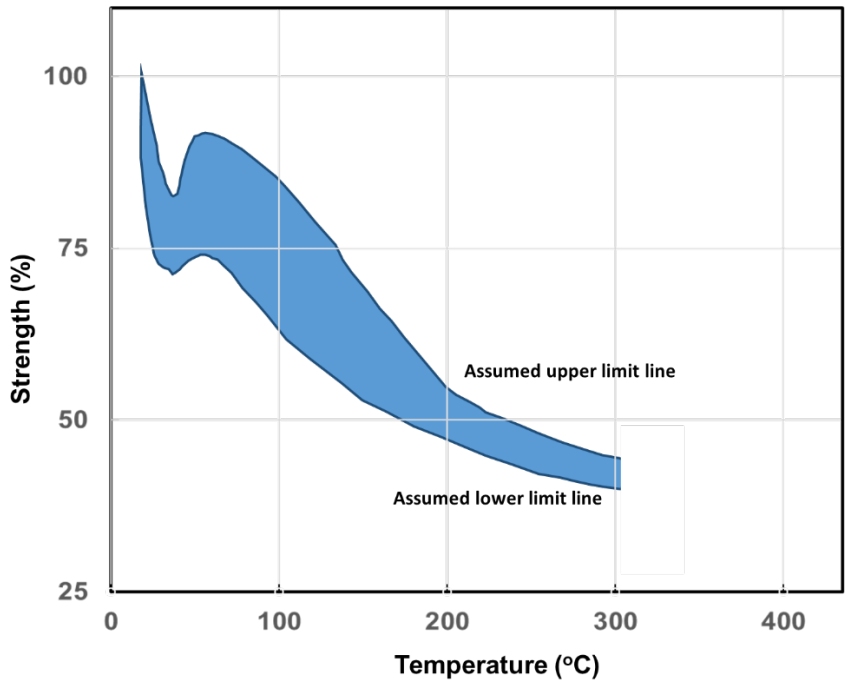

Figure 4-27 Comparison of the Effect of Elevated Temperature on the Relative Bond Strengths of Mild Steel to Concretes Fabricated Using Different Types of Conventional Aggregate Materials (Data from Sullivan [95] as referenced in Naus [14])

Similar to past studies, Kakae et al. [98] investigated how a number of different concrete compositions respond to heat. For a concrete composed of ordinary Portland cement and sandstone aggregate (w/c = 0.55), there was little change in compressive strength at 100°C compared to room temperature, but there was a significant drop of almost 40% in the elastic modulus. However, no samples were studied at intermediate temperatures.

4.3.1.2 Compressive Strength

Figure 4-28 shows the effect of thermal expansion on the compressive strength of neutron irradiated concrete. There is a very clear correlation between temperature and the mechanical properties of concrete and mortar: high environmental temperature can result in a significant reduction of mechanical properties at a high neutron irradiation level (> 1×10^{18} n/cm^2). Note that the absolute compressive strength reduction in Figure 4-28 is due to the combined effects of neutron radiation and elevated temperature. It is difficult to distinguish between the two effects through any theoretical or numerical modeling (i.e., whether they are independent or synergistic) because many experimental radiation studies in the literature did not have a control group for the temperature effect. In order to be consistent, the original properties for all samples (before irradiation testing) listed in our data collection were measured under normal ambient temperature instead of the testing temperatures. At a higher temperature, the difference in the thermal strains of the two phases becomes larger, which leads to higher long-term damage.

This observation is reinforced by information from thermal testing. As shown in Figure 4-29, a compilation of experimental data from thermal treatment tests on ordinary Portland cement

concrete (no radiation exposure) shows a clear drop in relative compressive strength above 300°C. There is quite a bit of scatter in the 100°C range, which can be attributed, in part, to differences in final preparation treatments and initial moisture contents. These results are consistent with data that show a dip in compressive strength between about 50 and 150°C (Figure 2.80 in Naus [14]; see also Schneider [99]) in some cases. Overall, the relative compressive strength is near 0.5 by the time 500°C is reached for the irradiated (Figure 4-28) and non-irradiated samples (Figure 4-29).

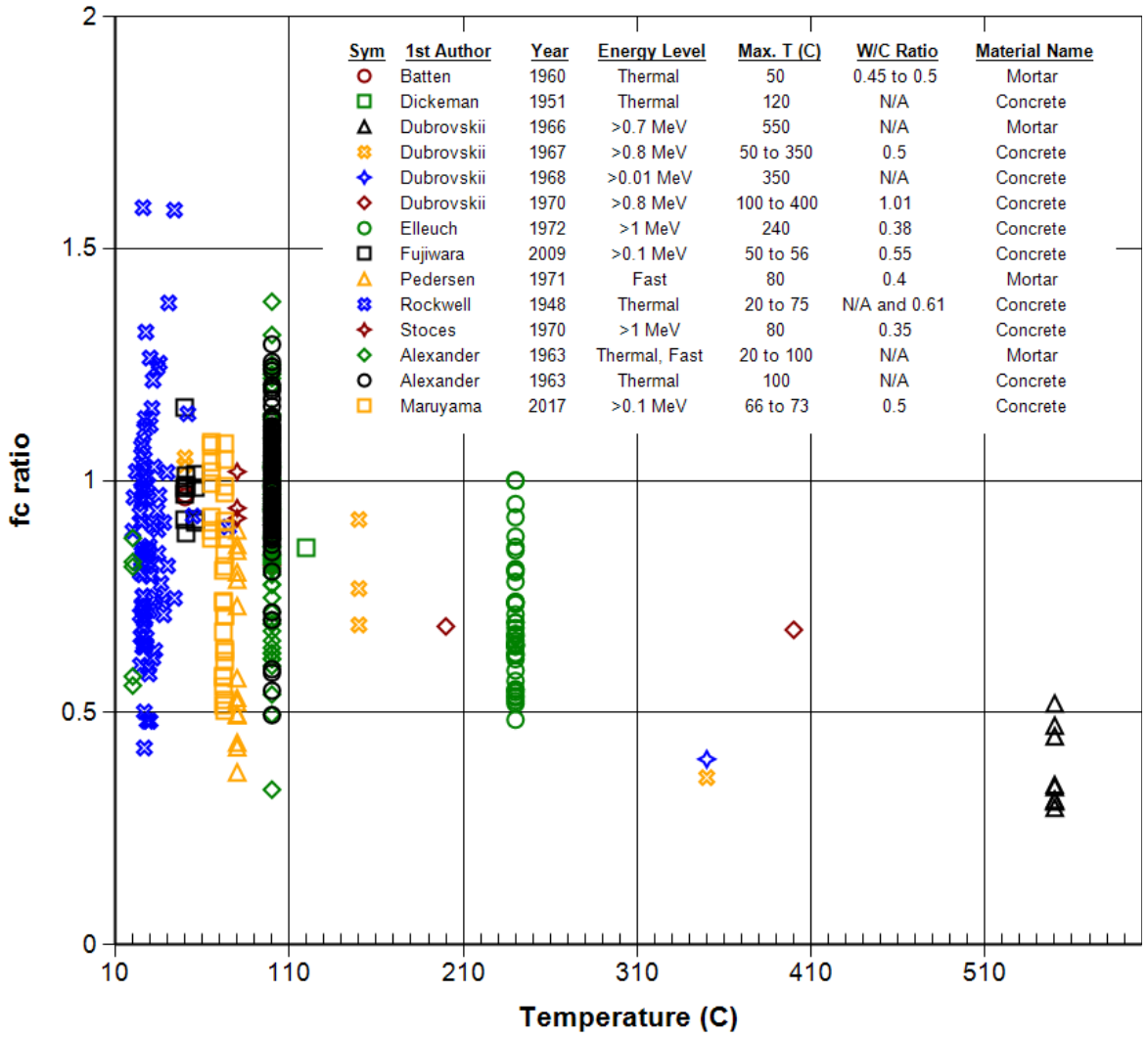

Figure 4-28 Effect of Temperature and Neutron Irradiation on the Compressive Strength of Concrete and Mortar (neutron fluence > 1 × 10^{18} n/cm^2)

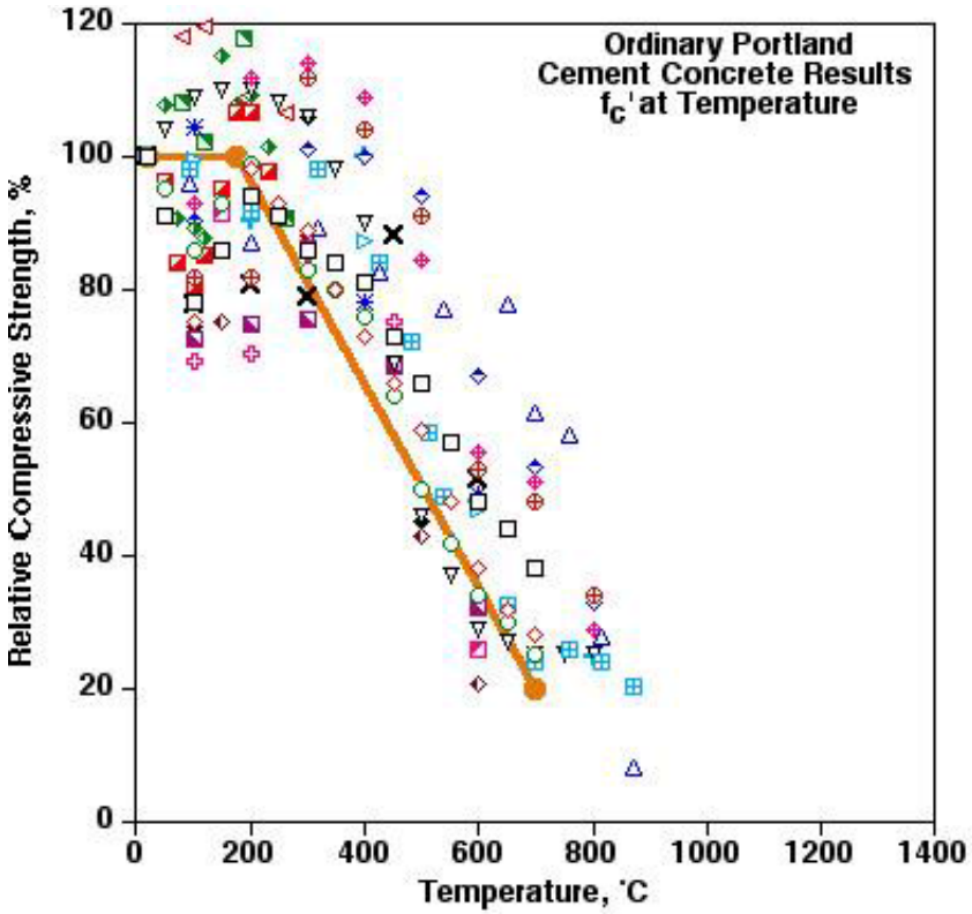

Figure 4-29 Effect of Temperature on the Compressive Strength of Portland Cement Concrete (no radiation) (Source: Naus [14], Figure 2.86)

This decrease in concrete compressive strength with an increase in temperature is consistent with studies on the effect of temperature on the mechanical properties of concrete in the absence of radiation [87]. Thus, although increasing temperature is expected to result in reduced compressive strength for concrete as a whole, the results by Elleuch et al. [73] suggest that the reduction is due to the aggregate–cement paste mismatch at a temperature of 240°C, as discussed above. For lower temperatures (<100°C), there is no phase transformation involved and the decrease of the compressive strength should mainly be due to the mismatch between the deformations of hardened cement paste and the aggregate, and the subsequent damage. When concretes are exposed to elevated temperatures (>100°C), the change of concrete properties results from the mismatch, and from the phase transformations in hardened cement paste and the deterioration of the cement paste–aggregate interface [100, 101].

4.3.1.3 Tensile Strength

Figure 4-30 shows the effect of temperature on the tensile strength of concrete and mortar, which is similar to the trend shown in Figure 4-28 for compressive strength. One can see a very clear correlation between temperature and the tensile strength of concrete and mortar. The downward trend as a function of temperature (shown in Figure 4-30) is mainly due to the difference in the thermal expansion between aggregate and cement paste, with some spread

due to neutron irradiation. At a higher temperature, the difference in the thermal strains of the two phases becomes larger, which leads to higher long-term damage. Similar to compressive strength, the tensile strength reduction in the figure is due to the combined effect of neutron radiation and elevated temperature. Combining the results from Figures 4-28 and 4-30, we can conclude that high environmental temperatures can significantly reduce mechanical properties at a high neutron irradiation level.

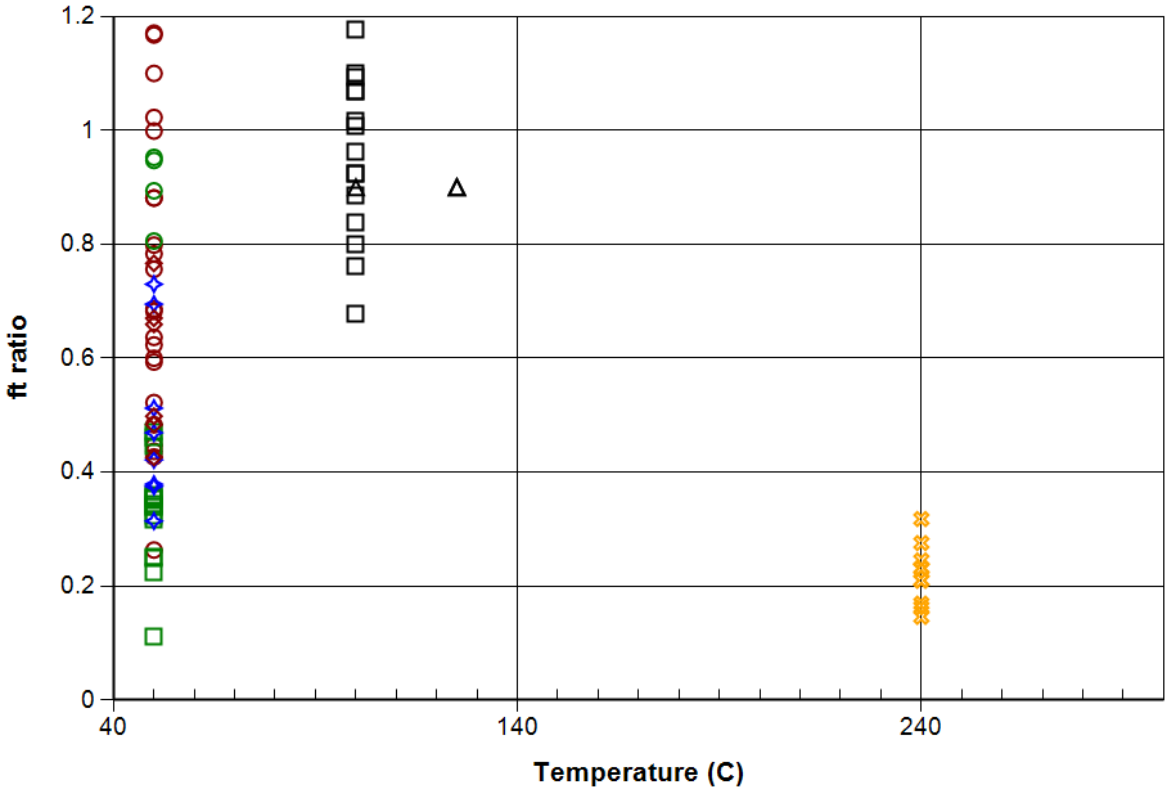

Sym	1st Author	Year	Energy Level	Ag. Frac.	W/C Ratio	Aggregate	Cement Type
○	Batten	1960	Thermal	0.67 to 0.84	0.45 to 0.5	Riversand	Portland cement
□	Batten	1960	Thermal	0.84	0.5	Riversand	Aluminous cement
△	Cristiani	1971	Fast	0.67	0.5	Limestone	Portland cement
✕	Elleuch	1972	>1 MeV	0.74	0.38	Serpentine	Aluminous cement
◇	Kelly	1969	Fast	0.67	0.36	Flint	Portland cement
◇	Kelly	1969	Fast	0.67	0.36	Limestone	Portland cement
○	Kelly	1969	Fast	N/A	N/A	Light weight rock, Sand	Portland cement
□	Alexander	1963	Thermal	N/A	N/A	Heston sand	Portland cement

Figure 4-30 Effect of Temperature (°C) on the Tensile Strength of Concrete and Mortar (neutron fluence > 1 × 10^{18} n/cm^2)

4.3.1.4 Elastic Modulus

The effects of temperature on *E* of irradiated concrete and mortar, cement paste, and aggregate are shown in Figures 4-31 through 4-33. The general trends shown by the test data are that the elastic modulus of concrete and mortar decreases significantly by temperature under a high level of neutron irradiation. The rate of reduction correlates nearly linearly with temperature. However, in Figure 4-31, two sets of data above 300°C show a different trend. One of them

used liquid glass [102] and the other one used normal Portland cement [74, 103]. The test data on cement paste and aggregate are very limited, and thus not conclusive.

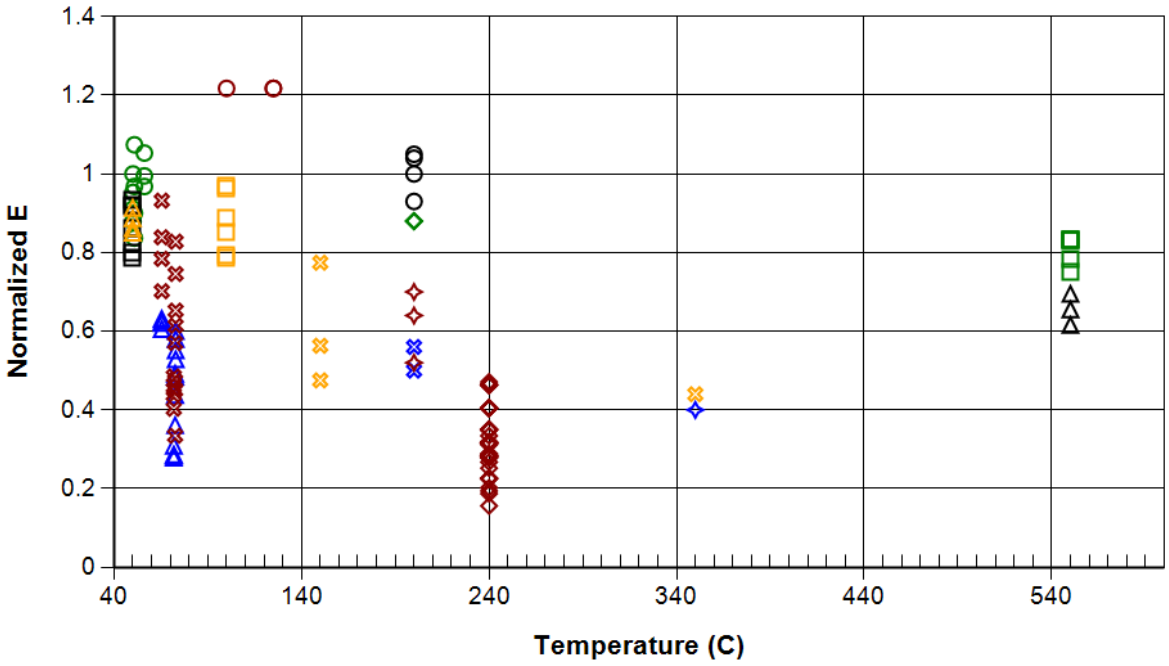

Sym	1st Author	Year	Energy Level	Ag. Frac.	W/C Ratio	Aggregate	Cement Type
○	Cristiani	1971	Fast	0.67	0.5	Limestone	Portland cement
□	Dubrovskii	1966	>0.7 MeV	N/A	N/A	Chromite	Portland cement
△	Dubrovskii	1966	>0.7 MeV	N/A	N/A	Chromite	Liquid glass
✕	Dubrovskii	1967	>0.8 MeV	0.76	0.5	Sandstone, Riversand(quartz)	Portland cement
◇	Dubrovskii	1968	>0.01 MeV	N/A	N/A	Serpentine	Portland cement
◇	Elleuch	1972	>1 MeV	0.74	0.38	Serpentine	Aluminous cement
○	Fujiwara	2009	>0.1 MeV	0.79	0.55	Gravel, Sand	Cement
□	Kelly	1969	Fast	0.67	0.36	Limestone	Portland cement
△	Kelly	1969	Fast	N/A	N/A	Light weight rock, Sand	Portland cement
✕	Van der Schaaf	1967	Fast	N/A	N/A	Barite	Portland cement
◇	Van der Schaaf	1967	Fast	N/A	0.5	Barite	Blastfurnace slag cement
◇	Van der Schaaf	1967	Fast	N/A	0.5	Magnetite	Portland cement
○	Van der Schaaf	1967	Fast	N/A	1	Sintered shale	Portland cement
□	Alexander	1963	Thermal	N/A	N/A	Heston gravel	Portland cement
△	Maruyama	2017	>0.1 MeV	0.77	0.5	Thermally altered tuff, Sandstone	high early-strength ordinary Portland cement
✕	Maruyama	2017	>0.1 MeV	0.77	0.5	Felsic sandstone, Sandstone	high early-strength ordinary Portland cement

Figure 4-31 Effect of Temperature (°C) on the Elastic Modulus of Concrete and Mortar (neutron fluence > 1 × 10^{18} n/cm^2)

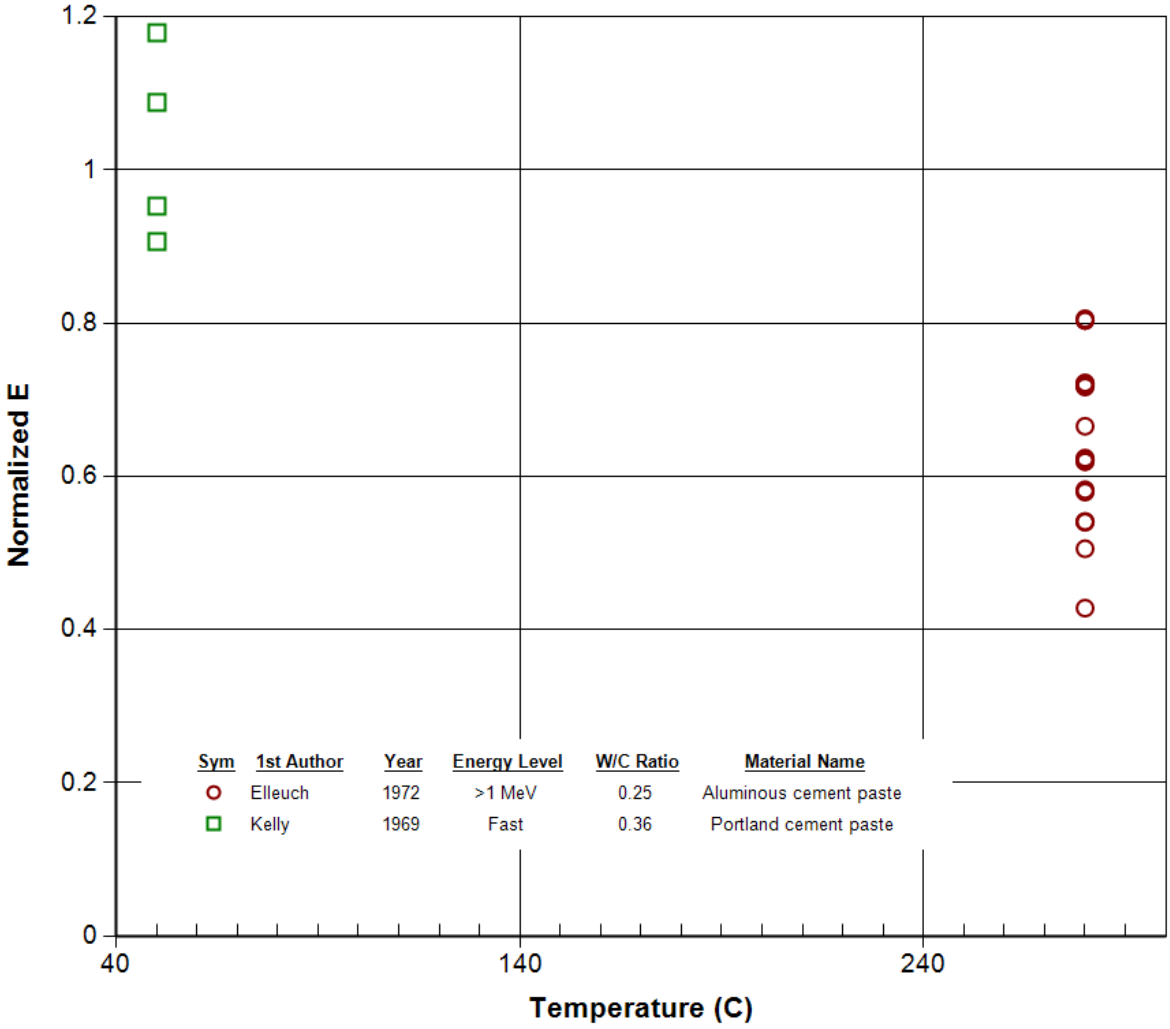

Figure 4-32 Effect of Temperature (°C) on the Elastic Modulus of Cement Paste

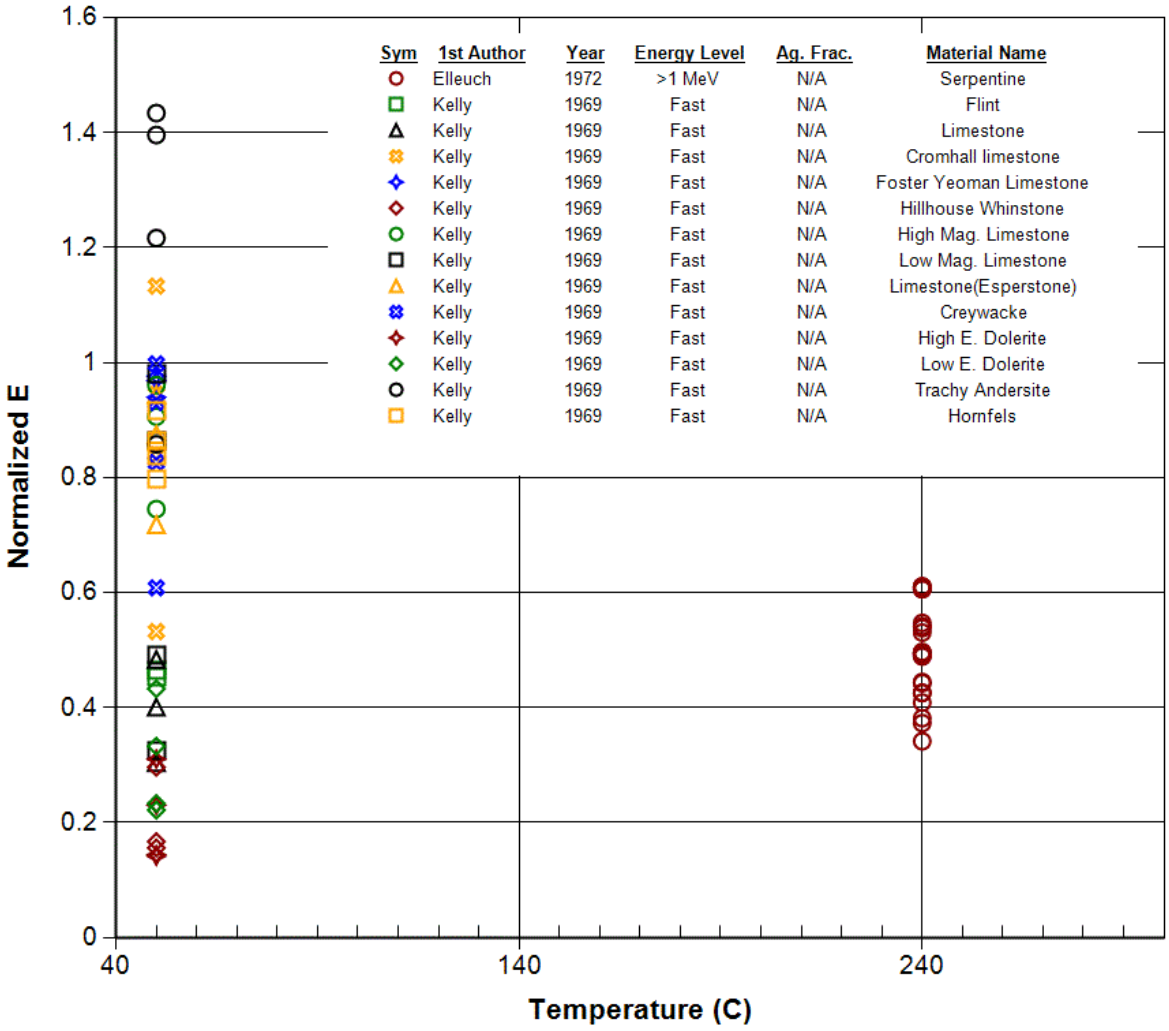

Figure 4-33 Effect of Temperature (°C) on the Elastic Modulus of Aggregates

4.3.1.5 Gamma Irradiation

Figure 4-34 shows the effect of both temperature and gamma irradiation on the normalized compressive strength of concrete and mortar. However, the existing data is for temperatures less than or equal to 100°C. The general trend may be to slightly higher compressive strengths with an increase in temperature to 100°C. The results are consistent with the scatter seen in results (Figure 4-29) for unirradiated concrete at these temperatures.

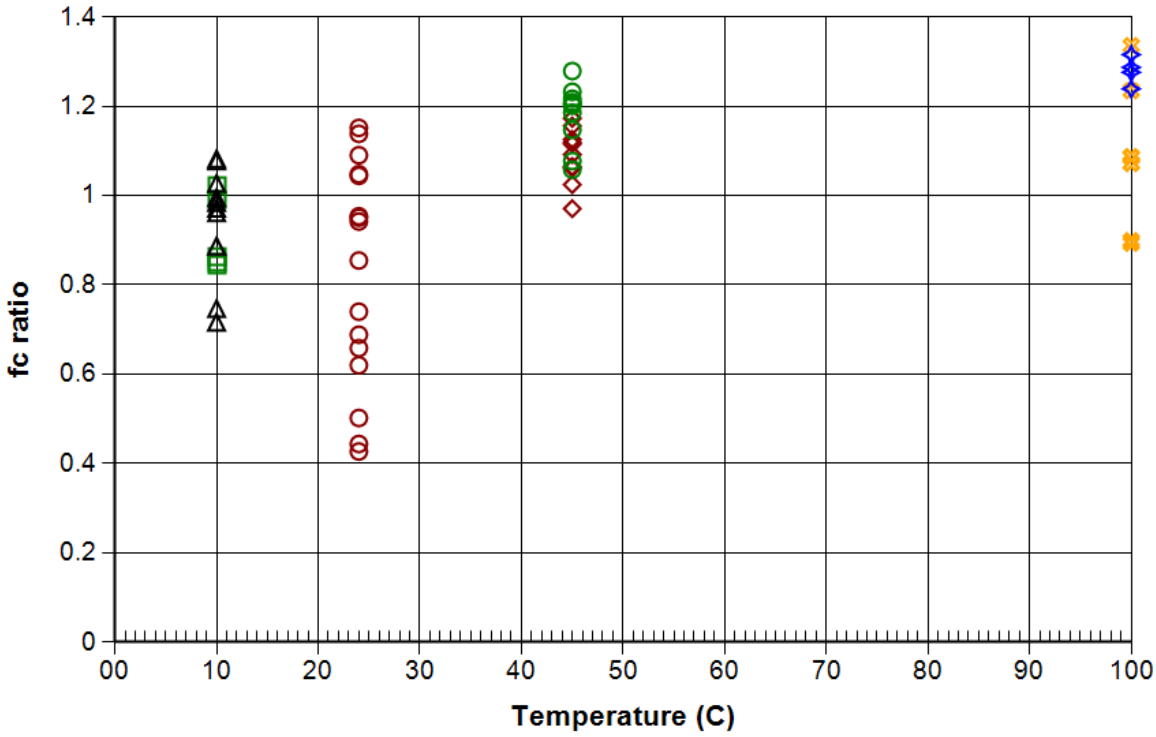

Sym	1st Author	Year	Ag. Frac.	W/C Ratio	Aggregate	Cement Type
○	Sommers	1969	0.8	0.46	Aggregate, Sand	Portland cement
□	Soo	1989	0.65	0.485	Standard Ottawa sand	Portland cement(Type I)
△	Soo	1989	0.65 to 0.66	0.4 to 0.485	Standard Ottawa sand	Portland cement(Type V)
✕	Alexander	1963	N/A	N/A	Heston sand	Portland cement
◇	Alexander	1963	N/A	N/A	Heston gravel	Portland cement
◇	Maruyama	2017	0.77	0.5	Thermally altered tuff, Sandstone	high early-strength ordinary Portland cement
○	Maruyama	2017	0.77	0.5	Felsic sandstone, Sandstone	high early-strength ordinary Portland cement

Figure 4-34 Normalized Compressive Strength as a Function of Temperature for Concrete and Mortar (under gamma only irradiation)

4.3.2 Carbonation

As discussed in Section 2.1, carbonation is the conversion of calcium hydroxide (in the form of portlandite) in the cement paste to calcium carbonate (in the form of calcite) through interaction with carbon dioxide (CO_2) and water. Carbonation is normally associated with the diffusion of CO_2 from the atmosphere through open pores in cement paste; therefore, carbonation is generally relegated to relatively small depths at the surface of the concrete.

No experimental studies have investigated synergistic effects involving carbonation and neutron irradiation. Only a handful of studies have simultaneously investigated carbonation and gamma irradiation effects.

Carbonation results in a reduced pore volume in the cement paste, due to the increased volume of calcite over portlandite, despite an increased number of pores in the nanometer size range [104]. Data from experiments involving the gamma irradiation of cement paste show enhanced natural carbonation with an increase in calcite content and a reduced average pore diameter as a function of dose [9, 83]. The data also suggest that gamma irradiation causes calcite to form at the expense of portlandite at the sample surface and in the center of the sample following a gamma dose of 10^7 Gy [83].

Separate experiments showed that gamma irradiation enhances carbonation at the cement paste surface. A gamma dose of 10^7 Gy over 6 months resulted in carbonation depths approximately 5 to 10 times deeper than reference samples under normal atmospheric conditions [80]. The reference samples (w/c = 0.45) showed average carbonation depths of 0.5–0.6 mm, whereas the irradiated samples showed an average depth of about 3 mm with depths up to 6 mm. It was shown that the degree of carbonation paralleled the radiolysis of water in the cement paste, which depended on the degree of saturation (w/c) of the samples [80]. The formation of micro-cracks during the radiolytic process was also thought to contribute to the increased carbonation rate. In addition, slightly less than stoichiometric amounts of oxygen gas were produced from hydrolysis, similar to other studies where the “missing” oxygen was assumed to be consumed in carbonate formation.

One potential synergistic effect could be an advancing front where neutron penetration increases as the water content is depleted by the gamma irradiation. Micro-crack formation during the radiolytic process could lead to further CO_2 and neutron penetration, enhancing carbonation and neutron damage. The neutron damage itself manifests by micro-crack formation in the concrete due to aggregate expansion and the resulting mismatch in bonding with the cement paste.

Similar to ASR in concrete, temperature and moisture changes induced by neutron and gamma irradiation can affect the carbonation of concrete. In studies of natural carbonation, higher w/c leads to less carbonation because pores are blocked by water [105]. In this case, there may be two competing effects: (1) the opening of pore space due to the reduction in water volume and (2) the reduction of pore volume due to calcite formation discussed above.

4.3.3 Alkali-Silica Reaction (ASR)

There are no direct experimental data on the combined synergistic effects of ASR and neutron or gamma irradiation on concrete performance. Ichikawa and co-workers demonstrated that argon ion irradiation of crystalline and amorphous quartz [85] and plagioclase [106] increased their reactivity toward alkali. Based on the implication that the disorder caused by argon ion bombardment of quartz can result in similar disorder caused by neutron irradiation [107], Ichikawa and Koizumi [85] proposed that the results strongly suggest that the disorder caused by neutron irradiation (aggregate degradation) would also increase reactivity toward alkali (i.e., leading to additional ASR in the presence of sufficient alkali). Thus, aggregates not typically prone to the ASR could be made susceptible through the disordering effect of neutron irradiation. Pignatelli et al. [108] also showed an increased reactivity of argon ion irradiated crystalline quartz in an alkaline environment. As pointed out by Maruyama et al. [109], the expansion strain imposed by aggregate expansion due to both neutron irradiation and ASR are similar. However, it is not clear whether an enhanced effect, higher strains within the concrete, would be achieved under a combined ASR/neutron irradiation environment rather than either effect separately.

In addition, as discussed earlier, environmental conditions such as the temperature and moisture could affect ASR in concrete. However, the moisture level in the bioshield is not expected to be high. In the reactor cavity, neutron and gamma irradiation can generate additional heat in concrete that could cause the evaporation of water, reducing the concrete moisture content and thus reducing the potential for ASR. Gamma irradiation could also reduce the moisture content in concrete through radiolysis. Therefore, radiation can affect the ASR in concrete through several different mechanisms.

4.3.4 Creep

As discussed in William et al. [10], the studies concerning concrete creep under irradiation are very limited. The effect of gamma radiation on the creep properties of concrete was investigated using a limestone aggregate concrete representative of that used in the pressure vessel of the Oldbury Nuclear Power Station [110]. Figure 4-35 presents test results of shrinkage and creep obtained from specimens subjected to an average gamma dose rate of 11.4×10^3 rad/h for 10 months, as well as unirradiated control specimens. In the figure, the creep of irradiated concrete decreases under gamma radiation. As noted, the modulus of elasticity of irradiated concrete is lower than that of regular concrete, and thus the creep of irradiated concrete would be expected to be higher. However, the results in Figure 4-35 show the opposite trend. One theory that explains this is that results for the irradiated concrete specimens could have been drier than the control specimens due to radiolysis of the absorbed water. In addition, increased viscosity caused by hindered water movement and high internal gas pressures under radiation could also affect concrete creep properties [110-112].

Gray [113] obtained creep data on Portland cement grout specimens under concurrent neutron and gamma irradiation. Figure 4-36 presents test results of shrinkage and creep obtained from the original paper. The irradiation test was done in the Herald test reactor in the UK, and the fast neutron fluence is about 0.75×10^{19} n/cm^2. The creep of specimens under irradiation is much higher than that before and after irradiation, which is very different from the results from McDowall [110]. The mechanisms are still unknown.

A recent numerical simulation of concrete specimens subject to irradiation-induced expansion and degradation [111] suggests that creep can play a favorable role in terms of LWRs long-term operation by delaying the initiation of damage from a higher fluence exposure.

4.3.5 Concrete–Metal Interactions

Many metallic components, including rebar and anchorages, are embedded in the concrete at NPPs. Embrittlement and other effects of nuclear radiation on metal are well documented and have previously been investigated in the area of metal RPV support components [114]. The current study is concerned with how nuclear radiation affects the bond between concrete and any embedments.

With one exception, no research data on the effect of radiation on the bond between concrete and metal reinforcement or metal anchorages was found. Kelly et al. [68] exposed concrete samples with embedded mild steel rods to a gamma dose of 3.6×10^8 Gy at 20°C while the samples were immersed in tap water. The ends of the steel rods exposed to water were corroded at the end of the experiment, but there was no evidence of any type of corrosion between the rods and the concrete.

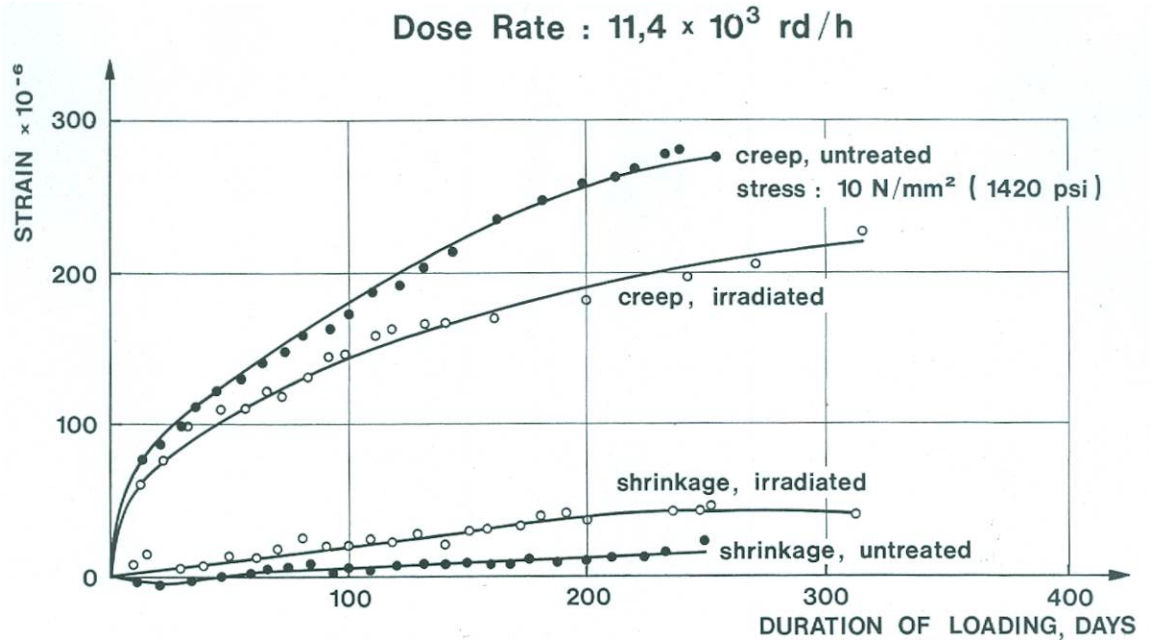

Figure 4-35 Effect of Gamma Radiation on Creep and Shrinkage of Concrete [110] (Note: rad = 0.01 Gy)

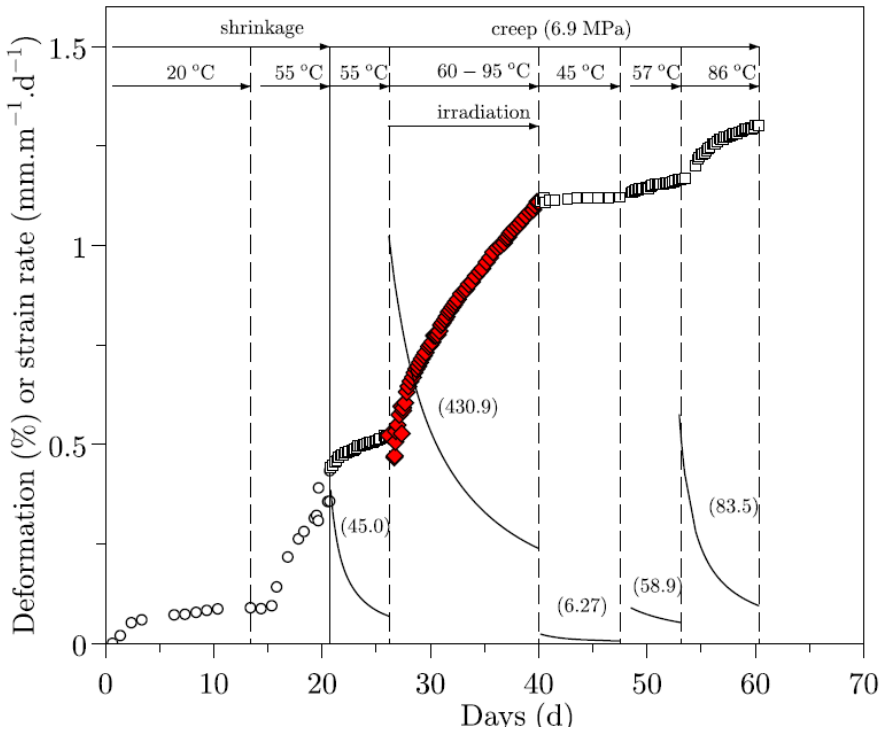

Figure 4-36 Measured Shrinkage and Creep Strain of Portland Cement Grout [111]

Most investigations of the bond deterioration between concrete and embedments such as rebar or anchorages have focused on the extent of the corrosion of the embedded steel because reinforced concrete structures are used extensively where they are exposed to the outdoor environment. Corrosion of the metal reinforcement decreases the size of the metal. However, there is an overall expansion effect, due to corrosion product formation, that leads to internal pressure and eventual crack formation. These studies are not appropriate for investigating the long-term degradation of the bond between metal embedments and concrete in an LWR cavity. The LWR setting of interest is a controlled environment where the corrosion of any metal embedments is expected to be minor.

Irradiation of concrete leads to the generation of cracks in concrete due to the aggregate mismatch caused by mechanisms such as the shrinkage of cement paste due to radiolysis or the expansion of aggregates under neutron bombardment. Such degradation (cracking) is expected to weaken the metal–concrete bond associated with metal embedments. In the absence of any direct irradiation data, some inference can be drawn from the work of Desnerck et al. [115], where the metal–concrete bond was investigated using pull-out tests involving cracked reinforced concrete samples. The bond strength was estimated to be reduced by 40% or more, depending on the extent of the cracks in the concrete around a section of rebar. Such an effect would vary with amount of radiation, aggregate type, and embedment configuration.

In an LWR environment, other confounding influences could include corrosion of the metal and shrinkage of the cement paste. Small amounts of metal embedment corrosion could actually lead to stronger metal-concrete bonding because the expansion due to corrosion product formation has not yet reached a point that would cause cracking [115, 116]. Cement paste shrinkage leads to crack formation and is dependent on the moisture content of the concrete, which in turn is influenced by exposure to the surrounding air, the humidity of the air, and the temperature of the environs.

4.4 Summary of Radiation Impacts

4.4.1 Neutron Impacts

Table 4-1 summarizes the effect of neutron radiation on concrete and its components. No weight loss due to neutron irradiation has been observed. At temperatures below 100°C, it is clear that neutrons have a much larger impact on aggregates than on cement paste because they cause disorder within the crystalline framework of an aggregate. The generally amorphous nature of cement paste is affected to a much lesser degree. In particular, neutrons appear to cause much more disruption to covalent aggregate crystal structures (e.g., silicates with a quartz lattice) than ionic aggregate crystal structures (e.g., calcite). However, this effect appears to be structure dependent; some silicates show little effect.

The disordering of the aggregate crystal structure results in volume expansion of the aggregate. The relative onset of the volume expansion of quartz under neutron irradiation is also temperature dependent. Aggregate volume expansion appears to lead to some reduction of the tensile strength and the elastic modulus of the aggregate. These impacts are noted at neutron fluence levels greater than 1×10^{19} n/cm^2. Observed degradation included calcareous aggregate as well as siliceous aggregates. As noted in Section 1.4, aggregates may be primarily calcareous or siliceous, but actual compositions are site-specific and some crystal structures are more susceptible than others.

The neutron irradiation of concrete leads to significant degradation of its mechanical properties (compressive strength, tensile strength, and modulus of elasticity) at neutron fluence levels greater than 1×10^{19} n/cm^2 at temperatures less than 100°C. The reduction in mechanical properties is due in part to the volume expansion of the aggregates, which results in a bonding mismatch with the cement paste. The volume expansion of the aggregate may also contribute to the reduction in tensile strength and the elastic modulus of the concrete.

There are no clear trends for the effect of the w/c and aggregate fraction of the concrete on the mechanical properties of concrete under neutron irradiation.

Table 4-1 Impact Summary of Neutron Irradiation on Concrete and Its Components

Property/ Variable	Summary Observations	Section
	Dimensional Change	
Cement paste	Little if any change. Potential slight shrinkage because of loss of water due to a high hydrogen cross-section, small temperature increase, and radiolysis due to secondary gamma radiation. As a generally overall amorphous solid, disordering by neutron bombardment is not expected to be significant.	3.1.2.1
Aggregates	Covalent bond nature and structure of crystalline quartz (SiO_2) make it more susceptible than ionic compounds such as calcite ($CaCO_3$) to damage and subsequent expansion due to neutron radiation. Volume changes of aggregates becomes more pronounced at fluence levels > 1×10^{19} n/cm^2. The volume expansion of quartz as a function of neutron fluence is temperature dependent, with the onset of significant expansion shifting about one order of magnitude (fluence of > 10^{19} to > 10^{20} n/cm^2) between temperatures of 30 to 95°C.	3.1.3.1
Concrete	Experiences expansion at fluence levels of about 1×10^{19} n/cm^2 and higher. Expansion is mainly attributed to the aggregate component, which includes the subsequent mismatch between the aggregate and cement paste. The degree of expansion may correlate with the silicate content of the aggregate.	3.1.4.1
	Weight Loss	
Cement paste	There is no clear trend as a function of neutron fluence. There may be a slight amount of potential weight loss due to water loss, as discussed above under dimensional changes.	3.1.2.2
Aggregates	In the limited studies available, no observable weight loss was recorded.	3.1.3.2

Table 4.1 Impact Summary of Neutron Irradiation on Concrete and Its Components (Cont.)

Property/ Variable	Summary Observations	Section
Concrete	There is no clear trend. Weight loss of about 5% or less was observed in some studies. However, the weight loss appears to correlate with changes in temperature rather than neutron fluence.	3.1.4.2
Compressive Strength		
Cement paste	There may be some reduction in strength depending on the type of cement.	4.1.1
Aggregates	Very limited data (one dataset at *T* up to 240°C) showed no loss in strength.	4.1.1
Concrete	Significant loss in strength, reductions down to about 40% of the original strength, at fluence levels greater than about 1×10^{19} n/cm^2 at temperatures less than 100°C.	4.1.1
Water/cement ratio	A higher w/c appears to result in less of a reduction in strength. One explanation is that the higher resultant porosity of the cement paste can better withstand the aggregate expansion caused by neutron irradiation.	4.1.1.1
Aggregate fraction	A higher aggregate fraction in concrete leads to less of a reduction in strength because aggregates are not significantly affected by compressive forces.	4.1.1.2
Tensile Strength		
Cement paste	Very limited data suggest that there is little to no effect on the tensile strength under neutron irradiation.	4.1.2
Aggregates	There is large scatter in the available data, but aggregates tend to exhibit a reduction in strength with neutron fluence.	4.1.2
Concrete	Significant loss in strength, reductions down to about 20% of the original strength, at fluence levels greater than about 1×10^{19} n/cm^2 at temperatures less than 100°C. Attributed to the volume mismatch between aggregates and cement paste.	4.1.2

Table 4.1 Impact Summary of Neutron Irradiation on Concrete and Its Components (Cont.)

Property/ Variable	Summary Observations	Section
Water/cement ratio	There are no clear trends in the data. Higher porosity as a result of increasing w/c could initially account for cement paste's better accommodation of aggregate expansion with neutron radiation until a point is reached where loss in bonding between the aggregate and cement paste begins to reduce the tensile strength.	4.1.2.2
Aggregate fraction	Based on limited data, an increase in aggregate content results in a reduction of tensile strength. This trend is consistent with the reduction in strength of the aggregates with neutron fluence. At higher fractions, the aggregate–cement bond strength might decrease due to insufficient amounts of cement paste between pieces of aggregate.	4.1.2.2
Modulus of Elasticity		
Cement paste	Very limited data suggest little or no effect of neutron irradiation on *E*.	4.1.3
Aggregates	Large scatter in data, but significant reductions in *E* are possible.	4.1.3
Concrete	Significant loss in *E*, reductions down to about 30% of the original values, at fluence levels greater than about 1×10^{19} n/cm^2 at temperatures less than 100°C. Attributed to reduction of *E* of the aggregates.	4.1.3
Water/cement ratio	There are no clear trends in the data. Higher porosity and *E* as the result of increasing w/c could reflect cement paste's better accommodation of aggregate expansion with neutron radiation. However, temperature effects could be in play and the w/c could have a relatively small, if any, effect on *E*.	4.1.3.1
Aggregate fraction	No clear trend in available data. Temperature effects could be involved.	4.1.3.2

4.4.2 Gamma Impacts

There is very limited data on the effects extended gamma irradiation has on concrete and its components, as summarized in Table 4-2. Cement paste and concrete experience weight loss due to the gamma radiolysis of water in the cement paste pores. Cement paste also shows shrinkage due to the water loss, but the limited data on concrete is inconclusive on shrinkage. Higher radiation exposures of Portland cement resulted in the partial disappearance of the original hydrated minerals and the loss of chemically bound water after a dose of 1.3×10^8 Gy

[82]. For example, a competing process with the opening of pore space due to the water loss is carbonation, the conversion of portlandite to calcium carbonate, which occupies more volume, caused by gamma irradiation. A slight increase in the compressive strength of concrete with a dose of 2×10^8 Gy was observed with an increase in carbonate formation. There is also the potential for water loss and shrinkage of cement paste due to heating caused by gamma irradiation. The very limited data on aggregate and concrete shows no apparent change in volume under gamma irradiation.

Table 4-2 Impact Summary of Gamma Irradiation on Concrete and Its Components

Property/Variable	Summary Observations	Section
Dimensional Change		
Cement paste	Shrinkage due to radiolysis of water.	3.2.2.1
Aggregates	Maruyama et al. [66] did not observe any significant change in volume with gamma dose.	3.2.3
Concrete	No change observed by Kelly and Davidson [88], but other studies that also involved neutron radiation saw a volume increase above 1×10^8 Gy.	3.2.4.2
Weight Loss		
Cement paste	Weight loss due to radiolysis of water.	3.2.2.1
Aggregates	No data available.	---
Concrete	Increases above a dose of 1×10^8 Gy due to the radiolysis of water.	3.2.4.1
Compressive Strength		
Cement paste	Based on very limited data, no significant effect up to 2×10^8 Gy. No data available at higher doses.	4.2.1
Aggregates	Based on very limited data, no significant effect up to 1×10^8 Gy. No data available at higher doses.	4.2.1
Concrete	Based on limited data, significant reduction by 1×10^9 Gy. Experiments were conducted underwater. No data available for samples in air.	4.2.1
W/c	No apparent effect based on limited data.	4.2.1
Aggregate fraction	No apparent effect based on limited data.	4.2.1

Table 4.2 Impact Summary of Gamma Irradiation on Concrete and Its Components (Cont.)

Property/Variable	Summary Observations	Section
Tensile Strength		
Cement paste	No data available.	—
Aggregates	No data available.	—
Concrete	No apparent effect based on limited data.	4.2.2
W/c	No data available.	---
Aggregate fraction	No data available.	---
Modulus of Elasticity		
Cement paste	No data available.	---
Aggregates	No data available.	---
Concrete	Not clear from the limited data available that there is a decrease caused by gamma irradiation.	4.2.3
W/c	Not clear from the very limited data available whether there is an effect.	4.2.3
Aggregate fraction	Not clear from the very limited data available whether there is an effect.	4.2.3

There is the potential for degradation of concrete properties at doses greater than 1×10^8 Gy, but no direct experimental results under conditions similar to an LWR cavity are available. No data are available for the effect of the w/c and aggregate fraction of the concrete on the mechanical properties of concrete under gamma irradiation.

4.4.3 Other Concerns

Due to the limited amount of qualified data available on gamma irradiated samples and the presence of gamma radiation during many of the neutron irradiation tests, the synergistic effects between neutron and gamma irradiation are largely unknown. Temperature does not play a significant role in volume change, but it can affect water loss from cement paste and influence the mechanical properties of concrete. Temperature can also affect the mechanical properties of concrete in the range experienced in LWR cavities.

When considering the implementation of a “threshold” or “cut-off” value for neutron fluence or gamma dose as they pertain to concrete degradation and failure to meet design criteria, it is important to account for several items. The first is that damage to concrete and its constituents occurs at any level of irradiation, and the extent of the damage increases with irradiation time. The extent of the damage depends on a variety of factors related to the nature of the concrete and its environmental surroundings, as previously discussed. The issue is trying to determine when the irradiation damage reaches a level that will compromise a concrete support structure’s

design. The second item is that there can be significant variation, possibly up to an order of magnitude, in the neutron fluence for the same reported values between experimental studies because the actual neutron distribution energies used in most cases are not known. Section 3.1.1 discusses the terminology used in the past and how a term such as “fast neutrons” may refer to different energy ranges.

Extreme care must be exercised when trying to infer structural performance under long-term radiation conditions from laboratory experiments that use small samples. The size effect of a test specimen is complicated. Depending on the failure mechanisms, the effect could be either deterministic or statistical. For discrete fracture failure with large cracks (e.g., a three-point bending test of a concrete beam), there is a deterministic size effect on the nominal strength of concrete, which relates to the energy release during the crack propagation. The size effect was studied in detail by Bazant and Planas [117] based on nonlinear fracture mechanics. For damage/failure with many micro-cracks, there is a statistical size effect called the Weibull size effect, which is based on the weakest link theory. In this theory, the failure of the whole structure is due to the failure of the weakest link (the weakest element) in the structure. The weakest element is associated with the largest defect in the material. The larger the volume of a structure, the higher its probability of having the largest defect. Therefore, the strength of concrete decreases with increasing specimen size. In general, the fracture size effect is much more significant than the statistical size effect for concrete. In the case of nuclear irradiation studies, the statistical size effect might dominate because the irradiation results in distributed damage in the concrete due to the formation of micro-cracks (e.g., from gamma-induced radiolysis or neutron-induced volume expansion of aggregates).

This review is concerned with the potential irradiation damage of concrete under conditions that are typically experienced in LWR cavities. However, there are situations where off-normal conditions exist and are incorporated into aging management plans. For example, the concrete at the location of certain RPV supports at the Farley NPP is subjected to a sustained temperature of about 190°F [118]. Another example is at the H.B. Robinson 2 plant, where water is dripping on some of the metal RPV supports and there is some standing water on the bioshield [119].

5 CONCRETE IN HIGH-RADIATION AREAS

Because of the intense neutron and gamma radiation given off by the nuclear fission process, an RPV in a commercial U.S. power plant is surrounded by a concrete shield wall to help reduce external radiation to a level deemed safe for plant workers. The shield wall, also known as a biological shield, or bioshield as used in this report, is typically a cylindrical concrete wall about 1.5 to 2 m thick that surrounds the RPV. The reactor cavity is the space between the RPV and the bioshield.

The concrete at the inner surface of the bioshield has the potential to receive the highest radiation exposure of any concrete support structure at a commercial NPP. In many cases, the bioshield is also the primary support structure for the RPV. Thus, it is necessary to ensure that any structural function of the bioshield is not compromised by radiation-induced degradation.

Section 5.1 provides a limited review of the different RPV/bioshield configurations used in currently operating commercial reactors. Rough estimates of the neutron fluence levels and gamma ray doses from 80 years of operation to critical areas surrounding the RPV for each NPP are estimated and the uncertainties are discussed in Section 5.2.

5.1 RPV/Bioshield Designs

There are 12 reactor types currently in the U.S. commercial NPP fleet, as summarized in Table 5-1. The BWR design in the area of the RPV remained fairly constant across Types 2 through 6, as discussed in Section 5.1.1. The PWR designs exhibit variations dependent on the manufacturer, the number of coolant loops, and the architect/engineer design for the RPV supports, as discussed in Section 5.1.2. Plant-specific information is required for a complete evaluation.

Table 5-1 Reactor Types Used in the U.S. Commercial NPP Fleet

Primary Type	Reactor Type	Number of Loops	Number of Reactors[a]
BWR	General Electric Type 2	N/A[b]	2
	General Electric Type 3	N/A	5
	General Electric Type 4	N/A	19
	General Electric Type 5	N/A	4
	General Electric Type 6	N/A	3
PWR	Babcock & Wilcox Raised-Loop	2	1
	Babcock & Wilcox Lowered-Loop	2	5
	Combustion Engineering	2	9
	Combustion Engineering System 80	2	3
	Westinghouse Two-Loop	2	5
	Westinghouse Three-Loop	3	13
	Westinghouse Four-Loop	4	29

[a] Operating reactors as of July 2016 (includes Clinton and Pilgrim 1).

[b] Not applicable.

5.1.1 Boiling-Water Reactors (BWRs)

All BWRs share a similar design for the configuration of the bioshield around the RPV. The RPV rests on a metal vessel support skirt on top of a concrete reactor pedestal, as depicted in Figure 5-1. The vessel support skirts are an integral part of the BWR vessel [120]. The cylindrical concrete bioshield also rests on the reactor pedestal, surrounding the core area of the RPV. The bioshield is a self-supporting structure and may be anchored at the top to the containment structure to maintain horizontal stability of the bioshield, as shown in Figure 5-2. In turn, horizontal stabilizers at the top of the bioshield may provide horizontal support for the upper end of the RPV and allow for thermal expansion and contraction of the RPV in some designs. Because the final implementation is architect/engineer dependent, evaluation needs to be on a plant-specific basis to properly assess load path and transfer mechanisms.

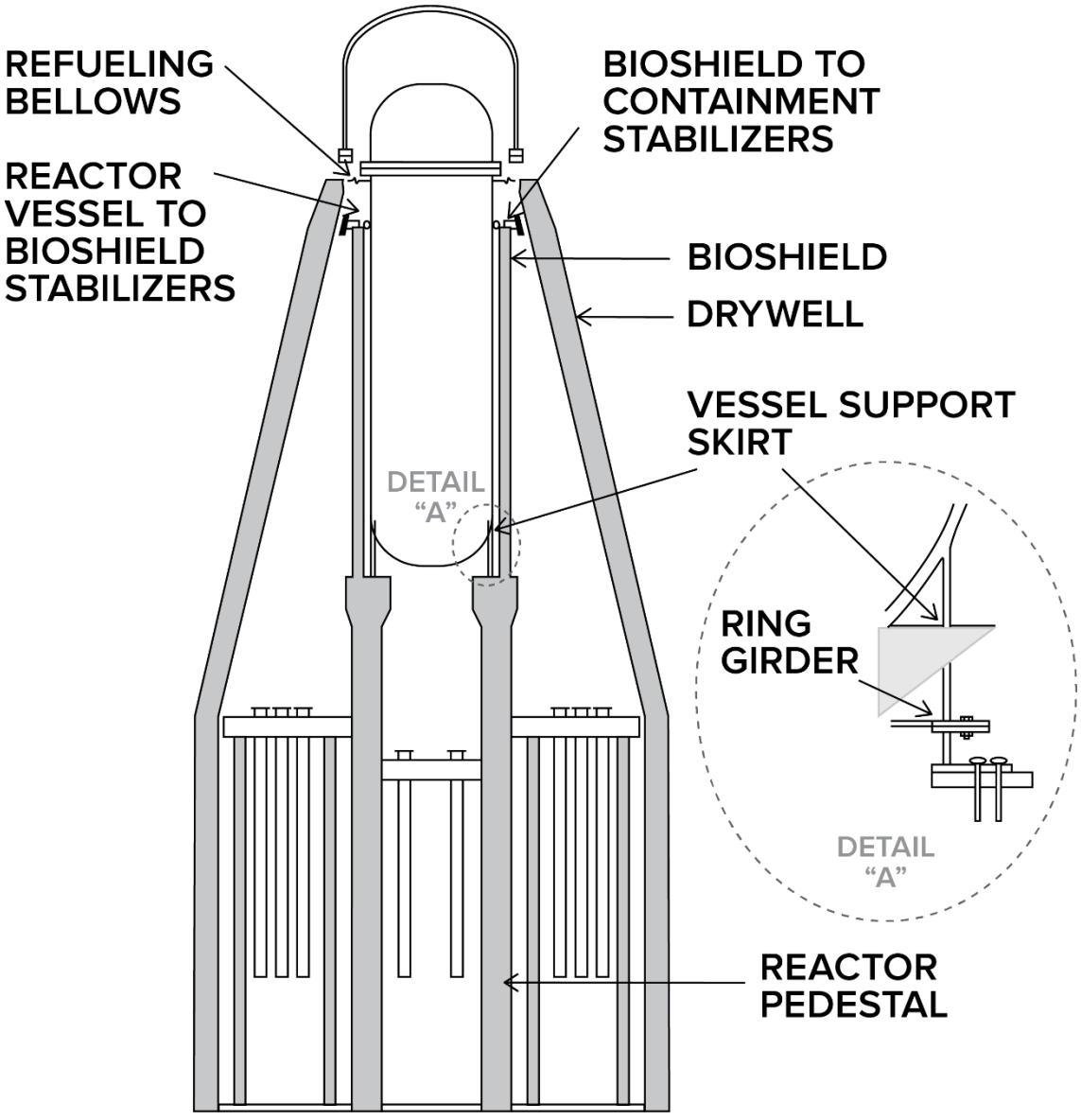

Figure 5-1 RPV Support and Bioshield (Source: NRC [121])

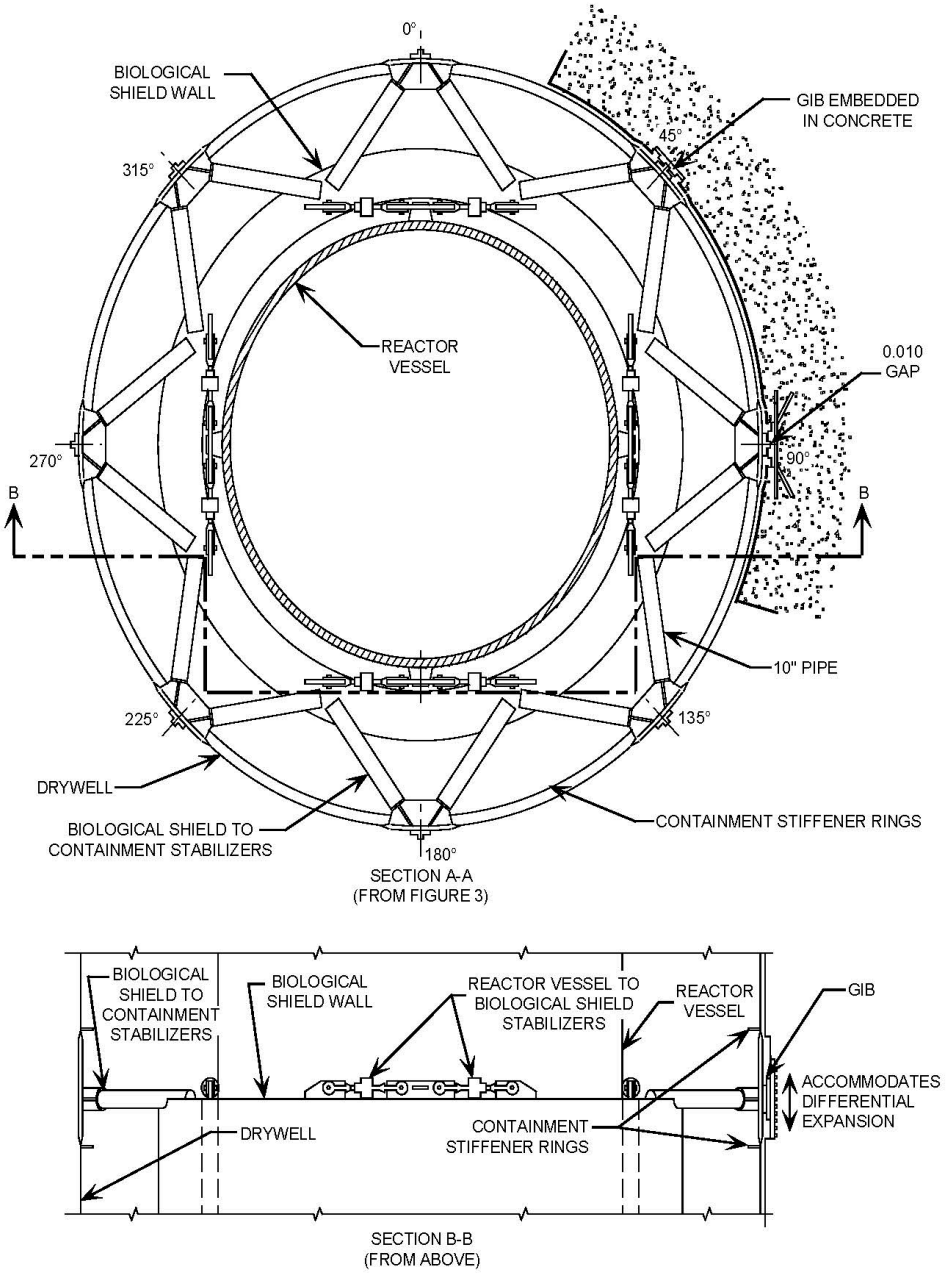

Figure 5-2 RPV Lateral Support (Source: NRC [121])

5.1.2 Pressurized-Water Reactors (PWRs)

There are seven different types of commercial PWRs in operation in the United States, as listed in Table 5-1. The primary difference among the PWR designs is the number of cooling loops (2, 3, or 4) used.

A variety of RPV support systems are used for PWRs, even among those with the same number of cooling loops. Six general support system design types are used. Two support system types rest on the concrete basemat, upon which the biological shield also sits; the remaining support types rest on the biological shield itself, which provides the structural support for the RPV.

The two PWR support types that rest on the concrete basemat are skirt and column support designs:

(1) Most Babcock and Wilcox PWRs in commercial operation incorporate a support skirt design similar to that used for BWRs (Fig. 5-3).

(2) Other PWRs are supported on the tops of columns, the bottoms of which are anchored on the basemat. The columns either support a ring girder that encircles the RPV under the inlet and outlet nozzles or are attached to supports under the inlet and/or outlet nozzles (Figure 5-4). Lateral support of the columns could include the use of a keyway assembly at the bottom of the column supports or anchoring or embedment of the columns in the biological shield. Figure D.10-1 in Appendix D shows an example of lateral supports embedded in the bioshield.

Per system design requirements, the RPV supports must restrict movement of the RPV under all design loading conditions. At the same time, the RPV must be allowed to expand and contract under varying temperature conditions. A “shoe” interface, also referred to as a “saddle,” is used under the inlet and/or outlet nozzles or under load brackets between nozzles; the shoe restricts vertical and tangential movement, but allows radial thermal growth of the RPV. The loadings on the shoe are transferred to the underlying support system. In the case of column supports, if the nozzle weldments are not bolted directly to the columns, the shoes sit on (are attached to) either the ring girder supported by the columns or on the columns themselves (e.g., see Figure D.10-1 in Appendix D).

In systems that are supported by the biological shield, the shoes may be anchored on any of the following:

(3) The top of the biological shield wall (i.e., either sitting directly on the top surface or set in a recess on the top surface) is most commonly used. The shoes are attached to metal weldments. These designs incorporate some type of air or water cooling to minimize heat transfer to the underlying concrete (e.g., see Appendix D, Section D.4). Some designs incorporate taller vertical plates that allow for better air cooling, but place the load-bearing baseplate of the weldment on the concrete, closer to the higher radiation fields at the beltline of the RPV (Figure 5-5).

(4) Cantilever beams that are anchored in the biological shield. The RPV is supported by fixtures that extend outward from the biological shield (Figure 5-6).

(5) A ring girder or other horizontal steel beams that are supported at the top or at the side of the biological shield (Figure 5-7). As in type 3, the shoes are generally water cooled to maintain the concrete temperature within design limits.

(6) The top of a neutron shield tank. The tank, in turn, is supported by the reinforced concrete basemat (Figure 5-8). In some cases, grout fills the gap between the shield tank and the primary shield wall to provide lateral stability for the RPV (e.g., see Appendix D, Section D.2).

Variations within these general designs exist because of the implementation used by the architect/engineer for each reactor. Thus, any complete analysis must consider impacts on a plant-specific basis.

5.1.3 Reactor Cavity Temperatures

Most PWR reactor cavities are designed to maintain a temperature of approximately 150°F during operating conditions, which helps to maintain the condition of concrete structures. Abnormal temperatures are recorded here as a repository for future use, if relevant in the degradation analysis.

Two of six reactor support concrete areas at the Farley NPP are at a temperature of approximately 190°F [118]. This off-normal condition is mitigated by periodic inspections of the supports as part of the licensee's structural monitoring program. Such an example reinforces the need for plant-specific analyses when evaluating the long-term effects of irradiation on concrete support structures.

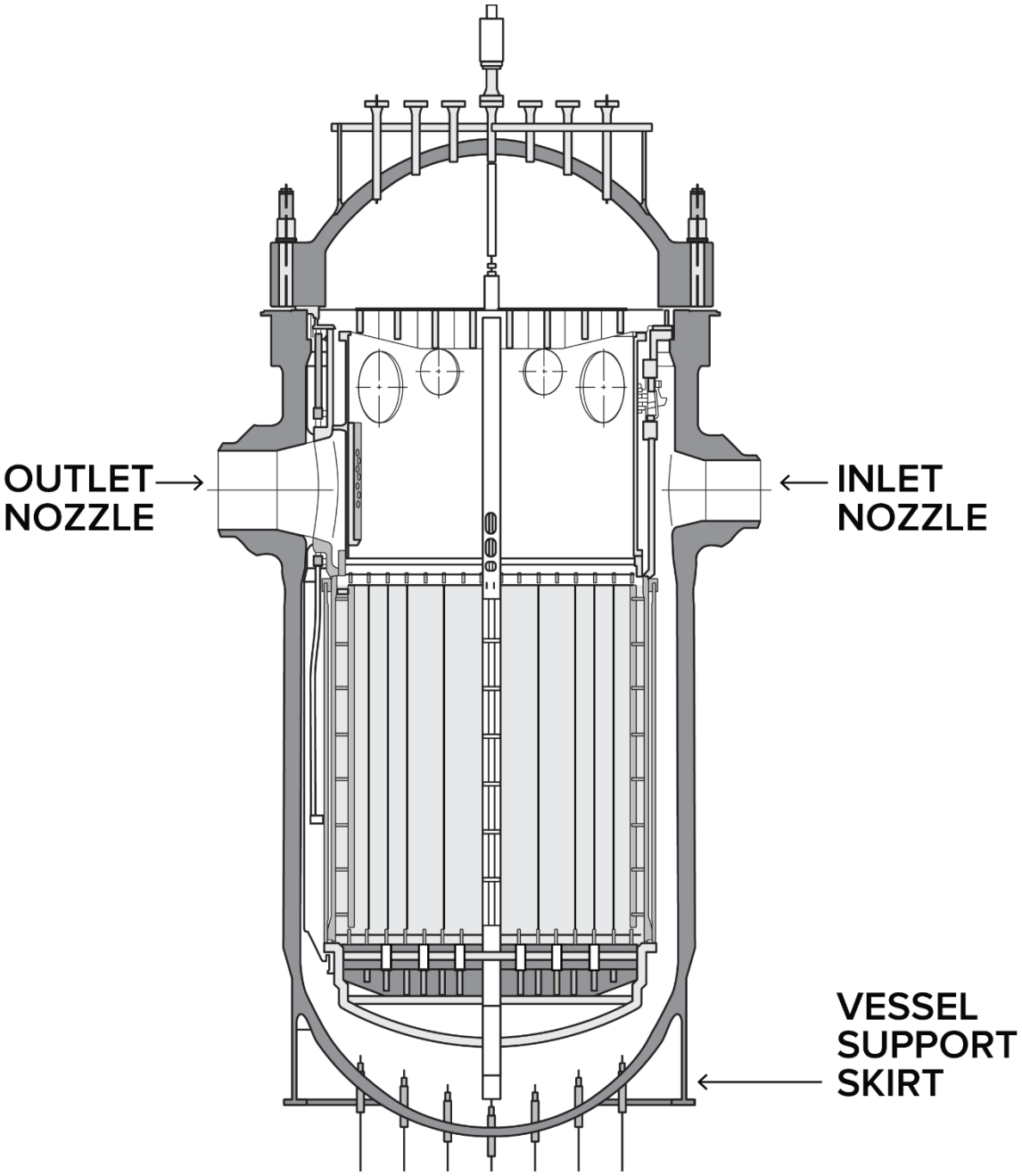

Figure 5-3 Example of a PWR RPV with a Support Skirt (Source: Cheverton et al. [122])

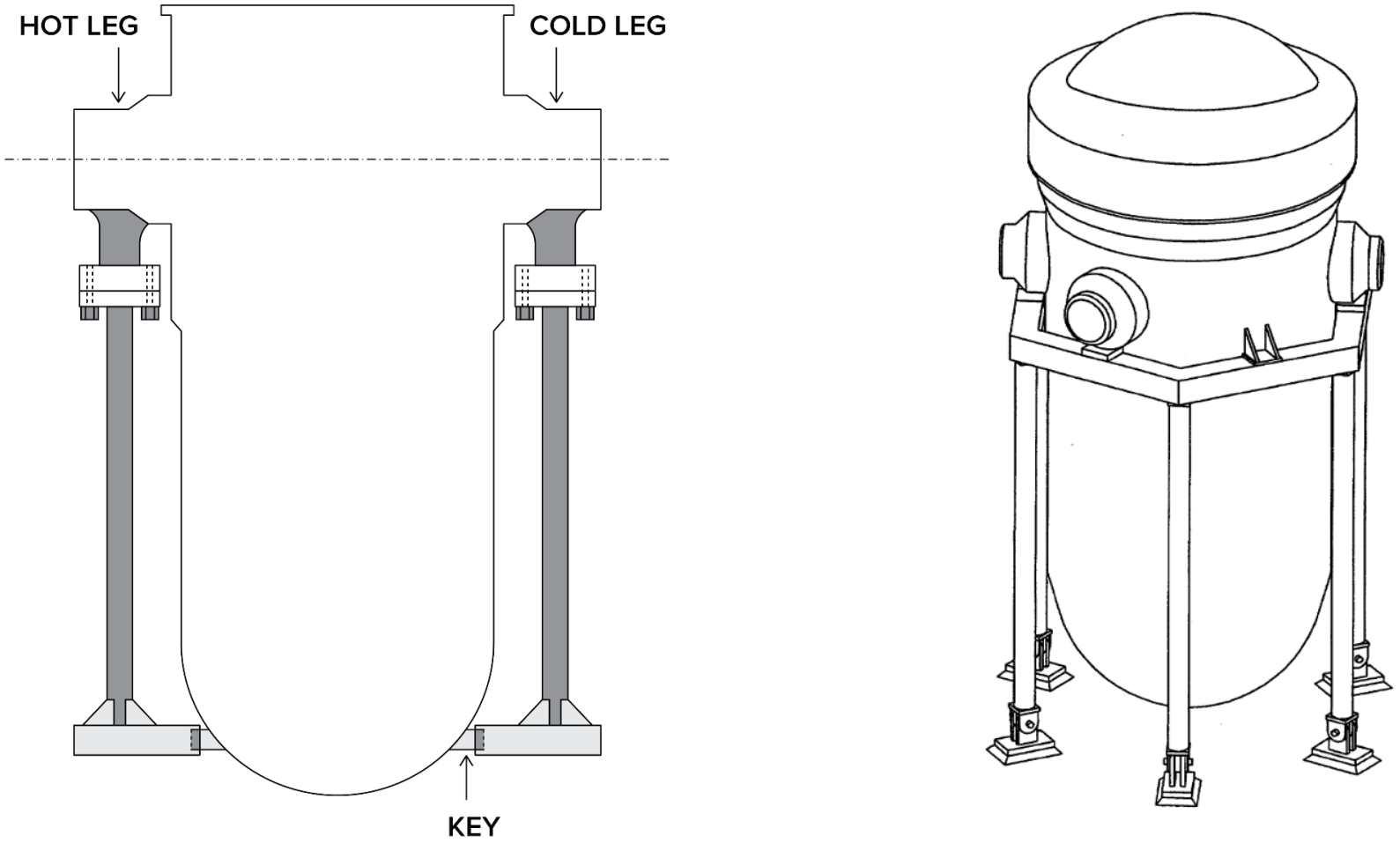

Figure 5-4 Examples of PWR RPVs Supported on Columns (Sources: Cheverton et al. [122] (left), Lapay et al. [123] (right))

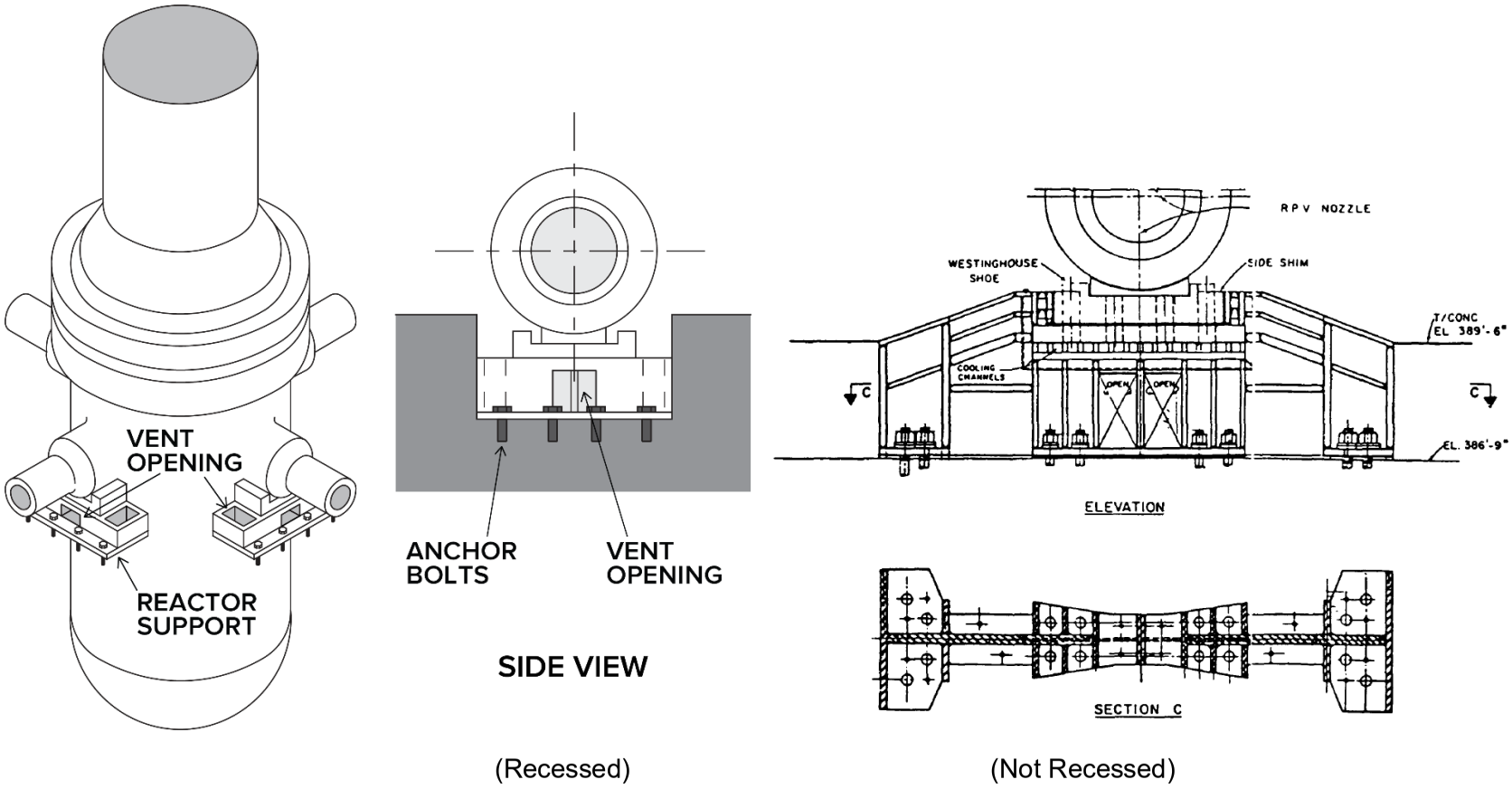

Figure 5-5 Examples of PWR RPV Supports Anchored to the Top of the Biological Shield Wall (Source: Cheverton et al. [122])

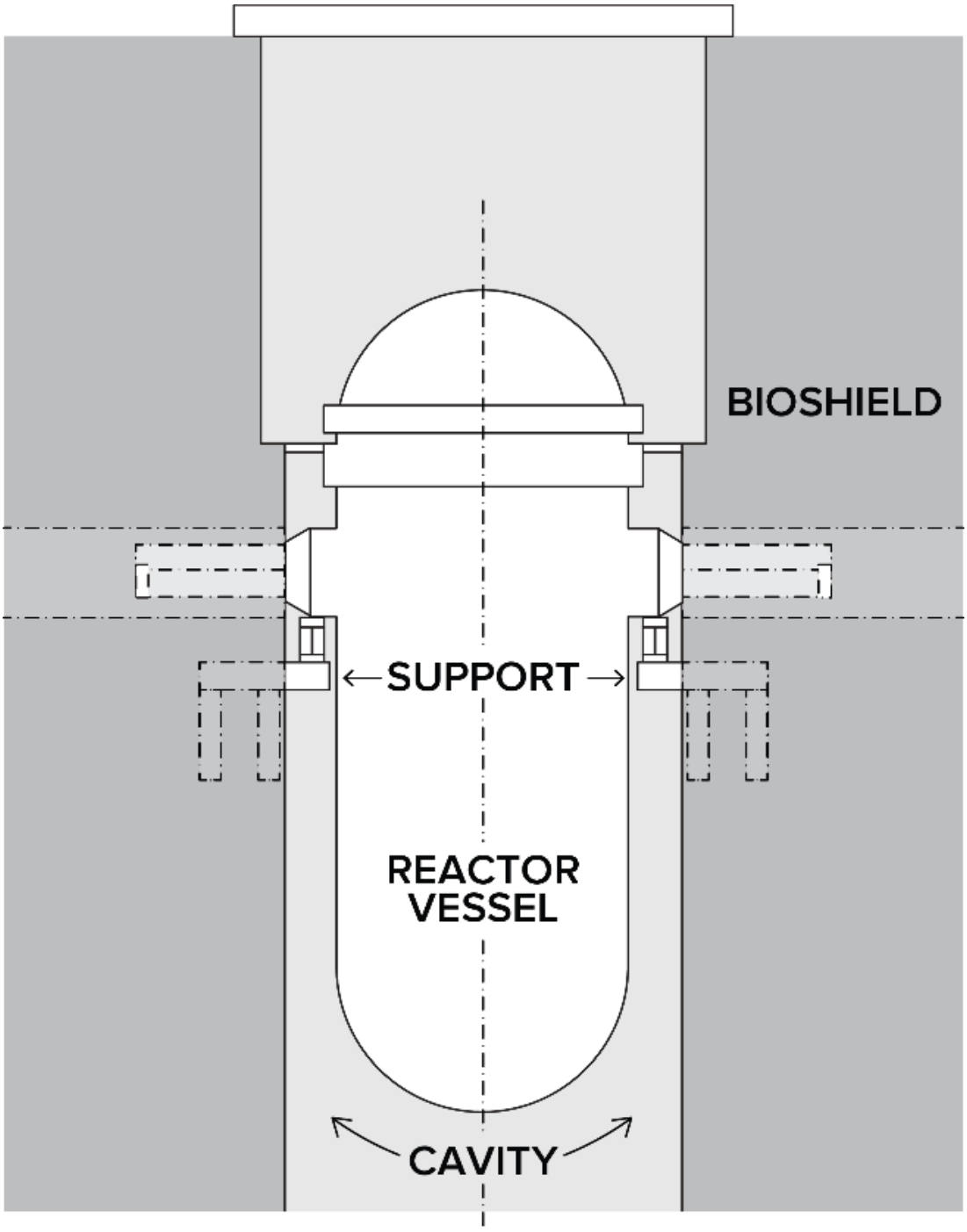

Figure 5-6 Example of a PWR Supported on Cantilevered Beams or Extended Supports (Source: Cheverton et al. [122])

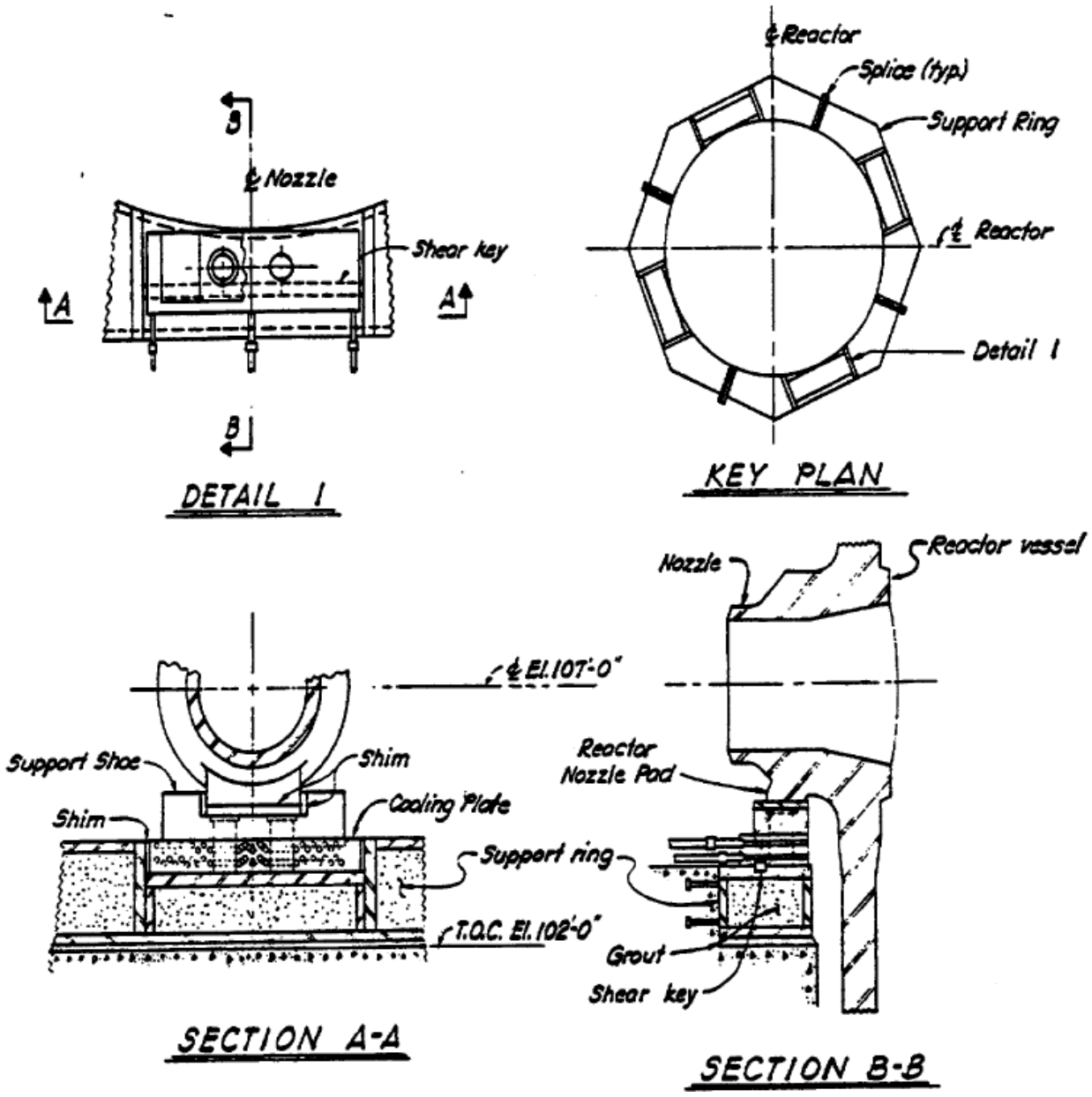

Figure 5-7 Examples of PWRs Supported by Steel Girders Embedded on the Biological Shield (Source: Lapay et al. [123])

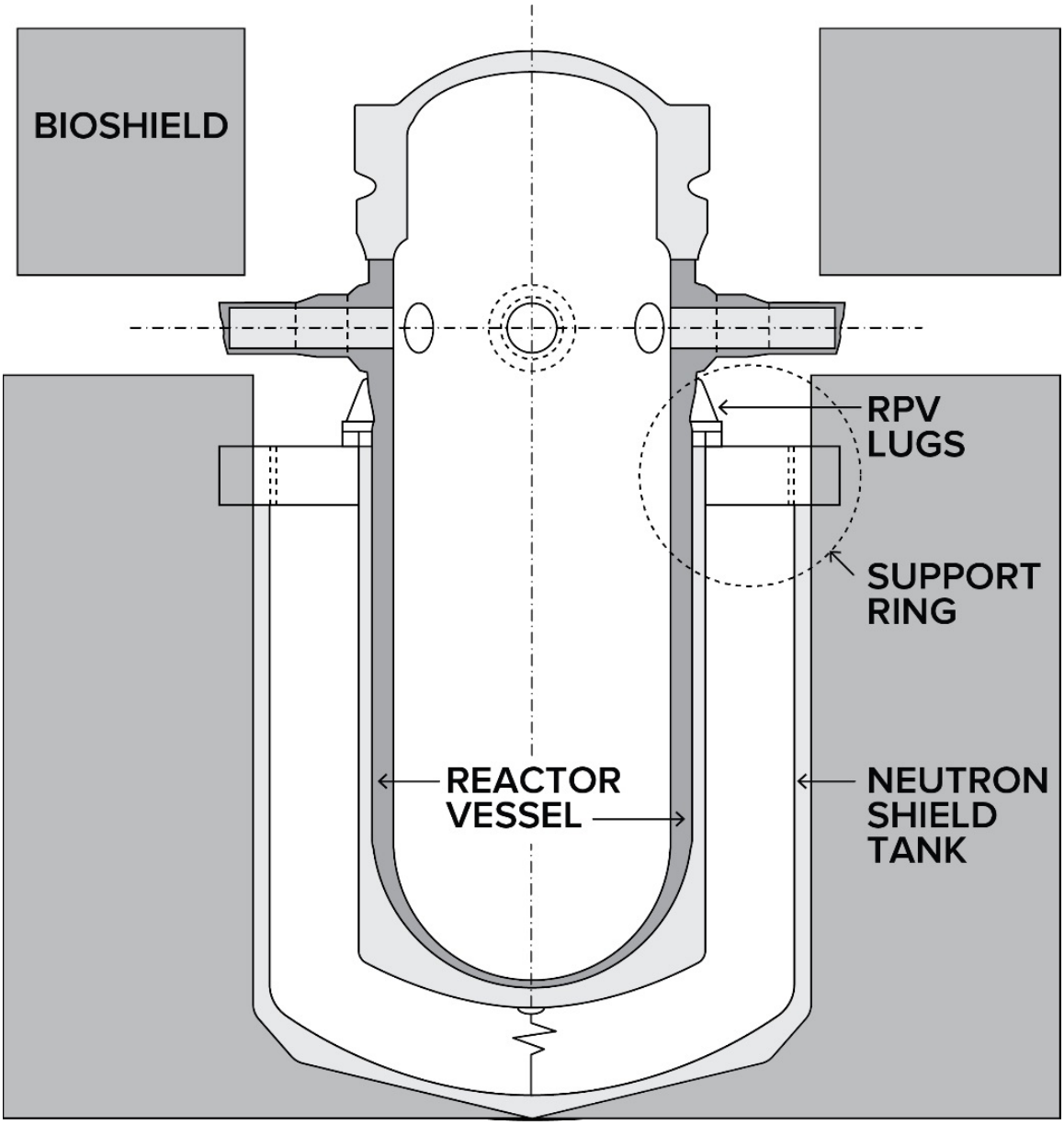

Figure 5-8 Example of PWR RPV Supports Mounted on a Neutron Shield Tank (Source: Lapay et al. [123])

5.2 Radiation Levels

The highest radiation levels outside of the RPV are in the belt-line region. During extended exposure periods, concrete support structures in this area are most susceptible to potential radiation damage. As shown in Section 5.1.2, most reactor designs include concrete support functions close to the highest radiation areas.

5.2.1 Neutron Radiation

The neutron radiation levels at critical concrete structure boundaries in the vicinity of the RPV have not been directly monitored in the past. For this review, approximate neutron fluence levels at the bioshield wall and associated concrete support interfaces are derived from estimates at the inner RPV wall for fast (neutron energies $E > 1.0$ MeV) neutrons, decayed for passage through the RPV wall, and then converted to $E > 0.1$ MeV dosimetry. Ex-vessel neutron dosimetry is now becoming available for some NPPs, and will provide an opportunity to more accurately evaluate neutron fluence in the reactor cavity in the vicinity of the reactor core.

Concrete degradation as a result of neutron irradiation is considered primarily due to interactions with fast neutrons ($E > 0.1$ MeV) [124], as discussed in Section 3.1. Through a series of steps, data obtained for neutron radiation for $E > 1.0$ MeV at the inner RPV wall is converted to an estimated fluence ($E > 0.1$ MeV) in the vicinity of concrete support structures in the reactor cavity. In each step of the calculation, there are variabilities and uncertainties that cannot be totally quantified at present without further confirmatory research and plant-specific information. Thus, the method presented here is a rough approximation that may not be conservative.

5.2.1.1 60-Year Neutron Fluence (E > 1.0 MeV) at the Inner RPV Wall

Information on neutron radiation levels at commercial U.S. NPPs can be obtained from data generated as a part of their RPV surveillance programs, as required by the NRC, to monitor RPV metal degradation due to neutron embrittlement effects. Estimated levels of neutron fluence for $E > 1.0$ MeV at the inner RPV wall are reported periodically for each reactor. At this time, most operating reactors have received a license renewal extension from 40 to 60 years. Estimates of the neutron fluence at the inner RPV wall after 60 years of operation were provided as part of a plant's license renewal application (LRA). These estimates are generally based on approximately 20 to 30 years of operating experience and were extrapolated out to 60 years. Figure 5-9 displays the estimated neutron fluence ($E > 1.0$ MeV) after 60 years of operation at the inside edge of the RPV wall (0T position) on the reactor core mid-plane for each reactor in the operating NPP fleet based on surveillance programs and operating history. The tabulated data is provided in Appendix C.

5.2.1.2 60-Year Neutron Fluence (E > 1.0 MeV) at the Outer RPV Wall

Attenuation of the neutron radiation as it passes through the RPV wall can be estimated using the exponential power law provided as Equation (3) of Regulatory Guide 1.99 [125]:

$$f = f_{surf} e^{-0.24x} \tag{5-1}$$

where f is the neutron fluence (10^{19} n/cm^2; $E > 1.0$ MeV) at the outer RPV wall (the 1T position), f_{surf} is the estimated neutron fluence at the inner surface of the RPV wall (10^{19} n/cm^2; $E > 1.0$ MeV), and x is the RPV wall thickness in inches. It has been suggested that a more appropriate value for the exponential term to estimate the neutron fluence in Equation (5-1) would be $-0.33x$ rather than $-0.24x$ [126, 127].

The value of -0.33 was used previously, but the adjustment to -0.24 was made for purposes related to the use of the fluence value in the calculation of the adjusted reference temperature. The adjustment accounts for changes in the displacements per atom as a function of depth in the metal relative to the neutron fluence, but the adjusted value is not properly representative of the actual neutron fluence.

To further validate the use of the -0.33 value in the exponential term, a number of capsule surveillance reports that had been previously reviewed for reactor fluence information were re-examined to extricate information on the relative intensity of the E > 1.0 MeV neutron flux (or fluence) at the outer edge of the RPV wall (1T position) and the clad-base metal interface (0T position). The relative intensity (ratio) of the neutron flux (or fluence) at the 1T position to that at the 0T position can be used to calculate the neutron fluence at the 1T position, if the fluence level at the 0T position is known. Comparison of this method with the use of Equation (5-1), which relies on RPV thickness and the fluence level at the 0T position, is shown in Table 5-2 for some PWRs. As shown, there is relatively good agreement, <10% difference, between the fluences estimated using the fluence ratios and those estimated using Regulatory Guide 1.99 [125]. For the calculations in this report, the exponential value of -0.33 was used [126].

Figure 5-10 displays the estimated neutron fluence (E > 1.0 MeV) after 60 years of operation at the outside edge of the RPV wall (1T position) on the reactor core mid-plane for each reactor in the operating NPP fleet.

Table 5-2 Estimation of Neutron Attenuation by the RPV

			60-Year Neutron Fluence (E > 1.0 MeV)			
Reactor	RPV Thickness (in)[a]	Maximum Reported Ratio (1T/0T, E > 1.0 MeV)	Clad-Base Metal Interface[b]	Outer RPV Using Reported Ratio	Outer RPV Using RG 1.99 with -0.33 in Exponent[b]	% Difference
Comanche Peak	8.622	0.061 [128]	3.38E+19	2.06E+18	1.96E+18	-4.7
Fort Calhoun	7.122	0.093 [129]	3.50E+19	3.26E+18	3.34E+18	2.5
McGuire 2	8.689	0.060 [130]	2.88E+19	1.73E+18	1.76E+18	2.0
Millstone 2	8.626	0.057 [131]	4.25E+19	2.42E+18	2.47E+18	1.8
Palisades	8.74	0.059 [132]	3.00E+19	1.77E+18	1.68E+18	-5.3
Palo Verde 2	8.902	0.048 [133]	2.83E+19	1.36E+18	1.42E+18	4.4
Salem 2	8.689	0.056 [134]	1.96E+19	1.10E+18	1.11E+18	1.5
St. Lucie 1	8.626	0.057 [135]	4.68E+19	2.67E+18	2.72E+18	1.9
Vogtle 1	8.622	0.064 [136]	3.20E+19	2.05E+18	1.86E+18	-9.3
Vogtle 2	8.622	0.064 [137]	3.02E+19	1.93E+18	1.75E+18	-9.3

[a] For reference only.

[b] As provided in Appendix C, Table C-1.

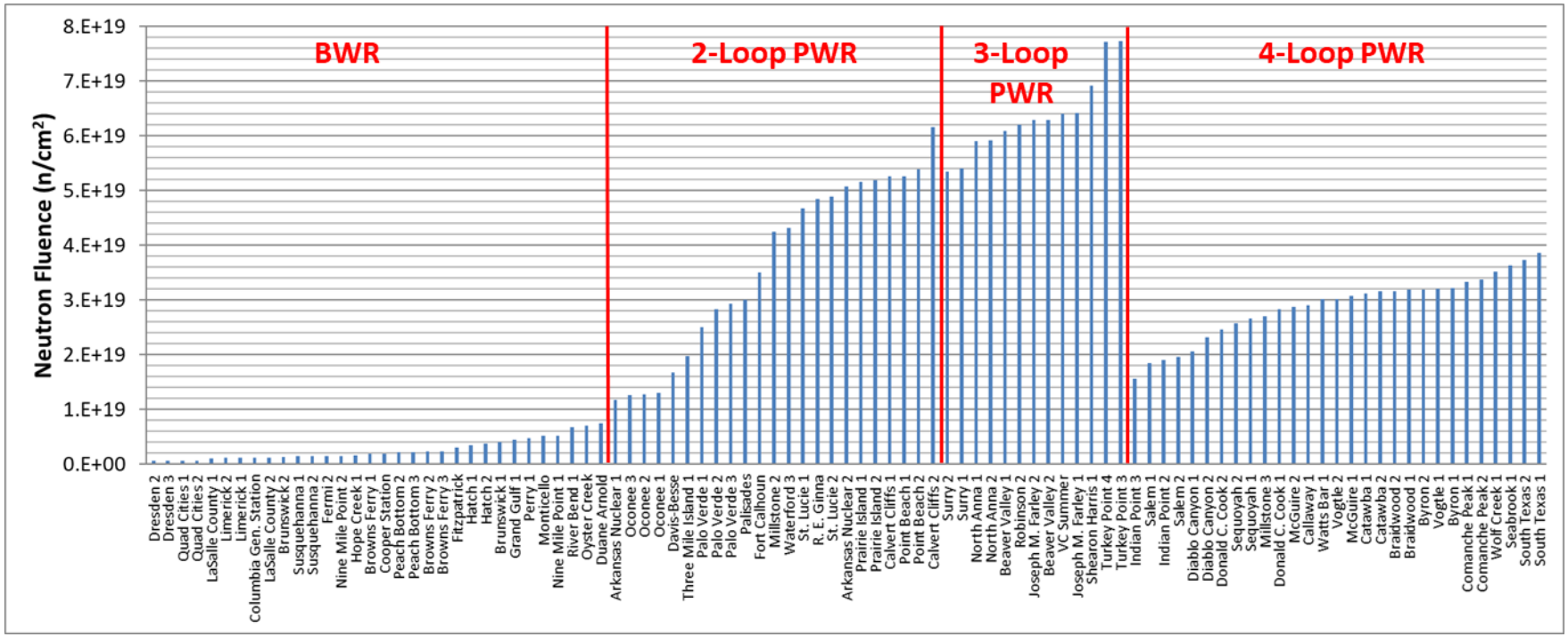

Figure 5-9 Estimated 60-Year Neutron Fluence (E > 1.0 MeV) at Inner RPV Wall (n/cm^2) for Each Operating U.S. NPP

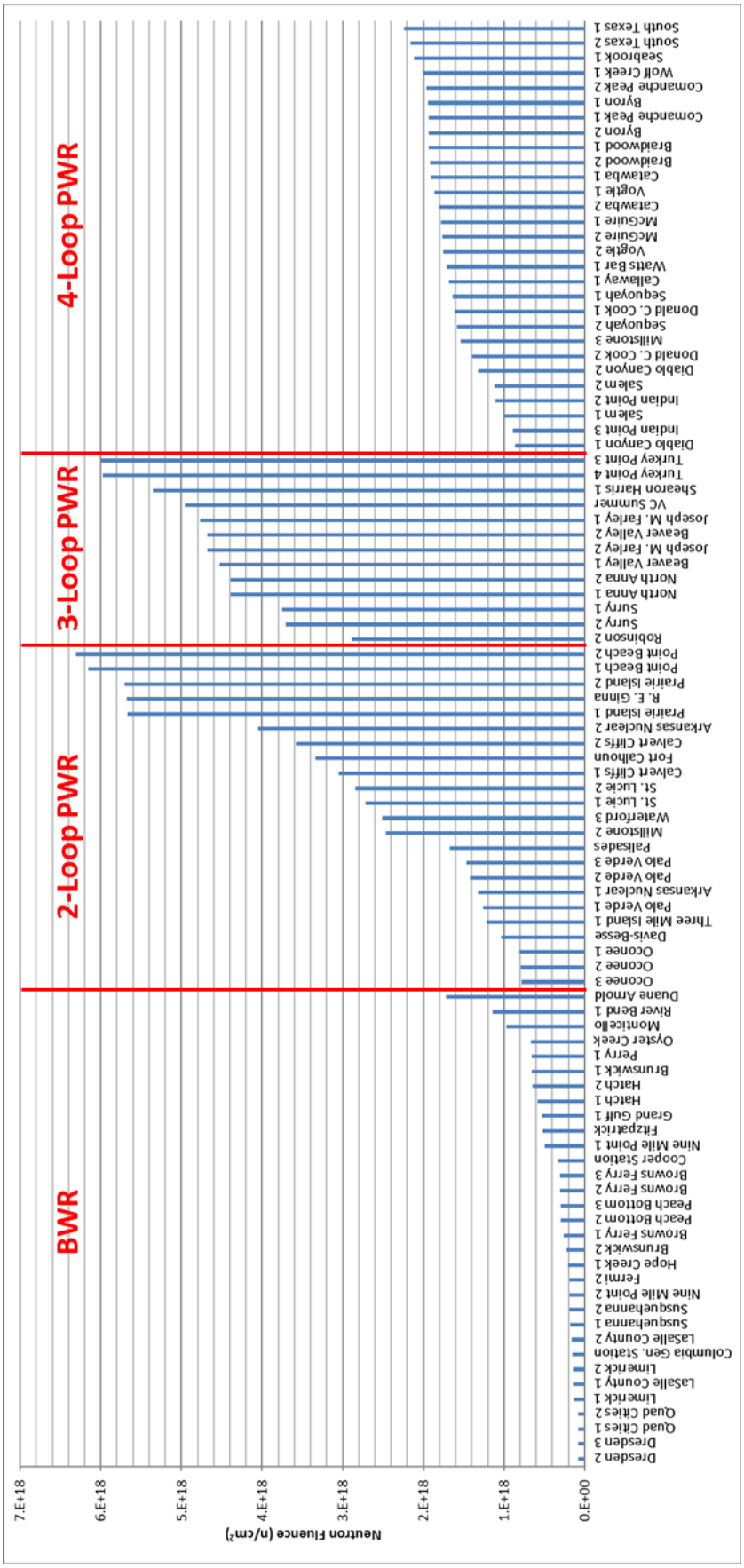

Figure 5-10 Estimated 60-Year Neutron Fluence ($E > 1.0$ MeV) at Outer RPV Wall (n/cm^2) for Each Operating U.S. NPP

5.2.1.3 80-Year Neutron Fluence (E > 1.0 MeV) at the Outer RPV Wall

As a first approximation, the neutron fluence (E > 1.0 MeV) after 80 years of operation at the outer RPV wall was calculated as a linear scaling of the fluence after 60 years of operation for each of the operating NPPs. An alternative approach would be to determine the effective full-power years (EFPYs) for each reactor at the end of an 80-year license and use it with the latest values of EFPY representative of the 60-year fluence levels to generate a scaling factor. In addition, changes in the fuel configuration and power generation (e.g., power uprates) before and after the 60-year operating EFPY timeframe are not considered. If it is eventually determined that fluence levels for a particular reactor may be of concern, it will be necessary to spend additional time and effort to take a closer look at these assumptions. The next step was to estimate the E > 0.1 MeV fluence from that for E > 1.0 MeV.

5.2.1.4 80-Year Neutron Fluence (E > 0.1 MeV) at the Outer RPV Wall

The ratio of E > 0.1 MeV to E > 1.0 MeV neutron fluence was calculated according to the approach taken by Esselman and Bruck [12]. In their report, a curve was fitted to six different pairs of fluence data, using an exponential power form. As shown in Table 5-3, the six different pairs of modeled fluence data from their report were used to generate a ratio curve based on RPV thickness. A curve fit to the data was made using an exponential power form as shown in Figure 5-11, with red lines indicating values within 25% of the curve fit for comparison purposes only. The resulting fit was used to scale the 80-year E > 1.0 MeV fluence levels to E > 0.1 MeV levels at the outer RPV wall. Figure 5-12 presents the estimated final neutron fluence levels (E > 0.1 MeV) for the U.S. NPPs after 80 years of operation. The calculated values are presented in Appendix C.

The curve fit used to convert E > 1.0 MeV fluence levels to E > 0.1 MeV levels at the outer RPV wall is only a rough estimate. To obtain a perspective on the validity of the conversion curve, ex-vessel neutron dosimetry results from several reports with estimated fluxes for both E > 1.0 MeV and E > 0.1 MeV neutrons were compared. The related conversion curve using the Esselman and Bruck data is represented by the blue diamonds in Figure 5-11. Ex-vessel capsule data from Braidwood 1, Braidwood 2, Palisades, H.B. Robinson, McGuire 2, Fort Calhoun, and St. Lucie 1 have been added and are relatively consistent with the original data. Table 5-3 provides the data used to generate Figure 5-11.

The scatter in the data presented in Figure 5-11 emphasizes the combination of uncertainties in the calculations for both the estimate of the E > 1.0 MeV neutron fluence at the outer RPV wall and the conversion to neutron fluence where E > 0.1 MeV. SLR reviews of the impacts of concrete degradation will need to be on a reactor-specific basis and there may be a need to further investigate the uncertainties based on available reactor-specific dosimetry.

Table 5-3 Neutron Fluence Ratio at the Outer RPV Wall

Study	*E* > 0.1 MeV	*E* > 1.0 MeV	RPV Thickness (in)	Ratio 0.1/1.0
Esselman and Bruck [12]				
Three-Loop ORNL	1.43E+10	1.04E+09	9.5	13.75
Three-Loop TwE	1.77E+10	1.31E+09	9.5	13.51
Two-Loop ORNL	3.04E+10	3.58E+09	6.5	8.49
“Thinner vessel” ORNL	1.96E+10	2.62E+09	7.38	7.48
“Medium thickness” ORNL	1.50E+10	1.23E+09	9.53	12.20
“Thickest vessel” ORNL	1.05E+10	5.00E+08	11.91	21.00
Braidwood 1 ex-vessel dosimetry [138]				
Capsule A, core midplane	5.23E+09	5.20E+08	8.5	10.06
Capsule B, core midplane	6.67E+09	6.74E+08	8.5	9.90
Capsule C, core midplane	7.84E+09	7.32E+08	8.5	10.71
Capsule E, core midplane	7.50E+09	6.79E+08	8.5	11.05
Capsule D, top of core	2.73E+09	2.41E+08	8.5	11.33
Capsule F, bottom of core	3.09E+09	2.97E+08	8.5	10.40
Braidwood 2 ex-vessel dosimetry [139]				
Capsule A, core midplane	5.13E+09	5.01E+08	8.5	10.24
Capsule B, core midplane	6.81E+09	6.64E+08	8.5	10.26
Capsule C, core midplane	7.86E+09	7.37E+08	8.5	10.66
Capsule E, core midplane	7.43E+09	6.60E+08	8.5	11.26
Capsule D, top of core	3.09E+09	2.74E+08	8.5	11.28
Capsule F, bottom of core	2.69E+09	2.49E+08	8.5	10.80
H.B. Robinson				
0° cavity, mid cycle 9 **[140]**	7.56E+09	6.51E+08	9.297	11.61
Capsule U, 1.69 m above core midplane **[141]**	2.83E+09	1.68E+08	9.297	16.85

Table 5-3 Neutron Fluence Ratio at the Outer RPV Wall (Cont.)

Study	*E* > 0.1 MeV	*E* > 1.0 MeV	RPV Thickness (in)	Ratio 0.1/1.0
Capsule V, 1.31 m below core midplane **[141]**	4.58E+09	3.13E+08	9.297	14.63
Palisades [132]				
84° cavity Cycle 9	8.05E+09	9.33E+08	8.74	8.63
84° cavity Cycle 10/11	5.40E+09	6.30E+08	8.74	8.57
74° cavity Cycle 8	1.05E+10	1.30E+09	8.74	8.08
74° cavity Cycle 9	6.92E+09	8.53E+08	8.74	8.11
74° cavity Cycle 10/11	5.39E+09	6.43E+08	8.74	8.38
64° cavity Cycle 8	8.50E+09	9.78E+08	8.74	8.69
64° cavity Cycle 9	6.33E+09	7.58E+08	8.74	8.35
64° cavity Cycle 10/11	5.09E+09	5.95E+08	8.74	8.55
54° cavity Cycle 10/11	4.36E+09	4.89E+08	8.74	8.92
39° cavity Cycle 8	6.69E+09	6.86E+08	8.74	9.75
39° cavity Cycle 9	4.62E+09	4.92E+08	8.74	9.39
39° cavity Cycle 10/11	4.19E+09	4.68E+08	8.74	8.95
24° cavity Cycle 10/11	4.54E+09	5.47E+08	8.74	8.30
McGuire 2 [130]				
0°, Cycle 12	4.80E+18	2.63E+17	8.689	18.27
15°, Cycle 12	3.67E+18	3.73E+17	8.689	9.83
30°, Cycle 12	3.82E+18	3.73E+17	8.689	10.24
45°, Cycle 12	2.06E+18	3.72E+17	8.689	5.55
Fort Calhoun [129]				
90°, Cycle 14	8.25E+18	1.01E+18	7.122	8.21
75°, Cycle 14	7.55E+18	9.20E+17	7.122	8.21
60°, Cycle 14	8.18E+18	9.86E+17	7.122	8.29

Table 5-3 Neutron Fluence Ratio at the Outer RPV Wall (Cont.)

Study	*E* > 0.1 MeV	*E* > 1.0 MeV	RPV Thickness (in)	Ratio 0.1/1.0
45°, Cycle 14	1.09E+19	1.36E+18	7.122	8.03
0°, Cycle 14	7.31E+18	8.99E+17	7.122	8.14
St. Lucie 1 [135]				
0°, Cycles 1–4	1.46E+10	1.41E+09	8.626	10.34
15°, Cycles 1–4	1.07E+10	9.35E+08	8.626	11.46
30°, Cycles 1–4	1.02E+10	9.08E+08	8.626	11.22
45°, Cycles 1–4	8.09E+09	6.95E+08	8.626	11.63
0°, Cycle 5	1.42E+10	1.37E+09	8.626	10.34
15°, Cycle 5	8.88E+09	7.76E+08	8.626	11.45
30°, Cycle 5	7.44E+09	6.66E+08	8.626	11.17
45°, Cycle 5	5.67E+09	4.85E+08	8.626	11.68
0°, Cycles 6–9	1.66E+10	1.89E+09	8.626	8.81
15°, Cycles 6–9	1.13E+10	1.17E+09	8.626	9.65
30°, Cycles 6–9	9.62E+09	9.96E+08	8.626	9.67
45°, Cycles 6–9	7.66E+09	7.58E+08	8.626	10.11
0°, Cycle 10	8.80E+09	9.95E+08	8.626	8.85
15°, Cycle 10	8.18E+09	8.58E+08	8.626	9.53
30°, Cycle 10	9.67E+09	1.01E+09	8.626	9.61
45°, Cycle 10	8.03E+09	7.98E+08	8.626	10.07
0°, Cycle 11	7.39E+09	8.42E+08	8.626	8.78
15°, Cycle 11	7.12E+09	7.54E+08	8.626	9.45
30°, Cycle 11	1.03E+10	1.07E+09	8.626	9.61
45°, Cycle 11	8.27E+09	8.27E+08	8.626	10.01
0°, Cycle 12	8.59E+09	9.79E+08	8.626	8.77

Table 5-3 Neutron Fluence Ratio at the Outer RPV Wall (Cont.)

Study	*E* > 0.1 MeV	*E* > 1.0 MeV	RPV Thickness (in)	Ratio 0.1/1.0
15°, Cycle 12	7.78E+09	8.20E+08	8.626	9.49
30°, Cycle 12	1.05E+10	1.09E+09	8.626	9.61
45°, Cycle 12	8.14E+09	8.09E+08	8.626	10.06
0°, Cycle 13	7.87E+09	8.93E+08	8.626	8.81
15°, Cycle 13	7.29E+09	7.70E+08	8.626	9.46
30°, Cycle 13	9.77E+09	1.02E+09	8.626	9.60
45°, Cycle 13	8.09E+09	8.04E+08	8.626	10.06
0°, Cycle 14	8.71E+09	9.89E+08	8.626	8.81
15°, Cycle 14	8.01E+09	8.42E+08	8.626	9.52
30°, Cycle 14	9.82E+09	1.02E+09	8.626	9.60
45°, Cycle 14	8.35E+09	8.32E+08	8.626	10.04
0°, Cycle 15	1.06E+10	1.20E+09	8.626	8.82
15°, Cycle 15	8.37E+09	8.75E+08	8.626	9.57
30°, Cycle 15	7.14E+09	7.43E+08	8.626	9.62
45°, Cycle 15	6.25E+09	6.21E+08	8.626	10.06

5.2.1.5 80-Year Neutron Fluence (E > 0.1 MeV) at the Inner Bioshield Wall

A slight reduction of the neutron fluence will occur in the air gap between the outer RPV wall and the inner wall of the bioshield. In RPV designs with a surrounding neutron shield tank, significant attenuation of the neutron fluence occurs. In many cases, the bioshield inner wall has a steel liner. However, attenuation of the neutron flux by the liner is not expected to be significant. In addition, the level of the neutron fluence will vary as one moves azimuthally or vertically away from the location of the reactor core mid-plane.

One issue that still needs resolution is the expected neutron fluence levels in the area of the nozzle supports (part of what is termed the extended belt-line region) compared to the belt-line fluence levels. Typical axial neutron fluence curves exhibit a rather sharp drop in fluence once past the top or bottom of the fuel core, as shown in Figure 5-13, with a drop of about a factor of 10 at a distance of 2 m (6 ft) from the core midplane. The curves shown are for neutron fluences (*E* > 1.0 MeV) at the clad-base metal interface in seven different azimuthal directions from the axial centerline of the core within one quadrant at a PWR after several operating cycles [132]. Note that overlaps occur at 15° and 75° as well as at 0° and 90° in Figure 5-13.

Fluence levels outside the RPV are expected to follow the same trend, but neutron streaming and scattering in the reactor cavity could cause elevated fluence levels above or below the belt-line [122, 142] and can even result in fast neutron fluence exposures to be higher outside of the RPV rather than at the clad-metal interface in locations away from the core midplane [143]. However, these elevated levels outside the RPV were lower than those fluences in the belt-line region. How much of an impact this has on concrete RPV nozzle support structures depends on how far the structure is from the top of the core, the structural details, the cavity gap, and whether or not a cavity liner is present.

The current focus on potential concrete radiation damage is on the two- and three-loop PWR designs based on the 80-year fluence levels estimated in the previous section. The highest estimated neutron fluence (E > 0.1 MeV) calculated was 7.5×10^{19} n/cm^2 at the outer RPV wall (see Appendix C); however, given the variability and uncertainty in the estimates, neutron fluence levels could approach 1×10^{20} n/cm^2 at the outer RPV wall. For example, a conservative estimate for the Turkey Point Unit 3 and Unit 4 reactors was 9.7×10^{19} n/cm^2 as provided in their SLR application [144]. Concrete support structures nearest the reactor core could be affected. For PWR two-loop and three-loop reactor designs, Tables 5-4 and 5-5, respectively, provide information on specific RPV concrete support characteristics for each reactor such as support type and the horizontal and vertical distances from the RPV outer wall and core mid-plane. In many cases, the shoe supports sit on concrete that is below the plane defined by the top of the core, which is typically 3.7–4.3 m (12–14 ft) long (e.g., see Figure D.3-2 in Appendix D).

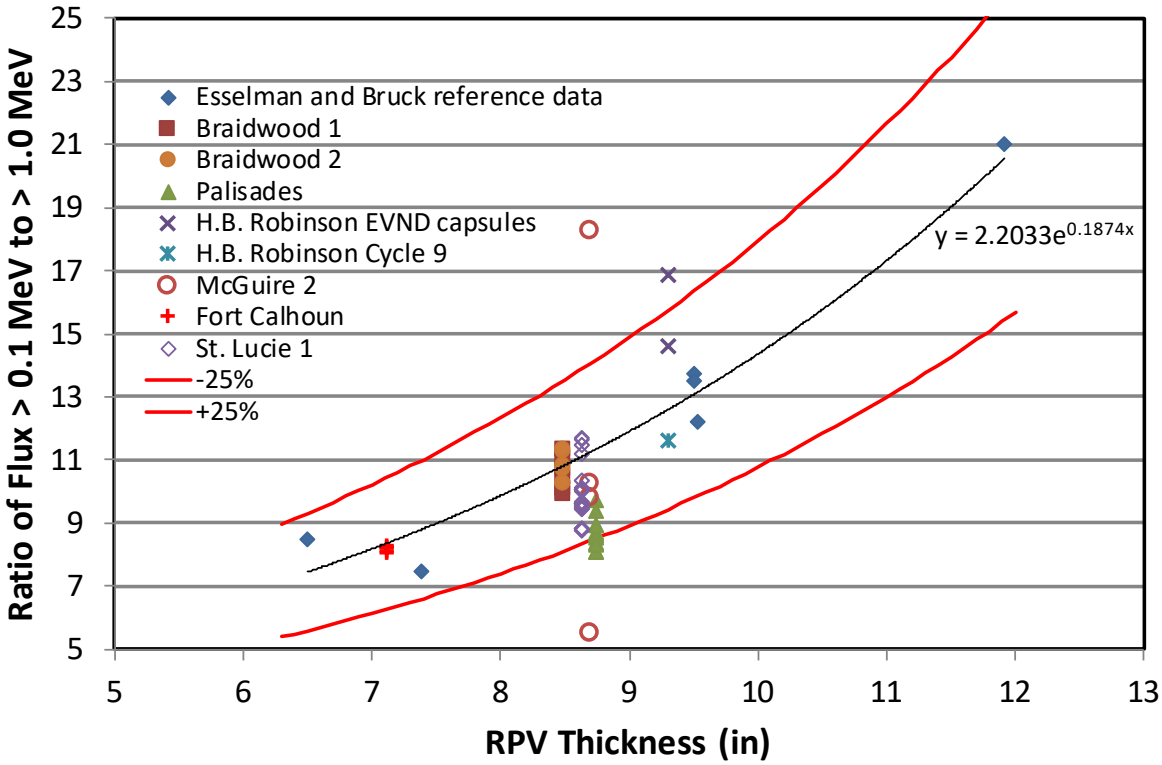

Figure 5-11 Ratio of Neutron Fluence (E > 0.1 MeV / E > 1.0 MeV) at the Outer Edge of the RPV Wall vs. RPV Thickness

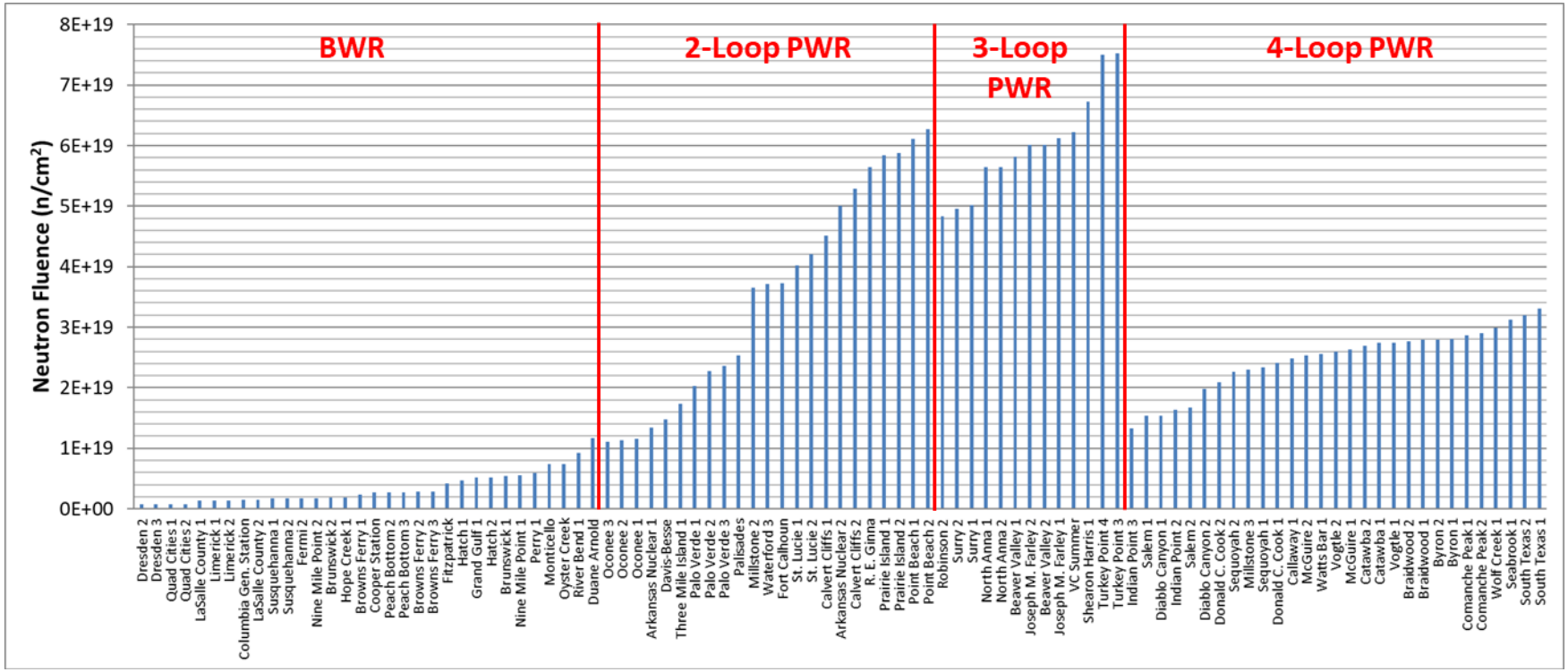

Figure 5-12 Estimated 80-Year Neutron Fluence (E > 0.1 MeV) at Outer RPV Wall (n/cm^2) for Each Operating U.S. NPP

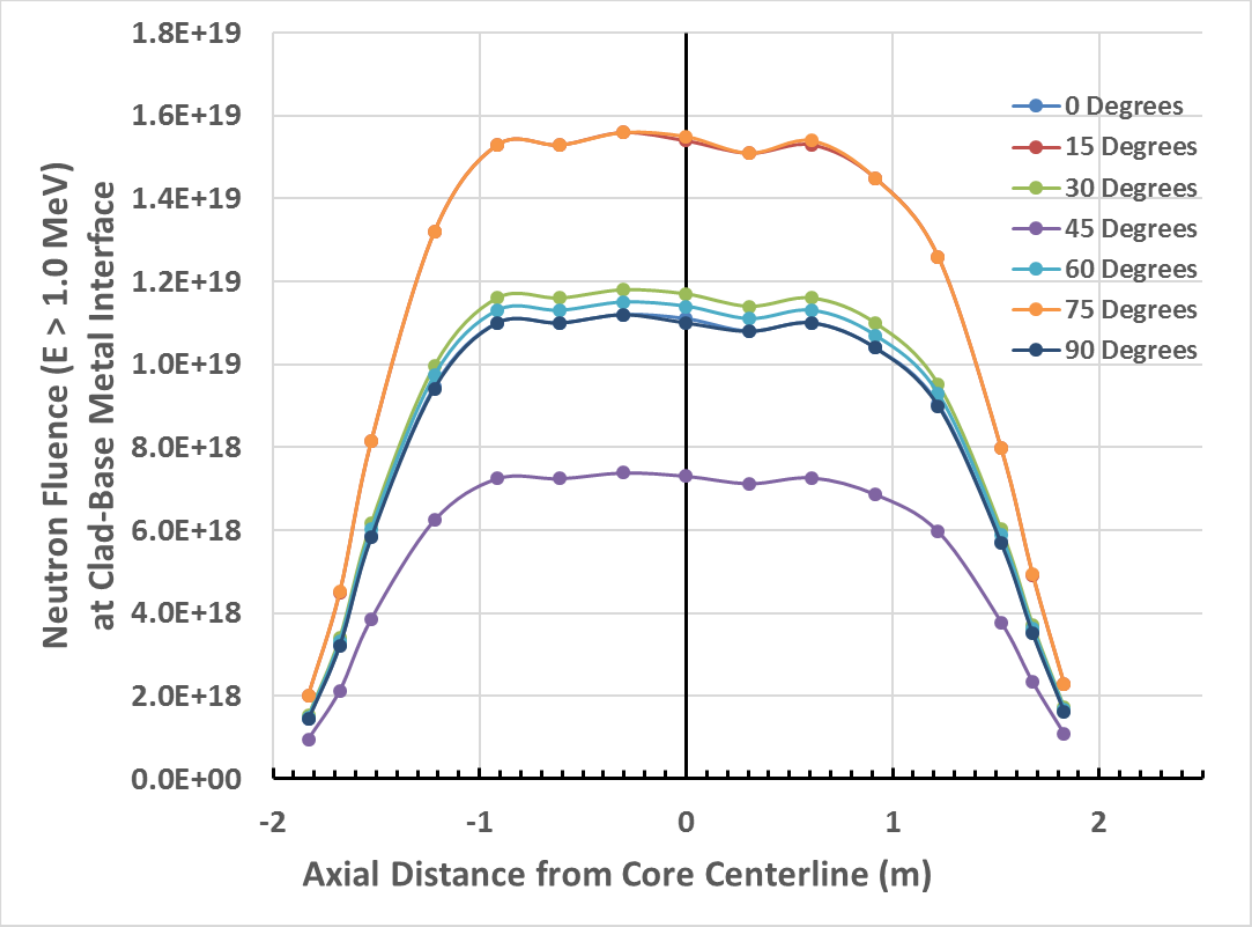

Figure 5-13 Neutron Fluence (*E* > 1.0 MeV) at Clad-Base Metal Interface through Cycle 14 at the Palisades NPP

5.2.2 Gamma Radiation

Few data are available on the expected gamma flux at the outer wall of a commercial RPV and in the reactor cavity. Remec et al. [145] provided an estimated maximum for two-loop PWRs (9.53×10^9/cm^2-s) and three-loop PWRs (3.29×10^9/cm^2-s) for $E > 0.01$ MeV. For a hypothetical 80-year reactor life of 80 years (72 EFPY), the resulting gamma dose at the outer RPV wall would be on the order of 1×10^{10} rad (1×10^8 Gy) or 4×10^9 rad (4×10^7 Gy), respectively. Because the radiation damage threshold for concrete is considered by some to be around 10^{10} rad (10^8 Gy) [5], there is the possibility for some gamma radiation damage by the end of a PWR's lifetime. As an example, the historical gamma flux spectrum (0.8–7.5 MeV) estimates for the Seabrook PWR [59], a four-loop design, result in a gamma dose of approximately 1×10^{10} rad (1×10^8 Gy) after 72 EFPY. Also, the recent SLR application for the Turkey Point Unit 3 and Unit 4 reactors [144] provided a conservative estimate of 3.4×10^{10} rad (3.4×10^8 Gy). Thus, the effects of gamma radiation and the combined effect of gamma and neutron radiation by the end of a PWR's lifetime need to be evaluated.

Table 5-4 PWR Two-Loop RPV Support Configurations and Potential Concrete Damage Areas

Reactor Type[a]	Plant	Number of RPV Support	Support Type	Potential Concrete Damage Area	Estimated Horizontal Distance from RPV Outer Wall	Estimated Vertical Distance from Core Mid-Plane	Ref.
WH	Ginna	6 (4 RPV nozzle supports, 2 RPV bracket supports)	Shoe support siting on shielding wall	Concrete underneath the RPV nozzle supports and bracket supports	6 in.	3 ft	[146]
WH	Point Beach 1, 2	6 (4 RPV nozzle supports, 2 RPV bracket supports)	Ring girder supported by columns	Concrete shelf around the support columns and concrete at base of the support columns	2 in.	12 ft (to column base)	[147-149]
WH	Prairie Island	6 (4 RPV nozzle support, 2 RPV bracket support)	Ring girder supported by columns. Each column is imbedded in the surrounding shielding wall	Concrete at base of each support column and concrete at shielding wall where the top of the column is anchored	NA[b]	NA	[150]
B&WLL	Oconee 1, 2, 3	1	Base skirt support	Concrete at base of the skirt support	0 ft	15 ft	[151]
B&WLL	TMI 1	1	Base skirt support	Concrete at base of the skirt support	0 ft	13 ft	[152]

Table 5-4 PWR Two-Loop RPV Support Configurations and Potential Concrete Damage Areas (Cont.)

Reactor Type[a]	Plant	Number of RPV Support	Support Type	Potential Concrete Damage Area	Estimated Horizontal Distance from RPV Outer Wall	Estimated Vertical Distance from Core Mid-Plane	Ref.
B&WLL	ANO-1	1	Base skirt support	Concrete at base of the skirt support	NA	NA	[153]
B&WRL	Davis-Besse	4 nozzle supports (at four inlets)	Nozzle support sitting on embedded cantilevered steel beam bracket, one under each cold leg nozzle	Concrete around the embedded cantilevered beam brackets that are located near the core mid-plane	3.8 ft	2.3 ft	[154, 155]
CE	ANO-2	3 nozzle supports (2 on inlet, 1 on outlet)	Columns under nozzle pads, horizontal support provided by horizontal beams at nozzle level	Concrete at base of the column supports and at shielding wall	0 ft	~6 ft (to column base)	[156], [157]
CE	Calvert Cliffs 1, 2	3 nozzle supports (2 on inlet, 1 on outlet)	Shoe support siting on shielding wall	Concrete underneath the shoe support	10 in.	2.8 ft	[158]
CE	Fort Calhoun	4 nozzle supports (at four inlets)	NA	NA	NA	NA	[159]

Table 5-4 PWR Two-Loop RPV Support Configurations and Potential Concrete Damage Areas (Cont.)

Reactor Type[a]	Plant	Number of RPV Support	Support Type	Potential Concrete Damage Area	Estimated Horizontal Distance from RPV Outer Wall	Estimated Vertical Distance from Core Mid-Plane	Ref.
CE	Palisades	3 nozzle supports (2 on inlet, 1 on outlet)	Shoe support sitting on concrete (unsure of configuration)	Concrete underneath the shoe support	8 in.	7.5 ft	[160]
CE	Millstone 2	3 nozzle supports (2 on inlet, 1 outlet)	Appears to be shoe support on shielding wall	Concrete underneath the shoe support	NA	NA	[161] [162]
CE	St. Lucie 1, 2	3 nozzle supports (2 on inlet, 1 on outlet)	Nozzle support pads on horizontal beams with their ends embedded in the shielding wall	Concrete around the support beams	8 in.	7.5 ft	[163]
CE	Waterford 3	4 nozzle supports on 4 inlets	Shoe support on embedded ring girder	Concrete underneath the shoe support	16 in.	8.5 ft	[164]
CE S80	Palo Verde 1, 2, 3	4 nozzle supports on 4 inlets	Column support with upper part of each column anchored to shield walling for lateral support	Concrete at column lateral support and base of each column	0 ft	8.5 ft (to column lateral support); 15 ft (to column base)	[58]

[a] WH: Westinghouse; B&WLL: Babcock & Wilcox Lowered-Loop; B&WRL: Babcock &Wilcox Raised-Loop; CE: Combustion Engineering; CE S80: Combustion Engineering System 80.

[b] Not publicly available.

Table 5-5 PWR Three-Loop RPV Support Configurations and Potential Concrete Damage Areas

Reactor Type[a]	Plant	Number of RPV Support	Support Type	Examples of Areas More Susceptible to Degradation	Estimated Horizontal Distance from RPV Outer Wall	Estimated Vertical Distance from Core Mid-Plane	Refs.
WH	Beaver Valley 1, 2	6 (1 under each RPV nozzle)	Shoe support sitting on neutron shield tank	Grout between shield tank and shielding wall on opposite side of RPV. Concrete at base of shielding tank skirt support	3.5 ft (grout) 6 in. (shielding tank skirt support)	6 ft (grout) 31 ft (to base of the shielding tank skirt support)	[56, 165]
WH	Joseph Farley 1, 2	6 (1 under each RPV nozzle)	Shoe support siting on shielding wall	Concrete below the shoe supports	8 in.	7.5 ft	[166]
WH	H.B. Robinson 2	3 (1 under alternating nozzles)	Shoe support sitting on shielding wall	Concrete below the shoe supports	NA[b]	NA	[167]
WH	North Anna 1, 2	6 (1 under each RPV nozzle)	Shoe support sitting on neutron shield tank	Shield tank grouted to shield wall on opposite side of tank from RPV; skirt of neutron shield tank sits on the concrete mat of the containment structure	6 in.	31 ft (to base of the shielding tank skirt support)	[57]
WH	Shearon Harris	6 (1 under each RPV nozzle)	Shoe support sitting on shielding wall	Concrete below the shoe supports	8 in.	7.5 ft	[168-170]

Table 5-5 PWR Three-Loop RPV Support Configurations and Potential Concrete Damage Areas (Cont.)

Reactor Type[a]	Plant	Number of RPV Support	Support Type	Potential Damage Area	Estimated Horizontal Distance from RPV Outer Wall	Estimated Vertical Distance from Core Mid-Plane	Refs.
WH	Surry 1, 2	6 (1 under each RPV nozzle)	Shoe support sitting on neutron shield tank	Limited if any. Neutron shield tank is skirt mounted and sits on the concrete mat of the containment structure	6 in.	31 ft (to base of the shielding tank skirt support)	[171]
WH	Turkey Point 3, 4	6 (1 under each RPV nozzle)	Shoe supports sitting on embedded cantilevered steel beam and column assembly	Concrete below the embedded cantilevered steel beam and column assembly	24 in.	~0 ft (to the bottom of the embedded cantilevered steel beam and column assembly)	[55]
WH	VC Summer 1	6 (1 under each RPV nozzle)	Shoe support sitting on top of embedded steel beam and column assembly	Concrete below the embedded steel beam and column assembly	6 in.	~0 ft (to the bottom of the embedded steel beam and column assembly)	[172]

[a] WH: Westinghouse.

[b] Not publicly available.

6 DESIGN CRITERIA, DEGRADATION, AND MODELING

Given the potential degradation characteristics of concrete after irradiation, a methodology is needed to determine whether a specific concrete structure will meet its design criteria after a period of time in a specific radiation environment. Chapter 4 reviewed the current understanding of concrete degradation due to neutron and gamma irradiation. Chapter 5 reviewed the reactor cavity designs and potential radiation fields that exist in currently operating NPPs. Here, we examine some of the important design criteria for the RPV supports and bioshields and how to relate the change in concrete properties (degradation) because of irradiation to the design criteria.

A short review of relevant design criteria is presented in Section 6.1. Section 6.2 describes the loss-of-coolant accident (LOCA) loads on reactor vessel supports and the concrete shielding wall. Also reviewed are some important factors that impact the structural integrity of reactor vessel supports and the shielding wall due to radiation effects on concrete under combined LOCA and safe shutdown earthquake (SSE) loads (Section 6.3).

Because the interactions within the concrete itself (cement paste–aggregate; rebar reinforcement effects; irradiation effects; temperature and humidity effects) are complex, a knowledge of how microscale interactions translate into macroscale performance is needed to better understand and eventually quantify structural performance in a long-term radiation environment. Section 6.4 reviews current work in this area.

6.1 Design Criteria

The current licensing basis (CLB) design and analysis for operating NPPs includes plant-specific design criteria. Some generic guidance is provided in Section 3.8.3 of the “Standard Review Plan for the Review of Safety Analysis Reports for Nuclear Power Plants” (NUREG-0800) with respect to concrete supports for the reactor, the primary shield wall (bioshield), and the reactor cavity. These criteria include:

- The PWR vessel should be supported and restrained to resist normal operating loads, seismic loads, and design basis accident loads such as loads induced by postulated pipe rupture, including LOCAs.

- The support and restraint system should restrain the movement of the vessel to within allowable limits under the applicable load combinations.

- LOCA loads applicable to the primary shield wall include a differential pressure created across the reactor cavity by a pipe break in the vicinity of the reactor nozzles, acting on the entire cavity or on portions of the cavity.

For reactors that have been shut down for refueling or other reasons, the concrete supports could also be subject to accidental loads such as heavy load drops (e.g., reactor head drop) during servicing/maintenance procedures identified in NUREG-0612 [173].

Another criterion that is important to the proper functioning of bioshield RPV supports is the behavior of anchorages (metal embedments, including those related to a protective metal reactor cavity liner, where applicable) under operating and accident conditions.

6.2 Loads Acting on the Reactor Vessel Support and Primary Shielding Wall

The RPV concrete supports must handle a number of loads simultaneously during normal conditions (startup, normal operations, and shutdown) and under potential accident conditions. Section 6.2.1 provides examples of loads and load combinations that could be encountered, and Section 6.2.2 discusses the more severe accident loads that need to be considered.

6.2.1 Example Loads and Load Combinations [164]

The four major load types considered with examples are:

1. Normal loads
    a. Dead load (D)
    b. Live load (L)
    c. Dead weight of equipment, piping, cable trays, etc. (L')
    d. Water load (F)

2. Severe environmental loads: loads that could infrequently be encountered during the life of a plant
    a. Loads generated by the operating basis earthquake (OBE) (E)

3. Extreme environmental loads
    a. Loads generated by the SSE (E')

4. Abnormal loads: loads generated by a postulated high-energy pipe break accident within the containment and/or compartment thereof
    a. Loss of coolant accident pressure load: pressure equivalent static load within or across a compartment generated by the postulated break and determined by analysis of pressure transients inside the primary and secondary shield wall (P)
    b. Equipment or pipe accident load: the static and dynamic loads exerted upon the containment internal structure by a pipe or piece of equipment because of a postulated LOCA (Q)
    c. Thermal accident load: loads under thermal conditions generated by postulated LOCA, where T' is associated with $1.0P$, whereas T'' is associated with $1.25P$, and T''' is associated with $1.5P$ (T', T'', T''')
    d. Internal missiles loads or jet forces: due to internal missiles associated with the postulated LOCA, like pipe whipping; the effect of jet impingement forces is also included (M)

The ultimate design load (U) considers all potential loads under a given situation. Actual load combinations follow the codes and standards in the CLB for an NPP. Examples of different load combinations for internal concrete structures are:

1. Normal operating
   $U = 1.5(D + L' + T) + 1.8A$

2. Normal shutdown
   $U = 1.5(D + L' + T + F) + 1.8L$
3. Abnormal
   $U = (1.0 \pm 0.1)(D + T) + 1.5P + 1.25(L' + M + A + Q) + T'''$

4. Severe environmental/normal operation
   a) $U = 1.25(D + L' + T + A + E)$
   b) $U = 0.9(D + L') + 1.1E + (1.0 \pm 0.1)T$

5. Severe environmental/normal shutdown
   c) $U = 1.25(D + L' + T + E + F)$
   d) $U = 0.9(D + L' + F) + 1.1E + (1.0 \pm 0.1)T$

6. Abnormal/severe environment
   $U = (1.0 \pm 0.1)(D + T) + 1.25(P + M + Q + A + L' + E) + T''$

7. Extreme environment/normal operation
   $U = (1.0 \pm 0.1)(D + T + L' + F) + 1.0E'$

8. Extreme environment/normal shutdown
   $U = (1.0 \pm 0.1)(D + T + L' + F) + 1.0E'$

9. Abnormal/extreme environment
   $U = (1.0 \pm 0.1)(D + T + L' + A) + 1.0(P + E' + M + Q) + T'$

6.2.2 Accident Loads

The maximum loading on RPV support structures would be expected during accident conditions such as during a LOCA or during a potential SSE.

In a seismic-induced pipe break LOCA event, the discharge water from a pipe break at a reactor vessel nozzle will result in three types of LOCA dynamic loads acting on the reactor vessel support and the primary shielding wall:

1. Forces due to the thrust force at the break (i.e., jet thrust load),

2. Forces due to the differential pressure as the decompression wave travels through reactor internals (i.e., reactor internal LOCA blowdown loads), and

3. Forces on the reactor vessel and shielding wall due to differential pressures in the reactor cavity. (i.e., reactor cavity differential pressure and thermal loads).

These three loads occur simultaneously, are short in duration, and must be combined with the load from the seismic event as part of the load combination in the licensing basis design.

PWR plants have higher primary system pressures and the potential for higher LOCA loads than BWR plants. The three types of LOCA loads and their impacts on reactor vessel supports and the reactor cavity shielding wall are described in the following subsections.

6.2.2.1 Jet Thrust (Impinge) Load

A strong jet of water and steam escaping from the pipe break point (e.g., reactor nozzle) creates an axial thrust force that acts on the pipe. This jet will impinge on nearby structures, potentially creating horizontal and vertical forces at a reactor vessel support. Figure 6-1 shows the pipe jet thrust load acting on the reactor vessel and the reactor vessel supports at the location of the pipe break. For PWRs, these breaks could be on the order of 75 cm (30 in.) in diameter.

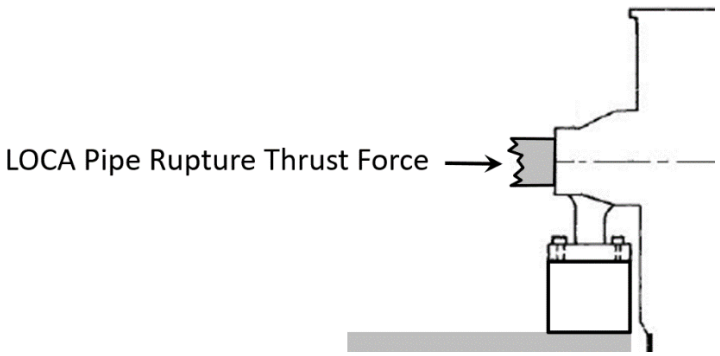

Figure 6-1 LOCA Pipe Rupture Thrust Force

6.2.2.2 Reactor Internal LOCA Blowdown Load

As coolant discharges from the pipe break, a depressurization wave will travel from the break point into the vessel, causing unbalanced loads in the RPV and its internals. These loads are called LOCA blowdown loads. As this decompression wave enters the reactor vessel and travels down the vessel-to-barrel annulus (see Figure 6-2), it will cause the core barrel to deflect sideways toward the side of the decompression wave due to differential pressures acting on the two sides of the core barrel. This sideways deflection of the core barrel will create horizontal and vertical compressive forces on the reactor vessel supports and reactor internals. Such transient differential pressures, although of short duration, could place a significant load on the reactor vessel supports and reactor internals.

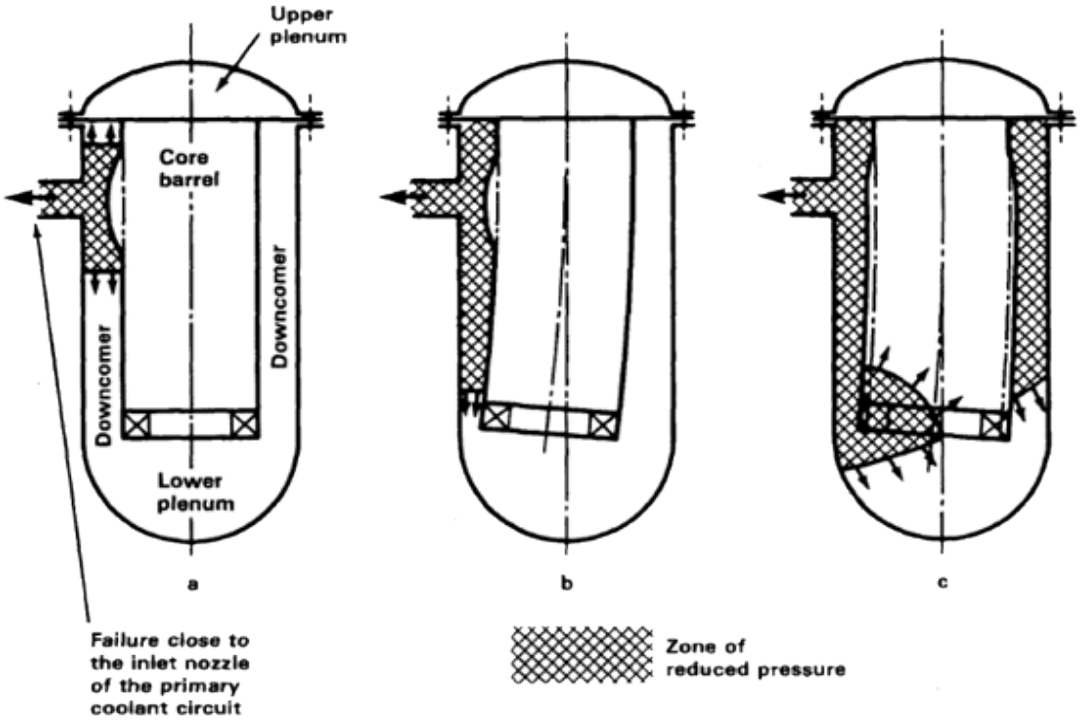

Figure 6-2 LOCA Asymmetric Blowdown Load (Source: NRC NUREG-1609, ADAMS Accession No. ML13255A427)

6.2.2.3 Reactor Cavity Differential Pressure and Thermal Loads

For pipe breaks at one of the reactor vessel nozzles, hot steam will rapidly fill the annulus between the vessel and the shield wall, as well as the cavity. The annulus between the reactor and biological shield wall could become asymmetrically pressurized, resulting in a differential pressure across the vessel in the reactor cavity, as shown Figure 6-3. An asymmetric force acting on the reactor vessel is created due to the transient differential pressures.

Similar to the asymmetric LOCA blowdown forces mentioned above, the asymmetric force acting on the exterior surface of the vessel will cause the reactor vessel to deflect sideways, creating horizontal and vertical forces on the reactor vessel supports. As shown in Figure 6-3, the differential pressures also create forces on the concrete shielding wall and the reactor vessel supports. In addition to the differential pressures, the buildup of hot steam pressure in the cavity will heat the concrete surface and exert thermal loads on the shielding wall and the reactor vessel supports.

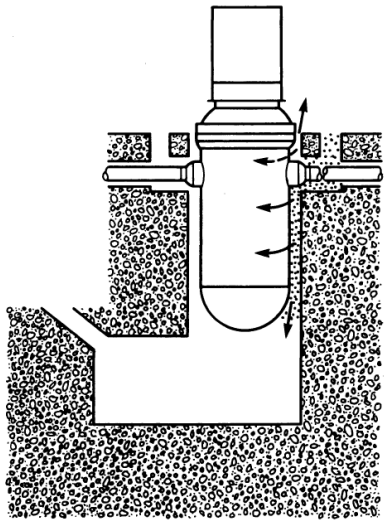

Figure 6-3 Differential Pressures in Reactor Cavity (Source: NRC NUREG-1609, ADAMS Accession No. ML13255A427)

6.3 Structural Analysis Considerations

As discussed in Section 5.1.2, the RPV support design where the RPV metal supports sit directly on top of the bioshield may be more susceptible to radiation damage, because the concrete support is close to the reactor core beltline, where the neutron fluence is higher over time. The maximum loads induced in PWR vessel supports of this type are those from the combined effects of postulated pipe rupture, SSE, and other loads per CLB. Generally, the peak horizontal loads and peak vertical loads do not occur at the same support. The largest vertical load occurs beneath the nozzle on the opposite side from the broken nozzle, and the peak horizontal load occurs on the supports that are mostly perpendicular to the broken nozzle.

The LOCA analyses in the Final Safety Analysis Reports (FSARs) for these reactors postulate a pipe rupture at the RPV inlet and outlet nozzles and the reactor coolant pump outlet nozzle. In a Westinghouse three-loop PWR, for example, the RPV is restrained by the six reactor vessel

support pads and shoes beneath each nozzle and the three reactor coolant loops, with the primary supports of the steam generators and reactor coolant pumps. Following a postulated pipe rupture at the reactor vessel nozzles, the reactor vessel is displaced by the time history loads on the reactor vessel due to the combined effects of three phenomena: reactor coolant loop mechanical loads, reactor cavity pressurization loads, and reactor internal hydraulic forces. The objective of the pipe rupture analyses is to determine the reactor vessel displacements and reactor vessel support loads.

However, analyses for pipe displacement restraints mounted in the primary shield wall estimated that the restraints would limit the break opening area of the vessel nozzle pipe breaks to less than approximately 650 cm^2 (100 $in.^2$) for the inlet nozzle and 200 cm^2 (30 $in.^2$). for the outlet nozzle [174]. Based on similar plant analyses, these areas represent an upper bound by using worst-case vessel and pipe relative motions. Detailed studies have shown that pipe breaks at the inlet and outlet reactor vessel nozzles, even with a limited break area, would give the highest reactor vessel support loads and the highest vessel displacements, primarily due to the influence of reactor cavity pressurization [174]. The displacements and rotation of and about a point represent the centerline of the nozzle attached to the coolant loop leg with the pipe rupture and the vertical centerline of the reactor vessel.

In the case of nozzle shoe supports that rest on the bioshield, care must be taken to properly distribute the loads among and within the shoe components. Each nozzle support consists of two parts: one part (the upper part) that is attached to the nozzle and a lower part that supports the upper and is in turn supported by the concrete bioshield. The baseplate of the lower part is anchored to the bioshield. The upper part is allowed to slide on the lower part to allow for thermal expansion of the RPV. See Figure 5-5 for an example. Thus, the structural analysis must account for the ability of the reactor nozzle to slide on the reactor support shoe, and, in addition, the bearing stress calculation also needs to consider thermal stresses at the reactor support concrete due to the presence of hot steam in the reactor cavity in a LOCA event for assessing the margin for the concrete under the reactor supports.

Regardless of whether normal operating loads or accident loads are considered, any structural analysis would need to account for any abnormal loading caused by concrete support degradation. For example, a decrease in compressive strength of the bioshield wall around RPV supports would lead to stresses and strains within the bioshield, as well as shifting loads on other support structures such as those involved in the reactor coolant system. If a portion of a concrete support structure is degraded, an eccentricity could develop associated with load transfer. Degradation of concrete around metal anchors or embedments could also affect the performance of their intended functions.

6.4 Micromechanical Degradation Models for Concrete under Nuclear Irradiation

Because only limited data is available on concrete degradation under LWR conditions, a methodology is necessary to quantify the radiation damage in a manner that can provide meaningful input to a structural evaluation, as discussed in Section 6.3. One such methodology is to extend existing multiscale models (micrometer to centimeter scale) down to the nanoscale and up to the meter level (macro-scale). Thus, the development of a nanoscale model based on the available degradation data and the application of a fundamental understanding of concrete and its interaction with neutron and gamma radiation at the molecular level can be extended to the macro-scale for use in structural analyses, as discussed in Sections 6.2 and 6.3.

6.4.1 Background

Almost all studies on the degradation of nuclear irradiated concrete are either experimental observations or qualitative descriptions, and there was a lack of modeling work until about 3 or 4 years ago. Publications in this area are very limited compared to the results from available experimental studies.

Finite element method (FEM) based numerical simulations [175-177] were used to study the deterioration of concrete structures under nuclear irradiation. The coupled hygro-thermo-mechanical field in concrete was calculated, and the scalar damage model was implemented to assess the total damage that resulted from thermo-chemo-mechanical and radiation damage. However, the radiation damage the models predicted was based on experimental evidence on the overall degradation of the modulus of elasticity of concrete under neutron radiation from papers such as Hilsdorf et al. [4]. The actual damage process that occurred within the concrete during the nuclear irradiation was not considered. For either analytical or numerical modeling, the radiation damage in the internal structure of the concrete constituents should be considered systematically.

Concrete is a multiphase heterogeneous material with constituent phases that span several scale levels from C-S-H (calcium silicate hydrates) at the nanometer level to crystal phases at the micrometer level such as CH (calcium hydroxide) to sand particles and gravels at the millimeter level (considered the meso-scale level). The constituent phases respond differently to nuclear irradiation, and thus different types of damage are generated. Micro-mechanical models that include all damage mechanisms of the constituent concrete phases due to radiation provide a very good approach to study the effects of radiation on concrete, as shown by the studies reviewed in Section 6.4.2.

There are two different ways to model the microstructure and mesostructure of concrete. One approach is to simplify the internal structures at different scale levels and then use available analytical models in composite mechanics and/or micromechanics to calculate effective properties of the composite (such as the effective modulus of elasticity of concrete) based on the properties of the constituents. The other approach is to simulate the internal structures using the finite element method (FEM) or finite difference method (FDM) at different scale levels. In this approach, the transition between different scale levels must be treated using methods developed in computational mechanics [178].

6.4.2 Review

Le Pape et al. developed a micromechanical model [179] based on an analytical approach that used the Hashin composite sphere model. Neutron radiation-induced effects on aggregate and on cement paste, as well as the interactions between them, were all taken into account. Gamma irradiation effects were not included. The volume change of the aggregate was the summation of neutron radiation induced expansion and thermal expansion. The volume change of the hardened cement paste was considered to be caused by the drying shrinkage and the thermal expansion of the cement paste. The cracking density follows Budiansky and O'Connell's analytical model [180]; a self-consistent scheme was adopted to quantify the damage in cement paste due to moisture loss and high temperature. Two tests with relatively complete information were used to validate the model. It was concluded that the expansion and damage of concrete was dominated by the expanding characteristic of the aggregates. In this model, the internal structures of concrete at small scales were characterized by analytical micromechanical models.

Another study (Giorla et al. [181]) published in the same year as Le Pape et al. [179] also treated the concrete as a two-phase material made of aggregate and cement paste. The difference with the study discussed above is that the two-phase composite was simulated by a two-dimensional mesoscale finite element model (not an analytical model) to analyze its deformation and damage mechanism. Each element had the properties and behavior of either cement paste or aggregate, depending on its location. In the numerical model, the cement paste phase was considered "a quasi-brittle material with a linear softening branch," and its deformation was the combination of elastic strain, creep strains, thermal expansion, and drying shrinkage. The aggregate phase was treated as purely elastic material, and its deformation was the summation of neutron radiation induced expansion of the aggregate and thermal expansion. Overall, concrete strains and continuum damage propagation in the cement paste phase surrounding the aggregate were obtained.

A follow-up study [182] investigated the combined effects of temperature and irradiation on concrete using the same numerical model developed by Giorla et al. [181]. The temperature-dependent volumetric expansion behavior of neutron-irradiated quartz was used as an example to demonstrate the "temperature-induced point-defect annealing phenomenon in minerals" under various radiation levels. The incremental volumetric expansion of quartz over time turned out to be a function of neutron fluence, temperature level, neutron flux, and temperature variation. Thus, using a constant neutron flux and temperature while modeling the radiation process may lead to unreliable results. Based on the same two-dimensional mesoscale finite element model, the progress of damage and viscoelastic processes in the irradiated concrete (and cement paste) were simulated with the implementation of a creep-damage algorithm (Giorla et al. [111]). The results showed that the creep can reduce the damage to concrete when irradiated. None of these studies [111, 179, 181, 182] included gamma irradiation effects, and radiation transport processes through the material are not considered, which indicates that the neutron fluence is spatially uniform within the material domain concerned.

A comprehensive numerical study was conducted in Japan [109] in which the behavior of nuclear irradiated concrete was evaluated in one dimension by coupling heat diffusion, moisture diffusion, a cement-based material model, and the deterministic radiation transport code "ANISN" [183]. The heat and moisture diffusion were modeled by the FDM. The material model provided the phase transformation during cement hydration and material properties. ANISN was used to calculate the neutron flux, gamma-ray dose, and radiation heat in concrete. The effect of gamma irradiation was analyzed but not included in the model. The temperature-dependent expansion behavior of neutron irradiated quartz was also used to take into account the neutron radiation effect on aggregate. The overall strain of the concrete was obtained by a composite analytical model. A relationship between expansive strain and compressive strength reduction of concrete was developed based on the available test data from neutron irradiation or ASR. This relationship was used to compute the degradation of the concrete compressive strength along the depth of a biological shielding wall. The predictions of the model were compared with the results from a compressive loading test of cores from a biological shielding wall in the Japan Power Demonstration Reactor.

Recently, a new micromechanics-based analytical model was developed by team members of the current review study [184]. This new model can predict the mechanical properties of nuclear irradiated concrete taking into account the deterioration mechanisms at multiscale levels and spatial distributions of the multiphase constituents. This model characterizes the mechanism of the degradation of the elastic modulus of the neutron-irradiated concrete and individually considers the effects of neutron radiation and temperature on the mechanical properties of

constituents of concrete. In other words, the effects of neutron irradiation and radiation heating on the modulus of elasticity of concrete were separated and calibrated by the available experimental data. The model also estimated the shrinkage of the hardened cement paste. The model can be used to predict the degradation of the modulus of elasticity and the volume change of neutron irradiated concrete under two different scenarios: (1) without experimental data of nuclear irradiation for a specific concrete—in this case, the model prediction will be based on available test data in the literature; or (2) when some experimental data of nuclear irradiation for a specific concrete in a NPP are available (such as the volume expansion of aggregate used in the concrete)—in this case, the experimental data can be incorporated in the model to enhance the accuracy of model prediction.

6.4.3 Future Directions

The currently available models are valid only from the centimeter scale (the so-called representative volume element, RVE) down to the micrometer level. The models need to be further developed in two directions in order to be used in structural analysis for concrete structures in NPPs. One direction is to consider the effects of nuclear irradiation on the nanostructure of C-S-H and on the expansion of aggregates. The current models depend on experimental results that were summarized by several empirical equations for C-S-H and for aggregates. What happens in C-S-H and aggregates under nuclear irradiation should be further studied and characterized. The other direction is to extend the multiscale models up to the meter level (the macro-structural level), because the degradation of concrete materials must be reflected in the structural analysis (as discussed in Section 6.3), which is the ultimate goal of the multiscale analysis. To this end, the multiscale models should be integrated with commercial finite element software, or their results accounted for in the models used by those codes, so that engineers can use the available software as a platform to consider the structural effects of nuclear irradiation.

7 PLANT-SPECIFIC DETAILS

7.1 Plant-Specific RPV/Bioshield Configurations with High Projected Fluence Levels

As shown in Figure 5-12, all PWRs have an estimated 80-year neutron fluence level greater than 1.0×10^{19} n/cm^2 ($E > 0.1$ MeV) at the outer RPV shell. For an initial comparison with the results from Esselman and Bruck [12], those two- and three-loop reactors were selected for which the estimated neutron fluence ($E > 0.1$ MeV) at the outer RPV shell was greater than that estimated in this review for the highest four-loop reactor estimate (3.3×10^{19} n/cm^2), as shown in Table 7-1. This cutoff level down-selects a more manageable number of 24 reactors for consideration, including all three-loop reactors, and provides a range of support configurations that cover all major support designs that will require evaluation as each of the U.S. fleet of PWRs applies for a license extension to 80 years. The four-loop reactors are a newer design expected to undergo SLR at a later time, generally exhibit lower neutron fluence levels, and have similar support structure designs.

The two major differences between Esselman and Bruck [12] and this review in the results are the use of different estimates for the 60-year fluences (often due to the availability of more recent data for use in this review) and scaling to 80 years. Scaling to 80 years by EFPY (which accounts for only the time during which the reactor is assumed to be in full operation for the remaining 20 years) was used by Esselman and Bruck versus scaling by year (assumes the reactor will have the same operation time versus down time as in its full previous history by multiplying the 60-year result by 80/60) in this review. There are also some differences in RPV thickness, but most of these were less than a difference of 0.75 cm (0.3 in.) and are likely due to reported thicknesses that may or may not include the inner cladding. The starting 60-year fluence and RPV thickness for North Anna 2 was the same in both studies.

As shown in Table 7-1, the 80-year fluence levels at the outer RPV wall are similar in both studies. Of interest is the location of the RPV supports, including the supporting concrete in the reactor cavity. In general, the more susceptible supports will be located closer to the reactor core, where radiation is the highest. The approximate horizontal and vertical distances from the core mid-plane to supporting concrete are listed in Table 7-1 and depicted in Figure 7-1.

The reactors that are more susceptible to concrete bioshield support degradation are those where the reactor supports sit on the concrete bioshield in close proximity, and directly exposed to, the core radiation (NPPs highlighted in yellow in Table 7-1). The PWRs resting on support skirts, neutron shield tanks, or pedestal (metal column) supports may not have any significant long-term concrete irradiation degradation issues because the distance from the core to the base of the reactor cavity is greater, and/or because they are shielded by a tank. However, the effect of irradiation on concrete support structures in close proximity to the core mid-plane requires evaluation, and the effect of irradiation on steel structures and components continues to be an item of interest for future evaluation, along with their impacts on concrete support structures. A summary of the reactor vessel support designs for the reactors listed in Table 7-1 is provided in Appendix D for reference.

None of the reactors identified in Table 7-1 rest on a support skirt. The reactor vessels at Beaver Valley 1 and 2, North Anna 1 and 2, and Surry 1 and 2 have shoe supports that are mounted on neutron shield tanks. The reactor vessels at ANO 2, Point Beach 1 and 2, and Prairie Island 1 and 2 are mounted on column supports that are anchored on the concrete

basemat. The tops of the support columns at ANO 2 are anchored to the bioshield by embedded horizontal steel braces. For the Point Beach reactors, the support legs pass through openings in a concrete shelf structure that comes within inches of the RPV outer wall. The narrow openings in the shelf structure are intended to provide some support of the pedestal legs, should they buckle under loads imposed by potential accidents [185]. The steel column supports for the Prairie Island reactors are embedded in the concrete bioshield, as noted in Table 5-4.

The VC Summer 1 and the Turkey Point reactors have reactor supports that sit on embedded steel cantilever beams near the inside edge of the bioshield opposite the reactor core. In those two cases, the concrete in question is between the vertical embedded steel beams and the reactor cavity.

St. Lucie 1 and St. Lucie 2 have support shoes that sit on steel beams that are supported by the bioshield. Waterford 3 rests on an embedded ring girder that extends into the reactor cavity from the side of the bioshield.

Table 7-1 Reactors with the Highest Estimated Neutron Fluence at 80 Years[a]

	Neutron Fluence (n/cm^2, $E > 0.1$ MeV)			Distance between Core Mid-Plane and Reactor Vessel Support[b]	
	This Review	Esselman and Bruck[12]	Support Configuration	Horizontal (D1)	Vertical (D2)
Arkansas Nuclear One 2	5.00E+19	6.11E+19	Column	~0 ft	~6 ft
Beaver Valley 1	5.82E+19	6.80E+19	Shield Tank	3.5 ft grout	6 ft grout
Beaver Valley 2	5.82E+19	5.97E+19	Shield Tank	3.5 ft grout	6 ft grout
Calvert Cliffs 1	4.52E+19	4.02E+19	Bioshield	10 in.	2.8 ft
Calvert Cliffs 2	5.29E+19	4.23E+19	Bioshield	10 in.	2.8 ft
Joseph M. Farley 1	6.13E+19	5.74E+19	Bioshield	8 in.	7.5 ft
Joseph M. Farley 2	6.01E+19	5.42E+19	Bioshield	8 in.	7.5 ft
Fort Calhoun[c]	3.72E+19				
R. E. Ginna	5.64E+19	6.64E+19	Bioshield	6 in.	3 ft
H.B. Robinson 2	6.12E+19	5.43E+19	Bioshield	NA[d]	NA

Table 7-1 Reactors with the Highest Estimated Neutron Fluence at 80 Years[a] (Cont.)

	Neutron Fluence (n/cm^2, $E > 0.1$ MeV)			Distance between Core Mid-Plane and Reactor Vessel Support[b]	
	This Review	Esselman and Bruck[12]	Support Configuration	Horizontal (D1)	Vertical (D2)
Shearon Harris 1	6.72E+19	6.66E+19	Bioshield	8 in.	7.5 ft
Millstone 2	3.65E+19	3.53E+19	Bioshield	NA	NA
North Anna 1	5.64E+19	6.13E+19	Shield Tank	6 in.	31 ft
North Anna 2	5.65E+19	5.91E+19	Shield Tank	6 in.	31 ft
Point Beach 1	6.12E+19	5.21E+19	Column	Concrete. Shelf[e]	Concrete. Shelf
Point Beach 2	6.27E+19	5.90E+19	Column	Concrete. Shelf	Concrete. Shelf
Prairie Island 1	5.84E+19	5.94E+19	Column	NA	NA
Prairie Island 2	5.87E+19	5.99E+19	Column	NA	NA
St. Lucie 1	4.02E+19	3.75E+19	Beam on Shield	8 in.	7.5 ft
St. Lucie 2	4.20E+19	3.91E+19	Beam on Shield	8 in.	7.5 ft
VC Summer	6.23E+19	6.46E+19	Cantilever	6 in.	~0 ft
Surry 1	5.01E+19	6.04E+19	Shield Tank	6 in.	31 ft
Surry 2	4.96E+19	5.91E+19	Shield Tank	6 in.	31 ft
Turkey Point 3	7.52E+19	6.70E+19	Cantilever	2 ft	~0 ft
Turkey Point 4	7.50E+19	6.70E+19	Cantilever	2 ft	~0 ft
Waterford 3	3.71E+19	5.36E+19	Ring Girder[f]	16 in.	8.5 ft

[a] Highest estimate at the outer wall of the RPV as calculated in this report. Entries highlighted in yellow identify reactors where the RPV supports rest on the bioshield wall near the core.

[b] See Figure 7-1. Distance is from the core mid-plane to the nearest concrete support structure. Distances are approximate.

[c] Not considered in this study. Reactor will not participate in SLR.

[d] Not publicly available.

Footnotes continued on next page.

Table 7-1 Reactors with the Highest Estimated Neutron Fluence at 80 Years[a] (Cont.)

[e] Support columns pass through holes in a concrete shelf adjacent to the RPV. See text for additional description.

[f] Waterford 3 is a CE PWR with the support shoes sitting directly on a concrete encased metal ring support extending from the bioshield.

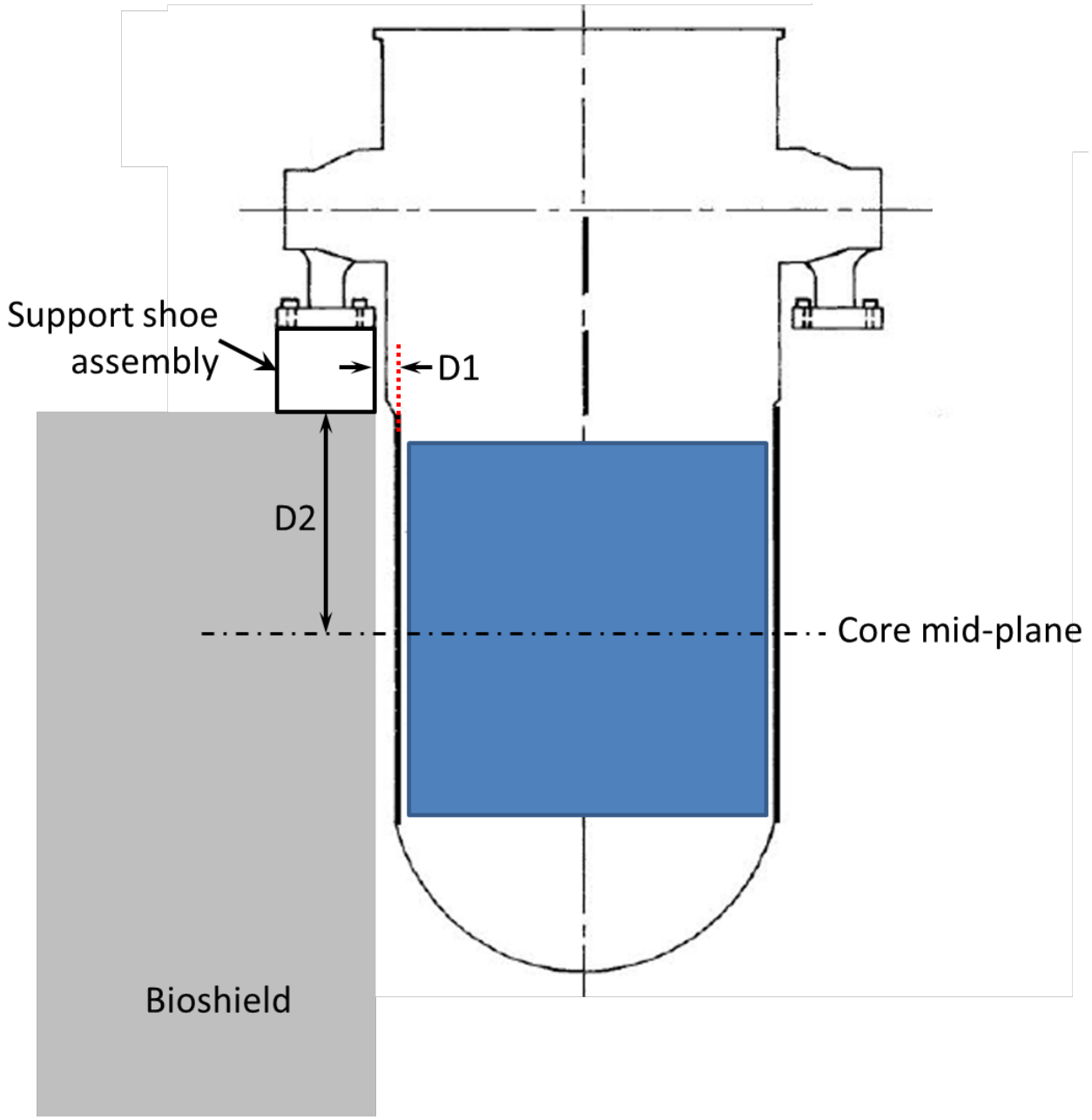

Figure 7-1 Schematic of the Horizontal (D1) and Vertical (D2) Distances between the Core Mid-plane and an RPV Support Assembly

7.2 Recommendations

A proper structural analysis that accounts for irradiation-induced concrete degradation for each reactor requires detailed knowledge of the reactor concrete supports, the potential neutron fluence levels, and the impacts on concrete from nuclear radiation. Such a structural analysis is limited by the uncertainties in these areas, discussed below, which require a detailed knowledge of each plant-specific design. Just as important, although not covered in this review, is the potential irradiation damage to the metal components of the support system. As for the interface and interaction between the metal and concrete components, little is known relative to irradiation degradation of this type of bonding in an LWR environment, as discussed in Section 4.3.5.

More detailed reactor support design and past, present, and future operating information than considered in this review is needed. Design information includes specific details on the interface of the metal reactor supports with the supporting concrete involving location and specific configuration (e.g., horizontal/vertical restrictions, tolerances, material specifications, loading conditions, surface area, and anchorages) as well as average operating conditions (e.g., temperature and humidity) and any off-normal conditions. Operating information includes up-to-date details on current EFPY, planned capacity factors (fraction of operating time versus total time; accounts for future EFPY), and configuration changes (e.g., power uprates, fuel type, loading patterns) for estimating the 80-year neutron fluence level.

From the limited available data, it is not clear which of the reactors supported directly on the bioshield, on cantilever beams, or on an extended ring girder would be the most susceptible to irradiation-assisted concrete degradation. The example group identified in Table 7-1 covers the major PWR support design variations estimated to experience the highest neutron fluence levels, but structural support systems for all PWRs need to be evaluated based on plant-specific conditions. Inclusion of the inherent uncertainties in the 80-year fluence level estimates for all PWRs could lower or extend estimates on an individual basis. For the PWRs at the lower end, uncertainties could extend estimates within the range of the levels considered in Table 7-1. The fluence levels generated for this study are intended to be reasonable estimates rather than overly conservative values. Thus, individual estimates presented in Table 7-1 could also be higher.

It is unlikely that reactors that are supported directly on neutron shield tanks or steel columns that rest on the concrete basemat will experience irradiation-induced concrete degradation that would compromise critical concrete support structures before the end of 80 years of operation. However, many of these designs also incorporate horizontal supports that are embedded in the bioshield in areas of higher nuclear radiation.

As shown in Appendix D, the PWR support design can vary widely for similar reactors. Thus, the actual design of each structural support system needs to be reviewed in order to assess its susceptibility to concrete degradation due to irradiation. Complete reactor support analyses are needed for all reactors for a proper structural analysis. As a result, the impact of nuclear radiation on critical concrete RPV support structures should be determined on a plant-specific basis for the purposes of SLR.

In addition, the reactor cavity has a steel liner for many reactors. While not a structural component itself, the liner itself has a structural impact on the bioshield at anchorage and support locations, imposing additional stress and strain on the bioshield. The liner also has an impact on the moisture content of the bioshield, as well as potentially imposing confinement and constraint on the face of the bioshield. These effects need to be considered synergistically with potential irradiation impacts. Another consideration is the location of the liner attachments to the bioshield that may be located in the highest radiation region in the reactor cavity.

8 SUMMARY AND CONCLUSION

The scope of this review was to evaluate the data available on the degradation of irradiated concrete as it pertains to critical RPV support structures at commercial NPPs in the context of the SLR application process. The review considered available data on the physical and mechanical properties of neutron- and gamma-irradiated concrete and its components, aggregate, and cement paste. Rough estimates of nuclear radiation levels in the reactor cavity accumulated over 80 years of operation were evaluated for each commercial NPP. Finally, a range of specific RPV support designs were reviewed.

8.1 Concrete Irradiation Damage

A more complete understanding of irradiation impacts on concrete is needed. As discussed in Chapters 3 and 4, we have a rudimentary knowledge of how nuclear irradiation causes alterations in concrete under LWR conditions. Further investigation of how neutrons and gamma-rays independently impact concrete and its constituents is required, particularly in the area of aggregate composition with respect to neutron radiation and concrete as a whole related to gamma radiation. Furthermore, studies are required to investigate the impacts of nuclear radiation on concrete–metal (steel) bonding to address the performance of steel reinforcements and anchorages. Knowledge of these effects will be useful in the development of the microscale model necessary to account for concrete irradiation damage and translate the results to the macroscale regime for traditional structural analysis.

Neutron fluence levels above 1×10^{19} n/cm^2 ($E > 0.1$ MeV) at temperatures found in LWR reactor cavities (below 100°C) can cause significant degradation of concrete's physical and mechanical properties, as summarized in Section 4.4.1. The onset of noticeable degradation appears at fluence levels above 1×10^{18} n/cm^2. The contributing factors and degradation mechanisms are not well understood. There is strong, but not conclusive, experimental evidence that the primary effect is related to the disordering effect of neutrons on aggregate structures, especially those with a covalent bond structure such as that found in siliceous minerals with a quartz structure. Since aggregates are a mix of different mineral types and not pure compounds, characterizing their composition and component grain sizes is important when determining their susceptibility to radiation induced degradation.

Gamma dose levels above 1×10^8 Gy may result in the degradation of concrete properties, but there is no data directly related to the isolated gamma irradiation of concrete in an air environment. The primary impact of gamma irradiation on concrete is water loss from the cement paste due to heating and radiolysis, which results in some shrinkage of the cement paste. The loss of water results in more open pore space within the cement paste, but this effect may be partially counteracted by gamma-induced carbonation of portlandite to calcite, where the calcite occupies slightly more volume than portlandite. These gamma irradiation impacts require additional study.

The synergistic effects neutron and gamma radiation have on concrete are not known at this time. Most of the reviewed neutron irradiation data were obtained using a nuclear reactor as a source, and much of this did not track the corresponding gamma dose or qualify the neutron spectrum. In addition, there is little neutron- or gamma-only data under LWR conditions available for comparative purposes.

The synergistic effects of nuclear radiation and heat are also not well-characterized. At temperatures below 100°C, thermal effects can solely lead to some degradation in mechanical properties. Higher temperatures also correlate with the apparent onset of quartz volume expansion under neutron irradiation shifting to higher neutron fluence values.

Issues that remain to be explored include those related to degradation depth, steel reactor cavity liners, and bonding between steel embedments and concrete. The neutron and gamma radiation are attenuated as they pass into the bioshield or other concrete support structure. At some depth, the radiation levels will be below those that cause significant degradation that could affect support functions. In addition, even if the degradation is limited to a short distance from the face of the inner bioshield wall, the degradation can lead to strains within the bioshield that extend much further. For NPPs with a steel cavity liner, the liner could confine and constrain concrete expansion due to neutron irradiation at the bioshield surface. The liner would also affect the relative amounts of water present in the concrete by limiting movement of water and its byproducts due to heating and radiolysis caused by gamma radiation. Steel embedments such as rebar and anchorages are used throughout the bioshield and RPV supports. Irradiation degradation of concrete support structures would be exacerbated by failure of the metal–concrete bond before failure of either the metal or concrete.

8.2 80-Year Radiation Levels and Reactor Support Designs

Rough values of the neutron fluence levels after 80 years of operation were estimated for all operating U.S. commercial reactors. The highest estimated fluence level at the outer face of the RPV wall was found to be greater than 1×10^{19} n/cm^2 ($E > 0.1$ MeV) for all PWRs, and less than 1×10^{19} n/cm^2 for all BWRs except one. These estimates are near or at the core mid-plane. The neutron fluence levels will rapidly decrease above the top and below the bottom of the reactor core. However, there are indications that streaming effects could increase the fluence levels near RPV supports in these areas, but not higher than the core mid-plane values.

In general, the distance from the RPV wall to the inner face of the bioshield is about 15 to 20 cm (a few inches), thus the radiation levels at the face of the bioshield will be roughly equivalent to that estimated at the face of the outer RPV wall. There are a variety of reactor designs and design/architecture/engineering implementations, even for the same reactor design. For the PWRs that are supported by the bioshield, the PWR concrete support locations on or in the bioshield are within a few feet of the highest radiation levels emanating from the reactor. PWRs resting directly on the bioshield or cantilever beams anchored in the bioshield across from the beltline region may be the most susceptible to concrete degradation issues over 80 years of operation because the concrete supports receive the most radiation. Other PWR designs such as those that rest on steel columns may have horizontal supports anchored in or on the bioshield within a few feet of the belt-line region.

Currently operating BWRs are supported on a metal skirt that rests on a concrete pedestal within the containment building. In most cases, radiation from the core is expected to be significantly attenuated by distance and intervening metallic components before it exits the RPV near its base and strikes the underlying concrete. Thus, because the neutron fluence is lower than in PWRs when compared at the core mid-plane and the aforesaid attenuation, significant degradation of the supporting concrete is not likely after 80 years. On the other hand, BWR installations vary somewhat due to the different generations of BWRs and the design/architecture/engineering implementation. For example, many of the BWRs have horizontal stabilizers above the core mid-plane that are anchored in the bioshield, which may experience higher fluence levels than the concrete under the support skirts.

8.3 Conclusion

The present review indicates that all operating PWRs have the potential to generate neutron fluence levels in the reactor cavity that could result in concrete degradation before 80 years of operation. However, the extent of any potential degradation of concrete RPV supports cannot be quantified in a general manner because of a need for specific detailed design information, an incomplete knowledge of the radiation levels at specific support locations, and an incomplete understanding of the effect and extent of nuclear irradiation on the concrete supports in an LWR operating environment. Although BWRs are expected to experience lower radiation levels and are not likely to experience issues related to concrete irradiation-induced degradation, certain aspects of a given design may need to be addressed. Furthermore, there are NPPs that are operating under off-normal conditions in some cases, that are monitored as part of their aging management plans, which could impact concrete irradiation degradation mechanisms. Thus, the impact of nuclear radiation on critical concrete support structures should be considered on a case-by-case basis as part of an SLR application.

9 REFERENCES

1. Naus, D.J., 2007, *Primer on Durability of Nuclear Power Plant Reinforced Concrete Structures - A Review of Pertinent Factors*, NUREG.CR-6927, Oak Ridge National Laboratory, for the U.S.Nuclear Regulatory Commission, Washington, DC, February.

2. U.S. Nuclear Regulatory Commission, 2010, *Standard Review Plan for Review of License Renewal Applications for Nuclear Power Plants,* NUREG-1800, Rev. 2, Office of Nuclear Reactor Regulation, Washington, DC.

3. U.S. Nuclear Regulatory Commission, 2017, *Standard Review Plan for Review of Subsequent License Renewal Applications for Nuclear Power Plants,* NUREG-2192, Office of Nuclear Reactor Regulation, Washington, DC. ADAMS Accession No. ML17188A158.

4. Hilsdorf, H.K., J. Kropp, and H.J. Koch, *The Effects of Nuclear Radiation on the Mechanical Properties of Concrete*, in *Douglas McHenry International Symposium on Concrete and Concrete Structures*. 1978, American Concrete Institute. p. 223-251.

5. Kontani, O., Y. Ichikawa, A. Ishizawa, M. Takizawa, and O. Sato, *Irradiation Effects on Concrete Structure*, in *International Symposium on the Ageing Management & Maintenance of Nuclear Power Plants*. 2010, Mitsubishi Research Institute. p. 173 - 182.

6. Fujiwara, K., M. Ito, M. Sasanuma, H. Tanaka, K. Hirotani, K. Onizawa, M. Suzuki, and H. Amezawa, *Experimental Study of the Effect of Radiation Exposure to Concrete*, in *20th International Conference on Structural Mechanics in Reactor Technology (SMiRT 20)*. 2009, International Association for Structural Mechanics in Reactor Technology: Espoo (Helsinki), Finland. p. 8 pages.

7. Kontani, O., Y. Ichikawa, A. Ishizawa, M. Takizawa, and O. Sato, *Irradiation Effects on Concrete Structures*, in *Infrastructure Systems for Nuclear Energy*, T.T.C. Hsu, C.-L. Wu, and J.-L. Lin, Editors. 2014, John Wiliey & Sons, Ltd. p. 459 - 473.

8. Kontani, O., S. Sawada, I. Maruyama, M. Takizawa, and O. Sato. *Evaluation of Irradiation Effects on Concrete Structure: Gamma-Ray Irradiation Tests on Cement Paste*. in *ASME 2013 Power Conference*. 2013. Boston, Massachusetts.

9. Vodák, F., K. Trtík, V. Sopko, O. Kapičková, and P. Demo, 2005, *Effect of γ-irradiation on strength of concrete for nuclear-safety structures.* Cement and Concrete Research. **35**(7): p. 1447-1451.

10. William, K., Y. Xi, and D. Naus, 2013, *A Review of the Effects of Radiation on Microstructure and Properties of Concretes Used in Nuclear Power Plants*, NUREG/CR-7171, U. of Houston, U. of Colorado, Oak Ridge National Laboratory, for the U.S.Nuclear Regulatory Commission, Washington, DC, November.

11. U.S. Department of Energy. *Light Water Reactor Sustainability (LWRS) Program*. 2016 [cited 2016 July 24, 2916]; Available from: http://www.energy.gov/ne/nuclear-reactor-technologies/light-water-reactor-sustainability-lwrs-program.

12. Esselman, T. and P. Bruck, 2018, *Expected Condition of Concrete Exposed to Radiation at Age 80 Years of Reactor Operation*, ORNL/TM-2018/769, Oak Ridge National Laboratory.

13. American Concrete Institute, 1971, *Building Code Requirements for Reinforced Concrete,* ACI Standard 318-71, Detroit, MI.

14. Naus, D.J., 2010, *A Compilation of Elevated Temperature Concrete Material Property Data and Information for Use in Assessments of Nuclear Power Plant Reinforced Concrete Structures*, NUREG/CR-7031, Oak Ridge National Laboratory, for U.S. Nuclear Regulatory Commission, Washington, DC, December.

15. Schneider, U. and H. Herbst, 2002, *Theoretical considerations about spalling in tunnels at high temperatures*, Technical University Vienna, Austria.

16. Castellote, M., C. Alonso, C. Andrade, X. Turrillas, and J. Campo, 2004, *Composition and Microstructural Changes of Cement Pastes Upon Heating, as Studied by Neutron Diffraction.* Cement and Concrete Research. **34**(9): p. 1633-1644.

17. Piasta, J., 1989, *Heat Deformation of Cement Phases and Microstruction of Cement Paste.* Materials and Structures. **17**(102): p. 415-420.

18. Mindess, S. and J.F. Young, 1981, *Concrete*, Prentice-Hall, New Jersey.

19. Feldman, R.F. and P.J. Sereda, 1968, *A Model for Hydrated Portland Cement Paste as Deduced from Sorption-Length Change and Mechanical Properties.* Materials and Structures. **1**(6): p. 509-520.

20. Chen, J., X. Jin, J. Nanguo, and Y. Tian, 2014, *A Nano-Model for Micromechanics-Based Elasticity Prediction of Hardened Cement Paste.* Magazine of Concrete Research. **66**(22): p. 1145-1153.

21. Roziere, E., A. Loukili, and F. Cussigh, 2009, *A Performance Based Approach for Durabiity of Concrete Exposed to Carbonation.* Construction and Building Materials. **23**: p. 190 - 199.

22. Papadakis, V.G., M.N. Fardis, and C.G. Vayenas, 1992, *Effect of Composition, Environmental Factors and Cement-Lime Mortar Coating on Concrete Carbonation.* Materials and Structures. **25**(149): p. 293-304.

23. Brunauer, S. and L.E. Copeland, 1964, *The Chemistry of Concrete.* Scientific American. **210**: p. 80 - 92.

24. Bensted, J., *Hydration of Portland Cement*, in *Advances in Cement Technology*, S.N. Ghosh, Editor. 1983, Pergamon Press: New York. p. 307 - 347.

25. Frigione, G., *Gypsum in Cement*, in *Advances in Cement Technology*, S.N. Ghosh, Editor. 1983, Pergamon Press: New York. p. 485 - 535.

26. Taylor, H.F.W., *Chemistry of Cement Hydration*, in *8th International Congress on the Chemistry of Cement*. 1986. p. 82 - 110.

27. Duguid, A. and G.W. Scherer, 2010, *Degradation of Oilwell Cement Due to Exposure to Carbonated Brine.* International Journal of Greenhouse Gas Control. **4**(3): p. 546-560.

28. Ho, D.W.S. and R.K. Lewis, 1987, *Carbonation of Concrete and Its Prediction.* Cement and Concrete Research. **17**: p. 489 - 504.

29. Vanzo, J., 2009, *A Nanochemomechanical Investigation of Carbonated Cement Paste*, Master of Science in Civil and Environmental Engineering, in Department of Civil and Environmental Engineering, Massachusetts Institute of Technology.

30. Zhang, C., J. Zhang, B. Peng, and H. Qiao, 2011, *Depth and Prediction Model of Oilwell Cement Stone Eroded by Carbon Dioxide.* Journal of the Chinese Ceramic Society. **38**(9): p. 1782 - 1787.

31. Hunkeler, F., *Corrosion in Reinforced Concrete: Processes and Mechanisms*, in *Corrosion in Reinforced Concrete Structures*, H. Bohni, Editor. 2005, CRC Press: Boca Raton. p. 1 - 45.

32. Kropp, J. and H.K. Hilsdorf, 1995, *Performance Criteria for Concrete Durability - a State of the Art Report*, RILEM Technical Committee TC 116-PCD, London.

33. Chang, J. and Y. Fang, 2015, *Quantitative Analysis of Accelerated Carbonation Products of the Synthetic Calcium Silicate Hydrate(C-S-H) by QXRD and TG/MS.* Journal of Thermal Analysis and Calorimetry. **119**(1): p. 57-62.

34. Ding, S., Z. Shui, T. Pan, W. Chen, and W. Xu, *Effects of Curing Conditions on Carbonation of Concrete Containing Expansive Admixture*, in *The 2013 World Congress on Advances in Structural Engineering and Mechanics (ASEM13)*. 2013: Jeju, Korea. p. 3298 - 3312.

35. Kawamura, M. and K. Iwahori, 2004, *ASR Gel Composition and Expansive Pressure in Mortars Under Restraint.* Cement & Concrete Composites. **26**(1): p. 47-56.

36. Stanton, T.E., 1940, *Expansion of Concrete Through Reaction Between Cement and Aggregate.* Proceedings, American Society of Civil Engineers. **66**: p. 1781-1811.

37. Shehata, M.H. and M.D.A. Thomas, 2000, *The Effect of Fly Ash Composition on the Expansion of Concrete due to Alkali-Silica Reaction.* Cement and Concrete Research. **30**(7): p. 1063-1072.

38. Jin, W., 1998, *Alkali-Silica Reaction in Concrete with Glass Aggregate - A Chemico-Physico-Mechanical Approach*, Ph.D. Dissertation, Columbia University: New York.

39. Bleszynski, R.F. and M.D.A. Thomas, 1998, *Microstructural Studies of Alkali-Silica Reaction in Fly Ash Concrete Immersed in Alkaline Solutions.* Advanced Cement Based Materials. **7**(2): p. 66-78.

40. Dent Glasser, L.S. and N. Kataoka, 1981, *The Chemistry of 'Alkali-Aggregate' Reaction.* Cement and Concrete Research. **11**: p. 1 - 9.

41. Dent Glasser, L.S. and N. Kataoka, 1982, *On the Role of Calcium in the Alkali-Aggregate Reaction.* Cement and Concrete Research. **12**: p. 321 - 331.

42. Deschenes, D.J., O. Bayrak, and K.J. Folliard, 2009, *ASR/DEF - Damaged Bent Caps: Shear Tests and Field Applications*, Texas Department of Transportation.

43. Diamond, S. *Chemistry and Other Characteristics of ASR Gels*. in *11th International Conference on Alkali-Aggregate Reaction in Concrete*. 2000. Quebec City, Canada.

44. Diamond, S. and N. Thaulow, 1974, *A Study of Expansion Due to Alkali - Silica Reaction as conditioned by the Grain Size of the Reactive Aggregate.* Cement and Concrete Research. **4**: p. 591-607.

45. Suwito, A., W. Jin, Y. Xi, and C. Meyer, 2002, *A Mathematical Model for the Pessimum Size Effect of ASR in Concrete.* Concrete Science and Engineering. **4**(13): p. 23-34.

46. Gago, R., J.V. Zulueta, and F. Abella, *The Ageing of Concrete Dams Due to Alkali-Silica Reactions*, in *Proceedings of the 21st Congress on Large Dams*. 2003: Montreal, Canada. p. 1083 - 1091.

47. Hobbs, D.W., *Alkali-Silica Reaction in Concrete*. 1988, London: Thomas Telford.

48. Mather, B., 1999, *How to Make Concrete That Will Not Suffer Deleterious Alkali-Silica Reaction.* Cement and Concrete Research. **29**: p. 1277 - 1280.

49. Touma, W.E., D.F. Fowler, and R.L. Carrasquillo, 2001, *Alkali-Silica Reaction in Portland Cement Concrete: Testing Methods and Mitigation Alternatives*, Research Report ICAR 301-1F, International Center for Aggregates Research, Austin, TX.

50. Meyer, C. and Y. Xi, 1999, *Use of Recycled Glass and Fly Ash for Precast Concrete.* Journal of Materials in Civil Engineering. **11**(2): p. 89 - 90.

51. Dron, R. and F. Brivot, 1993, *Thermodynamic and Kinetic Approach to the Alkali-Silica Reaction, Part 2: Experiment.* Cement and Concrete Research. **23**(1): p. 93 - 103.

52. Willam, K., Y. Xi, K. Lee, and B. Kim, 2009, *Thermal Response of Reinforced Concrete Structures in Nuclear Power Plants*, SESM No. 02-2009, University of Colorado at Boulder.

53. Evans, J.C., E.L. Lepel, R.W. Sanders, C.L. Wilkerson, W. Silker, C.W. Thomas, K.H. Abel, and D.R. Robertson, 1984, *Long-Lived Activation Products in Reactor Materials*, NUREG/CR-3474, Pacific Northwest Laboratory, for U.S. Nuclear Regulatory Commission, Washington, DC, August.

54. Duke Energy, 2017, *Oconee Nuclear Station Updated Final Safety Analysis Report, Revision 26,* Docket Nos. 50-269, 50-270, 50-287, Seneca, SC. ADAMS Accession No. ML17234A027.

55. Florida Power & Light Company, 2018, *Turkey Point Units 3 and 4 Updated Final Safety Analysis Report - Unit 4 Cycle 29 Update and License Renewal 10 CFR 54.37(b)*

Report, Docket Nos. 50-250 and 50-251, Homestead, FL. ADAMS Accession No. ML18117A091-Chapter 3; ML18117A092-Chapter 4; ML18117A093-Chapter 5.

56. First Energy Nuclear Operating Company, 2014, *Beaver Valley, Unit 2, Submittal of the Updated Final Safety Analysis Report, Revision 21,* Docket No. 50-412, Shippingport, PA. ADAMS Accession No. ML14339A419.

57. Virginia Electric and Power Company (Dominion), 2016, *North Anna Power Station Units 1 and 2 Updated Final Safety Analysis Report Revision 52,* Docket Nos. 50-338, 50-339, Richmond, VA. ADAMS Accession No. ML17033B477.

58. Arizona Public Service, 2017, *Palo Verde Nuclear Generating Station Units 1, 2, and 3 Updated Final Safety Analysis Report, Revision 19,* Docket Nos. 50-528, 50-529, 50-530, Phoenix, AZ. ADAMS Accession No. ML17193A009.

59. NextEra Energy Seabrook, LLC, 2019, *Seabrook Station Updated Final Safety Analysis Report, Revision 19,* Docket No. 50-443, Seabrook, NH. ADAMS Accession No. ML19101A185.

60. U.S. Nuclear Regulatory Commission, undated, *Westinghouse Technology Systems Manual,* Human Resources Training and Development, Chattanooga, TN. ADAMS Accession No. ML20057E160.

61. Glasstone, S. and A. Sesonke, *Nuclear Reactor Engineering*. 1967, New York: Van Nostrand Reinhold Company.

62. Jevremovic, T., *Nuclear Principles in Engineering*. 2nd ed. 2009, New York: Springer Science+Business Media LLC.

63. Bacon, G.E., *Neutron Scattering in Chemistry*. 1977, London: Butterworth & Co. (Publishers) Ltd.

64. Agrawal, H.M., *Nuclear Physics, Problem-based Approach Including MATLAB*. 2016, Delhi, India: PHI Learning Private Limited.

65. Dubrovskii, V.B., S.S. Ibragimov, V.V. Koronevskii, A.Y. Ladygin, V.K. Pergamenshchik, and V.S. Perevalov, 1970, *Hematite Concrete for Shielding Against High Neutron Fluxes.* Soviet Atomic Energy. **28**(3): p. 336 - 338.

66. Maruyama, I., O. Kontani, M. Takizawa, S. Sawada, S. Ishikawa, J. Yasukouchi, O. Sato, J. Etoh, and T. Igari, 2017, *Development of Soundness Assessment Procedure for Concrete Members Affected by Neutron and Gamma-Ray Irradiaion.* Journal of Advanced Concrete Technology. **15**: p. 440-523.

67. Alexander, S.C., 1963, *Effects of Irradiation on Concrete, Final Results*, AERE-R 4490, Atomic Energy Research Establishment, for U.K.A.E. Authority, Harwell, Berkshire, United Kingdom.

68. Kelly, B.T., J. Brocklehurst, D. Mottershead, S. McNerney, and I. Davidson, *The Effect of Reactor Radiation on Concrete*, in *Second information meeting on prestressed concrete reactor pressure vessels and their thermal isolation*. 1969, Commision of the European Communities: Brussels. p. 237 - 266.

69. Field, K.G., I. Remec, and Y.L. Pape, 2015, *Radiation effects in concrete for nuclear power plants – Part I: Quantification of radiation exposure and radiation effects.* Nuclear Engineering and Design. **282**: p. 126-143.

70. Primak, W., 1958, *Fast-Neutron-Induced Changes in Quartz and Vitreous Silica.* Physical Review. **110**(6): p. 1240-1254.

71. Wittels, M.C., 1957, *Structural behaviour of neutron irradiated quartz.* Philosophical Magazine. **2**(24): p. 1445-1461.

72. Bykov, V.N., A.V. Denisov, V.B. Dubrovskii, V.V. Korenewskii, G.K. Krivokoneva, and L.P. Muzalevskii, 1981, *Effect of Irradiation Temperature on the Radiation Expansion of Quartz.* Soviet Atomic Energy. **51**(3): p. 593 - 595.

73. Elleuch, L.F., F. DuBois, and J. Rappeneau, *Effects of Neutron Radiation on Special Concretes and Their Components*, in *Concrete for Nuclear Reactors*. 1972, American Concrete Institute: Berlin. p. 1071 - 1109.

74. Dubrovskii, V.B., S.S. Ibragimov, M.Y. Kulakovskii, A.Y. Ladygin, and B.K. Pergamenshchik, 1967, *Radiation Damage in Ordinary Concrete.* Soviet Atomic Energy. **23**(4): p. 1053 - 1058.

75. Gilmore, G.R., *Practical Gamma-ray Spectrometry*. 2nd ed. 2008, West Sussex, England: John Wiley & Sons, Ltd.

76. Martin, J.E., *Physics for Radiation Protection*. 3rd ed. 2013, Weinheim, Germany: Wiley-VCH Verlag GmbH & Co.

77. Chilton, A.B., J.K. Shultis, and R.E. Faw, *Principles of Radiation Shielding*. 1984, Englewood Cliffs, NJ: Prentice-Hall, Inc.

78. Evans, R.D., *The Atomic Nucleus*. 1955, New York: McGraw-Hill, Inc.

79. Mockel, H.J. and R.H. Koster, 1982, *Gas Formation During the Gamma Radiolysis of Cemented Low- and Intermediate-Level Waste Products.* Nuclear Technology. **59**(3): p. 494-497.

80. Bar-Nes, G., A. Katz, Y. Peled, and Y. Zeiri, 2008, *The Combined Effect of Radiation and Carbonation on the Immobilization of Sr and Cs Ions in Cementitious Pastes.* Materials and Structures. **41**(9): p. 1563-1570.

81. Bibler, N.E. and E.G. Orebaugh, 1977, *Radiolytic Gas Production from Tritiated Waste Forms, Gamma and Alpha Radiolysis Studies*, DP-1459, Savannah River Laboratory, Aiken, SC.

82. Lowinska-Kluge, A. and P. Piszora, 2008, *Effect of Gamma Irradiation on Cement Composites Observed with XRD and SEM Methods in the Range of Radiation Dose 0 - 1409 MGy.* Acta Physica Polonica A. **114**(2): p. 399 - 411.

83. Vodák, F., V. Vydra, K. Trtík, and O. Kapičková, 2011, *Effect of gamma irradiation on properties of hardened cement paste.* Materials and Structures. **44**(1): p. 101-107.

84. Mobasher, N., S.A. Bernal, H. Kinoshita, C.A. Sharrad, and J.L. Provis, 2015, *Gamma Irradiation Resistance of an Early Age Slag-Blended Cement Matrix for Nuclear Waste Encapsulation.* Journal of Materials Research. **30**(9): p. 1563-1571.

85. Ichikawa, T. and H. Koizumi, 2002, *Possibility of Radiation-Induced Degradation of Concrete by Alkali-Silica Reaction of Aggregates.* Journal of Nuclear Science and Technology. **39**(8): p. 880-884.

86. Kaplan, M.F., *Concrete Radiation Shielding: Nuclear Physics, Concrete Properties, Design and Construction*. 1989, Essex, England: Longman Scientic & Technical.

87. Naus, D.J., 2006, *The Effect of Eleveated Temperature on Concrete Materials and Structures - A Literature Review*, NUREG/CR-6900, Oak Ridge National Laboratory, for U.S. Nuclear Regulatory Commission, Washington, DC, March. ADAMS Accession No. ML060970563.

88. Kelly, B.T. and I. Davidson, *Irradiation Effects on Concrete*, in *Conference on Prestressed Concrete Pressure Vessels*. 1968, The Institution of Civil Engineers: Westminster. p. 173 - 175.

89. Van der Schaaf, C.F., *Effect of Heating and Radiation on Some Properties of Mortar and Concrete Specimens with Different Compositions*, in *Information meeting on work relating to prestressed concrete vessels and their isolation*. 1967, Euratom: Brussels.

90. Sommers, J.F., 1969, *Gamma Radiation Damage of Structural Concrete Immersed in Water.* Health Physics. **16**: p. 503 - 508.

91. Kitsutaka, Y. and K. Matsuzawa, *The Effect of Gamma Radiation on the Fracture Properties of Concrete*, in *Fracture Mechanics of Concrete and Concrete Structures - Recent Advances in Fracture Mechanics of Concrete*, B.H. Oh et. al, Editor. 2010, Korea Concrete Institute: Seoul.

92. Soo, P. and L.W. Milian, 1989, *Sulfate-Attack Resistance and Gamma-Irradiation Resistance of Some Portland Cement Based Mortars*, NUREG/CR-5279, Brookhaven National Laboratory, for U.S. Nuclear Regulatory Commission, Washington, DC.

93. Soo, P. and L.M. Milian, 2001, *The Effect of Gamma Irradiation on the Strength of Portland Cement Mortars.* Journal of Materials Science Letters. **20**: p. 4.

94. Blundell, R., C. Diamond, and R. Browne, 1976, *The Properties of Concrete Subjected to Elevated Temperatures*, Report No. 9, Construction Industry Research and Information Association,, London, June.

95. Sullivan, P.J.E., *The Effects of Temperature on Concrete*, in *Developments in Concrete Technology - 1*, F.D. Lydon, Editor. 1979, Applied Science Publishers: London.

96. Komonen, J. and V. Penttala, 2003, *Effects of High Temperature on the Pore Structure and Strength of Plain and Polypropylene Fiber Reinforced Cement Pastes.* Fire Technology. **39**(1): p. 23-34.

97. Rani, S.D. and M. Santhanam, 2012, *Influence of Moderately Elevated Temperatures on Engineering Properties of Concrete Used for Nuclear Reactor Vaults.* Cement & Concrete Composites. **34**(8): p. 917-923.

98. Kakae, N., K. Miyamoto, T. Momma, S. Sawada, H. Kumagai, Y. Ohga, H. Hirai, and T. Abiru, 2017, *Physical and Thermal Properties of Concrete Subjected to High Temperature.* Journal of Advanced Concrete Technology. **15**(6): p. 190-212.

99. Schneider, U., 1988, *Concrete at High-Temperatures - a General Review.* Fire Safety Journal. **13**(1): p. 55-68.

100. Graves, H., Y. Le Pape, D. Naus, J. Rashid, V. Saouma, A. Sheikh, and J. Wall, 2014, *Expanded Materials Degradation Assessment (EMDA), Volume 4: Aging of Concrete and Civil Structures*, Vol. 4, NUREG/CR-7153, Expert Panel, for the U.S.Nuclear Regulatory Commission, Office of Nuclear Regulatory Research, Washington, DC, ADAMS Accession No. ML14279A349.

101. Lee, J., Y. Xi, K. Willam, and Y. Jung, 2009, *A Multiscale Model for Modulus of Elasticity of Concrete at High Temperatures.* Cement and Concrete Research. **39**(9): p. 754-762.

102. Dubrovskii, V.B., S.S. Ibragimov, A.Y. Ladygin, and B.K. Pergamenshchik, 1966, *Effect of Neutron Irradiation on Some Properties of Heat-Resistant Concretes.* Soviet Atomic Energy. **21**(2): p. 5.

103. Dubrovskii, V.B., S.S. Ibragimov, A.Y. Ladygin, M.Y. Kulakovskii, and B.K. Pergamenshchik, 1968, *Radiation Stability of Serpentine Concrete.* Soviet Atomic Energy. **25**(6): p. 1345 - 1346.

104. Johannesson, B. and P. Utgenannt, 2001, *Microstructural Changes Caused by Carbonation of Cement Mortar.* Cement and Concrete Research. **31**(6): p. 925-931.

105. Houst, Y.F. and F.H. Wittmann, 2002, *Depth Profiles of Carbonates Formed During Natural Carbonation.* Cement and Concrete Research. **32**: p. 1923 - 1930.

106. Ichikawa, T. and T. Kimura, 2007, *Effect of Nuclear Radiation on Alkali-Silica Reaction of Concrete.* Journal of Nuclear Science and Technology. **44**(10): p. 1281-1284.

107. Douillard, L. and J.P. Duraud, 1996, *Swift Heavy Ion Amorphization of Quartz - A Comparative Study of the Particle Amorphization Mechanism of Quartz.* Nuclear Instruments & Methods in Physics Research Section B-Beam Interactions with Materials and Atoms. **107**(1-4): p. 212-217.

108. Pignatelli, I., A. Kumar, K.G. Field, B. Wang, Y. Yu, Y. Le Pape, M. Bauchy, and G. Sant, 2016, *Direct Experimental Evidence for Differing Reactivity Alterations of Minerals following Irradiation: The Case of Calcite and Quartz.* Sci Rep. **6**: p. 20155.

109. Maruyama, I., K. Haba, O. Sato, S. Ishikawa, O. Kontani, and M. Takizawa, 2016, *A Numerical Model for Concrete Strength Change Under Neutron and Gamma-Ray Irradiation.* Journal of Advanced Concrete Technology. **14**(4): p. 144-162.

110. McDowall, D.C., *The Effect of Gamma Irradiation on the Creep Properties of Concrete*, in *Results of Concrete Irradiation Programmes*, H. Benzler, Editor. 1971, Commission of the European Communities: Brussels. p. 55 - 69.

111. Giorla, A.B., Y. Le Pape, and C.F. Dunant, 2017, *Computing Creep-Damage Interactions in Irradiated Concrete.* Journal of Nanomechanics and Micromechanics. **7**(2): p. https://doi.org/10.1061/(ASCE)NM.2153-5477.0000118.

112. Pomaro, B., 2016, *A Review on Radiation Damage in Concrete for Nuclear Facilities: From Experiments to Modeling.* Modeling and Simulation in Engineering: p. 1-10.

113. Gray, B.S., *The Effects of Reactor Radiation on Cements and Concrete*, in *Results of Concrete Irradiation Programmes*, H. Benzler, Editor. 1972, Commission of the European Communities: Brussels. p. 17 - 39.

114. Johnson, R.E. and R.E. Lipinski, 1996, *Radiation Effects on Reactor Pressure Vessel Supports*, NUREG/CR-1509, Idaho National Engineering Laboratory, for the U.S.Nuclear Regulatory Commission, Washington, DC, April.

115. Desnerck, P., J.M. Lees, and C.T. Morley, 2015, *Bond Behaviour of Reinforcing Bars in Cracked Concrete.* Construction and Building Materials. **94**: p. 126-136.

116. Law, D.W. and C.K. Molyneaux, 2017, *Impact of Corrosion on Bond in Uncracked Concrete with Confined and Unconfined Rebar.* Construction and Building Materials. **155**: p. 550-559.

117. Bazant, Z. and J. Planas, *Fracture and Size Effect in Concrete and Other Quasibrittle Materials*. 1997, Boca Raton, FL: CRC Press.

118. U.S. Nuclear Regulatory Commission, 2001, *Task Interface Agreement 2000-10 RE: Evaluation of TIA 98-11 Regarding Reactor Vessel Support Concrete Temperature at Farley (TAC Nos. MA9311 and MA9312),* Office of Nuclear Reactor Regulation, Washington, DC. ADAMS Accession No. ML010650101.

119. Duke Energy Progress, 2013, *Relief Request (RR)-20 for Limited Examinations Performed in the Fourth Ten-Year Inservice Inspection Program Plan,* Docket No. 50-261, Hartsville, SC. ADAMS Accession No. ML13178A006.

120. Hopkins, W.G., *Reactor Pressure Vessel Supports for Pressurized Water Reactors and Boiling Water Reactors*, in *Residual Life Assessment of Major Light Water Reactor Components - Overview*, V.N. Shah and P.E. MacDonald, Editors. 1987, EG&G Idaho, Inc.: Idaho Falls, ID. p. 79-95.

121. U.S. Nuclear Regulatory Commission, 2009, *General Electric Systems Technology Manual, Chapter 2.1, Reactor Vessel System,* Washington, DC. ADAMS Accession No. ML11271A022.

122. Cheverton, R.D., W.E. Pennell, G.C. Robinson, and R.K. Nanstad, 1989, *Impact of Radiation Embrittlement on Integrity of Pressure Vessel Supports for Two PWR Plants*, NUREG/CR-5320, Oak Ridge National Laboratory, for the U.S.Nuclear Regulatory Commission, Office of Nuclear Regulatory Research, Oak Ridge, TN.

123. Lapay, W.S., C.Y. Yang, and C. Kim, 2000, *License Renewal Evaluation: Aging Management for Reactor Coolant System Supports*, WCAP-14422, Rev. 2-A, Westinghouse Electric Company, LLC, Pittsburgh, PA, December.

124. Remec, I., T.M. Rosseel, K.G. Field, and Y. Le Pape. *Characterization of Radiation Fields for Assessing Concrete Degradation in Biological Shields of NPPs*. in *Proc. ICRS-13 & RPSD-2016, 13th Int. Conf. on Radiation Shielding & 19th Topical Meeting of the Radiation Protection and Shielding Division of the American Nuclear Society*. 2016. EPJ Web of Conferences.

125. U.S. Nuclear Regulatory Commission, 1988, *Regulatory Guide 1.99, Rev. 2, Radiation Embrittlement of Reactor Vessel Materials,* Office of Nuclear Regulatory Research, Washington, DC.

126. Randall, P.N., *Basis for Revision 2 of the U. S. Nuclear Regulatory Commission's Regulatory Guide 1.99*, in *Radiation Embrittlement of Nuclear Reactor Pressure Vessel Steels: An International Review* L.E. Steele, Editor. 1986, American Society for Testing and Materials: Philadelphia. p. 149-162.

127. Remec, I., 1999, *Study of the Neutron Flux and Dpa Attenuation in the Reactor Pressure Vessel Wall*, ORNL/NRC/LTR-99/5, Oak Ridge National Laboratory, Oak Ridge, TN, June.

128. Leicht, A.E. and J. Chen, 2010, *Analysis of Capsule W from the Comanche Peak Unit No. 2 Reactor Vessel Radiation Surveillance Program*, Westinghouse Electric Company LLC, Pittsburgh, PA, September. ADAMS Accession No. ML102920160.

129. Anderson, S.L., 2000, *Fast Neutron Fluence Evaluations for the Fort Calhoun Unit 1 Reactor Pressure Vessel*, WCAP-15443, Westinghouse Electric Company LLC, Pittsburgh, PA, July. ADAMS Accession No. ML003738600.

130. Fero, A.H., 1999, *Duke Power Company Reactor Cavity Neutron Measurement Program for William B. McGuire Unit 2 Cycle 12*, Westinghouse Electric Company LLC, Pittsburgh, PA, November 1999. ADAMS Accession No. ML020870532.

131. Ledger, J.H., G.N. Wrights, and J. Conermann, 2003, *Analysis of Capsule W-83 from the Dominion Nuclear Connecticut Millstone Unit 2 Reactor Vessel Radiation Surveillance Program*, WCAP-16012, Westinghouse Electric Company LLC, Pittsburgh, PA, February. ADAMS Accession No. ML030710172.

132. Roberts, G.K., D.M. Chapman, S.L. Anderson, and J.D. Perok, 2000, *Palisades Reactor Pressure Vessel Neutron Fluence Evaluation*, WCAP-15353, Westinghouse Electric Company, LLC, Pittsburgh, PA, January. ADAMS Accession No. ML003686582.

133. Gift, F.C., E.T. Hayes, and J. Conermann, 2006, *Analysis of Capsule 230° from Arizona Public Service Company Palo Verde Unit 2 Reactor Vessel Radiation Surveillance Program*, WCAP-16524-NP, Westinghouse Electric Company LLC, Pittsburgh, PA, February. ADAMS Accession No. ML061040593.

134. Ledger, J.H., G.K. Roberts, and J. Conermann, 2001, *Analysis of Capsule Y from the Public Service Electric and Gas Company Salem Unit 2 Reactor Vessel Radiation Surveillance Program*, WCAP-15692, Westinghouse Electric Company LLC, Pittsburgh, PA, ADAMS Accession No. ML012910321.

135. Laubham, T.J., D.M. Chapman, and J. Conermann, 2002, *Analysis of Capsule 284' from the Florida Power & Light Company St. Lucie Unit 1 Reactor Vessel Radiation Surveillance Program*, WCAP-15446, Rev. 1, Westinghouse Electric Company LLC, Pittsburgh, PA, January. ADAMS Accession No. ML021280606.

136. Rosier, B.A., J. Conermann, and M.A. Hunter, 2009, *Analysis of Capsule W from the Vogtle Unit No. I Reactor Vessel Radiation Surveillance Program*, WCAP-17009-NP, Rev. 1, Westinghouse Electric Company LLC, Pittsburgh, PA, April 2009. ADAMS Accession No. ML091550357.

137. Rosier, B.A. and M.A. Hunter, 2011, *Analysis of Capsule Z from the Southern Nuclear Operating Company Vogtle Unit 2 Reactor Vessel Radiation Surveillance Program*, WCAP-17343-NP, Westinghouse Electric Company LLC, Cranberry Township, PA, March. ADAMS Accession No. ML110800302.

138. Mays, B.E. and A.B. Mohamed, 2016, *Analysis of Capsule V from the Exelon Generation Braidwood Unit 1 Reactor Vessel Radiation Surveillance Program*, WCAP-18092, Rev. 1, Westinghouse Electric Company, LLC, Cranberry Township, PA, May. ADAMS Accession No. ML16271A451.

139. Mays, B.E. and P.C. Cronstrand, 2016, *Analysis of Capsule V from the Exelon Generation Braidwood Unit 2 Reactor Vessel Radiation Surveillance Program*, WCAP-18107-NP, Westinghouse Electric Company LLC, Cranberry Township, PA, May. ADAMS Accession No. ML16271A452.

140. Williams, M.L., M. Asgari, and F.B.K. Kam, 1993, *Impact of ENDF/B-VI Cross-Section Data on H.B. Robinson Cycle 9 Dosimetry Calculations*, NUREG/CR-6071, Oak Ridge National Laboratory, for the U.S.Nuclear Regulatory Commission, Office of Nuclear Regulatory Research, Oak Ridge, TN, October.

141. Alpan, A. and J.J. Klingensmith, 2016, *Ex-Vessel Neutron Dosimetry Program for H.B. Robinson Unit 2 Cycles 16 through 29*, WCAP-18100-NP, Westinghouse Electric Company LLC, Cranberry Township, PA, March. ADAMS Accession No. ML16130A645.

142. Nanstad, R.K., T.M. Rosseel, M.A. Sokolov, W.L. Server, T. Arai, N. Soneda, R. Dyle, G.R. Odette, M.T. Kirk, B.N. Burgos, and J.B. Hall, 2014, *Expanded Materials Degradation Assessment (EMDA), Volume 3: Aging of Reactor Pressure Vessels*, Vol. 3, NUREG/CR-7153, Expert Panel, for the U.S.Nuclear Regulatory Commission, Office of Nuclear Regulatory Research, Washington, DC, ADAMS Accession No. ML14279A349.

143. Freed, A.E. and J. Chen, 2013, *Catawba Unit 1 Measurement Uncertainty Recapture (MUR) Power Uprate: Reactor Vessel Integrity and Neutron Fluence Evaluations*, WCAP-17669-NP, Westinghouse Electric Company LLC, Cranberry Township, PA, June. ADAMS Accession No. ML14353A029.

144. Florida Power & Light Company, 2018, *Turkey Point Nuclear Plant Units 3 and 4 Subsequent License Renewal Application and Reference Documents,* Docket Nos. 50-250 and 50-251, ADAMS Accession No. ML18113A146-SLR Application, Rev. 1; ML18113A148-reference documents.

145. Remec, I., T.M. Rosseel, K.G. Field, and Y. Le Pape. *Characterization of Radiation Fields in Biological Shields of Nuclear Power Plants for Assessing Concrete Degradation*. in *15th International Symposium on Reactor Dosimetry (ISRD)*. 2014. Aix en Provence, FRANCE: EPJ Web of Conferences.

146. Constellation Energy, 2008, *R.E. Ginna Nuclear Power Plant Updated Final Safety Analysis Report, Rev. 21,* Docket No. 50-244, Ontario, NY. ADAMS Accession No. ML092100074.

147. Sargent & Lundy LLC, 2005, *Analysis of Postulated Reactor Head Drop Onto the Reactor Vessel Flange,* ADAMS Accession No. ML051870299.

148. Nuclear Management Company, LLC, 2005, *Submittal of Supporting Analyses Regarding Control of Heavy Loads,* Docket No. 50-301, Two Rivers, WI. ADAMS Accession No. ML051720073.

149. Nuclear Management Company, LLC, 2005, *Supplement 3 to Request for Exigent Review of Heavy Load Analysis and Response to Request for Additional Information,* Docket No. 50-301, Two Rivers, WI. ADAMS Accession No. ML051800481.

150. Xcel Energy, 2018, *Prairie Island Nuclear Generating Plant Units 1 and 2, Updated Safety Analysis Report Revision 35,* Dockets 50-282 and 50-306, Welch, MN. ADAMS Accession No. ML18155A440 - Chapter 5; ML18155A456 - Chapter 12.

151. Duke Energy, 2015, *Fourth Ten-Year Inservice Inspection Plan, Relief Request No. 15-ON-004, Limited Visual Examinations from 1EOC27, 2EOC26 and 3EOC27 Outages,* Docket Nos. 50-269, 50-270, 50-287, Seneca, SC. ADAMS Accession No. ML15201A573.

152. Exelon Generation, 2018, *Three Mile Island Nuclear Station, Unit 1, Updated Final Safety Analysis Report (UFSAR), Revision 24 Fire Hazards Analysis Report (FHAR), Revision 28 UFSAR and FHAR Reference Drawings* Docket No. 50-289, Kennett Square, PA. ADAMS Accession No. ML19066A349.

153. Entergy Operations, Inc, 2000, *Arkansas Nuclear One - Unit 1 License Renewal Application,* Docket No. 50-313, Russellville, AR. ADAMS Accession No. ML003679667.

154. FirstEnergy Nuclear Operating Company, 2018, *Davis-Besse Unit 1 Update Final Safety Analysis Report, Rev. 32,* Docket No. 50-346, Oak Harbor, OH.

155. Lobner, P., C. Donahoe, and C. Cavallin, 1990, *Overview and Comparison of U.S. Commercial Nuclear Power Plants*, NUREG/CR-5640, Science Applications International Corporation, for the U.S.Nuclear Regulatory Commission, Washington, DC, September.

156. Entergy Operations, Inc, 2003, *Arkansas Nuclear One - Unit 2 License Renewal Application,* Docket No. 50-368, Russellville, AR. ADAMS Accession No. ML032890506.

157. Entergy Operations, Inc., 2016, *Arkansas Nuclear One - Unit 2, Safety Analysis Report Amendment 26,* Docket No. 50-368, Russellville, AR. ADAMS Accession No. ML18092A457.

158. Exelon Generation Company, LLC, 2017, *Calvert Cliffs Nuclear Power Plant Units 1 and 2, Updated Final Safety Analysis Report, Revision 49,* Docket Nos. 50-317 and 50-318, Kennett Square, PA. ADAMS Accession No. ML17354B239.

159. Omaha Public Power District, 2001, *10 CFR 50.59 Report and Updated Safety Analysis Report Revision for Fort Calhoun Station,* Docket No. 50-285, Omaha Nebraska. ADAMS Accession No. ML012890060 - Chapters 4 through 6.

160. Entergy Nuclear Operations, Inc., 2019, *Palisades Nuclear Plant Final Safety Analysis Report, Revision 34,* Docket 50-255, Covert, MI. ADAMS Accession No. ML19154A277 (Chptr. 4 figures).

161. Dominion, 2004, *Millstone Power Station Unit 2, Application for Renewed Operating License,* Docket No. 50-336, Richmond, VA.

162. Dominion Nuclear Connecticut, Inc., 2017, *Millstone Power Station Unit 2 Safety Analysis Report (Revision 35),* Docket No. 50-336, Waterford, CT. ADAMS Accession No. ML17212A045 - Chapter 4.

163. Florida Power & Light Company, 2019, *St. Lucie Unit 2 Updated Final Safety Analysis Report Amendment No. 25,* Docket No. 50-389, Jensen Beach, FL. ADAMS Accession No. ML19141A221-Chapter 3; ML19101A068-Chapter 4; ML19101A069-Chapter 5.

164. Entergy Operations, Inc., 2016, *Waterford Unit 3 Final Safety Analysis Report – Revision 309,* Docket No. 50-382, Killona, LA. ADAMS Accession No. ML16256A184-Section 3.7 figures; ML16256A186-Section 3.8; ML16256A244-Section 5.4; ML16256A249-App. 5.4A figures; ML16344A298-Section 5.4 figures.

165. First Energy Nuclear Operating Company, 2010, *Beaver Valley Power Station, Unit Nos. 1 and 2, Response to Request for Additional Information Related to Generic Letter 2004-02 (TAC Nos. MC4665 and MC4666)* Docket Nos. 50-334, 50-412, Shippingport, PA. ADAMS Accession No. ML102770023.

166. Southern Nuclear Operating Company, 2000, *Joseph M. Farley Nuclear Plant, Reactor Vessel Support Concrete Temperature, Reply to NCV 50-348, 364/00-01-01, Failure to Identify an USQ,* Docket Nos. 50-348 and 50-364, Birmingham, AL. ADAMS Accession No. ML003721316.

167. Carolina Power & Light (dba Progress Energy Carolinas), 2002, *Robinson Nuclear Plant License Renewal Application,* Docket No. 50-261, Hartsville, SC.

168. Carolina Power & Light Company, 1996, *Shearon Harris Nuclear Power Plant Final Safety Analysis Report Amendment No. 46,* Dockent No 50-400, New Hill, NC. ADAMS Accession No. ML18012A211.

169. Carolina Power & Light Company, 1997, *Shearon Harris Nuclear Power Plant Final Safety Analysis Report Amendment No. 48,* Docket No. 50-400, New Hill, NC. ADAMS Accession No. ML18022B032.

170. Duke Energy, 2019, *Shearon Harris Nuclear Power Plant, Unit 1, Final Safety Analysis Amendment No. 62,* Docket No. 50-400, New Hill, NC. ADAMS Accession No. ML19102A104-Chapter 3; ML19102A106-Chapter 5; ML19102A107-Chapter 6.

171. Virginia Electric and Power Company (Dominion), 2001, *Application for Renewed Operating Licenses, Surry Power Station Units 1 and 2,* Docket Nos. 50-280, 50-281, Richmond, VA.

172. South Carolina Electric & Gas Company, 2017, *Virgil C. Summer Nuclear Station (VCSNS) Unit 1 Final Safety Analysis Report (FSAR) - Updated Through April 30, 2017,* Docket No. 50-395, Jenkinsville, SC. ADAMS Accession No. ML17215A031-Chapter 3; ML17215A042-Chapter 5; ML17215A055-Chapter 12.

173. U.S. Nuclear Regulatory Commission, 1980, *Control of Heavy Loads at Nuclear Power Plants, Resolution of Generic Technical Activity A-36,* NUREG-0612, Office of Nuclear Reactor Regulation, Washington, DC. ADAMS Accession No. ML070250180.

174. Southern Nuclear, 2017, *Joseph M. Farley Nuclear Plant Updated Final Safety Analysis Report (Revision 27),* Docket Nos. 50-348 and 50-364, Birmingham, AL. ADAMS Accession No. Chapter 3 Pt. 2 - ML17117A368; Chapters 4 and 5 - ML17117A369.

175. Pomaro, B., V.A. Salomoni, F. Gramegna, G. Prete, and C.E. Majorana, 2011, *Radiation Damage Evaluation on Concrete Shielding for Nuclear Physics Experiments.* Annals of Solid and Structural Mechanics. **2**(2): p. 123-145.

176. Pomaro, B., V.A. Salomoni, F. Gramegna, G. Prete, and C.E. Majorana, 2011, *Radiation damage evaluation on concrete within a facility for Selective Production of Exotic Species (SPES Project), Italy.* J Hazard Mater. **194**: p. 169-77.

177. Salomoni, V.A., C.E. Majorana, B. Pomaro, G. Xotta, and F. Gramegna, 2014, *Macroscale and Mesoscale Analysis of Concrete as a Multiphase Material for Biological Shields Against Nuclear Radiation.* International Journal for Numerical and Analytical Methods in Geomechanics. **38**(5): p. 518-535.

178. Efendiev, Y. and T.Y. Hou, *Multiscale Finite Element Methods, Theory and Applications*. Surveys and Tutorials in the Applied Mathematical Sciences, ed. S.S. Antman, J.E. Marsden, and L. Sirovich. 2009, New York: Springer Science+Business Media, LLC.

179. Le Pape, Y., K.G. Field, and I. Remec, 2015, *Radiation effects in concrete for nuclear power plants, Part II: Perspective from micromechanical modeling.* Nuclear Engineering and Design. **282**: p. 144-157.

180. Budiansky, B. and R. O'Connell, 1976, *Elastic Moduli of a Cracked Solid.* International Journal of Solids and Structures. **12**(2): p. 81-97.

181. Giorla, A., M. Vaitová, Y. Le Pape, and P. Štemberk, 2015, *Meso-scale modeling of irradiated concrete in test reactor.* Nuclear Engineering and Design. **295**: p. 59-73.

182. Le Pape, Y., A. Giorla, and J. Sanahuja, 2016, *Combined Effects of Temperature and Irradiation on Concrete Damage.* Journal of Advanced Concrete Technology. **14**(3): p. 70-86.

183. Engle, J., Ward, W., 1967, *A User's Manual for ANISN, A One Dimensional Discrete Ordinates Transport Code with Anisotropic Scattering*, K-1693, Oak Ridge Gaseous Diffusion Plant, Oak Ridge, TN, March.

184. Jing, Y. and Y. Xi, 2017, *Theoretical Modeling of the Effects of Neutron Irradiation on Properties of Concrete.* Journal of Engineering Mechanics**. 143(12): 04017137**.

185. Sargent & Lundy LLC, 2005, *Analysis of Postulated Reactor Head Load Drop onto the Reactor Vessel Flange, Initial Summary Report,* ADAMS Accession No. ML051720073.

186. Exelon Generation Company, 2003, *License Renewal Application, Dresden Nuclear Power Station, Quad Cities Nuclear Power Station,* Docket Nos. 50-237, 50-249, 50-254, and 50-265, Warrenville, IL.

187. Mehta, A.R. and L.J. Tilly, 2004, *Pressure-Temperature Curves for Exelon Dresden Unit 2*, General Electric Company, San Jose, CA, May. . ADAMS Accession No. ML043360173.

188. Tilly, L.J., 2004, *Pressure-Temperature Curves for Exelon Dresden Unit 3*, General Electric Company, San Jose, CA, May. ADAMS Accession No. ML043360180.

189. Tilly, L.J., 2004, *Pressure-Temperature Curves for Exelon Quad Cities Unit 1*, General Electric Company, San Jose, CA, May. ADAMS Accession No. ML043360204.

190. Tilly, L.J., 2004, *Pressure-Temperature Curves for Exelon Quad Cities Unit 2*, General Electric Company, San Jose, CA, May. . ADAMS Accession No. ML043360217.

191. Exelon Generation Company, LLC, 2014, *License Renewal Application, LaSalle County Station, Units 1 and 2,* Docket Nos. 50-373 and 50-374, Kennett Square, PA.

192. Tilly, L.J., 2004, *Pressure-Temperature Curves for Exelon LaSalle Unit 1*, General Electric Company, San Jose, CA, May. ADAMS Accession No. ML101130371.

193. Exelon Generation Company, 2011, *License Renewal Application, Limerick Generating Station, Units 1 and 2,* Kennet Square, PA.

194. Energy Northwest, 2010, *License Renewal Application, Columbia Generating Station,* Docket No. 50-397, Richland, WA.

195. Tilly, L.J., 2004, *Pressure-Temperature Curves for Exelon LaSalle Unit 2*, General Electric Company, San Jose, CA, May. ADAMS Accession No. ML101130372.

196. PPL Susquehanna, LLC, 2006, *License Renewal Application, Susquehanna Steam Electric Station, Units 1 and 2,* Docket Nos. 50-387 and 50-388, Allentown, PA.

197. DTE Electric Company, 2014, *Fermi 2 License Renewal Application,* Docket No. 50-341, Detroit, MI.

198. Nine Mile Point Nuclear Station, LLC, 2004, *Application for Renewed Operating Licenses, Nine Mile Point Nuclear Stations 1 & 2* Docket Nos. , Annapolis, MD.

199. Inch, G.B., 2013, *Nine Mile Point Nuclear Station Nine Mile Point Unit 2 Pressure and Temperature Limits Report (PTLR)*, PTLR-2, Revision 0 (Draft B), Nine Mile Point Nuclear Station, LLC, November 2013. ADAMS Accession No. ML13311A054.

200. Carolina Power and Light Company, 2004, *Brunswick Steam Electric Plant License Renewal Application,* Docket Nos. 50-324 and 50-325, Raleigh, NC.

201. PSEG Nuclear LLC, 2009, *License Renewal Application, Hope Creek Generating Station,* Docket No. 50-354, Newark, NJ.

202. Tennessee Valley Authority, 2004, *Browns Ferry Nuclear Units 1, 2, and 3 License Renewal Application,* Docket Nos. 50-259, 50-260, 50-296, Knoxville, TN.

203. Nebraska Public Power District, 2008, *Cooper Nuclear Station License Renewal Application,* Docket No. 50-298, Columbus, NE.

204. U.S. Nuclear Regulatory Commission, 2003, *Safety Evaluation Report Related to the License Renewal of Peach Bottom Atomic Power Station, Units 2 and 3, Docket Nos. 50-277 and 50-278,* NUREG-1769, Office of Nuclear Reactor Regulation, Washington, DC.

205. Entergy Nuclear Fitzpatrick, LLC, 2006, *License Renewal Application, James A. Fitzpatrick Nuclear Power Plant,* Docket No. 50-333, Lycoming, NY.

206. Southern Nuclear Operating Company, Inc., 2000, *Edwin I. Hatch Nuclear Plant, Units 1 and 2 License Renewal Application,* Docket Nos. 50-321 and 50-366, Birmingham, AL.

207. Entergy Applications, Inc., 2011, *Grand Gulf Nuclear Station License Renewal Application,* Docket No. 50-416, Jackson, MI.

208. Palm, N., T. Hardin, M.P. Manahan Sr, and E. Jones, 2014, *BWRVIP-281 NP: BWR Vessel and Internals Project Testing and Evaluation of the Perry 177o Capsule*, EPRI Technical Report 3002003141, Electric Power Research Institute, Palo Alto, CA, October. ADAMS Accession No. ML14308A077.

209. FirstEnergy Nuclear Operating Company, 2002, *License Amendment Request Pursuant to 10 CFR 50.90: Revision of Pressure/Temperature Limit Curves for Non-Nuclear Heatup/Cooldown, Core Critical Operation, and Pressure Testing for Reactor Coolant Systems; Including an Exemption Request Pursuant to 10 CFR 50.60(b),* PY-CEI/NRR-2627L, Perry Nuclear Power Plant, Perry, OH. ADAMS Accession No. ML021650244.

210. Nuclear Management Company, LLC, 2005, *Application for Renewed Operating License, Monticello Nuclear Generating Plant,* Docket No. 50-263, Hudson, WI.

211. Amergen Energy Company, LLC, 2005, *License Renewal Application, Oyster Creek Generating Station,* Docket No. 50-219, Kennett Square, PA.

212. Carter, R., 2010, *River Bend 183 Degree Surveillance Capsule Report*, BWRVIP-113NP, EPRI, Palo Alto, CA, August 2010. ADAMS Accession No. ML102580248.

213. FPL Duane Arnold Energy Center, LLC, 2008, *Duane Arnold Energy Center License Renewal Application,* Juno Beach, FL.

214. Duke Energy Corporation, 1998, *Application for Renewed Operating Licenses, Oconee Nuclear Station, Units 1, 2, and 3, Volume III,* Docket Nos. 50-269, 50-270, and 50-287, Seneca, SC.

215. Duke Power Company, 1969, *Oconee Nuclear Station Units 1, 2 and 3, Final Safety Analysis Report, Volume 2,* Charlotte, NC. ADAMS Accession No. ML12268A123.

216. First Energy Nuclear Operating Company, 2010, *License Renewal Application, Davis-Besse Nuclear Power Station,* Docket No. 50-346, Akron, OH.

217. Amergen Energy Company, LLC, 2008, *License Renewal Application, Three Mile Island Nuclear Station Unit 1,* Docket No. 50-289, Kennertt Square, PA.

218. Arizona Public Service Company, 2009, *License Renewal Application, Palo Verde Nuclear Generating Station Unt 1, Unit 2, and Unit 3,* Docket Nos. 50-528, 50-529, and 50-530, Phoenix, AZ.

219. Byrne, S.T., F.P. Ferraraccio, B.R. Ganta, and V.A. Paggen, 2008, *Palo Verde Nuclear Generating Station Units 1, 2 and 3; Basis for RCS Pressure and Temperature Limits Report*, WCAP-16835-NP, Westinghouse Electric Company LLC, Pittsburgh, PA, June 2008. ADAMS Accession No. ML090641016.

220. Nuclear Management Company, LLC, 2005, *Palisades Nuclear Plant Application for Renewed Operating License,* Docket No. 50-255, Hudson, WI.

221. Freed, A.E., 2014, *Alternate Pressurized Thermal Shock (PTS) Rule Evaluation for Palisades*, WCAP-17628-NP, Revision 1, Westinghouse Electric Company LLC, Cranberry Township, PA, June 2014. ADAMS Accession No. ML14211A525.

222. Rosier, B.A. and A. Alpan, 2015, *Analysis of Capsule 83o from the Entergy Operations, Inc. Waterford Unit 3 Reactor Vessel Radiation Surveillance Program*, WCAP-17969-NP, Westinghouse Electric Company LLC, Cranberry Township, PA, April. ADAMS Accession No. ML15222A361.

223. U.S. Nuclear Regulatory Commission, 2013, *Fort Calhoun Station Unit 1 - Request for Approval of Proposed Changes to the Reactor Pressure Vessel Surveillance Capsule Withdrawal Schedules (TAC No. ME8219),* Office of Nuclear Reactor Regulation, Washington, DC. ADAMS Accession No. ML13017A467.

224. Florida Power & Light Company, 2001, *License Renewal Application, St. Lucie Units 1 & 2,* Docket Nos. 50-335 and 50-389, Juno Beach, FL.

225. Fournier, R.S., B. Reddy Ganta, and S.T. Byrne, 2010, *St. Lucie Unit 1 RCS Pressure and Temperature Limits and Low-Temperature Overpressure Protection Report for 54 Effective Full Power Years Westinghouse Non-Proprietary Class 3*, WCAP-17197-NP, Westinghouse Electric Company LLC, Pittsburgh, PA, February 2010. ADAMS Accession No. ML103560511.

226. Ferraraccio, F.P., 2007, *St. Lucie Unit 2 RCS Pressure and Temperature Limits and Low Temperature Overpressure Protection Report for 55 Effective Full Power Years*, Westinghouse Electric Company LLC, Windsor, CT, October 2007. ADAMS Accession No. ML080290135.

227. U.S. Nuclear Regulatory Commission, 2009, *Revision to Reactor Vessel Surveillance Capsule Withdrawal Schedule , Calvert Cliffs Nuclear Power Plant, Unit Nos. 1 and 2, Docket Nos. 50-317 and 50-318,* Office of Nuclear Reactor Regulation, Washington, DC. ADAMS Accession No. ML090270206.

228. Bishop, B.A., C.L. Boggess, and N.A. Palm, 2011, *Risk-Informed Extension of the Reactor Vessel In-Service Inspection Interval*, WCAP-16168-NP-A, Rev. 3, Westinghouse Electric Company LLC, Cranberry Township, PA, October 2011. ADAMS Accession No. ML11306A084.

229. Rochester Gas and Electric Corporation, 2002, *Application for Renewed Operating License, R. E. Ginna Nuclear Power Plant,* Docket No. 50-244, Rochester, NY.

230. Nuclear Management Company, LLC, 2008, *Application for Renewed Operating Licenses, Prairie Island Nuclear Generating Plant Units 1 and 2,* Docket Nos. 50-282 and 50-306, Minneapolis, MN.

231. Nuclear Management Company, LLC, 2004, *Application for Renewed Operating Licenses, Point Beach Nuclear Plant Units 1 & 2,* Docket Nos. 50-266 and 50-301, Hudson, WI.

232. Point Beach Nuclear Plant, 2000, *Technical Specifications Change Request 219, Adoption of Pressure and Temperature Limits Report and Revised P-T and LTOP Limits, Point Beach Nuclear Plant, Units 1 and 2*, NPL 2000-0123 Two Rivers, WI. ADAMS Accession No. ML003692932.

233. Virginia Electric and Power Company, 2002, *Virginia Electric and Power Company (Dominion), Surry and North Anna Power Stations Units 1 and 2, Response to Request for Supplemental Information, License Renewal Applications,* Richmond, VA. ADAMS Accession No. ML022960411.

234. Framatome Technologies, Inc., 1998, *Low Upper-Shelf Toughness Fracture Mechanics Analysis of Reactor Vessels of Surry Units 1 and 2 for Extended Life Through 48 Effective Full Power Years,* BAW-2323; FTI Document No. 77-2323-00, I.N. Services, Lynchburg, VA. ADAMS Accession No. ML022390143.

235. Virginia Electric and Power Company, 2005, *Virginia Electric and Power Company (Dominion) North Anna Power Station Units 1 and 2, Update to Reactor Vessel Integrity Database to Reflect License Renewal Period,* Richmond, VA. ADAMS Accession No. ML053480358.

236. First Energy Nuclear Operating Company, 2007, *Beaver Valley Power Station License Renewal Application,* Docket Nos. 50-334 and 50-412, Akron, OH.

237. Southern Nuclear Operating Company, Inc., 2003, *Joseph M. Farley License Renewal Application,* Docket Nos. 50-348 and 50-364, Birmingham, AL.

238. U.S. Nuclear Regulatory Commission, 2011, *Safety Evaluation by the Office of Nuclear Reactor Regulation, Reactor Vessel Surveillance Capsule Withdrawal Schedule Revision, Carolina Power and Light Company, H.B. Robinson Steam Electric Plant Unit No. 2, Docket 50-261,* Office of Nuclear Reactor Regulation, Washington, DC. ADAMS Accession No. ML11349A026.

239. U.S. Nuclear Regulatory Commission, 2004, *Safety Evaluation Report Related to the License Renewal of the Virgil C. Summer Nuclear Station, Docket No. 50-395,* NUREG-1787, Office of Nuclear Reactor Regulation, Washington, DC.

240. Carolina Power and Light Company, 2006, *Harris Nuclear Plan License Renewal Application,* Docket No. 50-400, Raleigh, NC.

241. DeVan, M.J. and S.Q. King, 1999, *Analysis of Capsule X, Carolina Power & Light Company, Shearon Harris Nuclear Power Plant - Reactor Vessel Material Surveillance Program*, BAW-2355, Framatone Technologies, Lynchburg, VA, October 1999. ADAMS Accession No. ML993220006.

242. Florida Power and Light Company, 2009, *Update to NRC Reactor Vessel Integrity Database and Exemption Request for Alternate Material Properties Bases Per 10 CFR 50.12 and 10 CFR 50.60 (b),* L-2009-023, ADAMS Accession No. ML090920408.

243. Entergy Nuclear Operations, Inc, 2007, *Indian Point Energy Center License Renewal Application,* Docket Nos. 50-247 and 50-286, White Plains, NY.

244. PSEG Nuclear LLC, 2009, *License Renewal Application, Salem Nuclear Generating Station,* Docket Nos. 50-272 and 50-311, Newark, NJ.

245. PSEG Nuclear LLC, 2009, *Relief Requests to Extend the Inservice Inspection Interval for ReactorVessel Weld Examinations,* LR-N09-0126, ADAMS Accession No. ML091740140.

246. Pacific Gas and Electric Company, 2009, *License Renewal Application, Diablo Canyon Power Plant, Unit 1 and Unit 2,* Docket Nos. 50-275 and 50-323, San Francisco, CA.

247. Indiana Michigan Power Company, 2003, *License Renewal Application, Donald C. Cook Nuclear Plant,* Docket Nos. 50-315 and 50-316, Columbus, OH.

248. Tennessee Valley Authority, 2013, *License Renewal Application, Sequoyah Nuclear Plant, Units 1 and 2,* Docket Nos. 50-327 and 50-328, Knoxville, TN.

249. Dominion, 2007, *Stretch Power Uprate Licensing Report, Millstone Power Station Unit 3,* ADAMS Accession No. ML072000400.

250. Ruminski, E.M. and A. Alpan, 2015, *Analysis of Capsule W from the Ameren Missouri Callaway Unit 1 Reactor Vessel Radiation Surveillance Program*, Westinghouse Electric Company LLC, Cranberry Township, PA, September.

251. Duke Energy Corporation, 2001, *Application to Renew the Operating Licenses of McGuire Nuclear Station, Units 1 & 2 and Catawba Nuclear Station, Units 1 & 2,* Docket Nos. 50-369, 50-370, 50-413, and 50-414, Charlotte, NC.

252. Tennessee Valley Authority, 2014, *Revision to Watts Bar Nuclear Plant, Unit 1, Reactor Vessel Surveillance Capsule Withdrawal Schedule, Revision 1,* Chattanooga, TN. ADAMS Accession No. ML14070A162.

253. Southern Nuclear Operating Company, Inc., 2007, *License Renewal Application, Vogtle Electric Generating Plant Units 1 and 2,* Docket Nos. 50-424 and 50-425, Birmingham, AL.

254. Duke Energy Corporation, 2009, *Duke Energy Carolinas, LLC, (Duke) McGuire Nuclear Station, Unit 1, Docket No. 50-369, Relief Request Serial #09-MN-003,* Huntersville, NC. ADAMS Accession No. ML091880423.

255. Exelon Generation Company, LLC, 2013, *License Renewal Application, Byron and Braidwood Stations, Units 1 and 2,* Docket Nos. 50-454, 50-455, 50-456, and 50-457, Kennett Square, PA.

256. Morrison, R.L. and L.C. Thomas, 2007, *Comanche Peak Nuclear Power Plant Stretch Power Uprate Licensing Report*, Westinghouse Electric Company LLC, Pittsburgh, PA, August. ADAMS Accession No. ML072490310, ML072490358.

257. Wolf Creek Nuclear Operating Corporation, 2006, *License Renewal Application, Wolf Creek Generating Station Unit 1,* Docket No. 50-482, Burlington, KS.

258. NextEra Energy Seabrook, LLC, 2010, *Seabrook Station License Renewal Application,* Docket No. 50-443, Juno Beach, FL.

259. South Texas Project Nuclear Operating Company, 2010, *License Renewal Application, South Texas Project Unit 1 and Unit 2,* Docket Nos. 50-498 and 50-499, Wadsworth, TX.

260. U.S.Nuclear Regulatory Commission, *Reactor Vessel Integrity Database Version 2.0.1*. 2000 March 27m 2014 [cited 2016 July]; Available from: https://www.nrc.gov/reactors/operating/ops-experience/reactor-vessel-integrity/database-overview.html#download.

261. Carolina Power & Light (dba Progress Energy Carolinas), 2017, *H.B. Robinson Steam Electric Plant, Unit 2, Revision 27 to Updated Final Safety Analysis Report,* Docket No. 50-261, Hartsville, SC. ADAMS Accession No. ML17298A849 - Chapter 3.

262. Virginia Electric and Power Company, 2007, *Updated Final Safety Analysis Report, Surry Power Station Units 1 and 2,* Docket Nos. 50-280, 50-281, Glen Allen, VA. ADAMS Accession No. ML072980817-Chapter 11; ML072980825-Chapter 15.

APPENDIX A
CONCRETE SPECIFICATIONS

A.1 Concrete Specifications

Specification	Title
ACI 211.1	“Standard Practice for Selecting Proportions for Normal, Heavyweight, and Mass Concrete”
ACI 224R	“Control of Cracks in Concrete Structures”
ACI 301	“Specifications for Structural Concrete for Buildings”
ACI 304	“Guide for Measuring, Mixing, Transporting, and Placing Concrete”
ACI 306	“Recommendation Practice for Cold Weather Concrete”
ACI 315	“Manual of Standard Practice for Detailing Reinforced Concrete Structures”
ACI 318	“Building Code Requirement for Reinforced Concrete”
ACI 347	“Recommended Practice for Concrete Framework”
ACI 349	“Code Requirements for Nuclear Safety Related Concrete Structures”
ACI 349.1R-07	“Reinforced Concrete Design for Thermal Effects on Nuclear Power Plant Structures”
ACI 605	“Recommended Practice for Hot Weather Concreting”
ACI 613	“Recommended Practice for Selecting Proportions for Concrete”
ACI 614	“Recommended Practice for Measuring, Mixing and Placing Concrete”

A.2 Related Specifications and Acceptance Test Procedures for Concrete Cement, Aggregate, and Water Quality

A.2.1 Cement

Type II cement (moderate heat of hydration and a low alkali content) is generally used in reactor internal structures such as concrete in the vicinity of the reactor vessel.

Specification	Title
ASTM C150	"Specification for Portland Cement"
ASTM C 114	"Standard Test Methods for Chemical Analysis of Hydraulic Cement"
ASTM C109-73	"Standard Method of Test for Compressive Strength of Hydraulic Cement Mortars"
ASTM C151	"Standard Method of Test for Autoclave Expansion of Portland Cement"
ASTM C191-74	"Standard Method of Test for Time of Setting of Hydraulic Cement by Vicat Needle"

A.2.2 Aggregate

Specification	Title
ASTM C33	"Specification for Concrete Aggregates"
ASTM C637	"Standard Specification for Aggregates for Radiation-Shielding Concrete"

ASTM tests for acceptability of aggregates include:

Test ID	Test Title
D75	Sampling
C33	Sand sample for gradation (Fine Aggregate)
C40	Organic test on sand
C40	Organic Impurities
C87	Mortar making properties
C88	Soundness
C117	Material Finer than No. 200 Sieve
C123	Lightweight Pieces
C127	Specific Gravity and Absorption Coarse
C128	Specific Gravity and Absorption Fine
C131	Los Angeles Abrasion
C136	Sieve Analysis
C142	Clay Lumps and Friable Particles
C227	Potential Reactivity (mortar bar)
C235	Soft Particles
C289	Potential Reactivity (Chemical)
C295	Petrographic Examination

A.2.3 Water

Water used in mixing concrete is free of injurious amounts of oil, acid, alkali, organic matter, or other deleterious substances as determined by the following ASTM tests:

Test ID	Test Title
ASTM C109	Standard Method of Test for Compressive Strength of Hydraulic Cement Mortars
ASTM C151	Standard Method of Test for Autoclave Expansion of Portland Cement
ASTM C191	Standard Method of Test for Time of Setting of Hydraulic Cement by Vicat Needle
ASTM D1888	Standard Test Methods for Particulate and Dissolved Matter, Solids, or Residue in Water
ASTM D512	Standard Test Methods for Chloride Ion in Water

APPENDIX B
BIBLIOGRAPHY OF IRRADIATED CONCRETE DEGRADATION STUDIES

1. Alexander, S.C., 1963, *Effects of Irradiation on Concrete, Final Results, AERE-R 4490, Atomic Energy Research Establishment*, for U.K.A.E. Authority, Harwell, Berkshire, United Kingdom.

2. Bar-Nes, G., A. Katz, Y. Peled, and Y. Zeiri, 2008, "The Combined Effect of Radiation and Carbonation on the Immobilization of Sr and Cs Ions in Cementitious Pastes." *Materials and Structures*. **41**(9): 1563–1570.

3. Bertero, V.V. and M. Polivka, 1972, *Influence of Thermal Exposures on Mechanical Characteristics of Concrete, in Concrete for Nuclear Reactors*. American Concrete Institute: Berlin. p. 505–531.

4. Bibler, N.E. and E.G. Orebaugh, 1977, *Radiolytic Gas Production from Tritiated Waste Forms*, Gamma and Alpha Radiolysis Studies, DP-1459, Savannah River Laboratory, Aiken, SC.

5. Bibler, N.E., 1978, *Radiolytic Gas Production from Concrete Containing Savannah River Plant Waste*, DP-1464, Savannah River Laboratory, Aiken, SC.

6. Blosser, T.V., G.W. Bond, L.A. Lee, D.T. Morgan, J.F. Nichols, R.C. Reid, . . . M.A. Welt, 1958, *A Study of the Nuclear and Physical Properties of the ORNL Graphite Reactor Shield*. ORNL-2195, A.E. Commission: Oak Ridge, Tennessee: Oak Ridge National Laboratory.

7. Bouchaala, F., C. Payan, V. Garnier, and J.P. Balayssac, 2011, "Carbonation assessment in concrete by nonlinear ultrasound." *Cement and Concrete Research.* **41**(5): 557–559.

8. Bouniol, P. and A. Aspart, 1998, "Disappearance of Oxygen in Concrete Under Irradiation: The Role of Peroxides in Radiolysis". *Cement and Concrete Research.* **28**(11): 13.

9. Bouniol, P. and E. Bjergbakke, 2008, "A comprehensive model to describe radiolytic processes in cement medium." *Journal of Nuclear Materials.* **372**(1): 1–15.

10. Bouniol, P., B. Muzeau, and V. Dauvois, 2013, "Experimental evidence of the influence of iron on pore water radiolysis in cement-based materials." *Journal of Nuclear Materials.* **437**(1-3): 208–215.

11. Browne, R.D., 1972, "Properties of Concrete in Reactor Vessels," in *Concrete for Nuclear Reactors.* American Concrete Institute: Berlin. p. 131–151.

12. Browne, R.D. and R. Blundell, 1972, "The Behaviour of Concrete in Prestressed Concrete Pressure Vessels." *Nuclear Engineering and Design.* **20**: 47.

13. Bykov, V.N., A.V. Denisov, V.B. Dubrovskii, V.V. Korenewskii, G.K. Krivokoneva, and L.P. Muzalevskii, 1981, "Effect of Irradiation Temperature on the Radiation Expansion of Quartz." *Soviet Atomic Energy.* **51**(3): 593–595.

14. Campbell-Allen, D., E.W.E. Low, and H. Roper, 1965, “An Investigation on the Effect of Elevated Temperatures on Concrete for Reactor Vessels.” *Nuclear Structural Engineering*. **2**: 7.

15. Chang, C.-F. and J.-W. Chen, 2006, “The experimental investigation of concrete carbonation depth.” *Cement and Concrete Research.* **36**(9): 1760–1767.

16. Chisholm-Batten, A.W., 1960, *Effect of Irradiation on the Strength of Concrete*. Harwell, Berkshire, U.K.: Atomic Energy Research Establishment, AERE-R 3332.

17. Clark, R.G., 1958, *Radiation Damage to Concrete*. A.E. Commission: General Electric Company/Hanford Atomic Products Operation.

18. Craeye, B, G. De Schutter, C. Vuye, and I. Gerardy, 2015, “Cement-Waste Interactions: Hardening Self-Compacting Mortar Exposed to Gamma Radiation.” *Progress in Nuclear Energy*. **83**: 212–219.

19. Crispino, E., C. Fizzotti, R. Gasparini, G. Gualtieri, A. Montagnini, and F. Rossi, 1972, *Irradiation Effects on Reactor Structural Materials, in Fourth International Conference on the Peaceful Uses of Atomic Energy*. United Nations and International Atomic Energy Agency: Geneva. p. 563–578.

20. Cristiani, G., S. Granata, and A. Montagnini, 1971, *Behaviour of Plastic Mortar Samples Under Temperature and Radiation Conditions, in Results of Concrete Irradiation Programmes*, H. Benzler, Editor. Commission of the European Communities: Brussels. p. 41–53.

21. Dickeman, R.L., 1951, *Shielding Studies*. Hanford Works.

22. Dubrovskii, V.B., S.S. Ibragimov, V.V. Koronevskii, A.Y. Ladygin, V.K. Pergamenshchik, and V.S. Perevalov, 1970, “Hematite Concrete for Shielding against High Neutron Fluxes.” *Soviet Atomic Energy*. **28**(3): 336–338.

23. Dubrovskii, V.B., S.S. Ibragimov, M.Y. Kulakovskii, A.Y. Ladygin, and B.K. Pergamenshchik, 1967, “Radiation Damage in Ordinary Concrete.” *Soviet Atomic Energy*. **23**(4): 1053–1058.

24. Dubrovskii, V.B., S.S. Ibragimov, A.Y. Ladygin, M.Y. Kulakovskii, and B.K. Pergamenshchik, 1968, “Radiation Stability of Serpentine Concrete.” *Soviet Atomic Energy.* **25**(6): 1345–1346.

25. Dubrovskii, V.B., S.S. Ibragimov, A.Y. Ladygin, and B.K. Pergamenshchik, 1966, “Effect of Neutron Irradiation on Some Properties of Heat-Resistant Concretes.” *Soviet Atomic Energy.* **21**(2): 5.

26. Elleuch, L.F., F. DuBois, and J. Rappeneau, 1972, “Effects of Neutron Radiation on Special Concretes and Their Components,” in *Concrete for Nuclear Reactors.* American Concrete Institute: Berlin. p. 1071–1109.

27. Field, K.G., I. Remec, and Y.L. Pape, 2015, “Radiation effects in concrete for nuclear power plants – Part I: Quantification of radiation exposure and radiation effects.” *Nuclear Engineering and Design.* **282**: 126–143.

28. Filmore, D.L., 2004, *Literature Review of the Effects of Radiation and Temperature on the Aging of Concrete.* Idaho Falls, Idaho: Idaho National Engineering and Envrionmental Laboratory.

29. Fujiwara, K., M. Ito, M. Sasanuma, H. Tanaka, K. Hirotani, K. Onizawa, . . . H. Amezawa, 2009, “Experimental Study of the Effect of Radiation Exposure to Concrete,” in *20th International Conference on Structural Mechanics in Reactor Technology (SMiRT 20).* International Association for Structural Mechanics in Reactor Technology: Espoo (Helsinki), Finland.

30. Giorla, A., M. Vaitová, Y. Le Pape, and P. Štemberk, 2015, “Meso-scale modeling of irradiated concrete in test reactor.” *Nuclear Engineering and Design.* **295**: 59–73.

31. Giorla, A.B., 2015, *Advanced Numerical Model for Irradiated Concrete*, ORNL/TM-2015/97, prepared by Oak Ridge National Laboratory, Oak Ridge, TN for U.S. Department of Energy, Office of Nuclear Energy, Washington, DC.

32. Giorla, A.B., Y. Le Pape, and C.F. Dunant, 2017, “Computing Creep-Damage Interactions in Irradiated Concrete.” *Journal of Nanomechanics and Micromechanics.* **7**(2):

33. Granata, S. and A. Montagnini, 1972, “Studies on Behavior of Concretes Under Irradiation,” in *Concrete for Nuclear Reactors.* American Concrete Institute: Berlin. p. 1163–1172.

34. Gray, B.S., 1971, *The Effects of Reactor Radiation on Cements and Concrete, in Results of Concrete Irradiation Programmes,* H. Benzler, Editor. Commission of the European Communities: Brussels. p. 17–39.

35. Guiglia, M. and M. Taliano, 2013, “Comparison of carbonation depths measured on in-field exposed existing r.c. structures with predictions made using fib-Model Code 2010.” *Cement and Concrete Composites.* **38**: 92–108.

36. Hansen, T.C. and L. Eriksson, 1966, *Temperature Change Effect on Behavior of Cement Paste, Mortar, and Concrete Under Load.* Proceedings, American Concrete Institute. p. 63.

37. Hilsdorf, H.K., J. Kropp, and H.J. Koch, 1978, “The Effects of Nuclear Radiation on the Mechanical Properties of Concrete,” in *Douglas McHenry International Symposium on Concrete and Concrete Structures*. American Concrete Institute. p. 223–251.

38. Hohmann, B.P., T.C. Esselman, and J.J. Wall, 2012, “Irradiated Concrete in Nuclear Power Plants: Bridging the Gap in Operational Experience,” in *3rd International Conference on NPP Life Management (PLIM) for Long Term Operations (LTO).* International Atomic Energy Agency: Salt Lake City, UT, USA.

39. Hookham, C.J., 1995, *In-Service Inspection Guidelines for Concrete Structures in Nuclear Power Plants.* Oak Ridge National Laboratory: Oak Ridge, TN.

40. Houst, Y.F. and F.H. Wittmann, 1994, “Influence of Porosity and Water-content on the Diffusivity of CO2 and O2 through Hydrated Cement Paste.” *Cement and Concrete Research.* **24**(6): 1165–1176.

41. Houst, Y.F. and F.H. Wittmann, 2002, “Depth profiles of carbonates fonned during natural carbonation.” *Cement and Concrete Research*. **32**(12): 1923–1930.

42. Ichikawa, T. and T. Kimura, 2007, “Effect of Nuclear Radiation on Alkali-Silica Reaction of Concrete.” *Journal of Nuclear Science and Technology.* **44**(10): 1281–1284.

43. Ichikawa, T. and H. Koizumi, 2002, “Possibility of Radiation-Induced Degradation of Concrete by Alkali-Silica Reaction of Aggregates.” *Journal of Nuclear Science and Technology.* **39**(8): 880–884.

44. Jing, Y. and Y. Xi, 2017, “Theoretical Modeling of the Effects of Neutron Irradiation on Properties of Concrete.” *Journal of Engineering Mechanics.* **143**(12): 04017137.

45. Kang, W.-H., T.-H. Kwon, H.-T. Kim, and K. Park, 2016, Design Strength Evaluation of RC Beams Under Radiation Environments for Nuclear Power Plants. 301: 101–110.

46. Kaplan, M.F., 1983, *Nuclear Radiation and the Properties of Concrete*. University of Cape Town.

47. Kelly, B.T., J. Brocklehurst, D. Mottershead, S. McNerney, and I. Davidson, 1969, “The Effect of Reactor Radiation on Concrete,” in *Second information meeting on prestressed concrete reactor pressure vessels and their thermal isolation.* Commision of the European Communities: Brussels. p. 237–266.

48. Kelly, B.T. and I. Davidson, 1968, “Irradiation Effects on Concrete,” in *Conference on Prestressed Concrete Pressure Vessels.* The Institution of Civil Engineers: Westminster. p. 173–175.

49. Kim, G., J.-Y. Kim, K.E. Kurtis, L.J. Jacobs, Y. Le Pape, and M. Guimaraes, 2014, “Quantitative evaluation of carbonation in concrete using nonlinear ultrasound.” *Materials and Structures.* **49**(1-2): 399–409.

50. Kitsutaka, Y. and K. Matsuzawa, 2010, “The Effect of Gamma Radiation on the Fracture Properties of Concrete,” in *Fracture Mechanics of Concrete and Concrete Structures - Recent Advances in Fracture Mechanics of Concrete,* B.H. Oh et al., Editors. Korea Concrete Institute: Seoul.

51. Kontani, O., Y. Ichikawa, A. Ishizawa, M. Takizawa, and O. Sato, 2010, “Irradiation Effects on Concrete Structure,” in *International Symposium on the Ageing Management & Maintenance of Nuclear Power Plants.* Mitsubishi Research Institute. p. 173–182.

52. Kontani, O., Y. Ichikawa, A. Ishizawa, M. Takizawa, and O. Sato, 2011, “Irradiation Effects on Concrete Durability of Nuclear Power Plants,” in *International Congress on Advances in Nuclear Power Plants 2011.* Societe Francaise D'Energie Nucleaire: Nice, France. p. 2352–2360.

53. Kontani, O., Y. Ichikawa, A. Ishizawa, M. Takizawa, and O. Sato, 2014, “Irradiation Effects on Concrete Structures,” in *Infrastructure Systems for Nuclear Energy,* T.T.C. Hsu, C.-L. Wu, and J.-L. Lin, Editors. John Wiley & Sons, Ltd. p. 459–473.

54. Kontani, O., S. Sawada, I. Maruyama, M. Takizawa, and O. Sato, 2013, “Evaluation of Irradiation Effects on Concrete Structure: Gamma-Ray Irradiation Tests on Cement Paste,” in *ASME 2013 Power Conference.* Boston, Massachusetts.

55. Kundu, T., J.N. Eiras, T. Kundu, J.S. Popovics, J. Monzó, M.V. Borrachero, and J. Payá, 2015, *Monitoring accelerated carbonation on standard Portland cement mortar by nonlinear resonance acoustic test*. p. 94380D.

56. Le Pape, Y., 2015, “Structural effects of radiation-induced volumetric expansion on unreinforced concrete biological shields”. *Nuclear Engineering and Design.* **295**: 534–548.

57. Le Pape, Y., K.G. Field, and I. Remec, 2015, “Radiation effects in concrete for nuclear power plants, Part II: Perspective from micromechanical modeling.” *Nuclear Engineering and Design*. **282**: 144–157.

58. Le Pape, Y., A. Giorla, and J. Sanahuja, 2016, “Combined Effects of Temperature and Irradiation on Concrete Damage.” *Journal of Advanced Concrete Technology.* **14**(3): 70–86.

59. Lowinska-Kluge, A. and P. Piszora, 2008, “Effect of Gamma Irradiation on Cement Composites Observed with XRD and SEM Methods in the Range of Radiation Dose 0 - 1409 MGy.” *Acta Physica Polonica A.* **114**(2): 399–411.

60. Lukesh, J.S., 1955, “Neutron Damage to the Structure of Vitreous Silica.” *Physical Review.* **97**(2): 345–346.

61. Maruyama, I., O. Kontani, A. Ishizawa, M. Takizawa, and O. Sato, 2012, “Development of System for Evaluating Concrete Strength Deterioration Due to Radiation and Resultant Heat,” in *3rd International Conference on NPP Life Management (PLIM) for Long Term Operations (LTO).* International Atomic Energy Agency: Salt Lake City, UT.

62. Maruyama, I., O. Kontani, S. Sawada, O. Sato, G. Igarashi, and M. Takizawa, 2013, “Evaluation of Irradiation Effects on Concrete Structure: Background and Preparation of Neutron Irradiation Test” in *Proceedings of the ASME 2013 Power Conference,* July 29–August 1, 2013, Boston MA.

63. Maruyama, I., Y. Nishioka, G. Igarashi, and K. Matsui, 2014, “Microstructural and bulk property changes in hardened cement paste during the first drying process.” *Cement and Concrete Research.* **58**: 20–34.

64. Maruyama, I., K. Haba, O. Sato, S. Ishikawa, O. Kontani, and M. Takizawa, 2016, “A Numerical Model for Concrete Strength Change under Neutron and Gamma-Ray Irradiation.” *Journal of Advanced Concrete Technology.* **14**(4): 144–162.

65. Maruyama, I., O. Kontani, M. Takizawa, S. Sawada, S. Ishikawa, J. Yasukouchi, O. Sato, J. Etoh, and T. Igari, 2017, “Development of Soundness Assessment Procedure for Concrete Members Affected by Neutron and Gamma-Ray Irradiaion.” *Journal of Advanced Concrete Technology.* **15**: 440–523.

66. McDowall, D.C., 1971, *The Effect of Gamma Irradiation on the Creep Properties of Concrete, in Results of Concrete Irradiation Programmes*, H. Benzler, Editor. Commission of the European Communities: Brussels. p. 55–69.

67. Mitchell, E.W.J. and E.G.S. Paige, CXI, 1956, “The optical effects of radiation induced atomic damage in quartz.” *Philosophical Magazine.* **1**(12): 1085–1115.

68. Mobasher, N., S.A. Bernal, H. Kinoshita, C.A. Sharrad, and J.L. Provis, 2015, “Gamma Irradiation Resistance of an Early Age Slag-Blended Cement Matrix for Nuclear Waste Encapsulation.” *Journal of Materials Research.* **30**(9): 1563–1571.

69. Mockel, H.J., and R.H. Koster, 1982, “Gas Formation during the Gamma Radiolysis of Cemented Low- and Intermediate-Level Waste Products.” *Nuclear Technology*. **59**: 494–497.

70. Naus, D.J., 2007, *Primer on Durability of Nuclear Power Plant Reinforced Concrete Structures - A Review of Pertinent Factors,* NUREG.CR-6927, Oak Ridge National Laboratory, for U.S. Nuclear Regulatory Commission, Washington, DC, February.

71. Nansted, R.K., 1976, *A Review of Concrete Properties for Prestressed Concrete Pressure Vessels*, ORNL/TM-5497, Oak Ridge National Laboratory, Oak Ridge, TN.

72. Ochbelagh, D.R., S. AzimKhani, and H.G. Mosavinejad, 2011, “Effect of Gamma and Lead as an Additive Material on the Resistance and Strength of Concrete.” *Nuclear Engineering and Design.* **241**: 2359–2363.

73. Park, K., H.-T. Kim, T.-H. Kwon, and E. Choi, 2016, “Effect of Neutron Irradiation on Response of Reinforced Concrete Members for Nuclear Power Plants.” *Nuclear Engineering and Design.* **310**: 15–26.

74. Pedersen, A., 1971, “Radiation Damage in Concrete - Measurements on Miniature Specimens of Cement Mortar,” in *Results of Concrete Irradiation Programmes,* H. Benzler, Editor. Commission of the European Communities: Brussels. p. 5–16.

75. Pomaro, B., V.A. Salomoni, F. Gramegna, G. Prete, and C.E. Majorana, 2011, “Radiation Damage Evaluation on Concrete Shielding for Nuclear Physics Experiments.” *Annals of Solid and Structural Mechanics.* **2**(2): 123–145.

76. Pomaro, B., V.A. Salomoni, F. Gramegna, G. Prete, and C.E. Majorana, 2011, “Radiation damage evaluation on concrete within a facility for Selective Production of Exotic Species (SPES Project), Italy.” *J Hazard Mater.* **194**: 169–177.

77. Pomaro, B., 2016, “A Review on Radiation Damage in Concrete for Nuclear Facilities: From Experiments to Modeling.” *Modeling and Simulation in Engineering*: p. 1–10.

78. Price, B.T., C.C. Horton, and K.T. Spinney, 1957, *Radiation Shielding*. New York: Pergamon.

79. Primak, W., 1953, *A Summary and Bibliography of Some Research on Radiation Damage in Ceramic Materials Performed at the Argonne National Laboratory*. Lemont, IL: Argonne National Laboratory. 14 pages.

80. Primak, W., 1955, "Experimental Evidence for Thermal Spikes in Radiation Damage." *Physical Review.* **98**(6): 1854–1855.

81. Primak, W., 1957, "Fast Neutron Damaging in Nuclear Reactors. III. The Radiation Damage Dosage." *Nuclear Science and Engineering.* **2**: 320–333.

82. Primak, W., 1958, "Fast-Neutron-Induced Changes in Quartz and Vitreous Silica." *Physical Review.* **110**(6): 1240–1254.

83. Primak, W., 1975, *The Compacted States of Vitreous Silica. Studies in Radiation Effects in Solids*, ed. G.J. Dienes and L.T. Chadderton. New York: Gordon and Breach Science Publishers.

84. Primak, W. and E. Edwards, 1962, "Radiation-Induced Dilatations in Vitreous Silica." *Physical Review.* **128**(6): 2580–2588.

85. Primak, W. and L.H. Fuchs, 1957, "Fast Neutron Damaging in Nuclear Reactors. I. Radiation Damage Monitoring with the Electrical Conductivity of Graphite." *Nuclear Science and Engineering.* **2**: 49–56.

86. Primak, W., L.H. Fuchs, and P. Day, 1953, "Radiation Damage in Insulators." *Physical Review.* **92**(4): 1064–1065.

87. Primak, W. and R. Kampwirth, 1968, "The Radiation Compaction of Vitreous Silica." *Journal of Applied Physics.* **39**(12): 5651.

88. Primak, W. and H. Szymanski, 1956, "Radiation Damage in Vitreous Silica: Annealing of the Density Changes." *Physical Review.* **101**(4): 1268–1271.

89. Rappeneau, J., M.F. Lagorio, J. Gilbert, and P. Piron, 1966, "Irradiation Experiments on Concretes." *Bull. Inform. Sci. Tech.* **110**: 31–48.

90. Rosseel, T.M., J.J. Wall, K.G. Field, Y. LePape, D.J. Naus, I. Remec, J.T. Busby, and P. Bruck, 2014, "Radiation Damage in Reactor Cavity Concrete." Fontevraud 8 – Contribution of Materials Investigations and Operating Experience to LWR's Safety, Performance and Reliability. September 14–18, Avignon, France.

91. Rosseel, T.M., K.G. Field, Y. LePape, I. Remec, A.B. Giorla, and J.J. Wall, 2015, "Recent Advances in Understanding Radiation Damage In Reactor Cavity Concrete." Division I, Paper ID 647, Transactions, (Structural Materials in Reactor Technology) SMiRT-23, August 10–14, Manchester, United Kingdom.

92. Rosseel, T.M., I. Maruyama, Y. LePape, O. Kontani, A.B. Giorla, I. Remec, J.J. Wall, M. Sircar, C. Andrade, and M. Ordonez, 2016, “Review of the Current State of Knowledge on the Effects of Radiation on Concrete.” *Journal of Advanced Concrete Technology.* **14**: 368–383.

93. Saouma, V.E. and M.A. Hariri-Ardebili, 2014, “A proposed aging management program for alkali silica reactions in a nuclear power plant.” *Nuclear Engineering and Design.* **277**: 248–264.

94. Short, M.P. and S. Yip, 2015, “Materials aging at the mesoscale: Kinetics of thermal, stress, radiation activations.” *Current Opinion in Solid State and Materials Science.* **19**(4): 245–252.

95. Simon, I., 1956, “Structure of Neutron-Disordered Silica.” *Physical Review*. **103**(5): 1587–1588.

96. Simon, I., 1957, “Structure of Neutron-Irradiated Quartz and Vitreous Silica.” *Journal of the American Ceramic Society.* **40**(5): 150–153.

97. Sommers, J.F., 1969, “Gamma Radiation Damage of Structural Concrete Immersed in Water. Health Physics.” **16**: 503–508.

98. Soo, P. and L.M. Milian, 2001, “The Effect of Gamma Irradiation on the Strength of Portland Cement Mortars.” *Journal of Materials Science Letters.* **20**: 4.

99. Soo, P. and L.W. Milian, 1989, *Sulfate-Attack Resistance and Gamma-Irradiation Resistance of Some Portland Cement Based Mortars*, NUREG/CR-5279, Brookhaven National Laboratory, for U.S. Nuclear Regulatory Commission, Washington, DC.

100. Sopko, V., K. Trtík, and F. Vodák, 2004, “Influence of Gamma Radiation on Concrete Strength.” *Acta Polytechnica*. **44**(1): 57–58.

101. Stoces, B., P. Otopal, V. Juricka, and J. Gabriel, 1970, *The Effect of Radiation on the Mechanical Properties of Concrete*.

102. Van der Schaaf, C.F., 1967, “Effect of Heating and Radiation on Some Properties of Mortar and Concrete Specimens with Different Compositions,” in *Information meeting on work relating to prestressed concrete vessels and their isolation.* Euratom: Brussels.

103. Vodak, F., R. Cerny, J. Drchalova, S. Hoskova, O. Kapickova, O. Michalko, . . . J. Toman, 1997, “Thermophysical Properties of Concrete for Nucelar-Safety Related Structures.” *Cement and Concrete Research*. **27**(3): 12.

104. Vodák, F., K. Trtík, V. Sopko, O. Kapičková, and P. Demo, 2005, “Effect of γ-irradiation on strength of concrete for nuclear-safety structures.” *Cement and Concrete Research.* **35**(7): 1447–1451.

105. Vodák, F., V. Vydra, K. Trtík, and O. Kapičková, 2011, “Effect of gamma irradiation on properties of hardened cement paste.” *Materials and Structures.* **44**(1): 101–107.

106. Vydra, V., F. Vodak, O. Kapickova, and S. Hoskova, 2001, “Effect of temperature on porosity of concrete for nuclear-safety structures.” *Cement and Concrete Research*. **31**(7): 1023–1026.

107. Weissmann, S. and K. Nakajima, 1963, “Defect Structure and Density Decrease in Neutron-Irradiated Quartz.” *Journal of Applied Physics.* **34**(3): 611.

108. Wilding, C.R., D.C. Phillips, C.E. Lyon, S.G. Burnay, J.A. Winter, and W.E. Spindler, 1991, *Nuclear Science and Technology, The Effects of Radiation on Intermediate-Level Waste Forms*, Task 3, Characterization of Radioactive Waste Forms, A Series of Final Reports (1985-89), No. 10, EUR 13559, prepared by the Chemistry Division, Harwell Laboratory, United Kingdom, for the Commission of the European Communities.

109. William, K., Y. Xi, and D. Naus, 2013, *A Review of the Effects of Radiation on Microstructure and Properties of Concretes Used in Nuclear Power Plants*, NUREG/CR-7171, U. of Houston, U. of Colorado, Oak Ridge National Laboratory, for U.S. Nuclear Regulatory Commission, Washington, DC, November.

110. Wittels, M., 1953, “The Lattice Expansion of Quartz Due to Fast Neutron Bombardment.” *Physical Review*. **89**(3): 656–657.

111. Wittels, M. and F.A. Sherrill, 1954, “Radiation Damage in SiO2 Structures.” *Physical Review*. **93**(5): 1117–1118.

112. Wittels, M.C., 1957, “Structural behaviour of neutron irradiated quartz.” *Philosophical Magazine.* **2**(24): 1445–1461.

113. Zubov, V.G. and A.T. Ivanov, 1966, “Expansion of Quartz Caused by Irradiation with Fast Neutrons.” *Soviet Physics - Crystallography*. **11**(3): 372–374.

APPENDIX C
NEUTRON FLUENCE ESTIMATES

Table C-1 60- and 80-Year Neutron Fluence Estimates (n/cm^2) at the Inner and Outer RPV Walls[a]

Type/Unit	Vendor[b]	No. of Loops	RPV Wall Thickness (in)	60-Year		80-Year		Ref. for 60-Year Neutron Fluence at Inner RPV Wall	Ref. for RPV Wall Thickness[c]
				Inner Wall (E > 1.0 MeV)	Outer Wall (E > 1.0 MeV)	Outer Wall (E > 1.0 MeV	Outer Wall (E > 0.1 MeV		
BWR									
Dresden 2	GET3	N/A[d]	6.125	5.70E+17	7.55E+16	1.01E+17	6.99E+17	[186]	[187]
Dresden 3	GET3	N/A	6.125	5.70E+17	7.55E+16	1.01E+17	6.99E+17	[186]	[188]
Quad Cities 1	GET3	N/A	6.125	5.70E+17	7.55E+16	1.01E+17	6.99E+17	[186]	[189]
Quad Cities 2	GET3	N/A	6.125	5.70E+17	7.55E+16	1.01E+17	6.99E+17	[186]	[190]
LaSalle County 1	GET5	N/A	6.13	1.06E+18	1.40E+17	1.87E+17	1.30E+18	[191]	[192]
Limerick 1	GET4	N/A	6.430	1.15E+18	1.38E+17	1.84E+17	1.35E+18	[193]	
Limerick 2	GET4	N/A	6.190	1.12E+18	1.45E+17	1.94E+17	1.36E+18	[193]	
Columbia Gen. Station	GET5	N/A	6.188	1.17E+18	1.52E+17	2.02E+17	1.42E+18	[194]	
LaSalle County 2	GET5	N/A	6.190	1.22E+18	1.58E+17	2.11E+17	1.48E+18	[191]	[195]
Susquehanna 1	GET4	N/A	6.188	1.41E+18	1.83E+17	2.44E+17	1.71E+18	[196]	

Table C-1 60- and 80-Year Neutron Fluence Estimates (n/cm^2) at the Inner and Outer RPV Walls[a] (Cont.)

Type/Unit	Vendor[b]	No. of Loops	RPV Wall Thickness (in)	60-Year		80-Year		Ref. for 60 Year Neutron Fluence at Inner RPVWall	Ref. for RPV Wall Thickness[c]
				Inner Wall (*E* > 1.0 MeV)	Outer Wall (*E* > 1.0 MeV)	Outer Wall (*E* > 1.0 MeV	Outer Wall (*E* > 0.1 MeV		
Susquehanna 2	GET4	N/A	6.188	1.42E+18	1.84E+17	2.46E+17	1.73E+18	[196]	
Fermi 2	GET4	N/A	6.125	1.43E+18	1.89E+17	2.53E+17	1.75E+18	[197]	[197]
Nine Mile Point 2	GET5	N/A	6.188	1.45E+18	1.88E+17	2.51E+17	1.76E+18	[198]	[199]
Brunswick 2	GET4	N/A	5.466	1.38E+18	2.27E+17	3.03E+17	1.86E+18	[200]	
Hope Creek 1	GET4	N/A	6.102	1.54E+18	2.06E+17	2.74E+17	1.90E+18	[201]	[201]
Browns Ferry 1	GET4	N/A	6.125	1.95E+18	2.58E+17	3.44E+17	2.39E+18	[202]	
Cooper Station	GET4	N/A	5.375	1.95E+18	3.31E+17	4.41E+17	2.66E+18	[203]	[203]
Peach Bottom 2	GET4	N/A	6.125	2.20E+18	2.91E+17	3.89E+17	2.70E+18	[204]	
Peach Bottom 3	GET4	N/A	6.125	2.20E+18	2.91E+17	3.89E+17	2.70E+18	[204]	
Browns Ferry 2	GET4	N/A	6.130	2.30E+18	3.04E+17	4.06E+17	2.82E+18	[202]	
Browns Ferry 3	GET4	N/A	6.130	2.30E+18	3.04E+17	4.06E+17	2.82E+18	[202]	
Fitzpatrick	GET4	N/A	5.375	3.05E+18	5.18E+17	6.90E+17	4.16E+18	[205]	
Hatch 1	GET4	N/A	5.38	3.47E+18	5.88E+17	7.84E+17	4.73E+18	[206]	[206]
Grand Gulf 1	GET4	N/A	6.438	4.44E+18	5.31E+17	7.07E+17	5.21E+18	[207]	[207]

Table C-1 60- and 80-Year Neutron Fluence Estimates (n/cm^2) at the Inner and Outer RPV Walls[a] (Cont.)

Type/Unit	Vendor[b]	No. of Loops	RPV Wall Thickness (in)	60-Year		80-Year		Ref. for 60 Year Neutron Fluence at Inner RPVWall	Ref. for RPV Wall Thickness[c]
				Inner Wall (E > 1.0 MeV)	Outer Wall (E > 1.0 MeV)	Outer Wall (E > 1.0 MeV	Outer Wall (E > 0.1 MeV		
Hatch 2	GET4	N/A	5.380	3.82E+18	6.47E+17	8.63E+17	5.21E+18	[206]	[206]
Brunswick 1	GET4	N/A	5.496	4.00E+18	6.52E+17	8.70E+17	5.37E+18	[200]	
Nine Mile Point 1	GET2	N/A	7.125	5.21E+18	4.96E+17	6.62E+17	5.54E+18	[198]	
Perry 1	GET6	N/A	6.00	4.73E+18	6.53E+17	8.71E+17	5.91E+18	[208]	[209]
Monticello	GET3	N/A	5.063	5.17E+18	9.72E+17	1.30E+18	7.38E+18	[210]	[210]
Oyster Creek	GET2	N/A	7.125	6.97E+18	6.64E+17	8.85E+17	7.41E+18	[211]	
River Bend 1	GET6	N/A	5.406	6.82E+18	1.15E+18	1.53E+18	9.27E+18	[212]	[212]
Duane Arnold	GET4	N/A	4.469	7.51E+18	1.72E+18	2.29E+18	1.17E+19	[213]	[213]
					PWR				
Oconee 3	B&WLL	2	8.4375	1.26E+19	7.78E+17	1.04E+18	1.11E+19	[214]	[215]
Oconee 2	B&WLL	2	8.4375	1.28E+19	7.91E+17	1.05E+18	1.13E+19	[214]	[215]
Oconee 1	B&WLL	2	8.4375	1.31E+19	8.09E+17	1.08E+18	1.16E+19	[214]	[215]
ANO 1	B&WLL	2	6.60	1.17E+19	1.33E+18	1.77E+18	1.34E+19	[153]	
Davis-Besse	B&WRL	2	8.44	1.68E+19	1.04E+18	1.38E+18	1.48E+19	[216]	[216]

Table C-1 60- and 80-Year Neutron Fluence Estimates (n/cm^2) at the Inner and Outer RPV Walls[a] (Cont.)

Type/Unit	Vendor[b]	No. of Loops	RPV Wall Thickness (in)	60-Year		80-Year		Ref. for 60 Year Neutron Fluence at Inner RPVWall	Ref. for RPV Wall Thickness[c]
				Inner Wall (E > 1.0 MeV)	Outer Wall (E > 1.0 MeV)	Outer Wall (E > 1.0 MeV	Outer Wall (E > 0.1 MeV		
Three Mile Island 1	B&WLL	2	8.44	1.97E+19	1.22E+18	1.62E+18	1.74E+19	[217]	[217]
Palo Verde 1	CES80	2	9.06	2.51E+19	1.26E+18	1.68E+18	2.03E+19	[218]	[219]
Palo Verde 2	CES80	2	9.07	2.83E+19	1.42E+18	1.89E+18	2.28E+19	[218]	[219]
Palo Verde 3	CES80	2	9.07	2.93E+19	1.47E+18	1.96E+18	2.36E+19	[218]	[219]
Palisades	CE	2	8.74	3.00E+19	1.68E+18	2.24E+18	2.53E+19	[220]	[221]
Millstone 2	CE	2	8.626	4.25E+19	2.47E+18	3.29E+18	3.65E+19	[161]	
Waterford 3	CE	2	8.622	4.32E+19	2.51E+18	3.35E+18	3.71E+19	[222]	
Fort Calhoun	CE	2	7.122	3.50E+19	3.34E+18	4.45E+18	3.72E+19	[223]	[129]
St. Lucie 1	CE	2	8.625	4.68E+19	2.72E+18	3.62E+18	4.02E+19	[224]	[225]
St. Lucie 2	CE	2	8.625	4.89E+19	2.84E+18	3.79E+18	4.20E+19	[224]	[226]
Calvert Cliffs 1	CE	2	8.625	5.26E+19	3.05E+18	4.07E+18	4.52E+19	[227]	
ANO 2	CE	2	7.666	5.08E+19	4.05E+18	5.40E+18	5.00E+19	[156]	
Calvert Cliffs 2	CE	2	8.625	6.16E+19	3.58E+18	4.77E+18	5.29E+19	[227]	[228]
R. E. Ginna	W2L	2	6.500	4.85E+19	5.68E+18	7.57E+18	5.64E+19	[229]	
Prairie Island 1	W2L	2	6.692	5.16E+19	5.67E+18	7.56E+18	5.84E+19	[230]	[230]

Table C-1 60- and 80-Year Neutron Fluence Estimates (n/cm^2) at the Inner and Outer RPV Walls[a] (Cont.)

Type/Unit	Vendor[b]	No. of Loops	RPV Wall Thickness (in)	60-Year		80-Year		Ref. for 60 Year Neutron Fluence at Inner RPVWall	Ref. for RPV Wall Thickness[c]
				Inner Wall (*E* > 1.0 MeV)	Outer Wall (*E* > 1.0 MeV)	Outer Wall (*E* > 1.0 MeV	Outer Wall (*E* > 0.1 MeV		
Prairie Island 2	W2L	2	6.692	5.19E+19	5.70E+18	7.60E+18	5.87E+19	[230]	[230]
Point Beach 1	W2L	2	6.500	5.26E+19	6.16E+18	8.21E+18	6.12E+19	[231]	[232]
Point Beach 2	W2L	2	6.500	5.39E+19	6.31E+18	8.41E+18	6.27E+19	[231]	[232]
Surry 2	W3L	3	8.08	5.34E+19	3.71E+18	4.95E+18	4.96E+19	[233]	[234]
Surry 1	W3L	3	8.08	5.40E+19	3.75E+18	5.00E+18	5.01E+19	[233]	[234]
North Anna 1	W3L	3	7.875	5.90E+19	4.39E+18	5.85E+18	5.64E+19	[235]	
North Anna 2	W3L	3	7.875	5.91E+19	4.40E+18	5.86E+18	5.65E+19	[235]	
Beaver Valley 1	W3L	3	7.874	6.09E+19	4.53E+18	6.04E+18	5.82E+19	[236]	[228]
Joseph M. Farley 2	W3L	3	7.875	6.29E+19	4.68E+18	6.24E+18	6.01E+19	[237]	
Beaver Valley 2	W3L	3	7.874	6.29E+19	4.68E+18	6.24E+18	6.01E+19	[236]	
Robinson 2	W3L	3	9.297	7.84E+19	3.65E+18	4.86E+18	6.12E+19	[238]	
Joseph M. Farley 1	W3L	3	7.875	6.41E+19	4.77E+18	6.36E+18	6.13E+19	[237]	
VC Summer	W3L	3	7.750	6.40E+19	4.96E+18	6.61E+18	6.23E+19	[239]	
Shearon Harris 1	W3L	3	7.75	6.91E+19	5.36E+18	7.14E+18	6.72E+19	[240]	[241]

Table C-1 60- and 80-Year Neutron Fluence Estimates (n/cm^2) at the Inner and Outer RPV Walls[a] (Cont.)

Type/Unit	Vendor[b]	No. of Loops	RPV Wall Thickness (in)	60-Year		80-Year		Ref. for 60 Year Neutron Fluence at Inner RPVWall	Ref. for RPV Wall Thickness[c]
				Inner Wall (E > 1.0 MeV)	Outer Wall (E > 1.0 MeV)	Outer Wall (E > 1.0 MeV	Outer Wall (E > 0.1 MeV		
Turkey Point 4	W3L	3	7.750	7.71E+19[e]	5.98E+18	7.97E+18	7.50E+19	[144]	[242]
Turkey Point 3	W3L	3	7.750	7.73E+19[e]	5.99E+18	7.99E+18	7.52E+19	[144]	[242]
Indian Point 3	W4L	4	8.689	1.56E+19	8.87E+17	1.18E+18	1.33E+19	[243]	
Salem 1	W4L	4	8.840	1.84E+19	9.95E+17	1.33E+18	1.53E+19	[244]	[245]
Diablo Canyon 1	W4L	4	9.625	2.06E+19	8.60E+17	1.15E+18	1.53E+19	[246]	[246]
Indian Point 2	W4L	4	8.622	1.91E+19	1.11E+18	1.48E+18	1.64E+19	[243]	
Salem 2	W4L	4	8.689	1.96E+19	1.11E+18	1.49E+18	1.67E+19	[244]	[134]
Diablo Canyon 2	W4L	4	8.689	2.32E+19	1.32E+18	1.76E+18	1.97E+19	[246]	
Donald C. Cook 2	W4L	4	8.689	2.46E+19	1.40E+18	1.86E+18	2.09E+19	[247]	
Sequoyah 2	W4L	4	8.450	2.57E+19	1.58E+18	2.11E+18	2.26E+19	[248]	
Millstone 3	W4L	4	8.689	2.70E+19	1.53E+18	2.05E+18	2.30E+19	[249]	
Sequoyah 1	W4L	4	8.450	2.66E+19	1.64E+18	2.18E+18	2.34E+19	[248]	

Table C-1 60- and 80-Year Neutron Fluence Estimates (n/cm^2) at the Inner and Outer RPV Walls[a] (Cont.)

Type/Unit	Vendor[b]	No. of Loops	RPV Wall Thickness (in)	60-Year		80-Year		Ref. for 60 Year Neutron Fluence at Inner RPVWall	Ref. for RPV Wall Thickness[c]
				Inner Wall (*E* > 1.0 MeV)	Outer Wall (*E* > 1.0 MeV)	Outer Wall (*E* > 1.0 MeV	Outer Wall (*E* > 0.1 MeV		
Donald C. Cook 1	W4L	4	8.689	2.83E+19	1.61E+18	2.15E+18	2.41E+19	[247]	
Callaway 1	W4L	4	8.630	2.90E+19	1.68E+18	2.24E+18	2.49E+19	[250]	[250]
McGuire 2	W4L	4	8.465	2.88E+19	1.76E+18	2.35E+18	2.53E+19	[251]	[130]
Watts Bar 1	W4L	4	8.689	3.01E+19	1.71E+18	2.28E+18	2.56E+19	[252]	
Vogtle 2	W4L	4	8.625	3.02E+19	1.75E+18	2.34E+18	2.59E+19	[253]	[137]
McGuire 1	W4L	4	8.630	3.07E+19	1.78E+18	2.37E+18	2.63E+19	[251]	[254]
Catawba 2	W4L	4	8.689	3.16E+19	1.80E+18	2.40E+18	2.69E+19	[251]	
Catawba 1	W4L	4	8.465	3.12E+19	1.91E+18	2.55E+18	2.74E+19	[251]	
Vogtle 1	W4L	4	8.625	3.20E+19	1.86E+18	2.48E+18	2.75E+19	[253]	[136]
Braidwood 2	W4L	4	8.5	3.16E+19	1.91E+18	2.55E+18	2.76E+19	[255]	[255]
Braidwood 1	W4L	4	8.5	3.19E+19	1.93E+18	2.57E+18	2.79E+19	[255]	[255]
Byron 2	W4L	4	8.5	3.19E+19	1.93E+18	2.57E+18	2.79E+19	[255]	[255]
Byron 1	W4L	4	8.5	3.21E+19	1.94E+18	2.59E+18	2.81E+19	[255]	[255]
Comanche Peak 1	W4L	4	8.622	3.33E+19	1.94E+18	2.58E+18	2.86E+19	[256]	

Table C-1 60- and 80-Year Neutron Fluence Estimates (n/cm^2) at the Inner and Outer RPV Walls[a] (Cont.)

Type/Unit	Vendor[b]	No. of Loops	RPV Wall Thickness (in)	60-Year		80-Year		Ref. for 60 Year Neutron Fluence at Inner RPVWall	Ref. for RPV Wall Thickness[c]
				Inner Wall (*E* > 1.0 MeV)	Outer Wall (*E* > 1.0 MeV)	Outer Wall (*E* > 1.0 MeV	Outer Wall (*E* > 0.1 MeV		
Wolf Creek 1	W4L	4	8.689	3.51E+19	2.00E+18	2.66E+18	2.99E+19	[257]	
Seabrook 1	W4L	4	8.622	3.63E+19	2.11E+18	2.81E+18	3.12E+19	[258]	
South Texas 2	W4L	4	8.630	3.73E+19	2.16E+18	2.88E+18	3.20E+19	[259]	
South Texas 1	W4L	4	8.630	3.86E+19	2.24E+18	2.98E+18	3.31E+19	[259]	

[a] Grouped by reactor type in increasing value of number of loops and neutron fluence (*E* > 0.1 MeV at the outer wall for 80-years of operation).

[b] B&W: Babcock and Wilcox Two-Loop Lower; CE: Combustion Engineering; CE80: Combustion Engineering System 80; W2L: Westinghouse 2-Lop; W3L: Westinghouse Three-Loop; W4L: Westinghouse Four-Loop; GET2: General Electric Type 2; GET3: General Electric Type 3; GET4: General Electric Type 4; GET5: General Electric Type 5; GET6: General Electric Type 6.

[c] RPV wall thickness values taken from Esselman and Bruck [12] unless otherwise specified, values without a specific reference listed are consistent with the corresponding value in the Reactor Vessel Integrity Database [260].

[d] N/A = Not applicable.

[e] Neutron fluence values for Turkey Point Units 3 and 4 at the inner wall (E > 1.0 MeV) after 60 years of operation (assumed to be 54 EFPY) were estimated by taking the average of the estimated 48 and 60 EFPY values provided in their SLR application reference documents [144].

APPENDIX D
PWR SUPPORT DESIGNS

This appendix summarizes 14 reactor support designs for the pressurized water reactor (PWR) nuclear power plants (NPPs) discussed in Section 7.1. These reactor supports were estimated to receive some of the highest neutron fluence levels during 80 years of operation. Excerpts from license application documentation are used to provide descriptions of the support systems. Figures called out in these excerpts can be found in the original documentation. Where possible, these figures are called out and provided in the main text of this appendix. All information, figures and sketches are obtained from available public resources at the time of the development of this document.

D.1 Arkansas Nuclear One Unit 2

Arkansas Nuclear One (ANO) Unit 2 is a Combustion Engineering design two-loop PWR. Figures and referenced text are from Safety Analysis Report (SAR) Amendment 26 [157]. The ANO 2 RPV incorporates a column support design:

> ***5.5.14.2.1 Reactor Vessel Supports***
> *The reactor vessel is supported by three vertical columns located under the reactor vessel nozzles (see Figure 5.5-12). The columns are sufficiently flexible to allow radial thermal expansion of the vessel. Keyways on the sides of the integral support pads under the nozzles guide the vessel during thermal expansion and maintain the location of the vessel vertical centerline. A key on the lower vessel head provides additional seismic restraint.*

Figures D.1-1 through D.1-3 provide views of the reactor vessel and its supports. The reactor vessel is supported on three vertical columns with the columns resting on the basemat, but there are horizontal reactor supports at the top of the columns which are embedded in the bioshield (see Figure D.1-1) and serve to limit motion under accident scenarios (SAR Section 3.6.4.2.1.2).

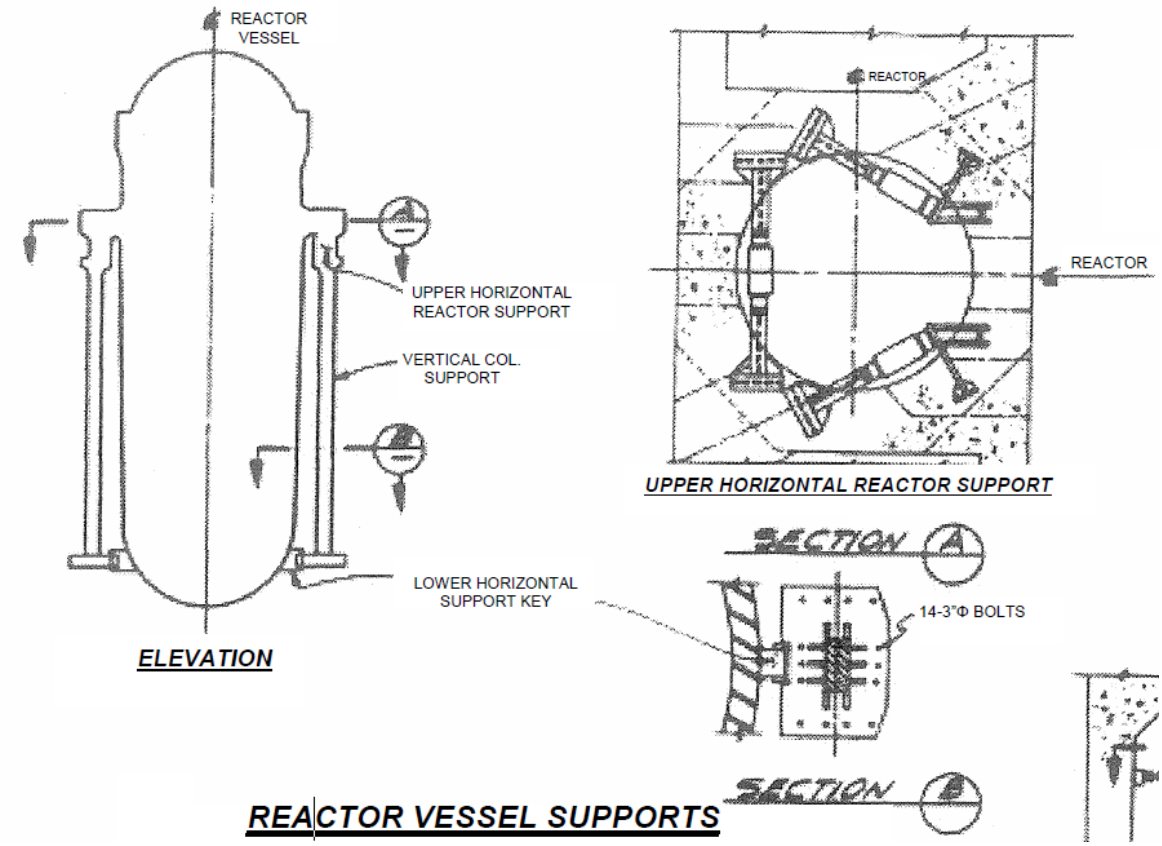

Figure D.1-1 ANO 2 Reactor Vessel Supports (taken from SAR Figure No. 3.8-13A)

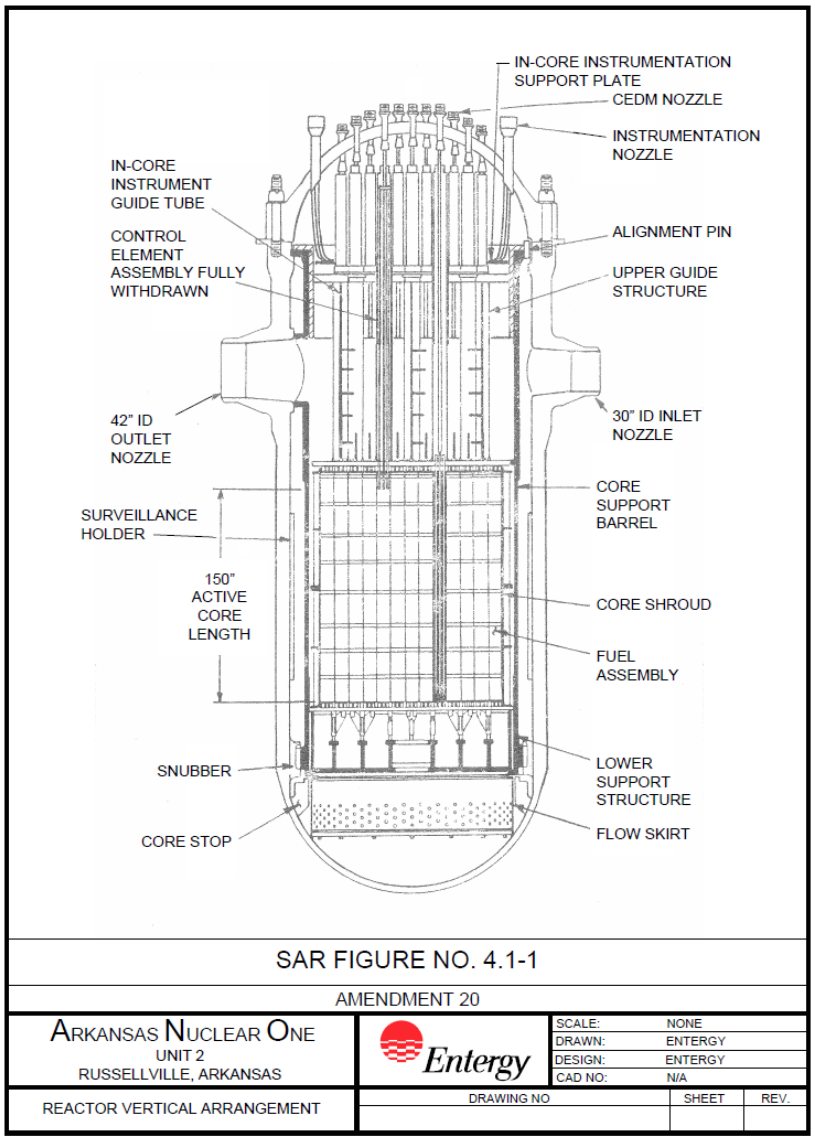

SAR FIGURE NO. 4.1-1

AMENDMENT 20

ARKANSAS NUCLEAR ONE UNIT 2 RUSSELLVILLE, ARKANSAS	Entergy	SCALE: NONE DRAWN: ENTERGY DESIGN: ENTERGY CAD NO: N/A	
REACTOR VERTICAL ARRANGEMENT	DRAWING NO	SHEET	REV.

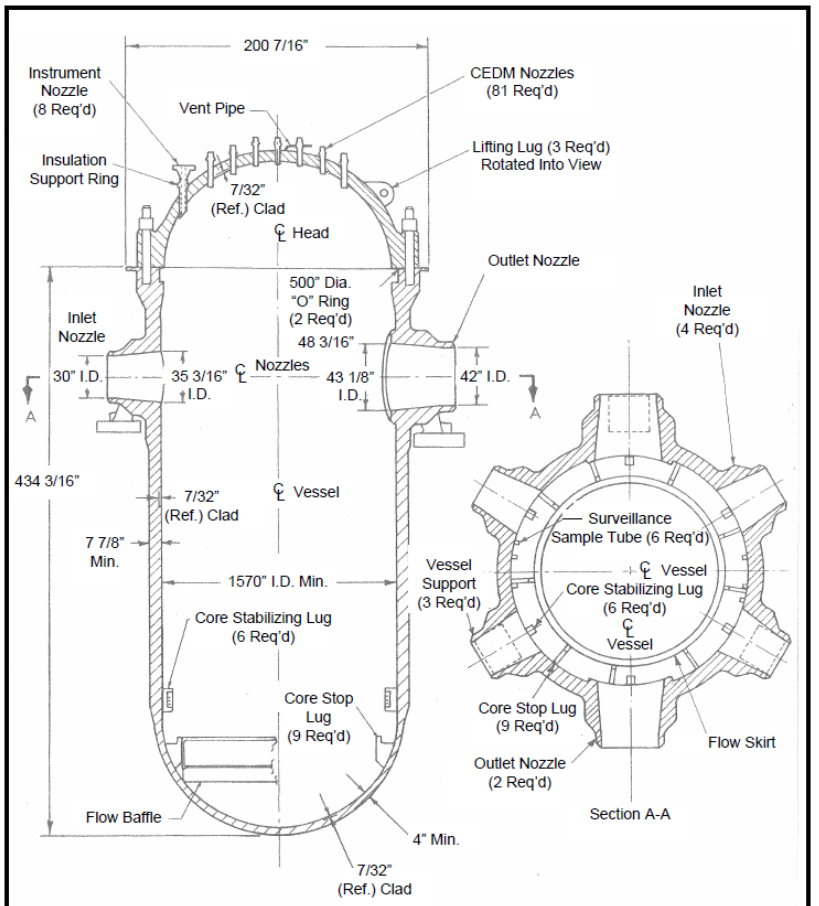

SAR FIGURE NO. 5.4-1

AMENDMENT 20

ARKANSAS NUCLEAR ONE UNIT 2 RUSSELLVILLE, ARKANSAS	Entergy	SCALE: NONE DRAWN: ENTERGY DESIGN: ENTERGY CAD NO: N/A	
REACTOR VESSEL	BASED ON DRAWING NO	SHEET	REV.

Figure D.1-2 ANO 2 RPV

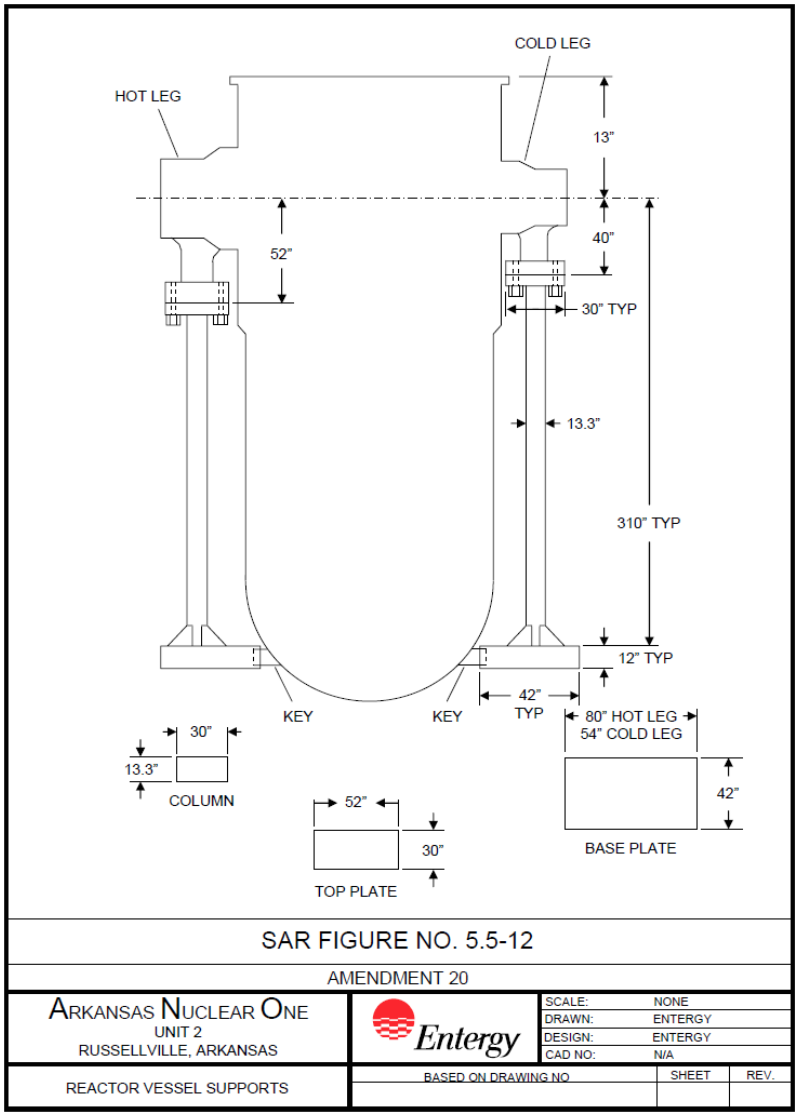

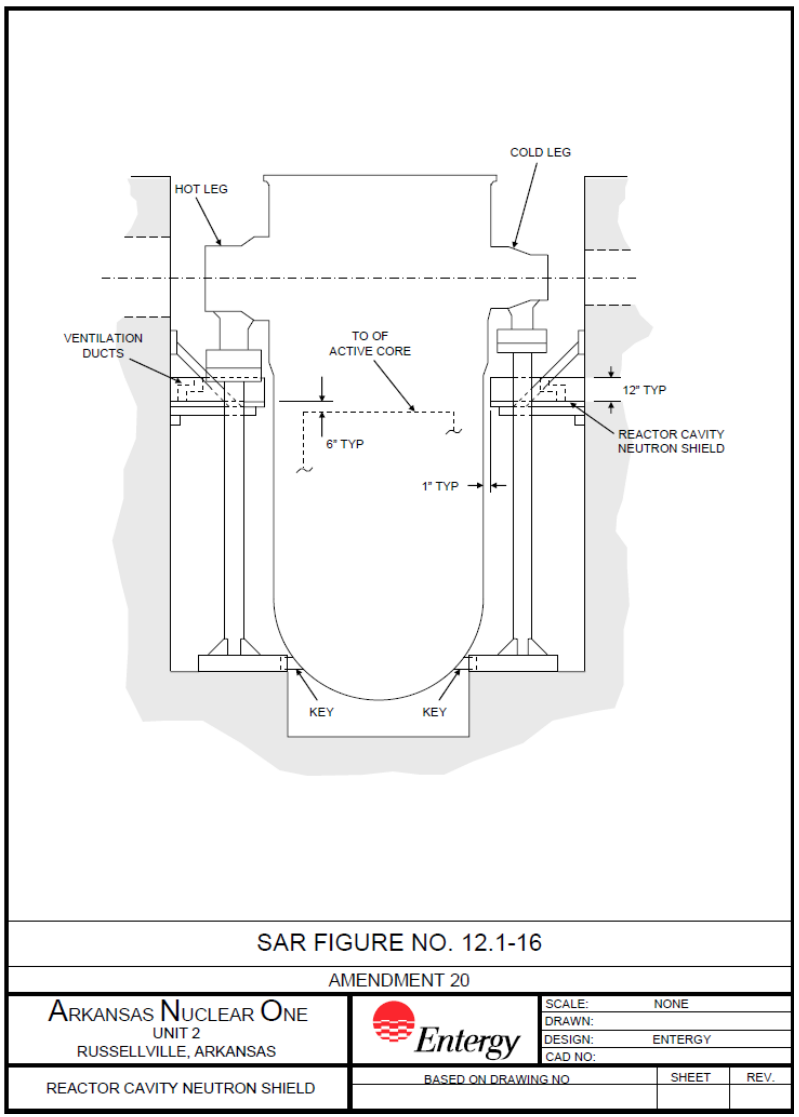

Figure D.1-3 ANO 2 RPV Support Columns

D.2 Beaver Valley Units 1 and 2

Beaver Valley Units 1 and 2 are Westinghouse PWR three-loop reactors. They employ a neutron shield tank that surrounds the reactor and is supported by the bioshield as shown in Figures D.2-1 through D.2-4.

The reactor vessel support system is described in the Updated Final Safety Analysis Report (UFSAR) [56]:

> *5.4.14.2.1 Reactor Vessel Structural Support*
>
> *The RVSS is a cylindrical, skirt-supported, double-walled structure designed to transfer loadings to the reinforced concrete mat of the containment structure and to the surrounding primary shield wall; it is fabricated of SA-516, Gr-70 plate. This component support is designed to restrain vertical, lateral, and rotational movement of the reactor vessel while permitting thermal expansion/contraction of the reactor vessel during plant operation. The reactor vessel is set on leveling devices between each of the six RPV loop nozzle pads and the top of the support structure. This support is also designed to provide neutron shielding and thermal protection to the surrounding structure by means of a water-filled annular section, as well as to house and cool the ex-core neutron detectors. The RVSS is shown on Figure 5.4-10.*
>
> *The reactor vessel support/leveling device, fabricated with material in compliance with the ASTM A-668-72 Type K material specification, is shown on Figure 5.4-11. The triple wedge shape device is positioned (without mechanical attachment) between each of the six reactor vessel nozzle pads and a lubricated plate which is fastened to the top surface of the reactor vessel structural support. The functional requirement of the RPV support/leveling device is to provide vertical adjustment at each RPV nozzle restraint pad during installation of the reactor vessel. Each support/leveling device has a screw assembly to produce relative horizontal translation of the wedge shaped plates, which results in a limited vertical adjustment of the reactor vessel during installation. During all plant conditions, this support system is designed to transfer only vertically downward (compression) loads from the reactor vessel nozzle pads to the reactor vessel structural support. Upward loads are reacted by gib keys (Figure 5.4-11).*

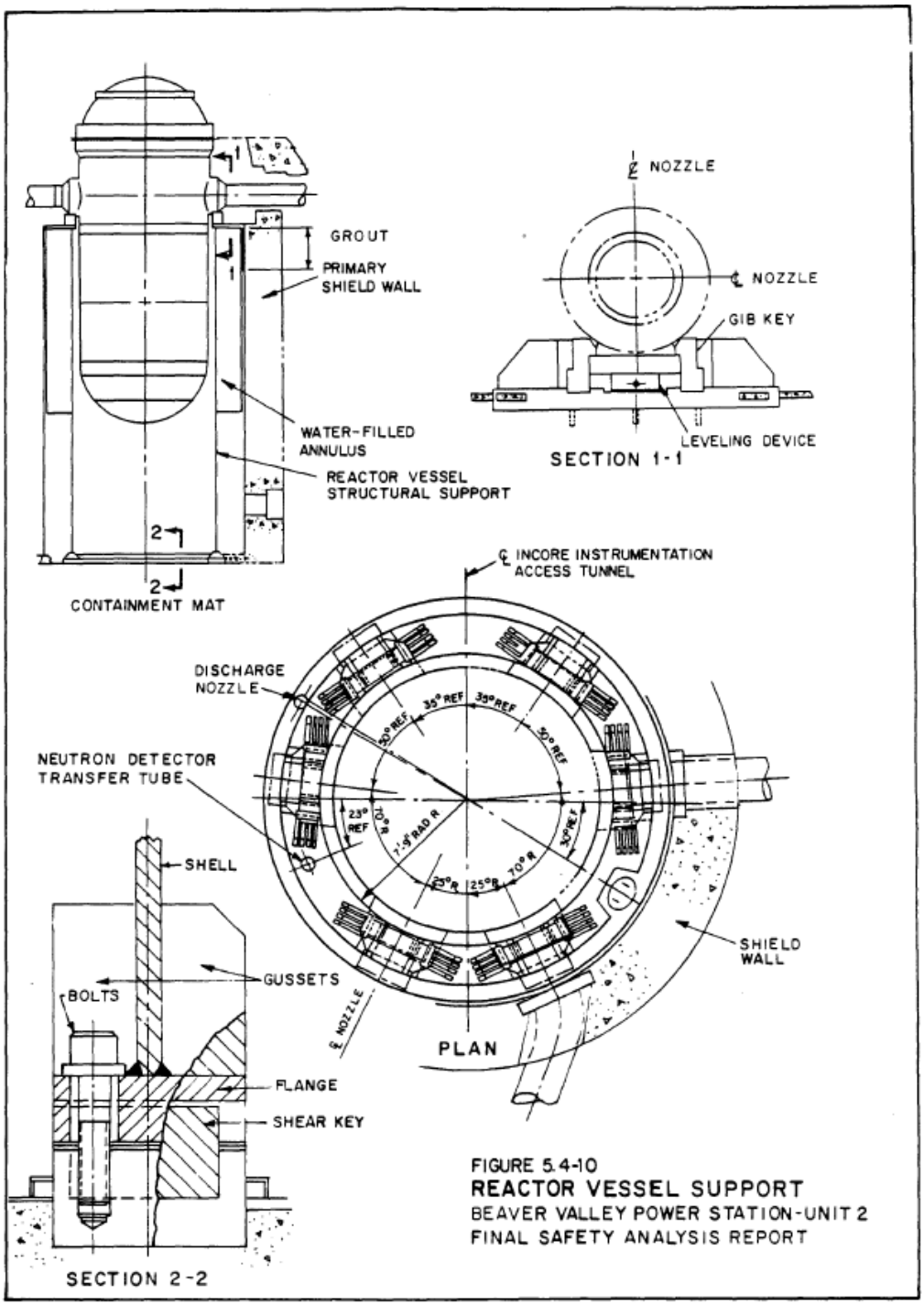

Figure D.2-1 Beaver Valley Unit 2 Reactor Vessel Support Design (UFSAR, Section 5 [56])

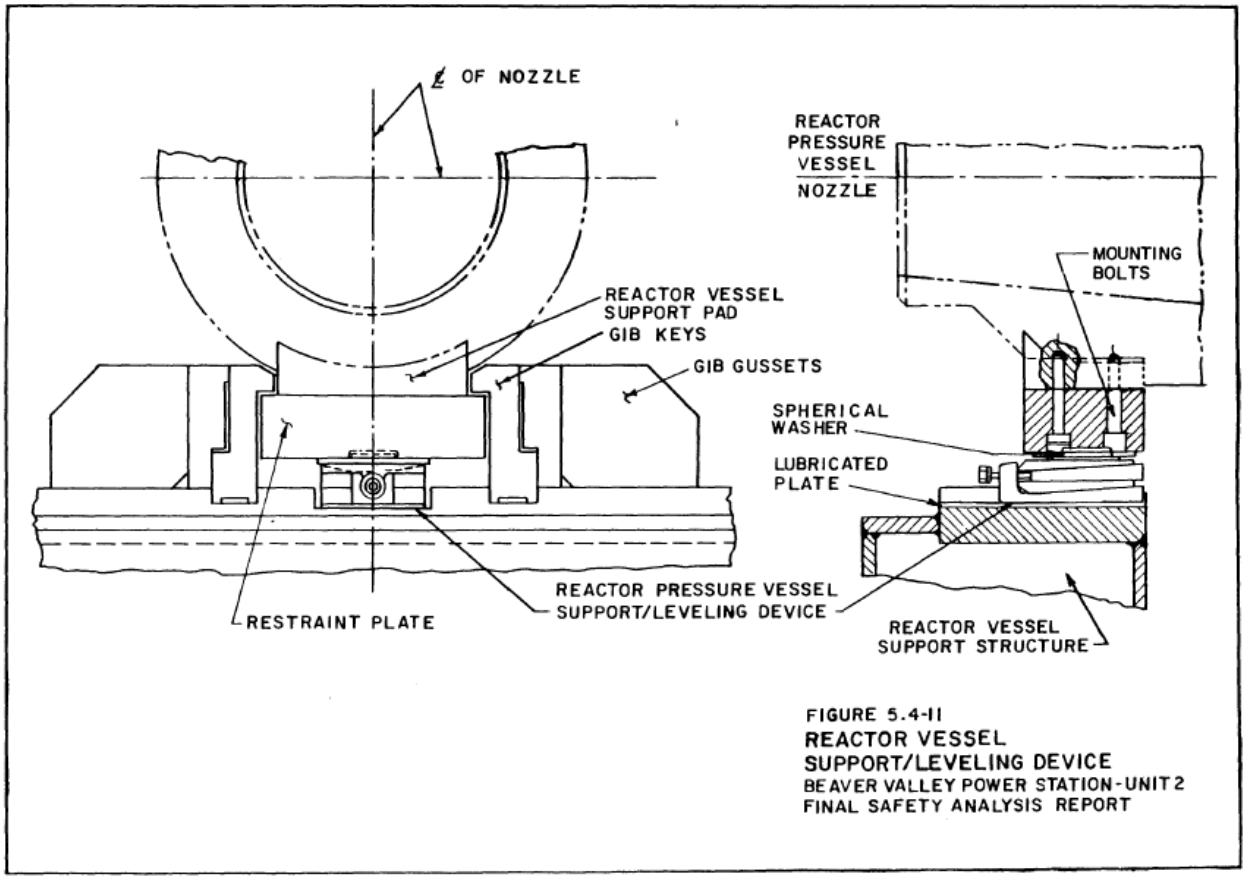

Figure D.2-2 Beaver Valley Unit 2 Reactor Vessel Support Shoe Design (UFSAR, Section 5 [56])

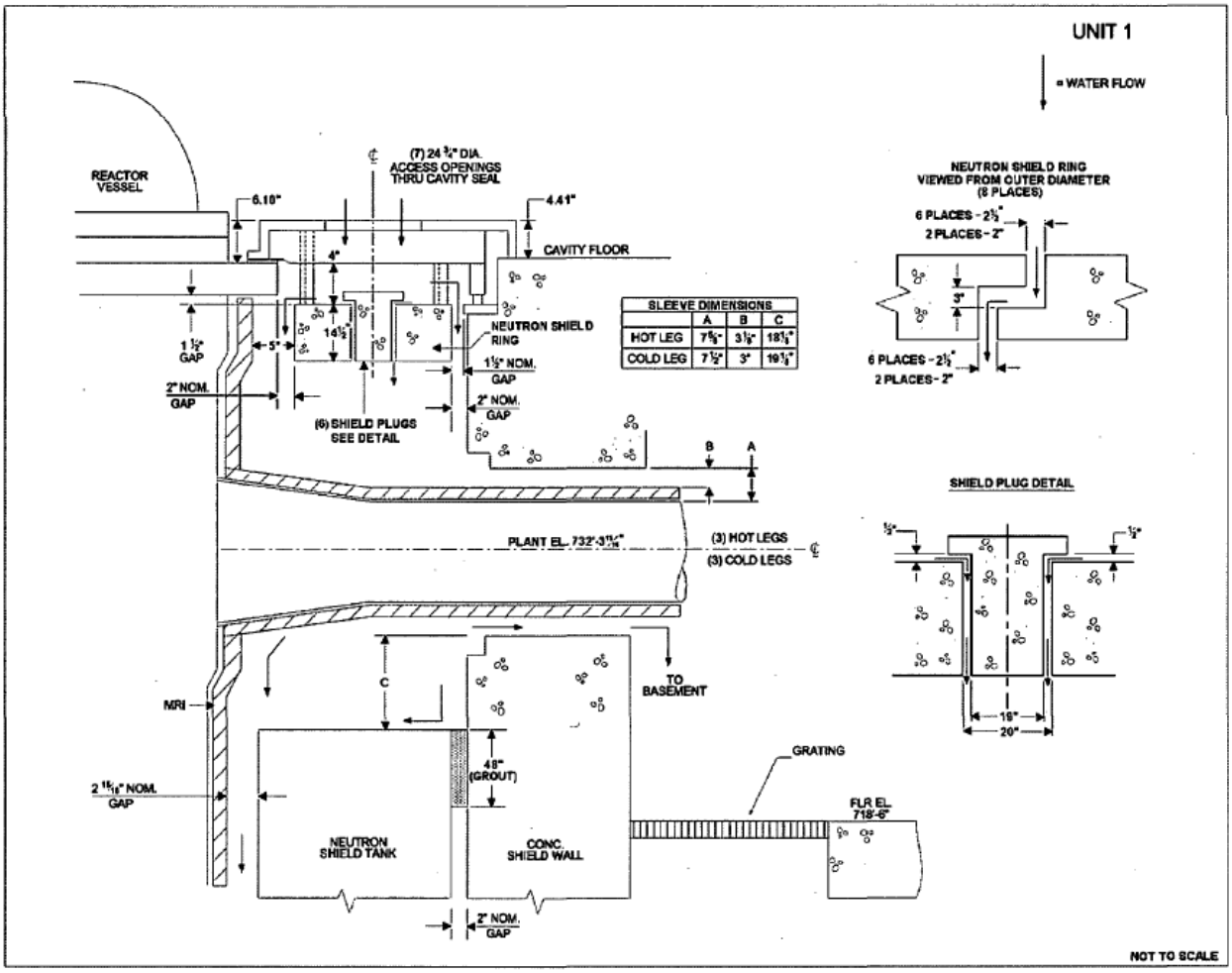

Figure D.2-3 Beaver Valley Unit 1 Upper Support Details (Figure 4-2 in [165])

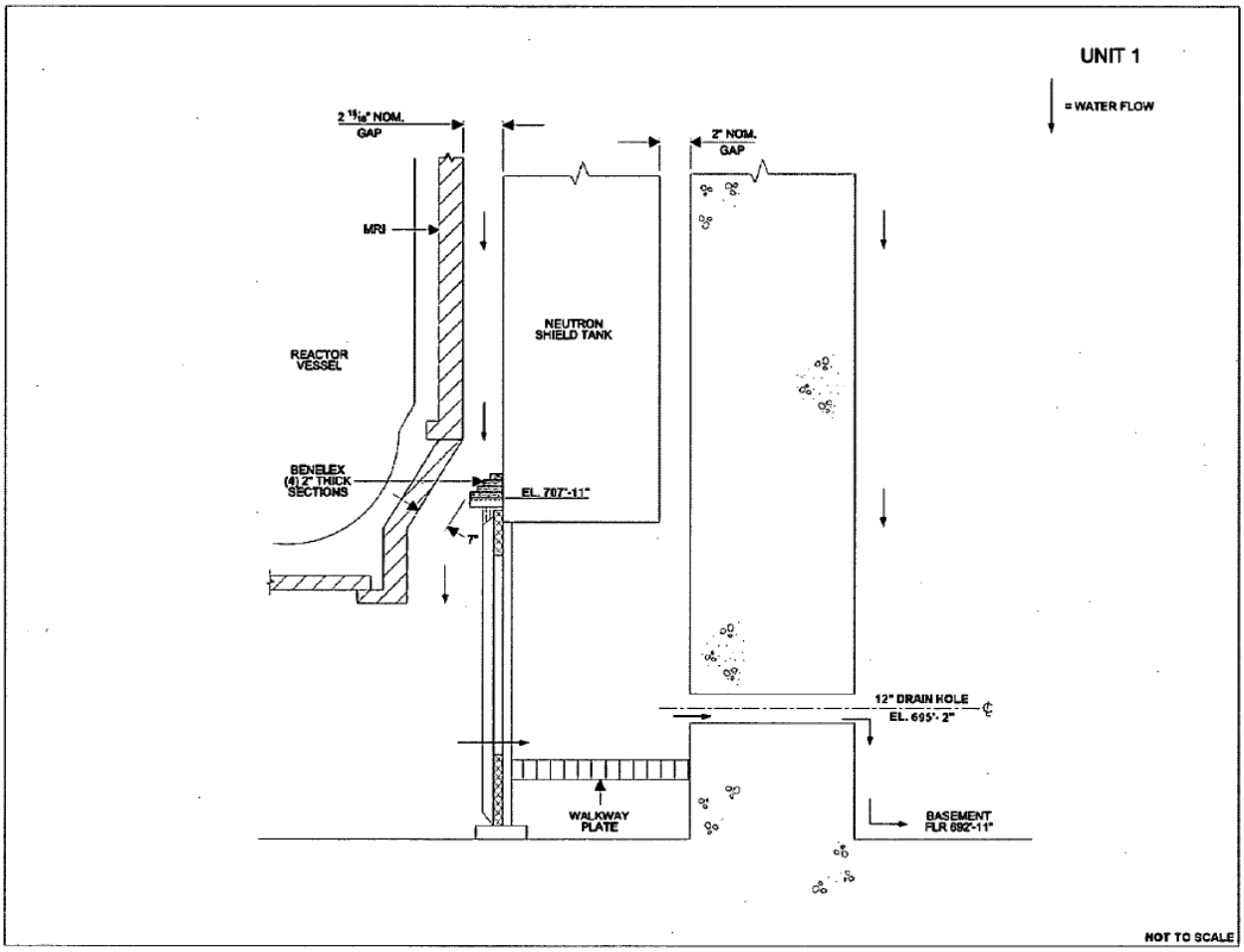

Figure D.2-4 Beaver Valley Unit 1 Lower Neutron Shield Tank Detail (Figure 4-1 in [165])

D.3 Calvert Cliffs Units 1 and 2

Calvert Cliffs Units 1 and 2 each incorporate a Combustion Engineering design two-loop PWR. All figures and references are from the UFSAR (Rev. 49) [158].

The support design is described as:

> *4.1.3.1 Reactor Vessel*
> *The reactor vessel (Figure 4-2) is supported vertically and horizontally by three pads welded to the underside of the reactor vessel nozzles. Each assembly consists of the following:*
>
> *a. A support foot (SA-508 CL2) welded to a reactor coolant nozzle;*
> *b. A socket [American Society for Testing and Materials (ASTM A283-67)] bolted to the support foot with Allenoy cap screws; and*
> *c. A sliding bearing (ASTM B22, Alloy E) whose spherical crown fits into the socket and whose flat sliding surface rests on a base plate (AISI-4140).*
>
> *The arrangement of the vessel supports allows radial growth of the reactor vessel due to thermal expansion while maintaining it centered and restrained from movement caused by seismic disturbances.*

5.1.2.3 <u>Equipment Supports</u>

a. Reactor Vessel Supports

1. *Restrain the vessel to maintain the integrity of emergency core cooling systems and to prevent the rupture of additional primary pipes should LOCA occur due to single pipe rupture;*
2. *Permit slow radial thermal expansion of the vessel under normal operation; and*
3. *Restrain the vessel against seismic and LOCA jet forces.*

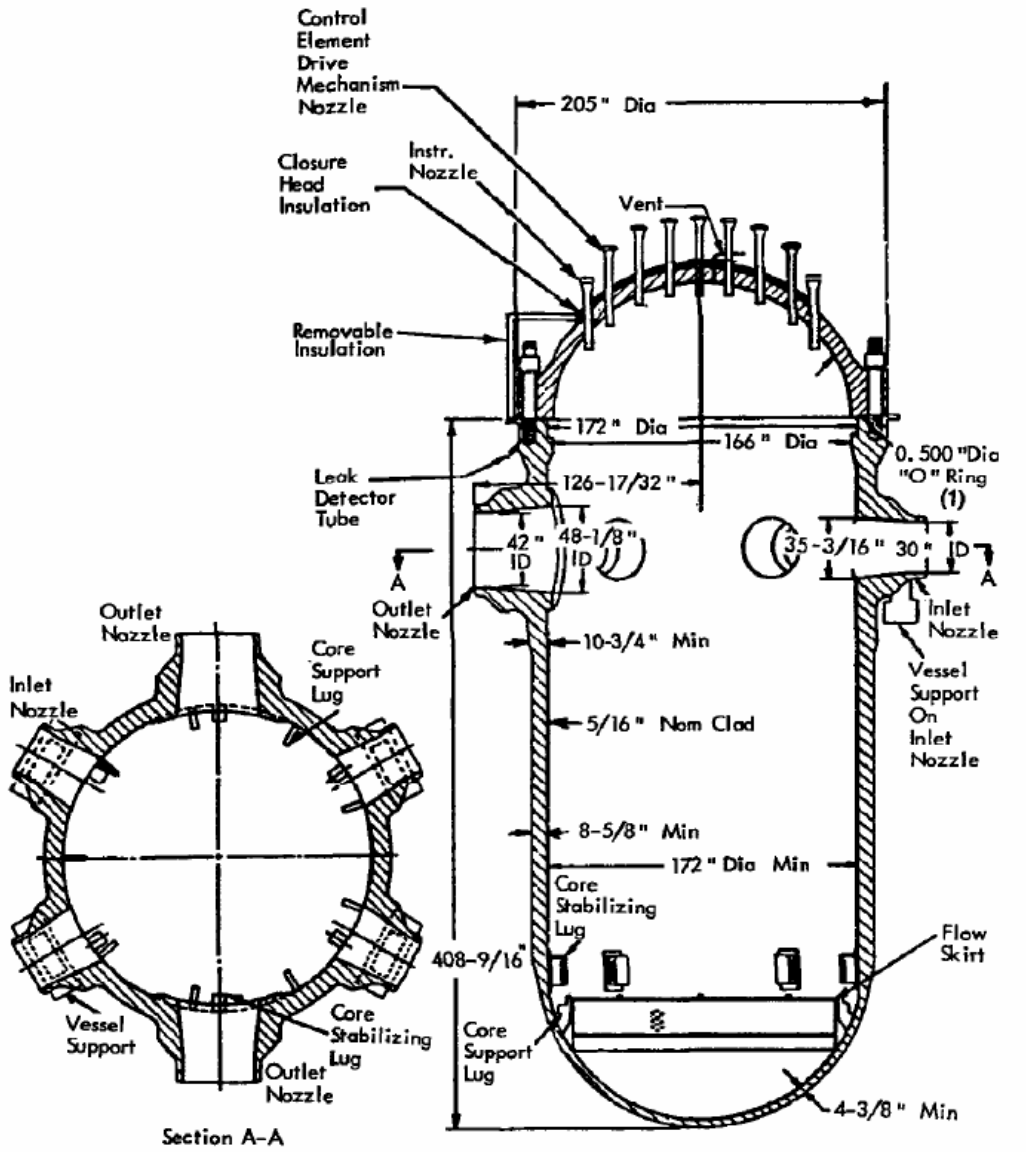

(1) The actual dimension depends on manufacturer's design and manufacturing tolerances.

Calvert Cliffs Nuclear Power Plant	REACTOR VESSEL	Figure 4-2 Rev. 38

Figure D.3-1 Calvert Cliffs Units 1 and 2 Reactor Vessel Dimensions

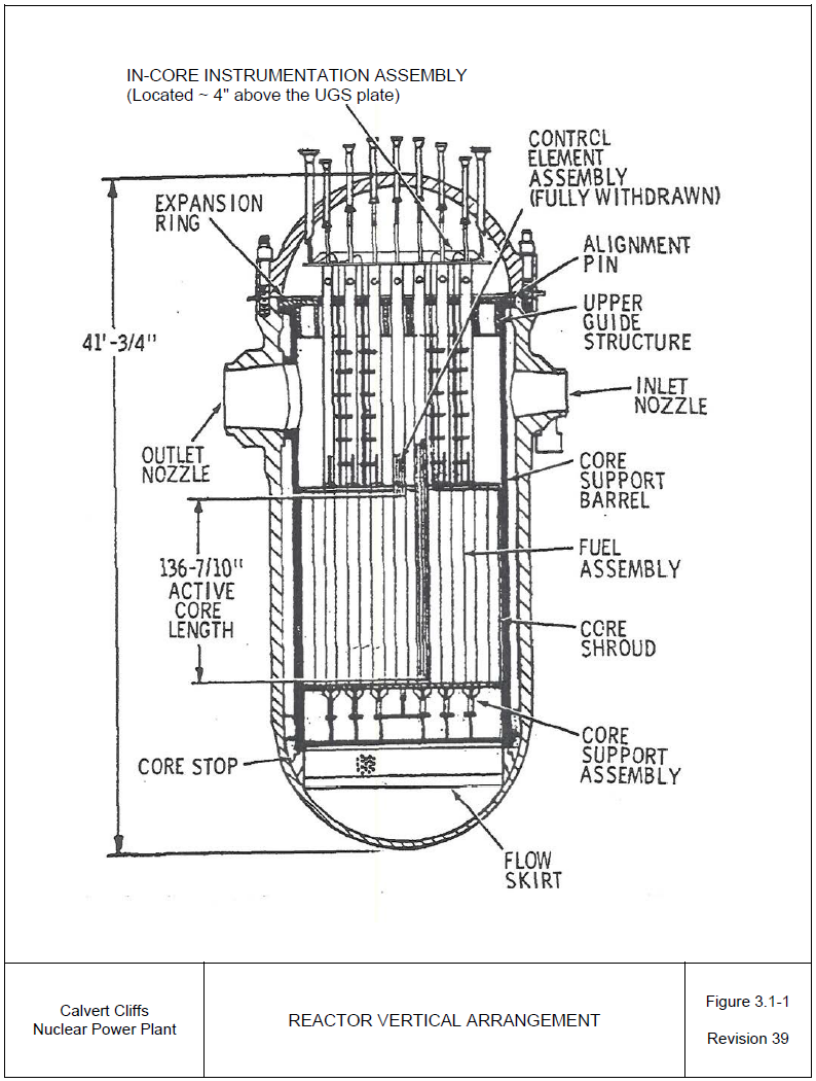

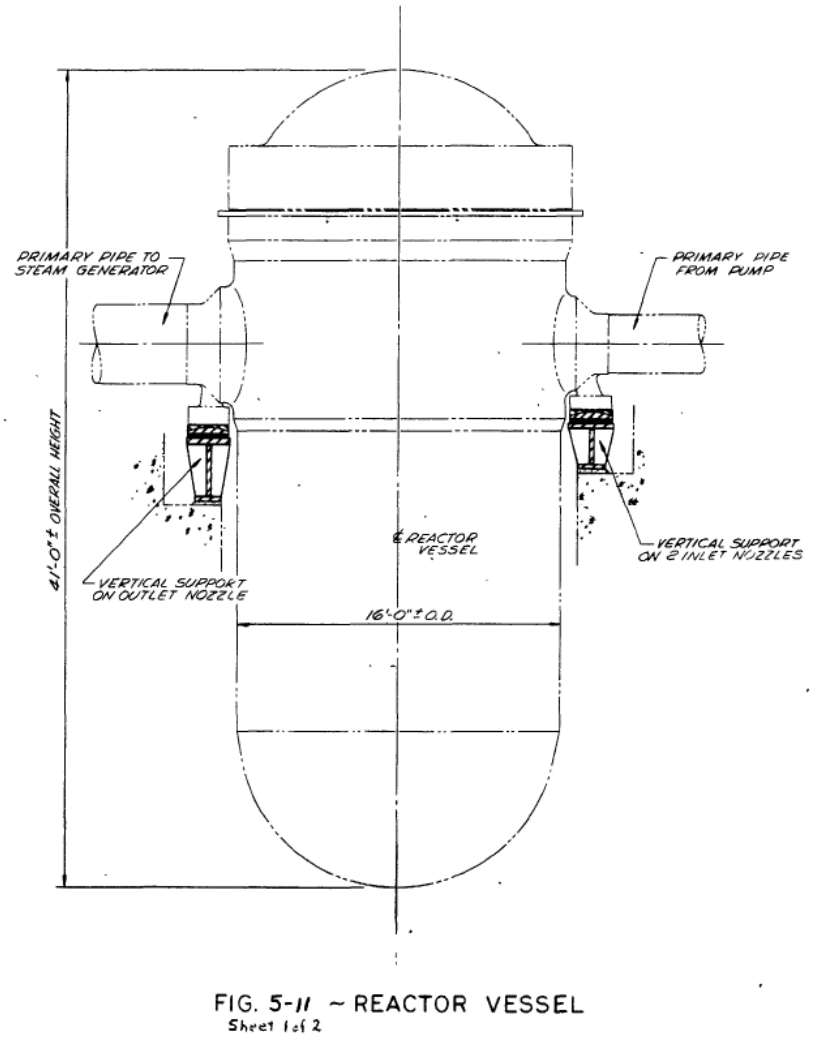

Figure D.3-2 Calvert Cliffs Units 1 and 2 Reactor Core Position Relative to Supports

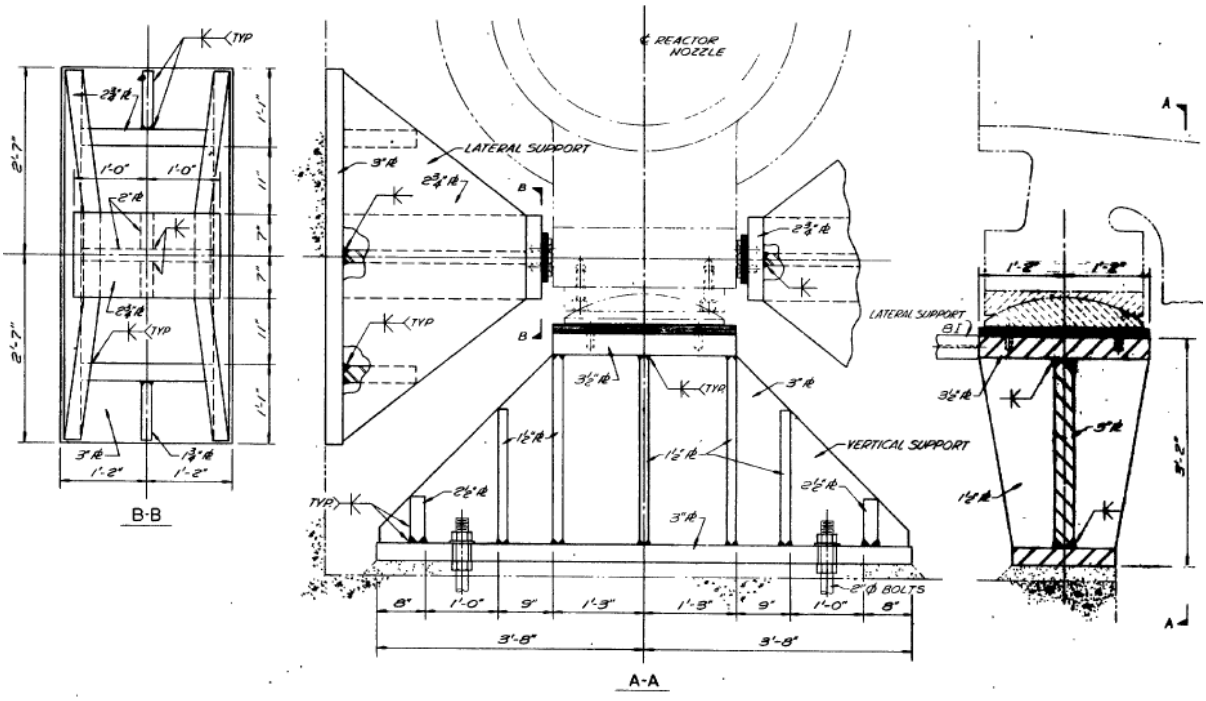

FIG. 5-11 ~ REACTOR VESSEL SUPPORTS
Sheet 2 of 2

Figure D.3-3 Calvert Cliffs Units 1 and 2 Reactor Vessel Support Detail

D.4 Joseph M. Farley Units 1 and 2

Farley units 1 and 2 are Westinghouse three-loop PWRs. Their reactor vessel supports sit on the bioshield and are described in Section 5.5.14.1 of the FSAR [174]:

A. Vessel

Supports for the reactor vessel (figure 5.5-7) are individual, air-cooled, rectangular-box structures beneath the vessel nozzles bolted to the primary shield wall concrete. Each box structure consists of a horizontal top plate that receives loads from the reactor vessel shoe, a horizontal bottom plate supported by and transferring loads to the primary shield wall concrete, and connecting vertical plates. The supports are air-cooled to maintain the supporting concrete temperature at or below 190°F at a flow rate of 2000 ft^3/min with an air temperature of 120°F to meet the acceptance criteria for the localized concrete temperature of 200°F. However, recognizing the potential degradation of the RPV supports subjected to sustained temperatures higher than 150°F, FNP has committed (NEL letter #00-279 to USNRC) to an augmented program to inspect the structural components including portions of the reactor vessel system (RVS) in the containment buildings as part of the maintenance rule structural monitoring program. This program will ensure that significant cracking of RVS that could affect the structural support of the reactor vessel or cause out of plumbness conditions will be detected and corrected [NRC commitment CTS #10533].

Figures D.4-1 through D.4-3 are drawings from the FSAR of the general support design, the support shoe, and the support box, respectively.

An additional description of the Farley reactor vessel support system appears in the response to a cited violation with respect to the maximum localized temperature limit to the reactor vessel supports [166]:

> ***Attachment 4***
> ***Description of the FNP Reactor Vessel Supports***
>
> ***DESIGN DESCRIPTION***
>
> *The primary shield wall provides shielding for the Reactor Pressure Vessel (RPV). The primary shield wall also provides support for the RPV. The primary shield wall is a massive heavily steel reinforced concrete structure having walls approximately 9.7 feet in thickness. It is octagonal in shape on the exterior perimeter with a circular shaped center cavity. The height of the primary shield wall is 12.4 feet, from the elevation at which the RPV rests to the top of the containment base slab, and continues an additional 34.25 feet from the top of the containment base slab to the bottom of the reactor cavity base slab. The center cavity is lined with steel plate material which is also welded to the bottom part of the RPV supports.*
>
> *The Reactor Pressure Vessel (RPV) rests on six steel supports which are located underneath the RPV nozzles. There are six supports; one support for each of the three hot leg nozzles and one support for each of the three cold leg nozzles. Each nozzle support consists of two parts, one part (the upper part) which is attached to the nozzle and the lower part which supports the upper part and is in turn supported by the concrete primary shield wall. The lower part is anchored into the concrete primary shield wall. The upper part is allowed to slide on the lower part to allow for thermal expansion of the RPV. The load path from the RPV is the nozzle support upper part through the lower part to the concrete surface. The gross cross-sectional area of the primary shield wall is approximately 835 square feet, as compared to sum of the footprint areas of the six supports, which is approximately 76.6 square feet. Based on these areas, the supports occupy less than ten percent of the cross-sectional area of the primary wall.*

The accompanying figures (presented here as Figures D.4-4 through D.4-7) provide an overhead view of the shield wall and reactor, a side view of the reactor and the provisions for air-cooling of the supports, and details of the support shoe and support box.

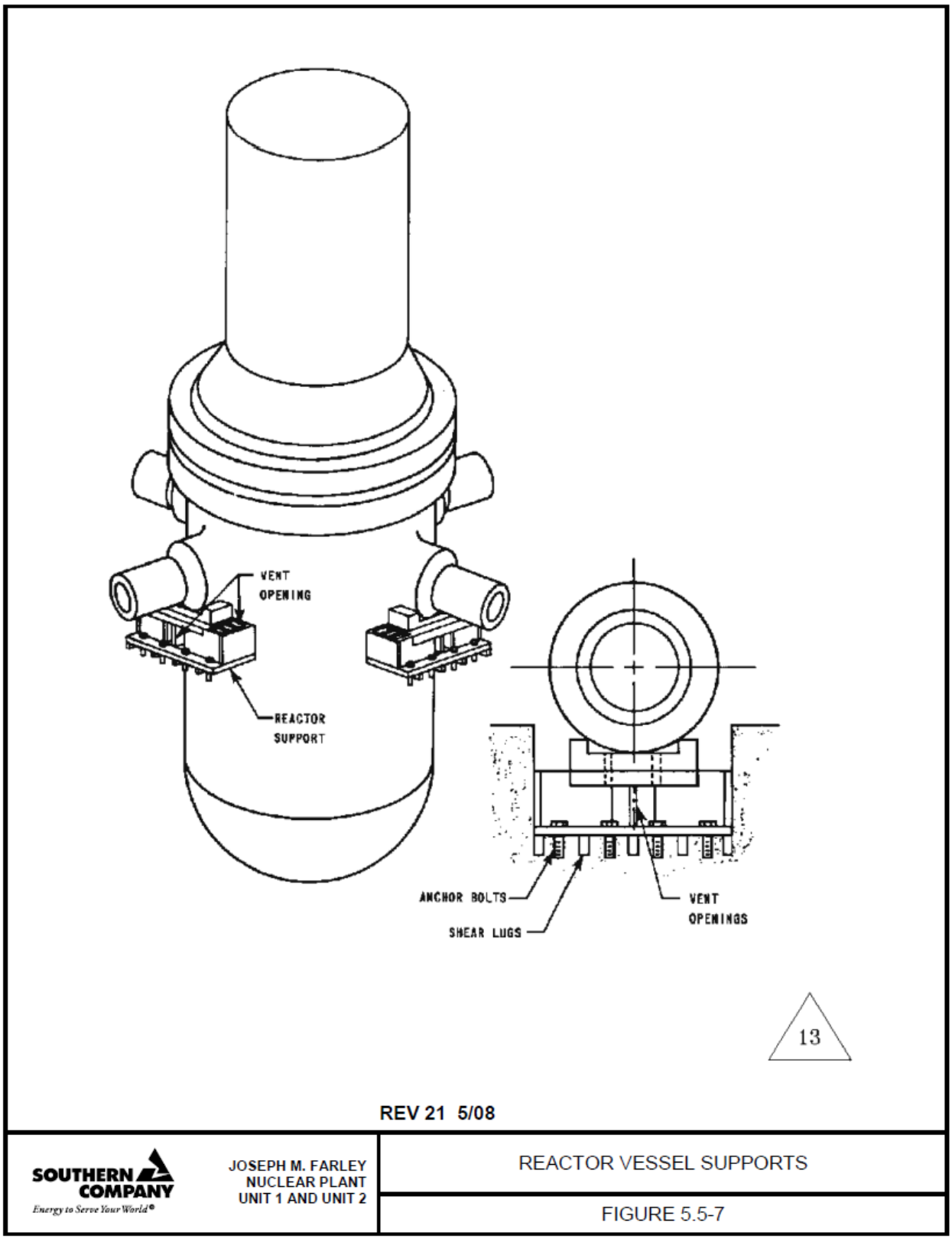

Figure D.4-1 Farley Units 1 and 2 Reactor Vessel Support Design [174]

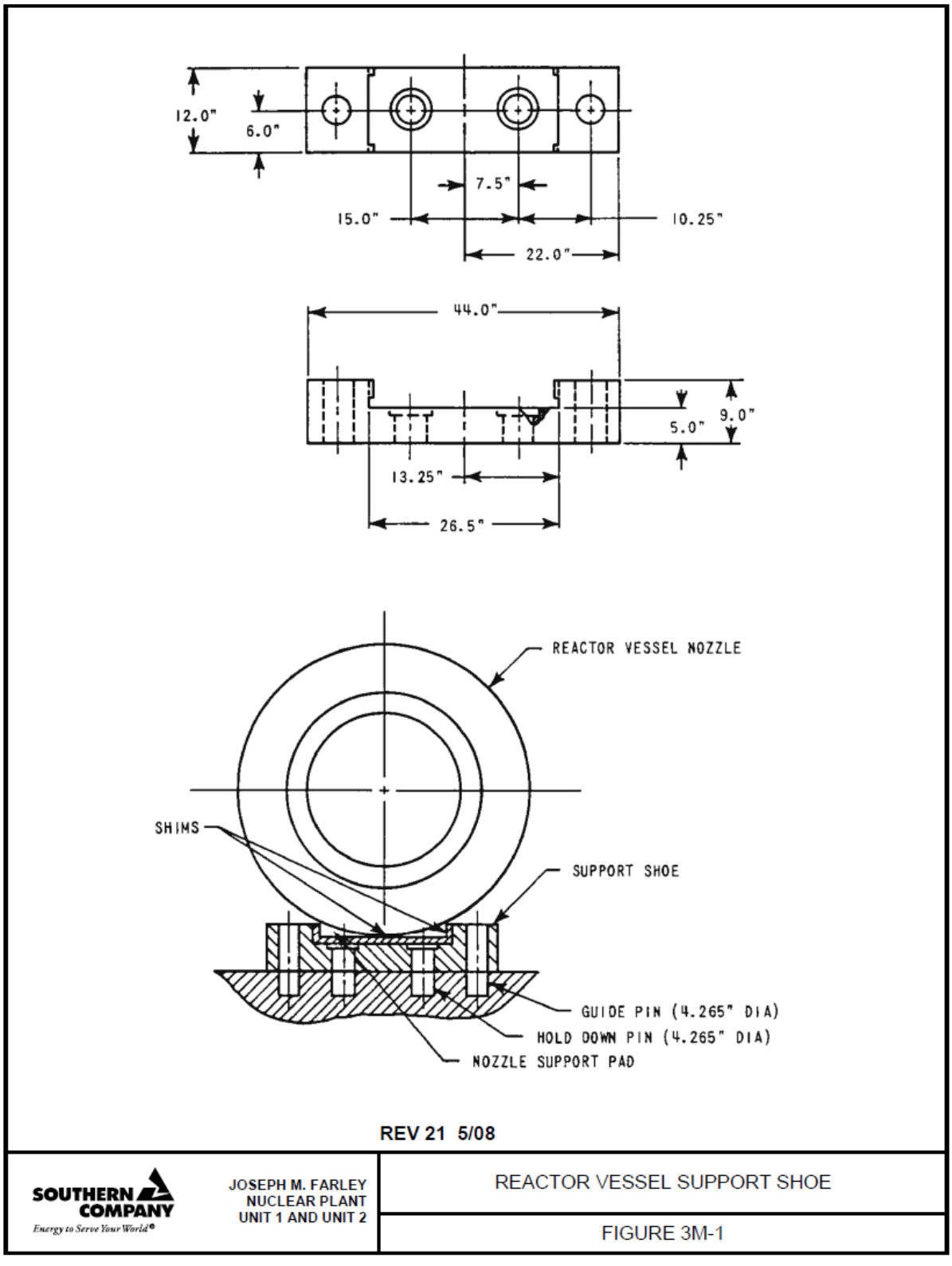

Figure D.4-2 Farley Units 1 and 2 Reactor Vessel Support Shoe [174]

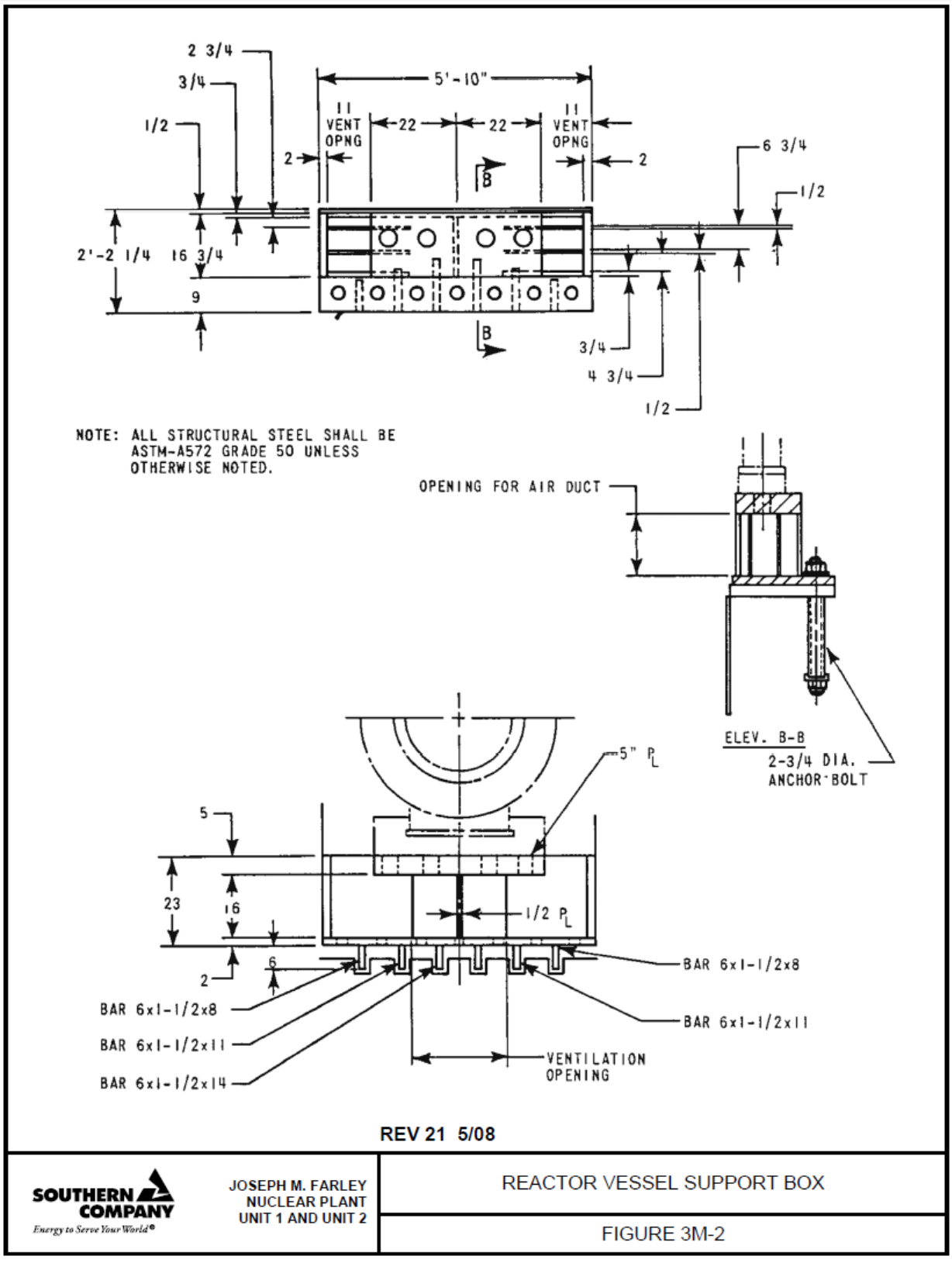

Figure D.4-3 Farley Units 1 and 2 Reactor Vessel Support Box [174]

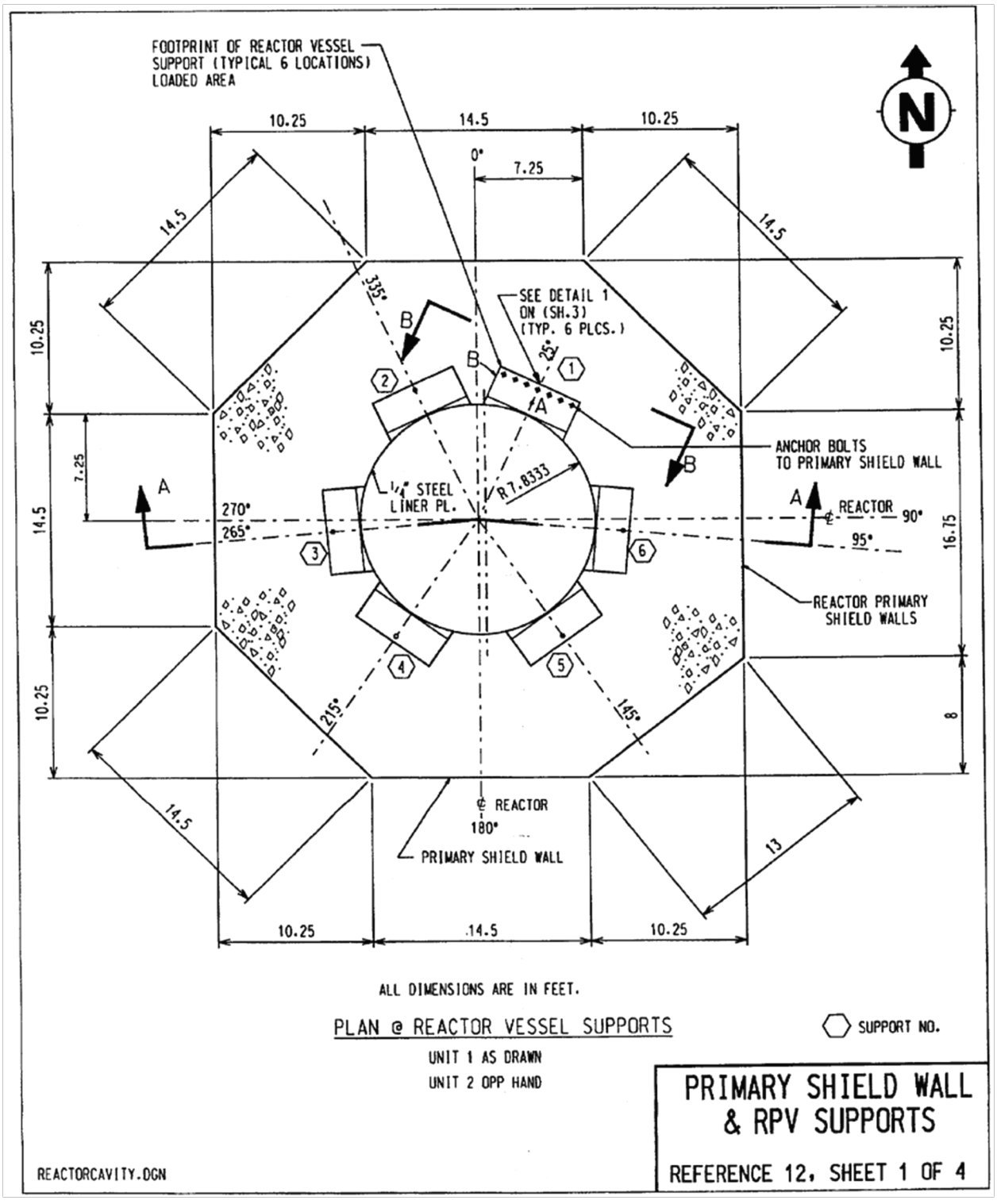

Figure D.4-4 Overhead View of Farley Units 1 and 2 Reactor Vessel and Shield Wall [166]

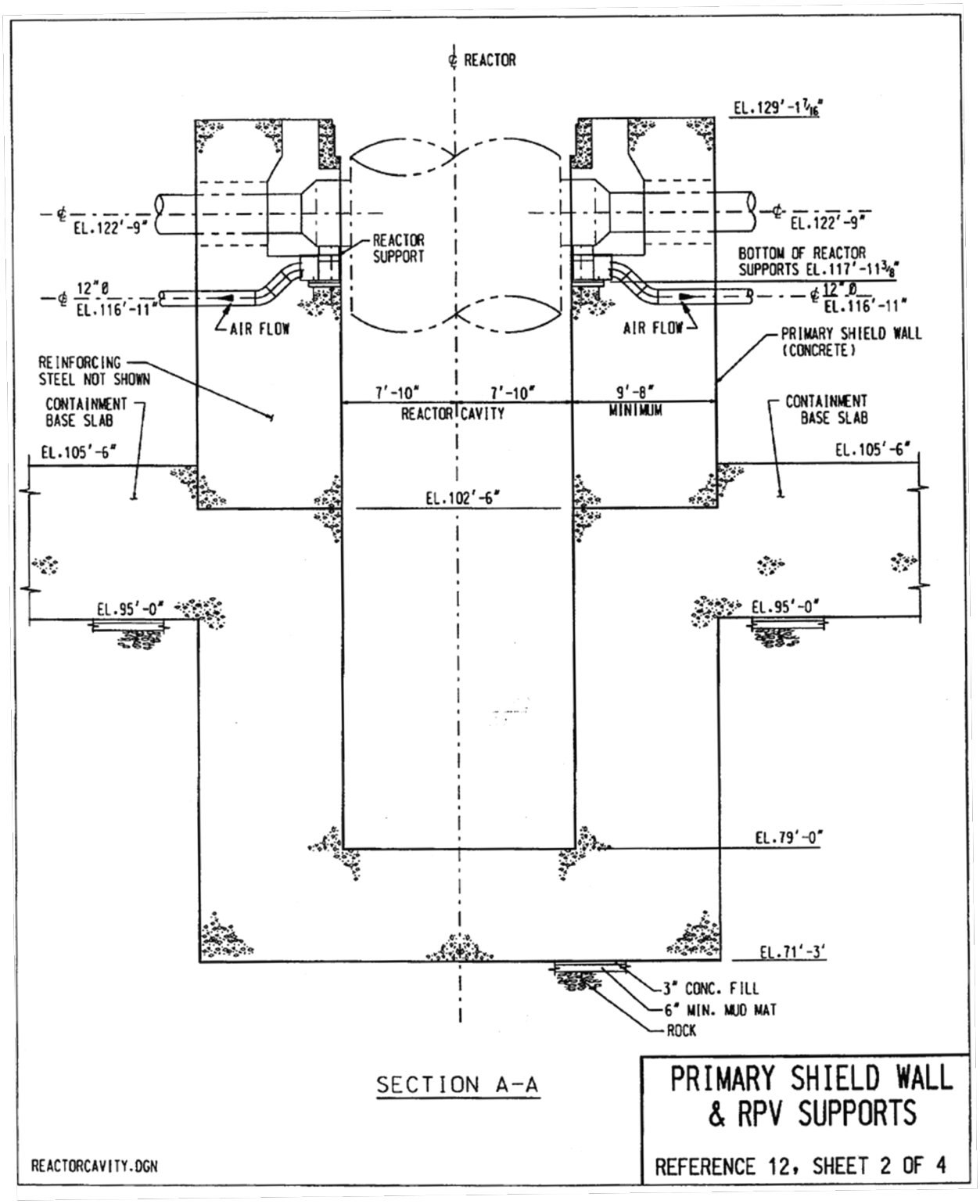

Figure D.4-5 Side View of Farley Units 1 and 2 Reactor Vessel and Shield Wall with Detail on Air Cooling of the Supports [166]

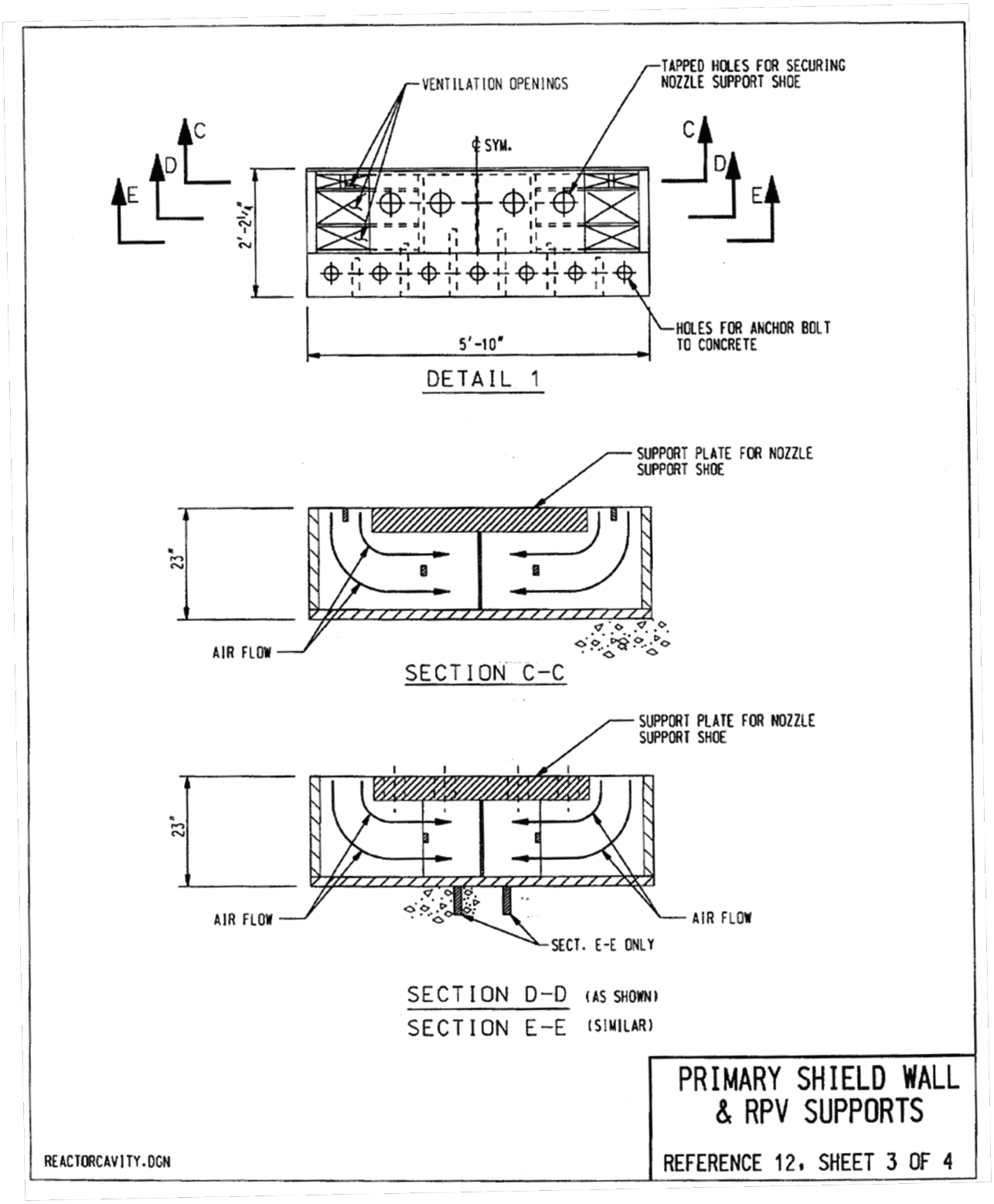

Figure D.4-6 Farley Units 1 and 2 Reactor Vessel Support Box Detail [166]

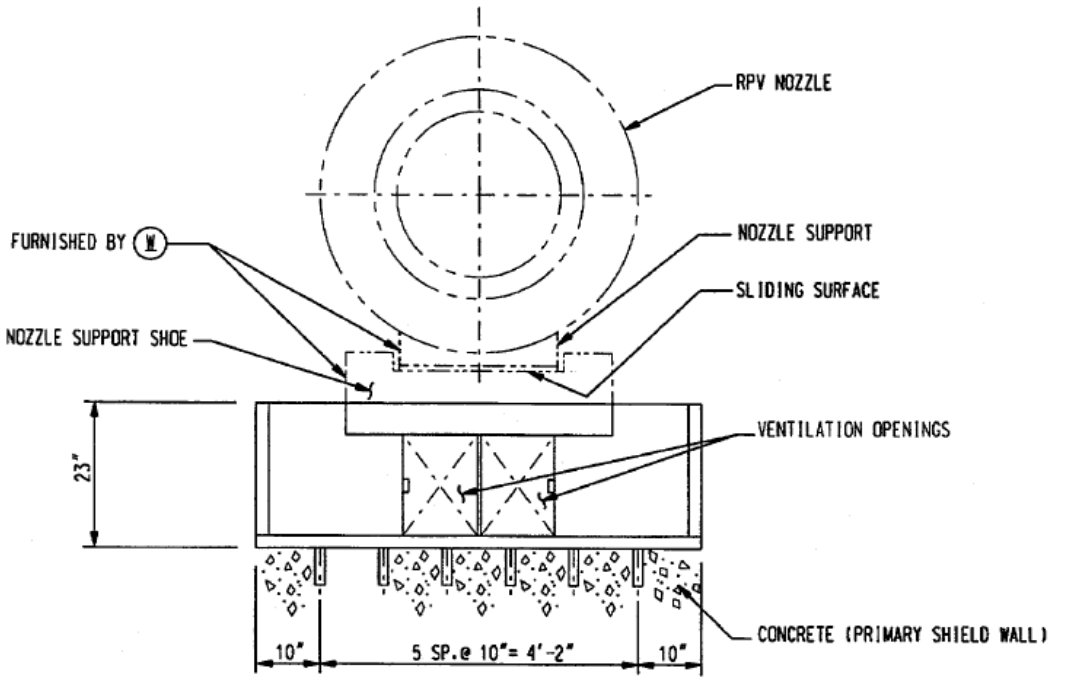

SECTION B-B

(NOZZLE SUPPORT, NOZZLE SUPPORT SHOE
AND STRUCTURAL STEEL SUPPORT TO CONCRETE SURFACE)
ALL PIECES ARE STEEL PLATE OR STEEL BAR

APPROXIMATE FLOW PER SUPPORT BASED ON ORIGINAL STARTUP TESTS		
SUPPORT NO.	FLOW (CFM)	PEAK CALCULATED TEMPERATURE °F
1	≲ 2150	≲ 183
2	≲ 2600	≲ 165
3	≲ 4700	≲ 120
4	≲ 3250	≲ 140
5	≲ 2700	≲ 160
6	≲ 2000	≲ 190

PRIMARY SHIELD WALL
& RPV SUPPORTS

REFERENCE 12, SHEET 4 OF 4

REACTORCAVITY.DGN

Figure D.4-7 Farley Units 1 and 2 Reactor Vessel Support Shoe Mounting Detail [166]

D.5 R.E. Ginna

Ginna is a Westinghouse two-loop PWR. A description of the reactor vessel supports is provided in the FSAR [146]:

> *5.4.11.2.1 Reactor Vessel Supports*
> *The vessel is supported on six individual pedestals. Each pedestal rests upon plates that are in turn supported upon the circular concrete primary shield wall.*
>
> *The reactor vessel has six supports comprising four support pads located one on the bottom of each of the primary nozzles and two gusset support pads. One of the reactor inlet nozzles is centered approximately 2 degrees counterclockwise from the 90-degree axis and the other is centered approximately 2 degrees counterclockwise from the 270-degree axis.*
>
> *Each support bears on a support shoe, which is fastened to the support structure. The support shoe is a structural member that transmits the support loads to the supporting structure. The support shoe is designed to restrain vertical, lateral, and rotational movement of the reactor vessel, but allows for thermal growth by permitting radial sliding at each support, on bearing plates.*
>
> *The seismic resistance of the reactor vessel supports was evaluated as part of SEP Topic 111-6. It was concluded, based on experience for nozzle-supported vessels, that the seismically induced stresses in the nozzles and adjacent shells are very small and that the governing element for reactor vessel support is the concrete shield wall. The shield wall was considered to be adequate to withstand the 0.2g safe shutdown earthquake according to the NRC review (Reference 47).*

No detailed drawings of the Ginna vessel support system are publicly available. Figures D.5-1 and D.5-2 provide an overview of the RPV and bioshield in containment and the position of the nozzle supports, respectively. A figure of the reactor vessel itself is available in the FSAR, but it does not show how the RPV is supported or the support structure.

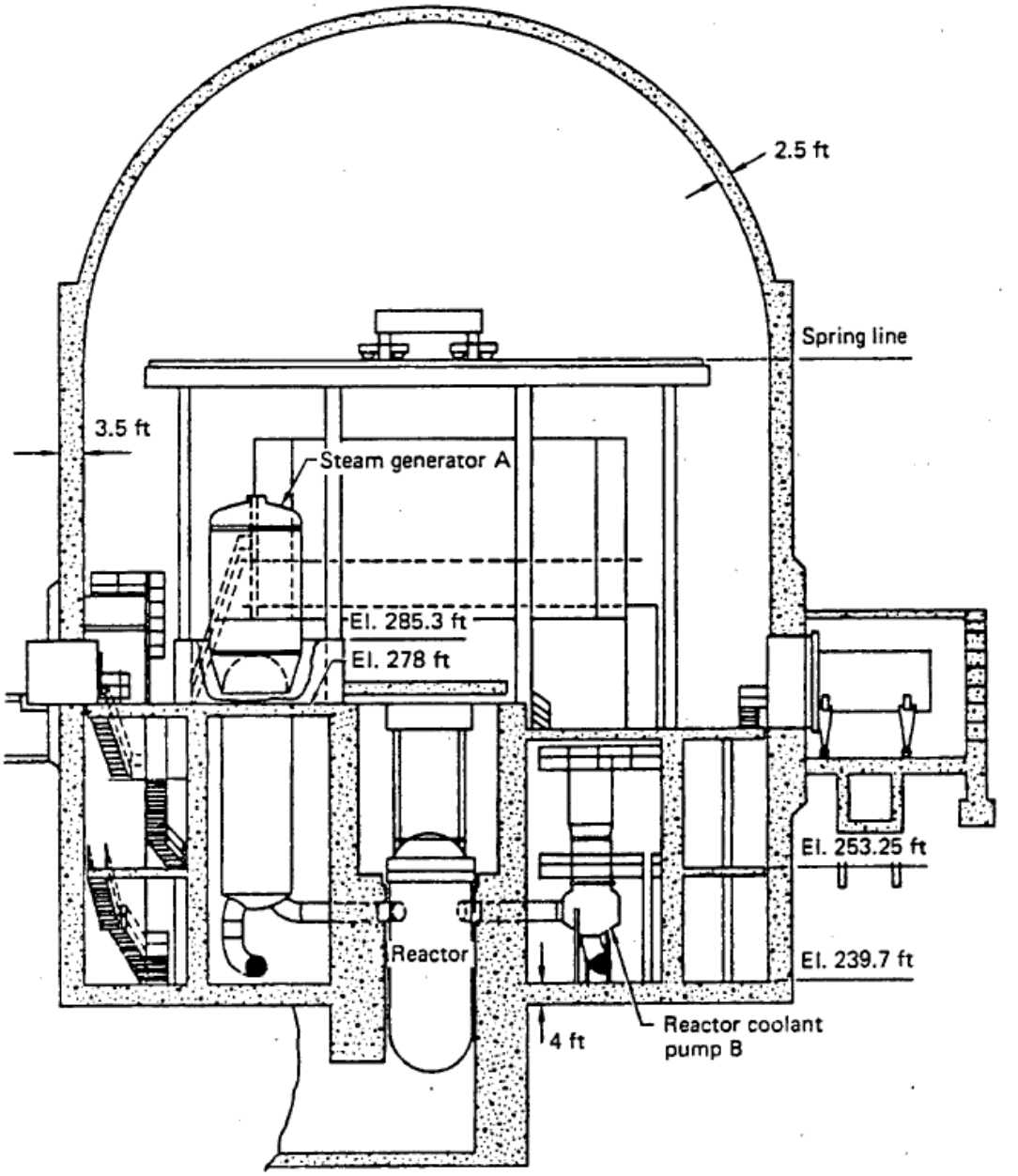

ROCHESTER GAS AND ELECTRIC CORPORATION
R.E. GINNA NUCLEAR POWER PLANT
UPDATED FINAL SAFETY ANALYSIS REPORT

Figure 3.8-55

Reactor Containment Internal Structures

Figure D.5-1 Containment for Ginna [146]

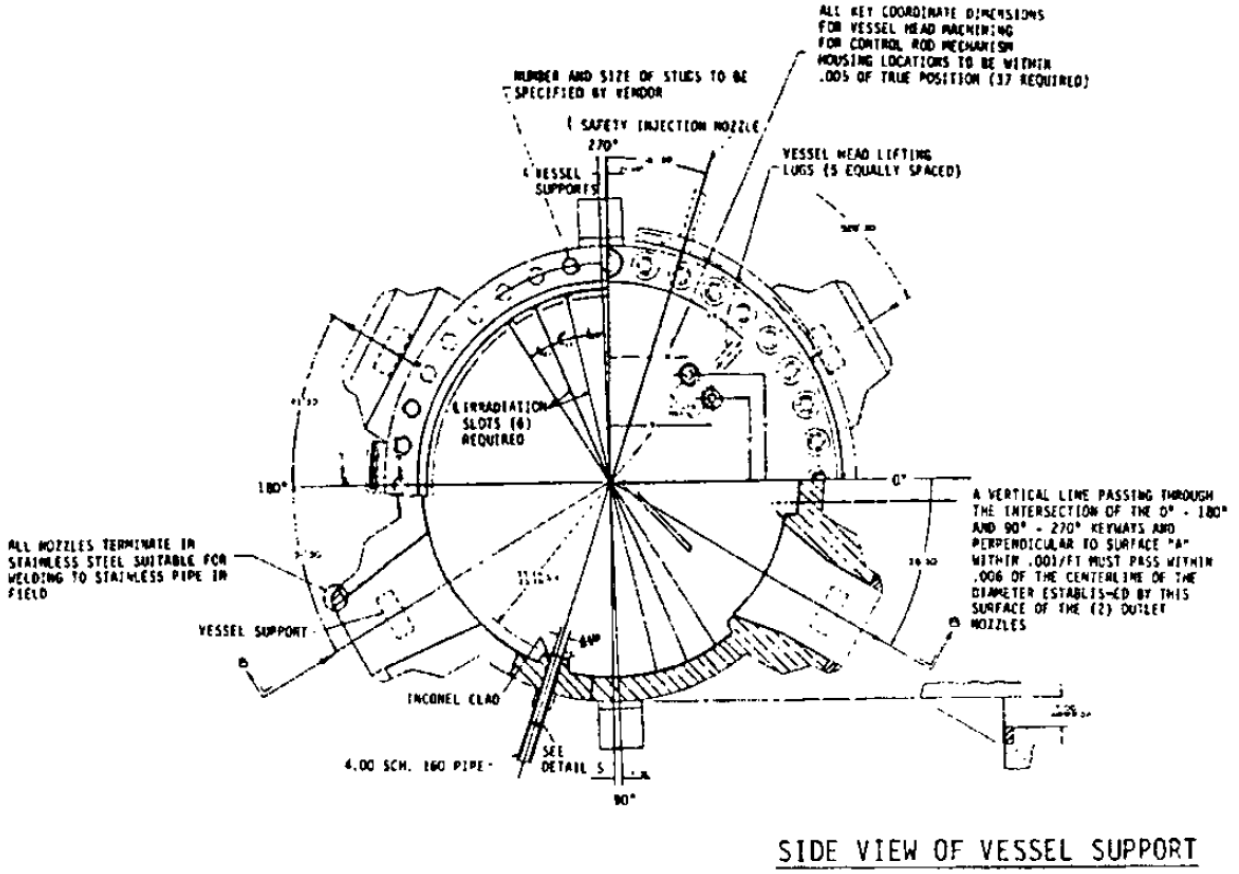

Figure D.5-2 Reactor Nozzle Support Positions for Ginna (extracted from Figure 5.3-1 Sheet 2 of the UFSAR [146]

D.6 H.B. Robinson 2

Robinson is a Westinghouse three-loop PWR. Its vessel support system is described in the FSAR [261]:

> *3.8.3.1.3 Reactor Vessel Support Structure*
> *The reactor vessel support structure consists of a circular box section ring girder, fabricated of carbon steel plates. The bottom flange of the girder is in continuous contact (except for openings for neutron detectors) with a non-yielding concrete foundation.*
>
> *The reactor vessel has three supports located at alternate nozzles. Each support bears on a support shoe, which is fastened to the support structure. The support shoe is a structural member that transmits the support loads to the supporting structure. Each support shoe is designed to restrain vertical, lateral, and rotational movement of the reactor vessel, but allows for thermal growth by permitting radial sliding on bearing plates*.

Detailed drawings of the RPV support structure are not available.

D.7 Shearon Harris Unit 1

Shearon Harris Unit 1 is a Westinghouse three-loop PWR. A complete FSAR does not appear to be publicly available. The following descriptions were provided in Amendments 46 and 48 to the FSAR [168, 169].

The description of the RPV supports is provided in the FSAR [169] as:

> *3.8.3.1.7 Reactor Vessel Support System*
> *The reactor pressure vessel (RPV) is supported and restrained to resist normal operating loads, seismic loads, and loads induced by the postulated pipe ruptures, including a LOCA. The RPV is supported at six points, the three inlet and three outlet nozzles, so that adjacent supports are 50 or 70 degrees apart. Steel pads, which are an integral part of the nozzles, rest on a steel bearing block atop a steel support pedestal as shown on Figure 5.4.14-1. The steel support pedestal is welded to a stiffened base plate at its bottom. The base plate is attached to the reinforced concrete by anchor bolts. The base plate has shear bars on its underside to resist part of the lateral loads, including piping loads.*
>
> *The transfer of horizontal seismic and postulated accident loads from the RPV and the connecting piping system into the concrete primary shield wall is performed through embedded steel structures as shown on Figure 3.8.3-9. These structures consist of billet plates welded to vertical circular plates, anchored into the concrete wall by using anchor bolts and embedded structural steel assemblies. The gap between the vertical RPV supports and the horizontal RPV supports is shimmed in the cold condition with a predetermined allowance for thermal expansion.*
>
> *5.4.14.2.1 Reactor pressure vessel. Supports for the reactor vessel (Figure 5.4.14-1) are individual air cooled rectangular box structures beneath the vessel nozzles bolted to the primary shield wall concrete. Each box structure consists of a horizontal top plate that receives loads from the reactor vessel shoe, a horizontal bottom plate which transfers the loads to the primary shield wall concrete, and connecting vertical plates. The supports are air cooled to maintain the supporting concrete temperature within acceptable levels.*

From Section 6.2.2.1 [168]:

> *10. The Primary Shield Cooling system and the Reactor Supports Cooling System are designed to supply cooling air to the annular clearance between the reactor vessel and primary shield wall, the reactor vessel supports and the annular space between the reactor coolant legs and the concrete wall. The systems are designed to limit the temperature of' the shielding concrete, instrumentation and concrete base at the reactor vessel supports to a maximum of 150'F. The systems are designed to Safety Class 3 and Seismic Category I requirements.*

Figure 5.4.14-1 as referenced in the FSAR is the same as Figure D.4-1.

D.8 North Anna Units 1 and 2

North Anna Units 1 and 2 are Westinghouse three-loop PWRs. Supported by shoes under all six nozzles, each RPV sits directly on a neutron shield tank, which is grouted into the shield wall.

The shield wall provides lateral stability for the shield tank, and the shield tank is supported by the concrete base mat. The support shoe design is shown in Figure D.8-1. Figure D.8-2 shows the neutron shield tank between the reactor vessel and shield wall. Figure D.8-3 is an overhead view of the reactor vessel on the shield tank. This summary and the following figures were taken from the FSAR [57].

From Section 3.8.2.2.1:

> *Within the primary shield area, the reactor vessel is supported on the steel neutron shield tank, which transfers the vessel weight directly to the containment foundation mat. The neutron shield tank will not be damaged by the design differential pressure of 130 psi within the primary shield resulting from a design basis accident, nor will resulting deflections impair the functioning of the reactor supports, which are designed to withstand resulting reaction forces. The neutron shield tank is grouted into and dependent on the reinforced-concrete primary shield cavity wall for lateral support. This wall is designed for a differential pressure of 130 psi.*

From Chapter 5:

> *5.5.9.2.1 Reactor Vessel Support*
> *The reactor vessel is supported by six sliding foot assemblies mounted on the neutron shield tank as shown in Figure 5.5-8. These foot assemblies were fabricated from modified AISI 4330 steel forgings. The support feet are designed to restrain seismic movement of the reactor vessel, while allowing radial thermal expansion. The neutron shield tank is a double-walled cylindrical structure of ASTM A516, Grade 60 steel that transfers the loadings to the heavily reinforced concrete mat and internal structures of the containment building. The tank also serves to minimize gamma and neutron heating of the primary concrete shield, and to attenuate neutron radiation outside of the primary shield to acceptable limits. The shield tank is securely fastened by anchor bolts. Overturning moments and horizontal forces induced on the tank during normal operation or accident condition are taken by the shield tank anchor bolts and the reinforced-concrete primary shield wall poured around the neutron shield tank. Any resulting vertical force and torque is taken by the anchor bolts.*

From Section 12.1.2.1:

> *The primary shield consists of a water-filled neutron shield tank and a concrete shield. The neutron shield tank has a radial thickness of approximately 3 feet, and it is surrounded by 4.5 feet of reinforced concrete. The shield tank prevents the overheating and dehydration of the primary shield wall concrete and minimizes the activation of the plant components within the reactor containment. A cooling system is provided for the water in the neutron shield tank. (The neutron shield tank cooling water subsystem is discussed in Section 9.2.2.)*

A 15 ft. 8 in. high x 2 inch thick cylindrical lead shield located beneath the neutron shield tank protects station personnel servicing the neutron detectors during reactor shutdown.

Figure 5.5-8
REACTOR VESSEL SUPPORT

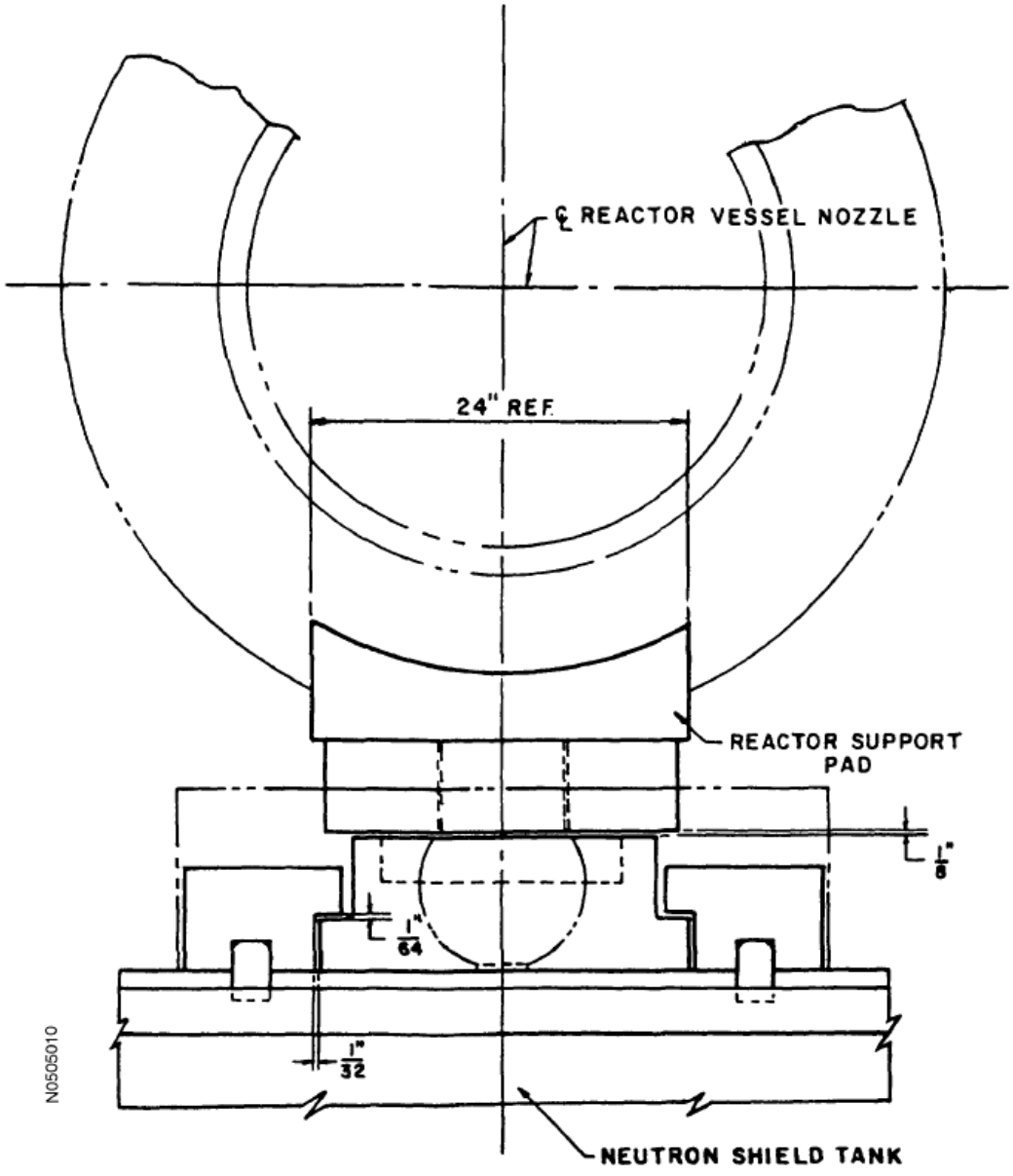

Figure D.8-1 Reactor Vessel Support

Figure 12.1-8
SHIELD ARRANGEMENT ELEVATION

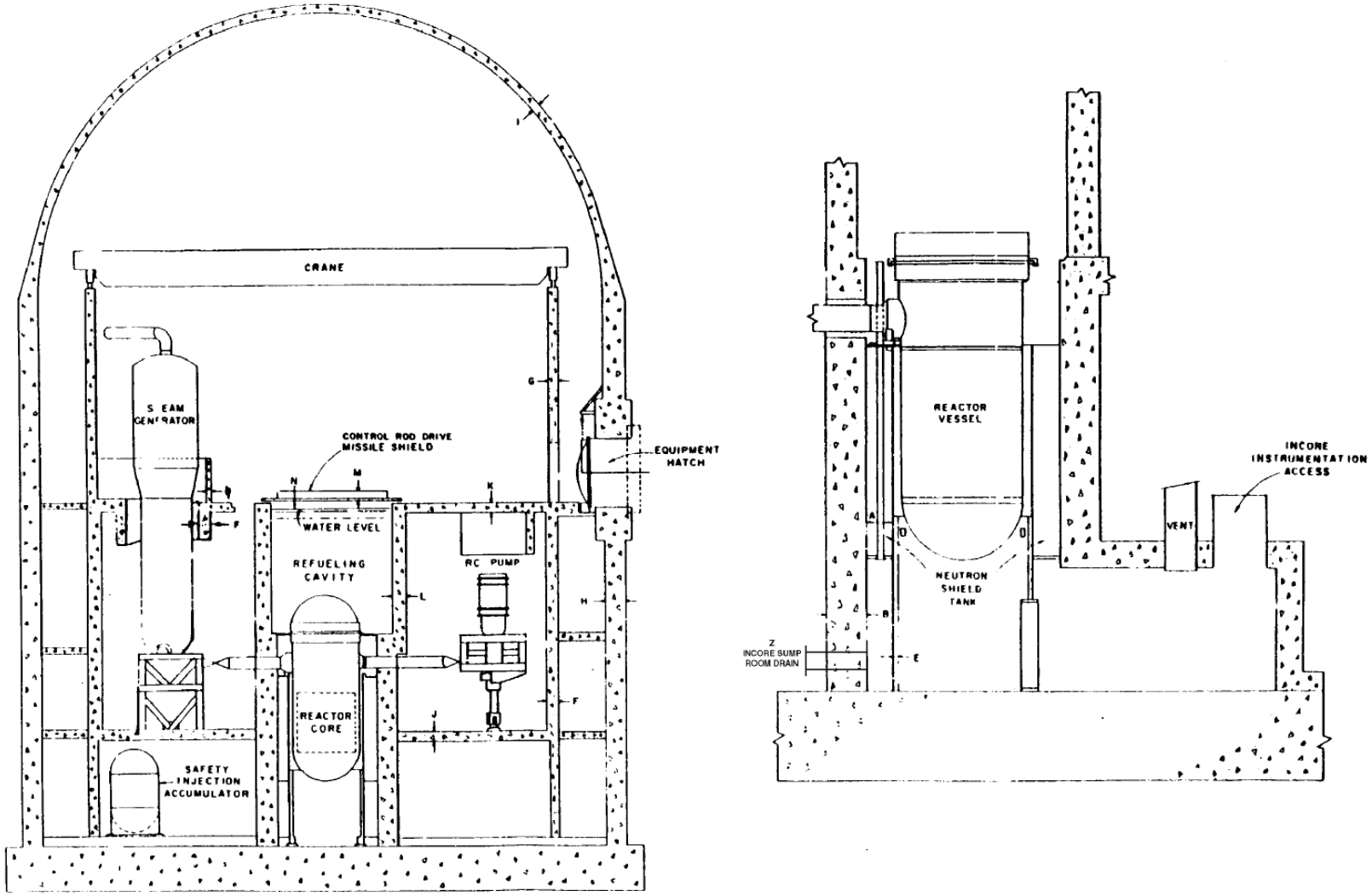

Figure D.8-2 Reactor Vessel on Neutron Shield Tank in Containment

Figure 12A-6
LOCATION OF SUPPLEMENTARY NEUTRON SHIELDS

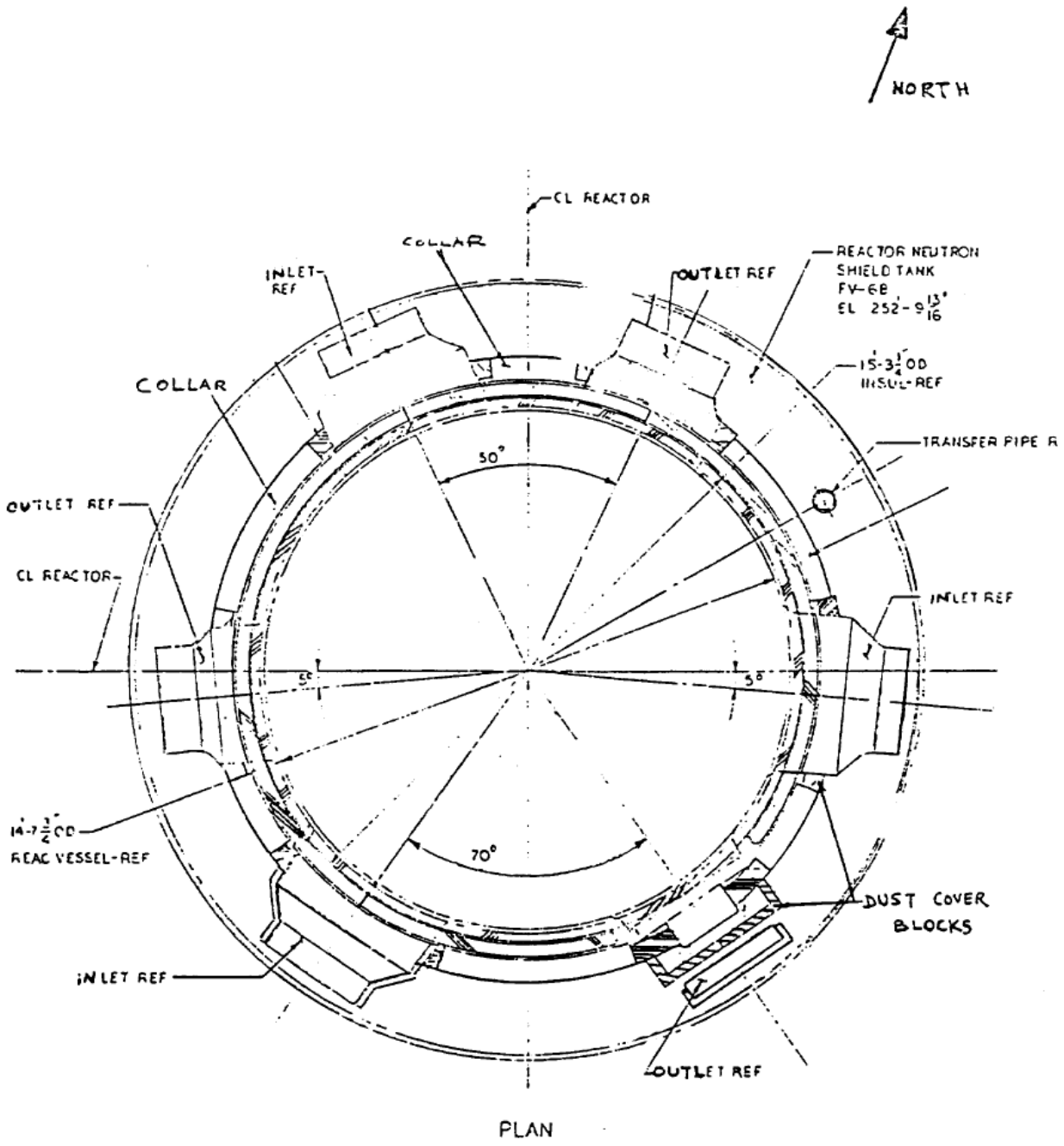

Figure D.8-3 Overhead View of Reactor Vessel on Neutron Shield Tank

D.9 Point Beach Units 1 and 2

Point Beach Units 1 and 2 are Westinghouse two-loop PWRs. The reactors sit on ring girders supported by steel columns that rest on the basemat as described in the excerpts from the FSAR listed below.

From Section 4.2 (FSAR, ML16251A154):

> *Reactor Vessel - Support Structure*
> *The Reactor Support Structure consists of a six sided structural steel ring supported at each apex by steel columns extending downward to a point below the reactor vessel and, at the center of each segment of the ring, by structural members imbedded in the surrounding concrete.*
>
> *The reactor vessel has six supports, one at each of four reactor vessel nozzles with pads, and one at each of two reactor vessel support brackets. Each support bears on a support shoe, which is fastened to the support structure. The support shoe is a structural member that transmits the support loads to the supporting structure. The support shoe is designed to restrain vertical, lateral, and rotational movement of the reactor vessel, but allows for thermal growth by permitting radial sliding at each support on bearing plates.*

From Chapter 11 (FSAR, ML16251A162):

> *11.6.2.2 Shielding Design*
> *Primary Shielding*
> *The primary shielding consists of the reactor internals, the reactor vessel wall, and a concrete structure surrounding the reactor vessel.*
>
> *The primary shielding immediately surrounding the reactor vessel consists of a reinforced concrete structure extending from the base of the containment to an elevation of 66.0 ft. The lower portion of the shield is a minimum thickness of 6.5 ft. of concrete and is an integral part of the main structural concrete support for the reactor vessel. It extends upward to the operating floor, forming a portion of the refueling cavity. This cavity is approximately rectangular in shape, and has concrete sidewalls which are 5 ft. 5 in. thick adjacent to areas in which fuel is transported.*
>
> *The primary concrete shielding is air cooled to prevent overheating and dehydration from the heat generated by radiation absorption in the concrete. Eight "windows" have been provided in the primary shield for insertion of the out-of-core nuclear instrumentation. Cooling for the primary shield concrete, nuclear instrumentation, and vessel supports is provided by circulating 26,000 cfm of containment air between the reactor vessel wall and the surrounding concrete structure.*

D.10 Prairie Island Units 1 and 2

Prairie Island Units 1 and 2 are Westinghouse two-loop PWRs. They are each supported on six steel columns that are welded to/braced by a surrounding metal band at the top, all of which are embedded in the concrete bioshield. As discussed in the excerpt from Section 12.2.4.1.4 in the USAR below, the metal support structure was designed to carry the entire load. Figures D.10-1 and D.10-2 provide details of the overall support design and the detail of the ventilated support shoes, respectively. The following sections from the USAR provide more detail.

From Section 4.4.2 of the USAR [150]:

> *The Reactor Support Structure consists of six structural steel columns extending downward to the bottom of the reactor cavity. The top of each column (Reactor Vessel Ventilated Support Pad discussed in Section 5.2.2.3.1.3) is anchored by structural members imbedded in the surrounding steel reinforced concrete.*
>
> *The reactor vessel has six supports, four pads, one at each nozzle, and two brackets. Each support bears on a ventilated support pad, which is fastened to the support structure (discussed in Section 12.2.5). The support shoe is a structural member that transmits the support loads to the supporting structure. The support pad is designed to restrain lateral and rotational movement of the reactor vessel, but allows for thermal growth by permitting radial sliding at each support on bearing plates.*

From Chapter 5 of the USAR [150]:

> ***5.2.2.3.1.3 Reactor Vessel Support Pads Cooling***
> *The reactor vessel is supported on six individual air-cooled support pads. The support pads are hollow box-type built-up plate structures equipped with ten 1/4-inch plate split steel cooling fins welded to the inside walls. Approximate outside dimensions of the pad structures are 15-inches wide x 18-inches high x 58 inches long. The boxes are welded to the top cap plates of six full-length support columns that are embedded in the concrete shield structure. The box structures support the reactor vessel shoes supplied with the vessel. Attachment of the shoes is by means of bolting.*
>
> *The support pads provide for the vertical and lateral support of the reactor vessel. In addition, the pads provide a means to obtain a suitable temperature gradient between the reactor vessel support points and the supporting concrete and steel structures of the building.*
>
> *The pads are cooled by an interconnecting forced air duct system embedded in the concrete shield structure.*
>
> *The pads are structurally designed for (1) reactor vessel vertical loads, (2) radial temperature expansion friction forces of the reactor vessel, (3) lateral seismic and pipe rupture loads, and (4) temperature stresses caused by temperature gradients within the supports pads.*
>
> *The pad structure was analyzed as a closed box type structure using STRUDL computer codes.*
>
> *The main purpose of pad-cooling is to maintain a satisfactory temperature profile along the support coordinate, rather than heat-removal from the support system. The optimum operating conditions are such that the temperature at the bottom plate of the rectangular ventilated pad is kept sufficiently low so that heat transferred from the pads into the surrounding concrete becomes negligible. Based on a design temperature of 650°F for the reactor vessel, the design criteria of thermal gradients across the support system are as follows:*
>
> 1. *The minimum temperature at the integral nozzle interface is 300°F, equivalent to a maximum permissible temperature drop of 350°F in the nozzle.*

2. *The temperature drop across the side walls of the rectangular finned pad must not exceed 150°F.*
3. *The temperature at the bottom plate of the rectangular pad is 150°F or lower.*

Thermocouples were installed in Unit 1 and were used to confirm that criteria (2) and (3) were satisfied.

With an air flow rate of 1500 cfm per support at 120°F available for the pad cooling, a rectangular finned pad as shown in Figure 5.2-10 was designed to satisfy all the criteria mentioned above.

From Section 12.2.4.1.4 of the USAR [150]:

To provide generous margins in the design of the six structural steel columns that support the reactor vessel and that are embedded in the concrete of this region, the structure was analyzed as an independent vertical support system and was assumed to carry the total reactor vertical load without relying on the surrounding concrete. The embedded structural steel members were designed in accordance with the requirements of the AISC, "Specifications for the Design, Fabrication, and Erection of Structural Steel for Buildings".

The design was reviewed to assure that any resulting deflections or distortions do not prevent the proper functioning of the structure or piece of equipment, do not endanger adjacent structures or components, do not allow the uncontrolled release of radioactive material, and do not prevent the safe shutdown and isolation of the reactor. Stresses resulting from earthquake were compared with stresses implied by the damping values used to assure that the analysis was consistent.

From Section 12.2.5.2 of the USAR [150]:

a. Reactor Vessel Support (Figure 12.2-22)
The Reactor Vessel is supported on six vertical steel H-Columns embedded in the biological shield concrete. The tops of these columns are furnished with ventilated support structures to provide for a suitable temperature gradient between the heated parts of the Reactor Vessel coming in contact with the supports and the supporting steel columns and surrounding concrete below.
Fitted key slot blocks that are furnished with the reactor and bolted to the ventilated support structures provide for the free radial thermal expansion of the Reactor Vessel. Machined keys that are integral with the Reactor Vessel nozzles and support lugs are shimmed for sliding fit in the key slots and restrain the Reactor Vessel from movement in any horizontal direction. Thus the center point of the Reactor Vessel is rigid and has a "zero" movement.

The tops of the steel H-Columns are connected together by means of a structural tee horizontal bracing system that is welded to a continuous outer steel band. This entire bracing system is embedded in concrete to provide a rigid anchorage. Stud anchors are welded to the flanges and web of the column length to assure the composite action of concrete in carrying the vessel loads thereby providing additional load carrying margins in the supporting structural system.

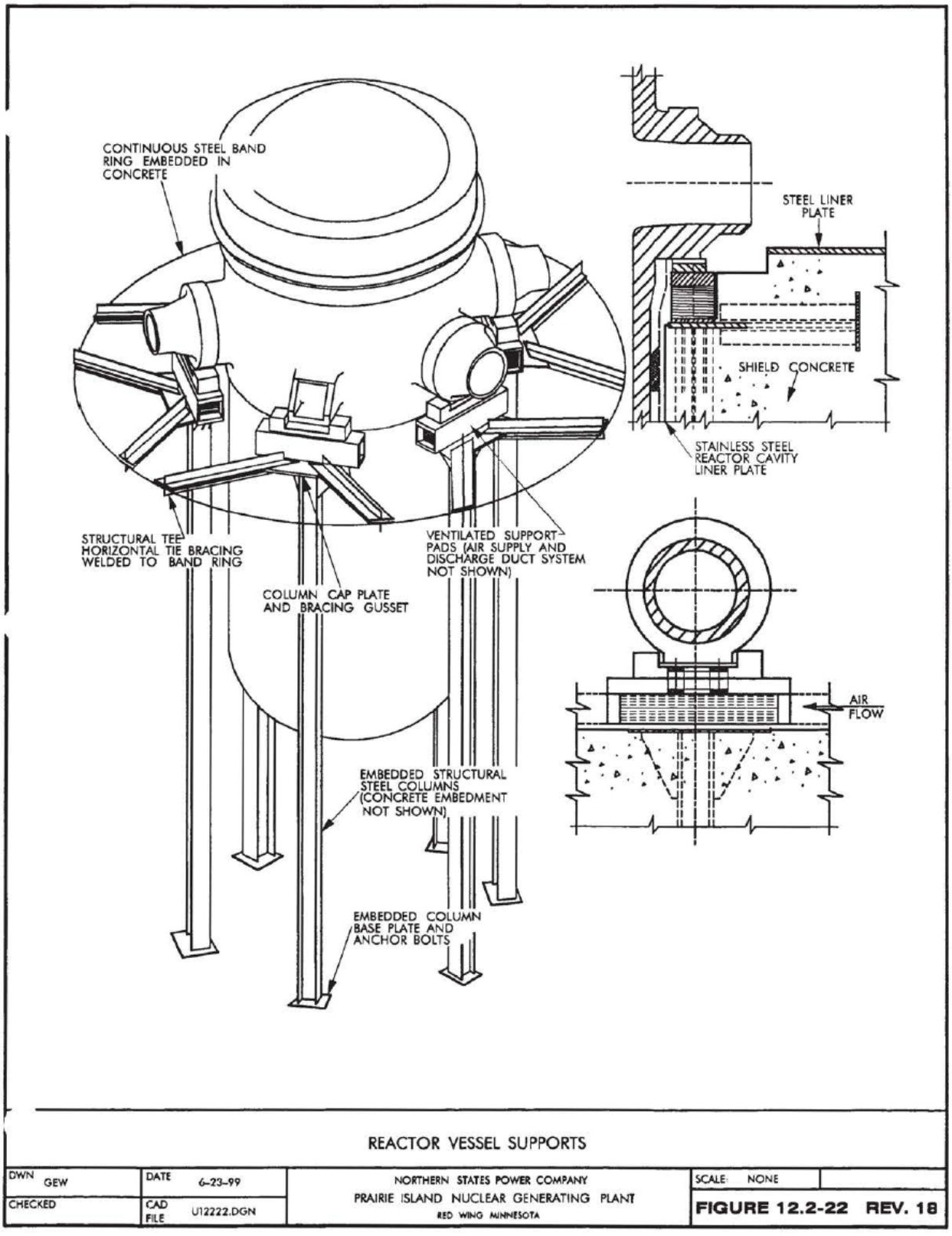

Figure D.10-1 Prairie Island Reactor Vessel Support Design [150]

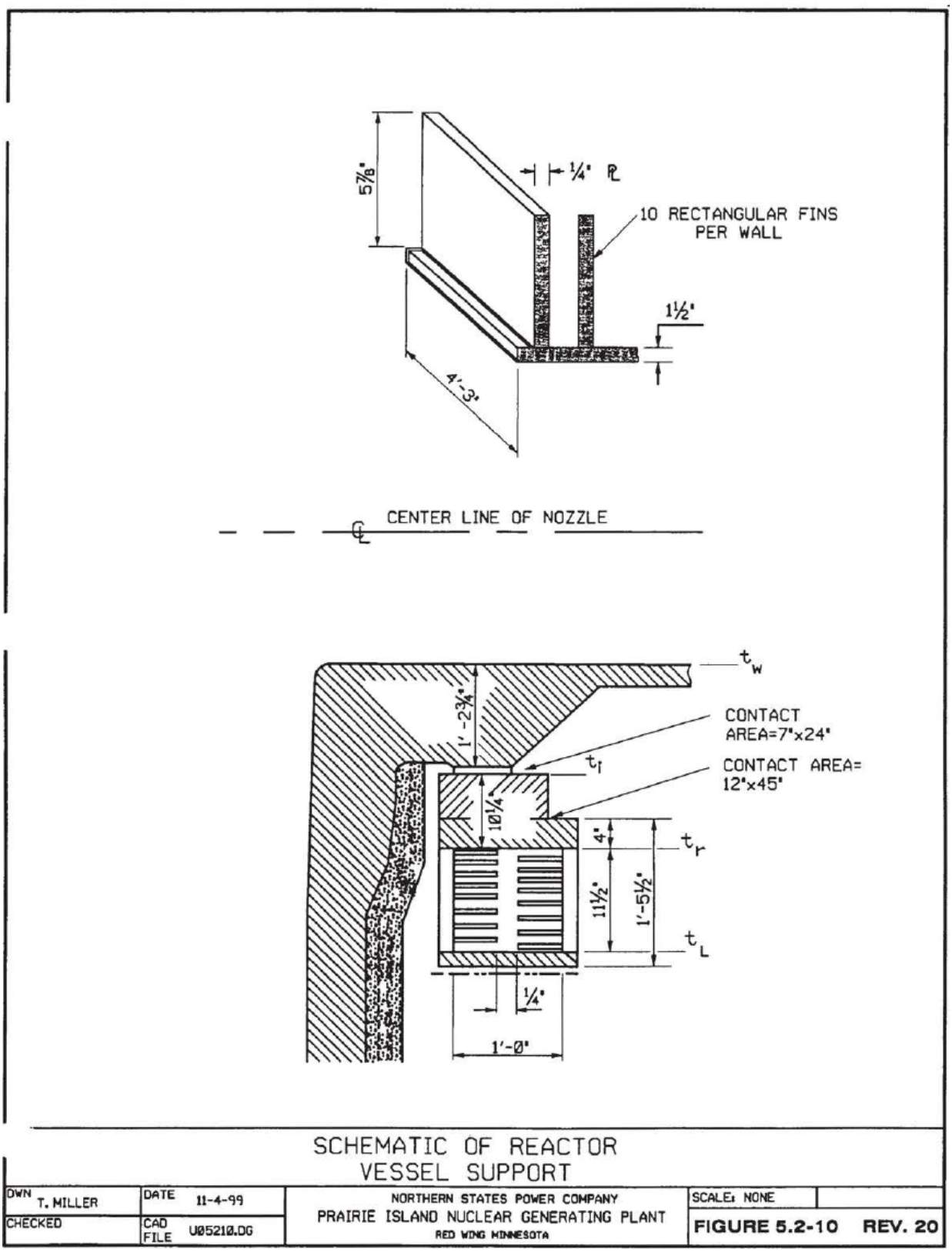

Figure D.10-2 Prairie Island Support Shoe Detail [150]

D.11 Virgil C. Summer

Virgil C. Summer Unit 1 is a Westinghouse three-loop PWR. The reactor vessel is supported under each of the six nozzles by a shoe support that rides on an air-cooled box structure bolted to embedded steel plates in the bioshield. Figure D.11-1 provides an overall view of the RPV and the support structure. Figure D.11-2 provides more detail on the embedded steel supports. The cooling system for the RPV supports is depicted in Figure D.11-3. Figures D.11-4 through D.11-7 provide additional detail on the shoe support and underlying support box structures.

The following text from Chapters 3 and 5 of the UFSAR [172] provide additional descriptions of the supports and their function.

From Chapter 3 of the UFSAR:

> *3.8.3.1.5.2 Primary Shield Wall and Embedded Steel Assemblies*
> *Embedded steel assemblies provide support for the reactor vessel support system, provide pipe rupture restraint for the reactor coolant piping, and restrict the buildup of pressure and temperature on the primary shield wall and on the reactor vessel, should a loss of coolant accident (LOCA) occur.*
>
> > *3. Anchor Assemblies under Reactor Vessel Supports*
> > *Anchorage assembly embedments are provided under each reactor vessel support to transfer loads from the reactor vessel support to the primary shield wall. See Figures 3.8-43, 3.8-49, and 3.8-50.*
> >
> > *Each assembly functions as a bearing shear lug assembly supported by wide flange sections cast into the primary shield wall. The anchorage assembly attachments transfer vertical, radial, and tangential loads from the reactor vessel support to the primary shield wall.*

From Section 5.5.14.1 of the UFSAR:

> *1. Vessel*
> *Supports for the reactor vessel (see Figure 5.5-7) are individual air cooled rectangular box structures beneath the vessel nozzles bolted to the primary shield wall concrete. Each box structure consists of a horizontal top plate that receives loads from the reactor vessel shoe, a horizontal bottom plate supported by and transferring loads to the primary shield wall concrete, and connecting vertical plates. The supports are air cooled to maintain the supporting concrete temperature within acceptable levels.*

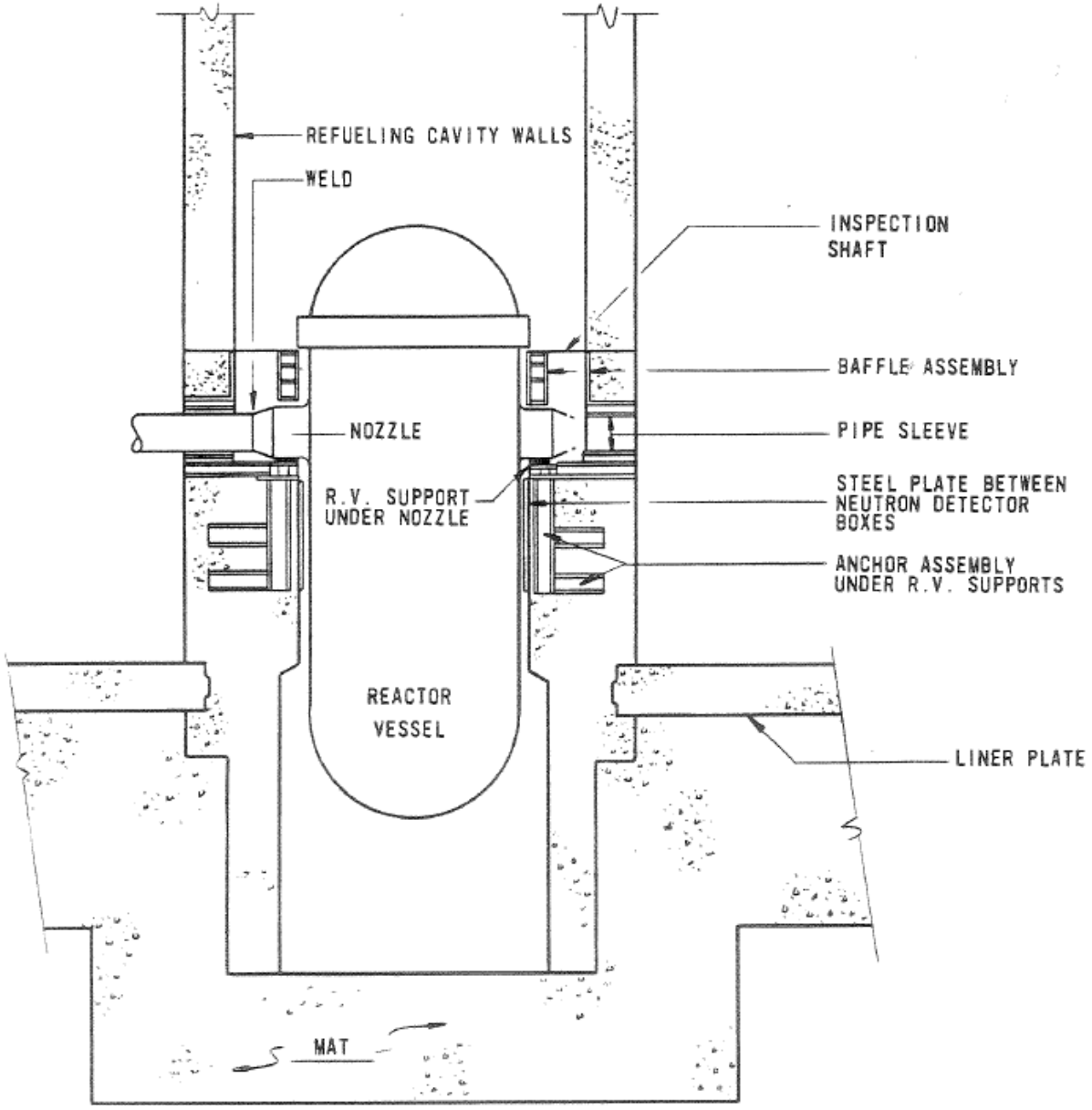

Figure D.11-1 VC Summer Reactor Vessel Support Structure (Figure 3.8-43 from UFSAR, [172])

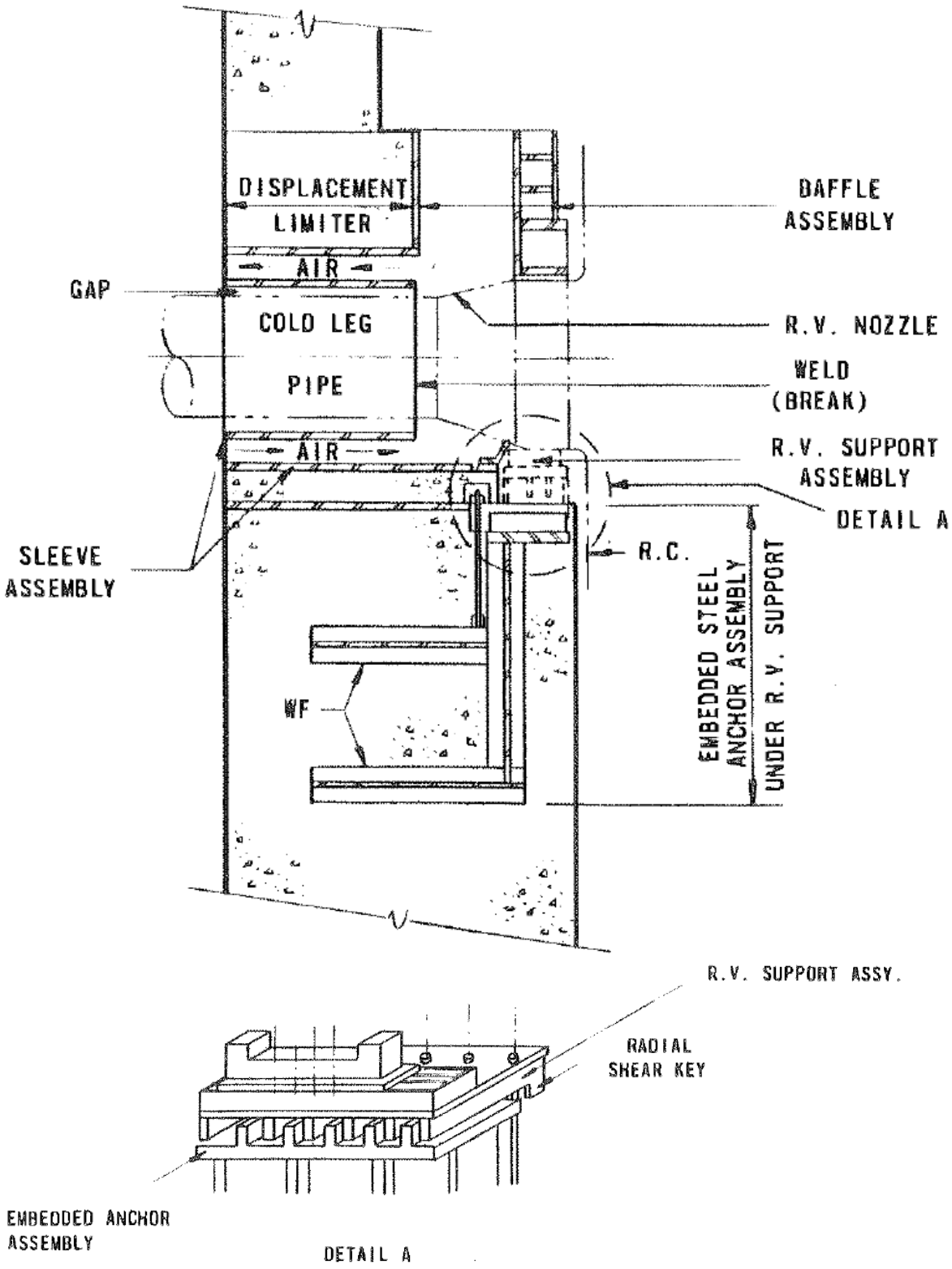

Figure D.11-2 VC Summer Reactor Vessel Support Anchorage Assembly (Figure 3.8-50 from UFSAR, [172])

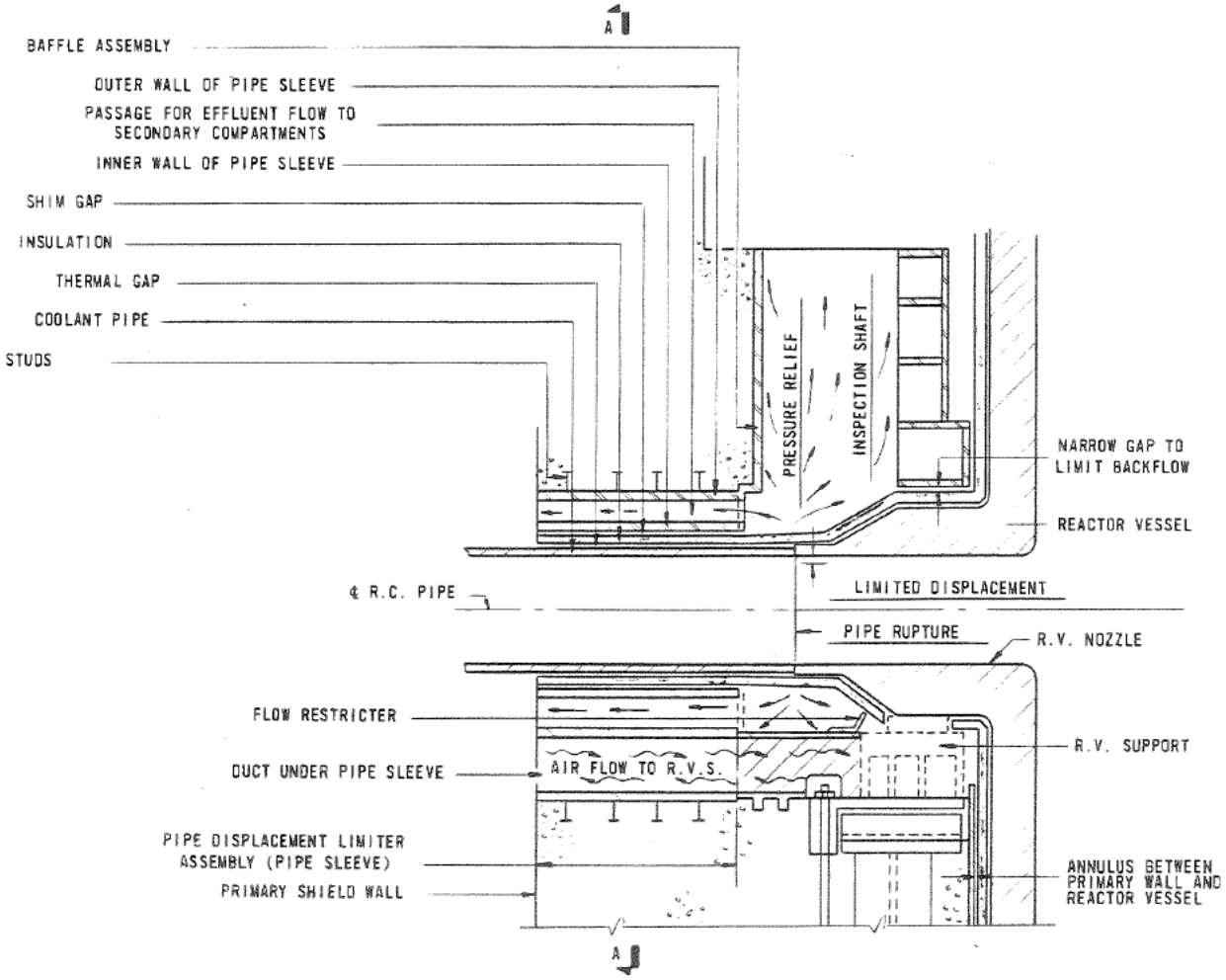

Figure D.11-3 VC Summer Reactor Cooling Pipe Structure Detail Including the Reactor Support (Figure 3.8-46 from UFSAR,[172])

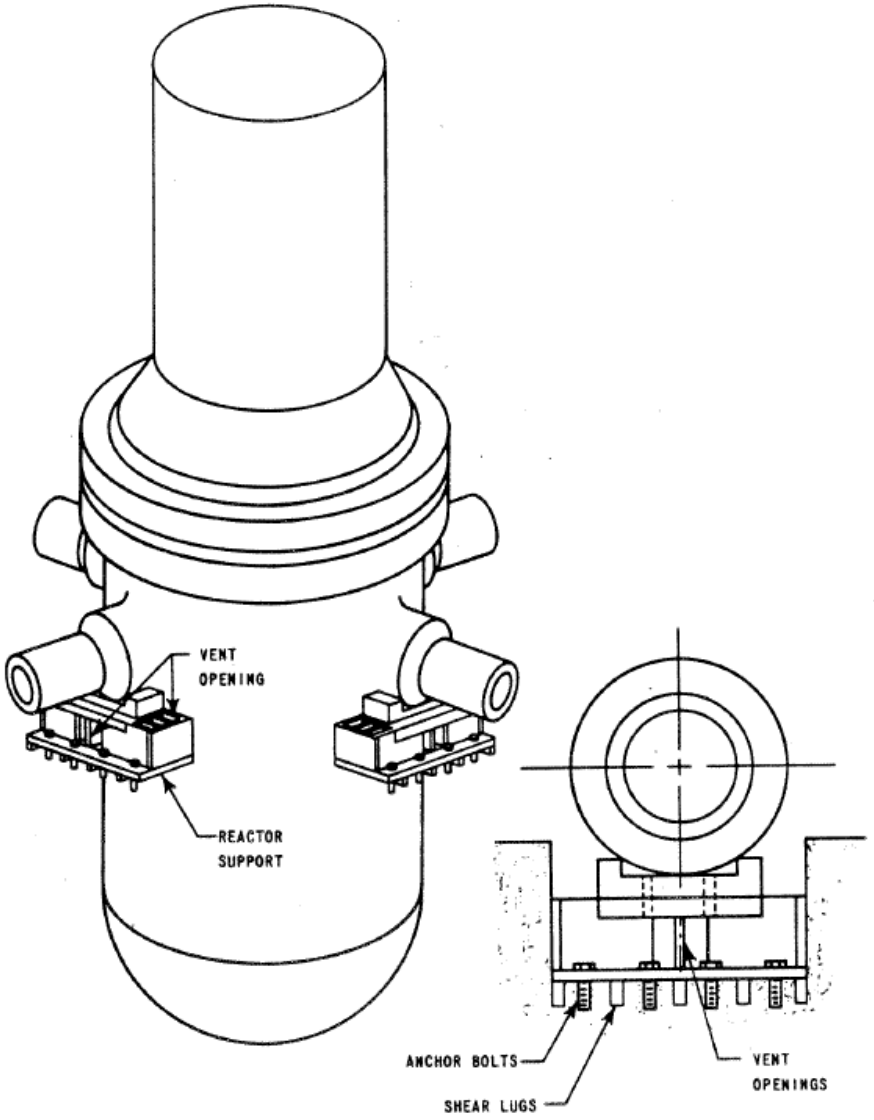

SOUTH CAROLINA ELECTRIC & GAS CO.
VIRGIL C. SUMMER NUCLEAR STATION

Reactor Vessel Supports

Figure 5.5-7

Amendment 0
August 1984

Figure D.11-4 VC Summer Reactor Vessel Support Diagram (UFSAR, [172])

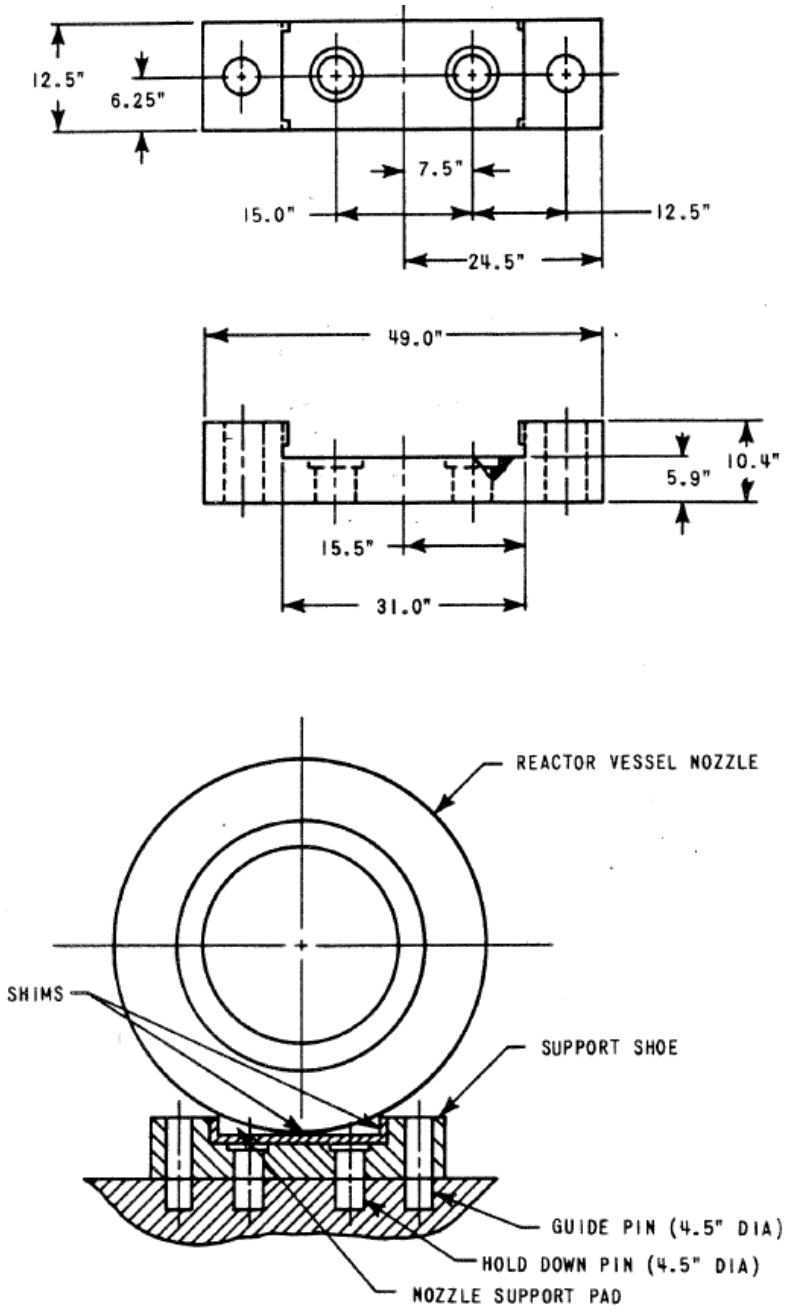

Figure D.11-5 VC Summer Reactor Vessel Support Shoe (UFSAR, [172])

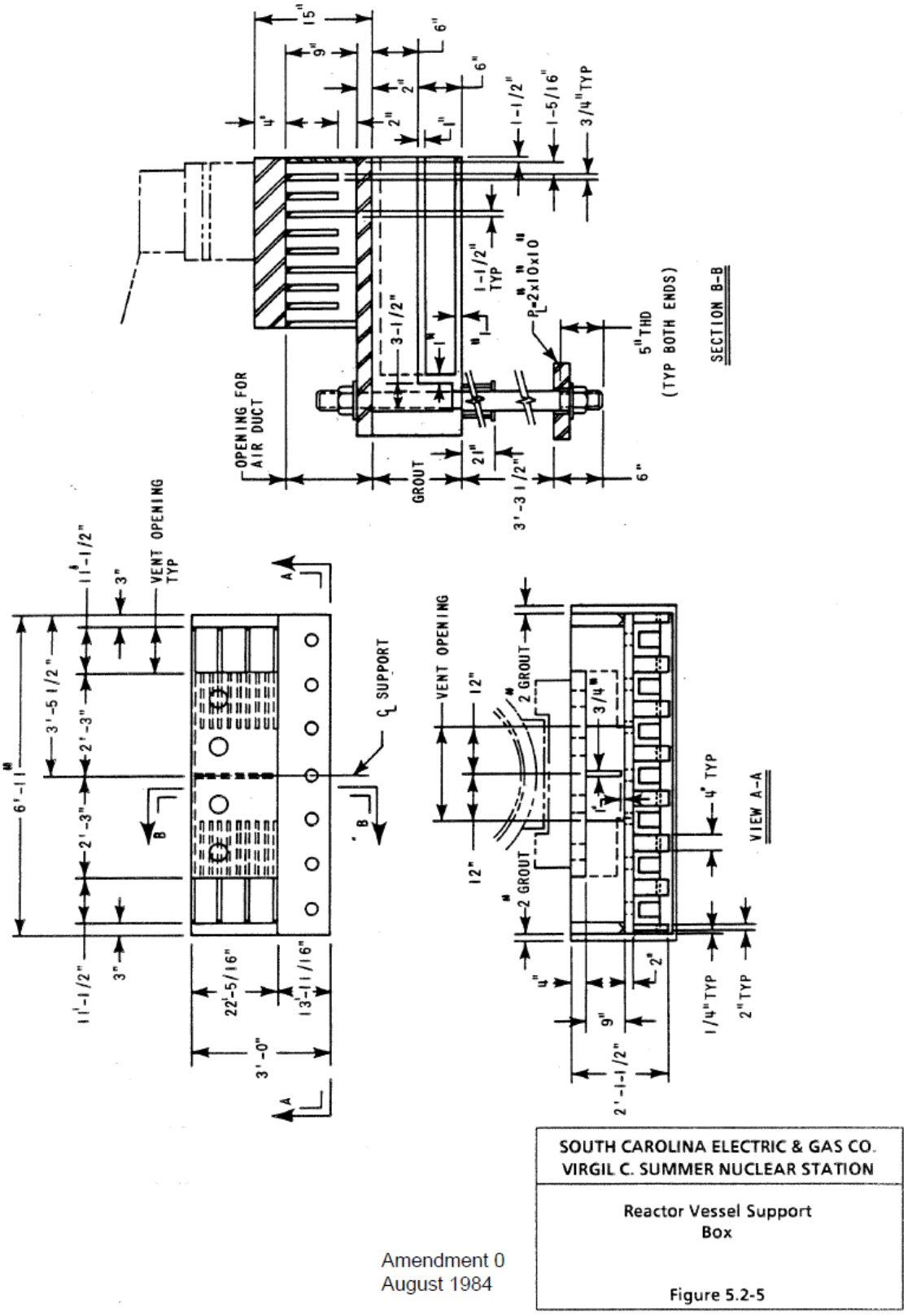

Figure D.11-6 VC Summer Reactor Vessel Support Box (UFSAR, [172])

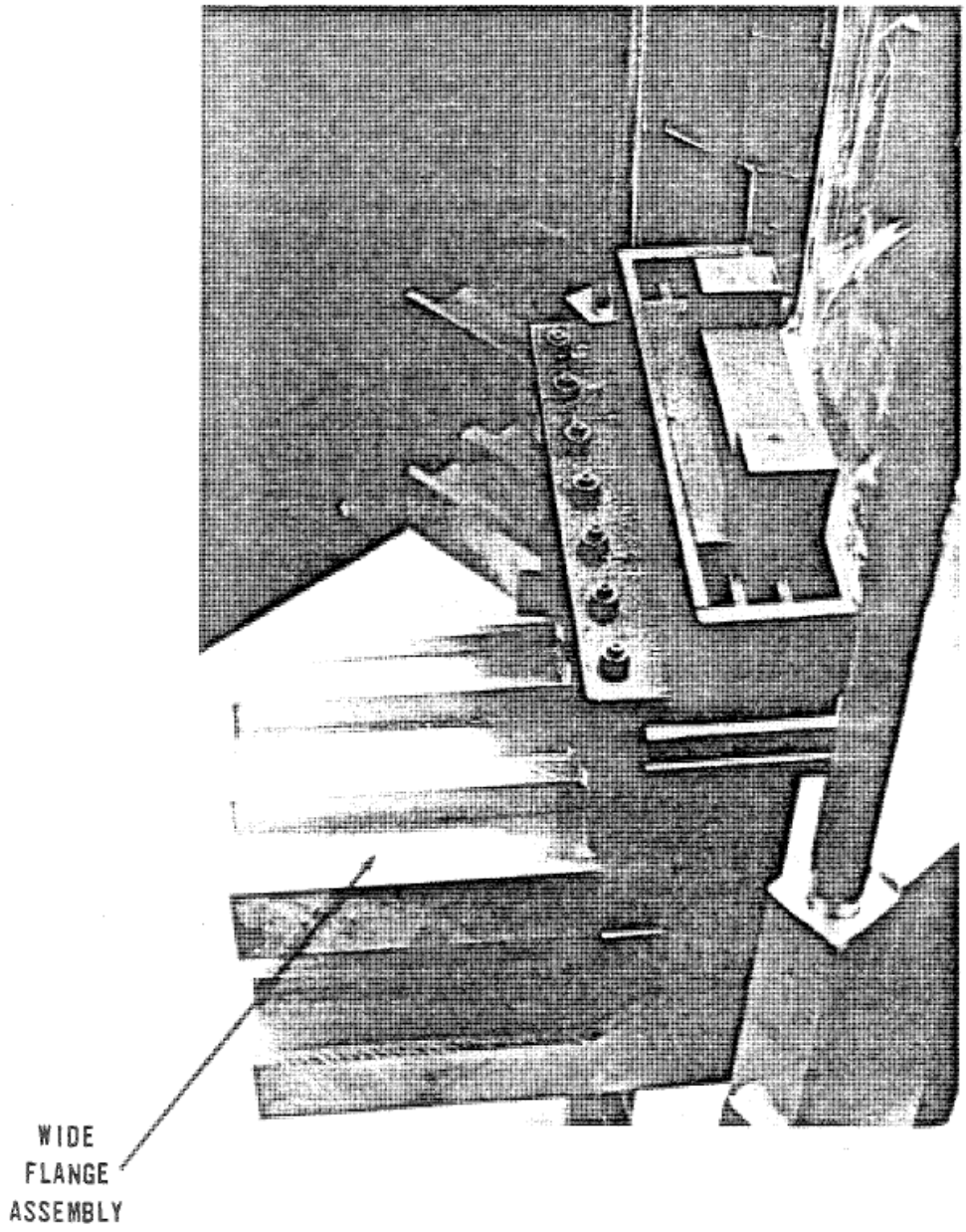

SOUTH CAROLINA ELECTRIC & GAS CO.
VIRGIL C. SUMMER NUCLEAR STATION

Reactor Vessel Support and Wide Flange Anchor Assembly

Figure 3.8-49

Figure D.11-7 VC Summer Reactor Vessel Support (UFSAR, [172])

D.12 Surry Units 1 and 2

Surry Units 1 and 2 are Westinghouse three-loop PWRs. As described in the UFSAR [262], each reactor is supported by six support shoes, one under each nozzle, that are mounted on a neutron shield tank:

> *15.6.2.2.1 Reactor Vessel Support*
> *The reactor vessel is supported by six sliding foot assemblies mounted on the neutron shield tank. The support feet are designed to restrain lateral and rotational movement of the reactor vessel while allowing thermal expansion. The neutron shield tank is a double-walled cylindrical structure that transfers the loadings to the heavy reinforced-concrete mat of the containment structure. The tank also serves to minimize gamma and neutron heating of the primary concrete shield, and to attenuate neutron radiation outside of the primary shield to acceptable limits (Section 11.3.2.1). The neutron shield tank assembly and material listing are shown on Figure 15.6-1.*
>
> *Sliding support blocks mounted on top of the shield tank support the reactor vessel. These sliding support blocks permit radial thermal expansion of the reactor vessel, while preventing translation, rotation, or uplifting. The support blocks are also designed to adjust to the correct height for plumbing the reactor vessel and for distributing the load properly among the six supports.*

A schematic of the support structure is provided in Figure D.12-1. Figure D.12-2 provides a general view of the reactor and neutron shield tank within containment.

Figure 15.6-1
REACTOR NEUTRON SHIELD TANK ASSEMBLY

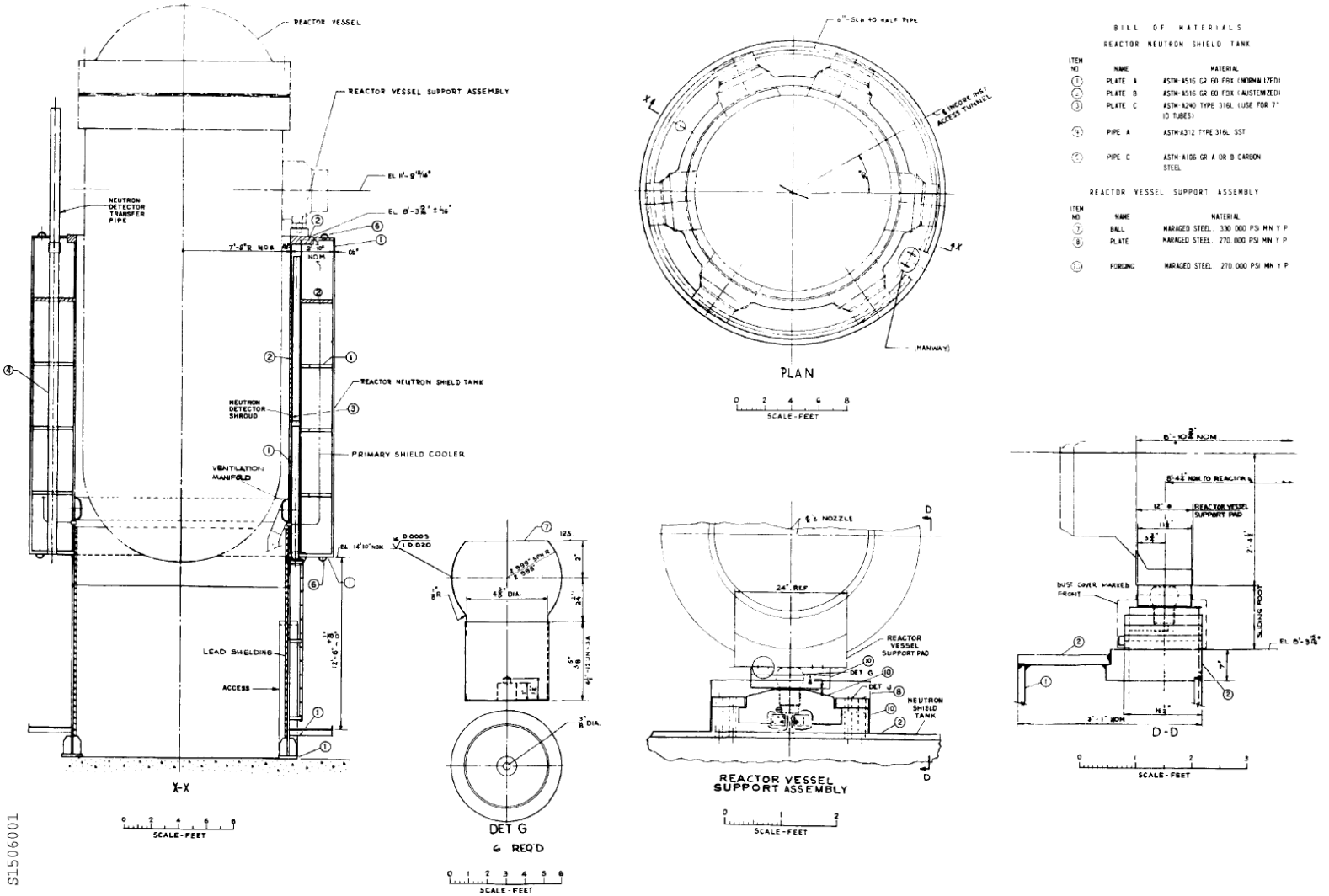

S1506001

Figure D.12-1 Surry Reactor Vessel Support (UFSAR, [262])

Figure 11.3-2
SHIELD ARRANGEMENT, ELEVATION, UNIT 1

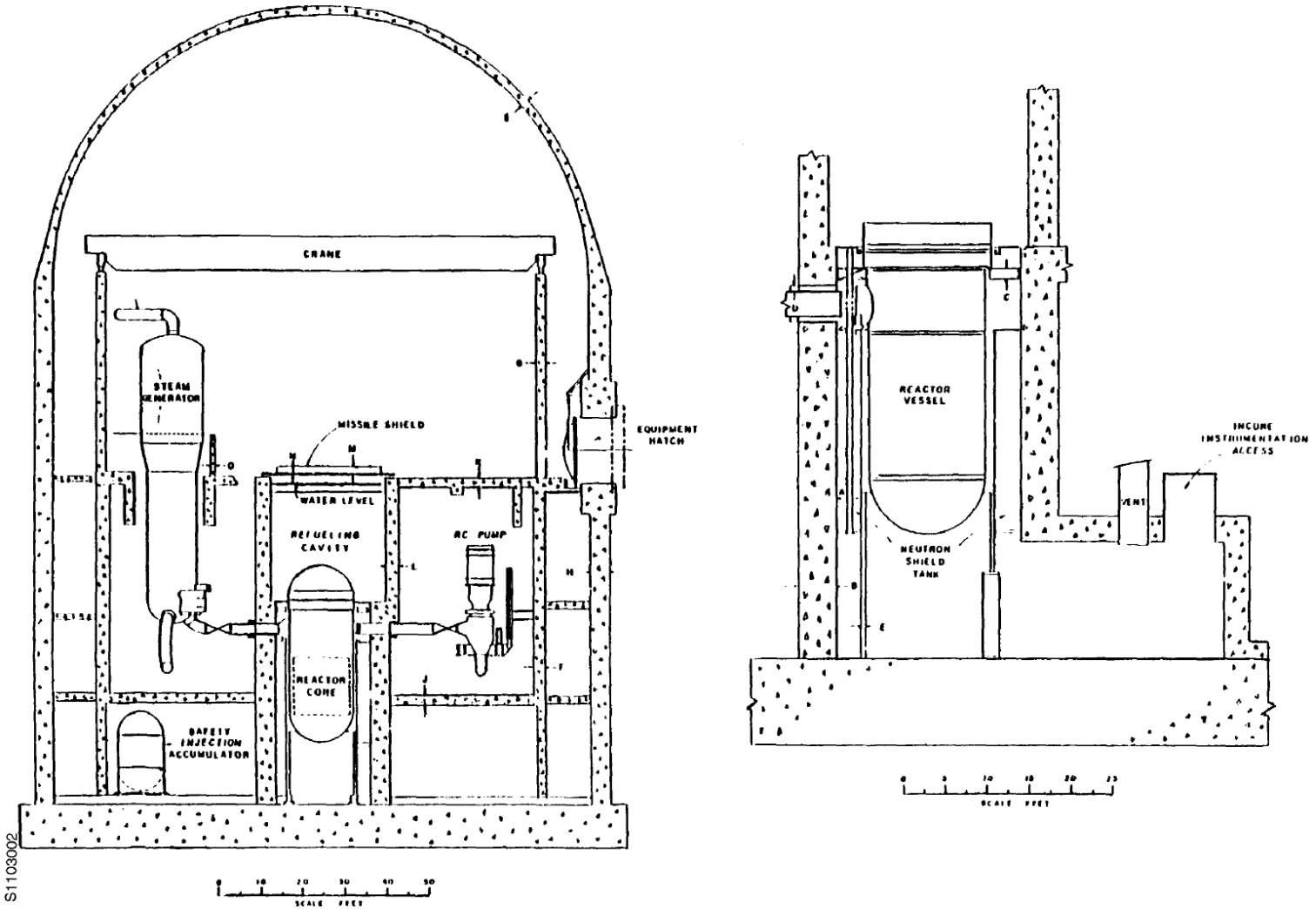

Figure D.12-2 Surry Unit 1 Reactor Vessel and Supporting Neutron Shield Tank in Containment (UFSAR, [262])

D.13 Turkey Point Units 3 and 4

Turkey Point Units 3 and 4 are Westinghouse three-loop PWRs. Each is supported on six nozzle supports that are anchored on cantilevered beams as described in the UFSAR [55]:

> *5.1.9.3 Reactor Vessel Supports*
> *The vessel is supported and restrained on its six nozzles. Each nozzle bears on three rollers set on a girder which is carried by three beams cantilevered from the primary shield wall. A shear lug on either side of the nozzle shoe provides tangential restraint. (See Fig. 5.1.20).*
>
> *Roller supports permit nearly free thermal growth. Cantilevered steel beams and lateral sheer lugs provide vertical and lateral restraints to resist operating and seismic loads. The non-ruptured loops piping are protected by absorbing the rupture forces in the support system as moments, shears and axial loads. Together, they prevent excessive movements of the vessel. No vertical hold down clamps are provided to resist upward forces since the dead weight of the vessel combined with the stiffness of the unruptured primary loop pipes provide enough resistance against uplift.*

Figure D.13-1 provides a view of the support system taken from Cheverton et al. [122]. More detail on the metal support structure can be found in that document. Figure D.13-2 provides some detail on the embedded cantilevered beams and an end view of the shoe support (three embedded beams side-by-side under the nozzle support the rollers).

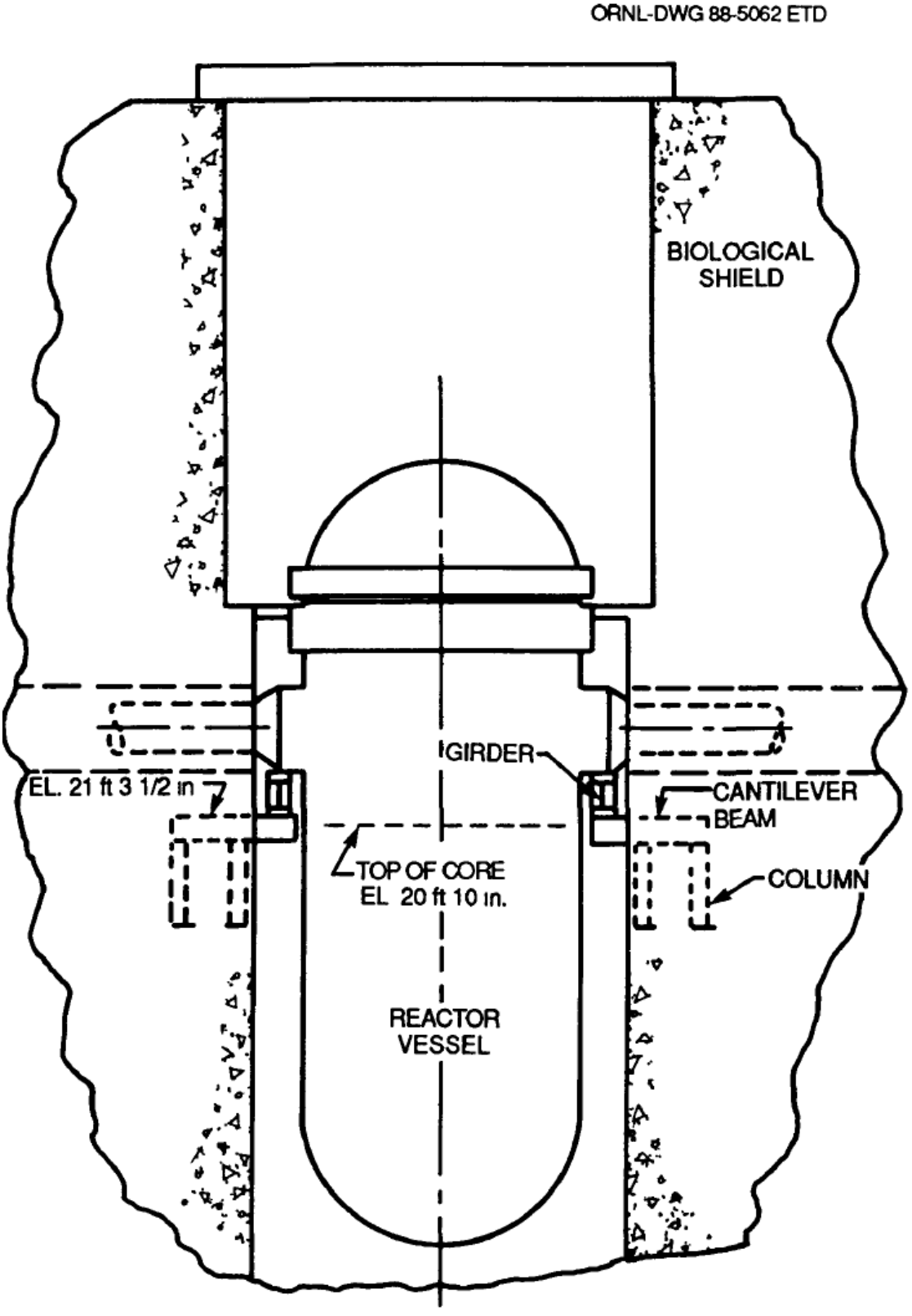

Figure D.13-1 Reactor Vessel Support Structure for Turkey Point Units 3 and 4 (Source: Cheverton et al. [122], Figure 7.2)

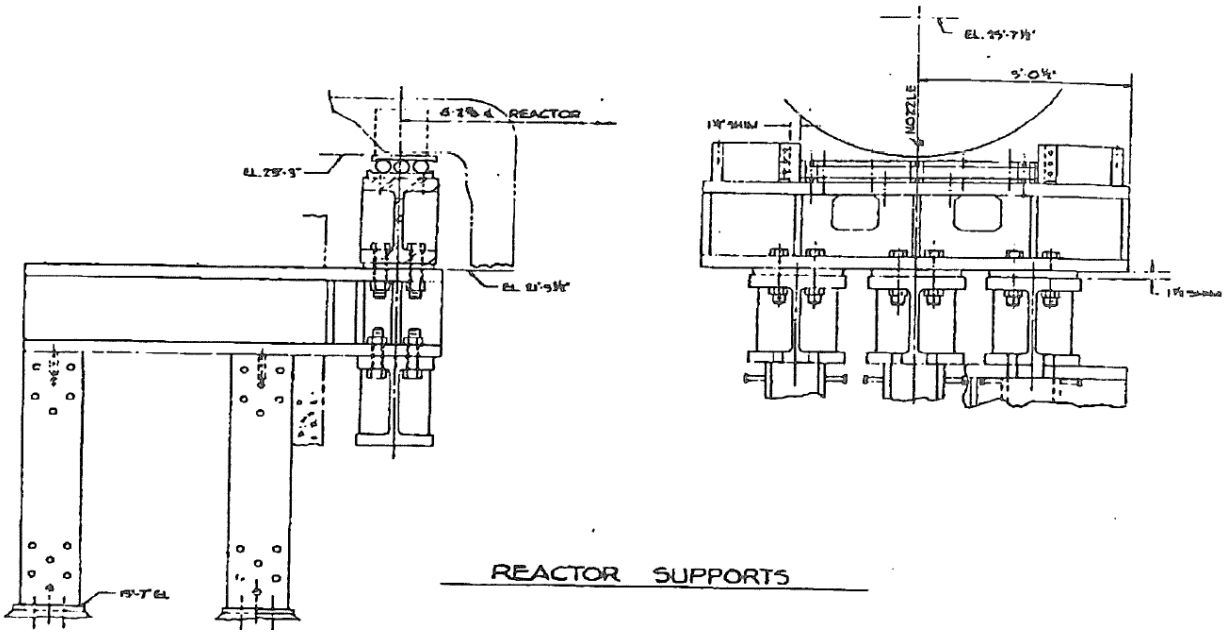

Figure D.13-2 Cantilever Beam and Support Block Detail for Turkey Point Units 3 and 4 (from Figure 5.1-20 in UFSAR, [55])

D.14 Waterford Unit 3

Waterford is a Combustion Engineering two-loop PWR. The reactor vessel is supported under each of the four inlet nozzles by welded metal pads that sit on an embedded ring girder.

The following excerpts from UFSAR [164] Sections 3.8 and 5.4 describe the vessel support system.

> *3.8.3.1.5 Steel Internal Structures*
> *The reactor vessel is supported on a 21.25 ft. diameter centerline to centerline built up ring girder, 5.0 ft deep by 2.75 ft. wide. The load is transferred from the reactor vessel to the built up steel ring at the four reactor vessel cold legs and the loads are then transferred from the steel ring to the supporting concrete by means of embedded floor plates and embedded ring plates (see Figure 3.8-34).*
>
> *5.4.14.2.1 Reactor Vessel Supports*
> *The reactor vessel integral supports consist of four pads welded to the underside of the vessel inlet nozzles. Vertically, the pads rest on lubricated bearing plates, and contain studs that act as holddown devices for the vessel. Horizontal keyways interface with the pads. The arrangement of the vessel supports allows radial growth of the reactor vessel due to thermal expansion while maintaining it centered. The supports are designed to accept normal loads and seismic and pipe rupture accident loads.*
>
> *Reactor vessel supports are shown in Figure 5.4-13 and Figure 3.8-34.*

Figure D.14-1 depicts the welded support pads under the inlet nozzles. Figure D.14-2 provides a drawing of the reactor vessel showing the relative positions of the inlet nozzles to the reactor core. Figures D.14-3 and D.14-4 provide more detail on the overall support structure.

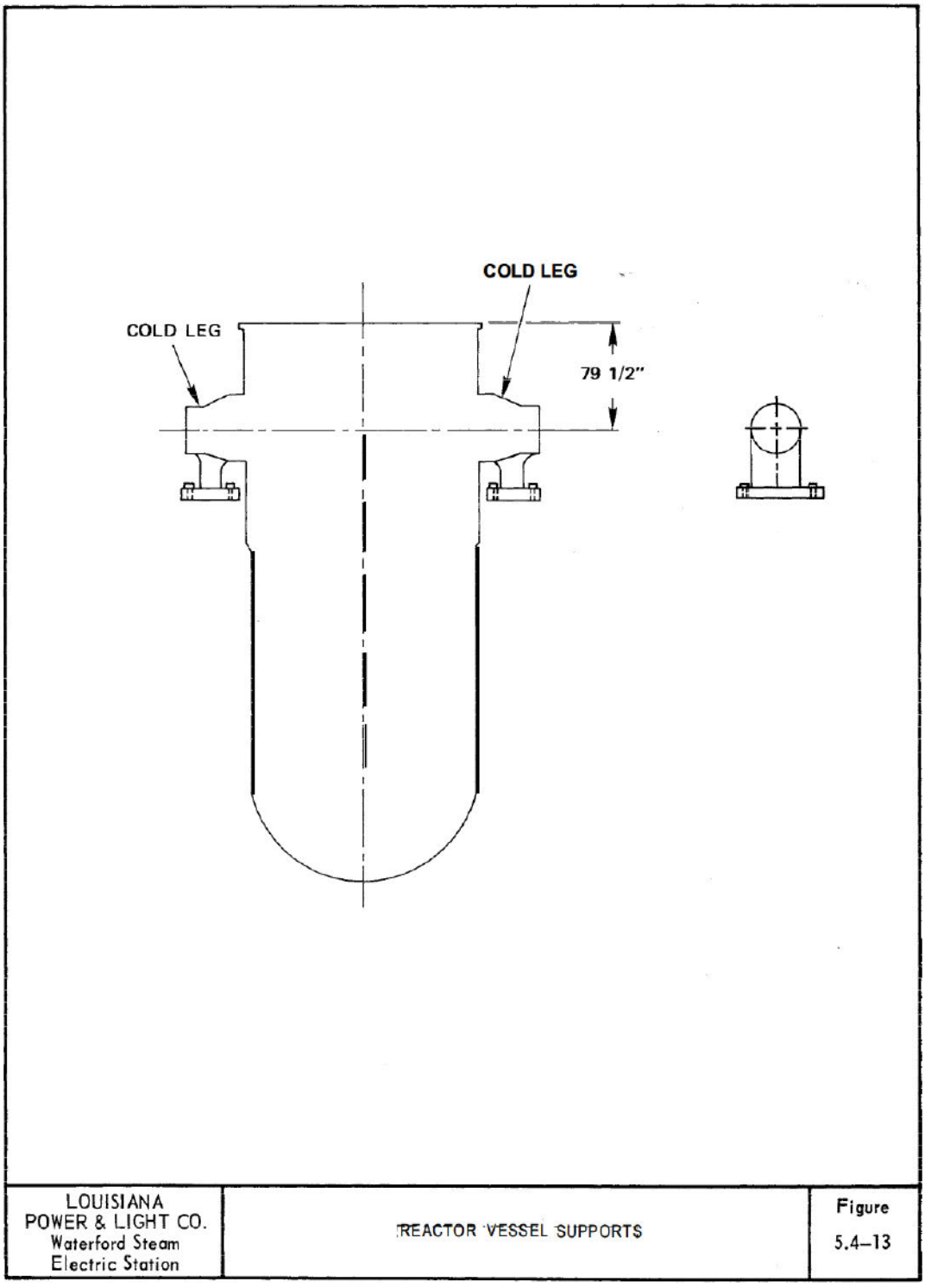

Figure D.14-1 Reactor Vessel Supports Welded to Underside of Inlet Nozzles at Waterford Unit 3 (UFSAR, [164])

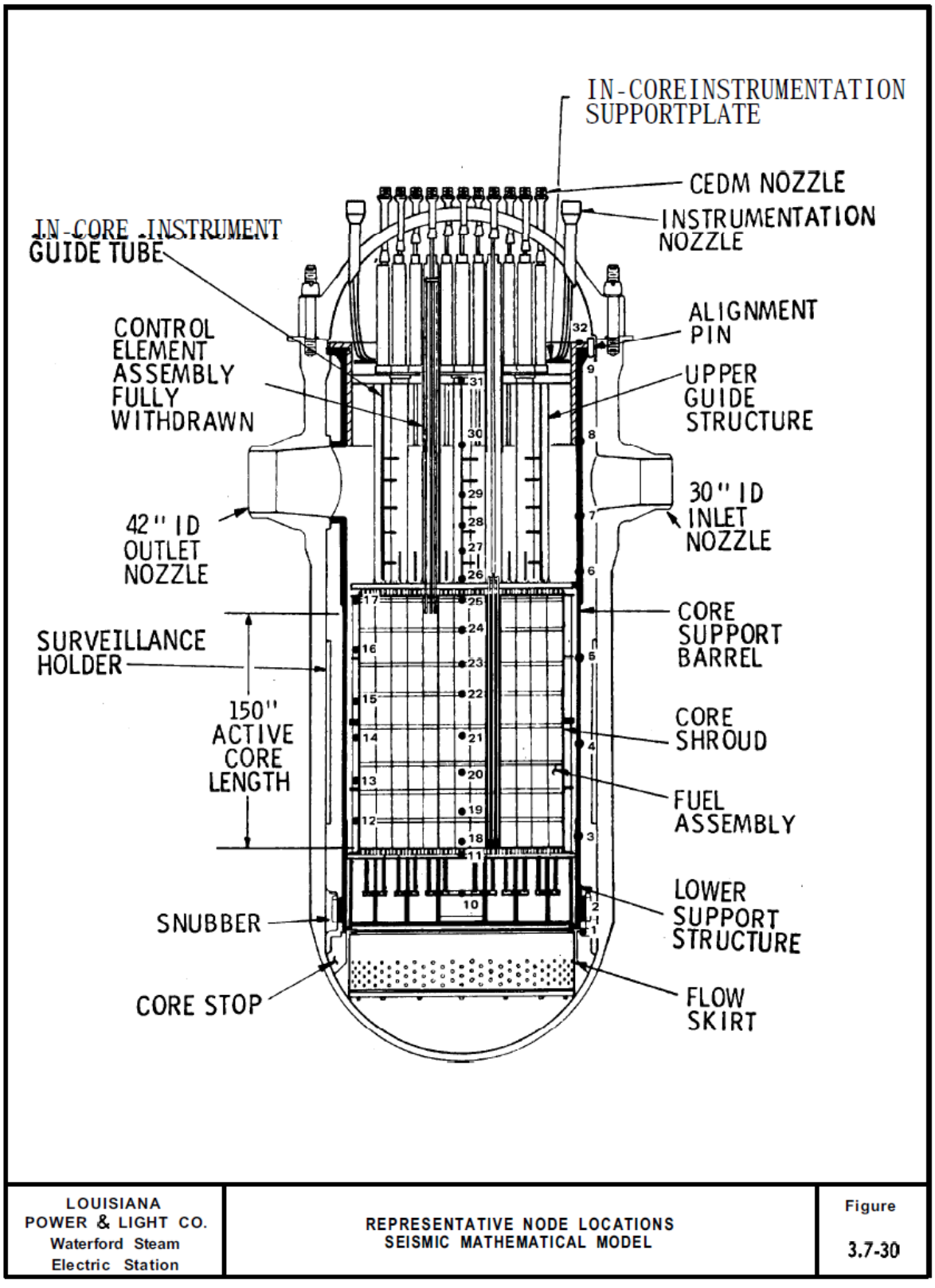

Figure D.14-2 Relative Position of Reactor Core to Inlet Nozzles at Waterford Unit 3 (UFSAR, [164])

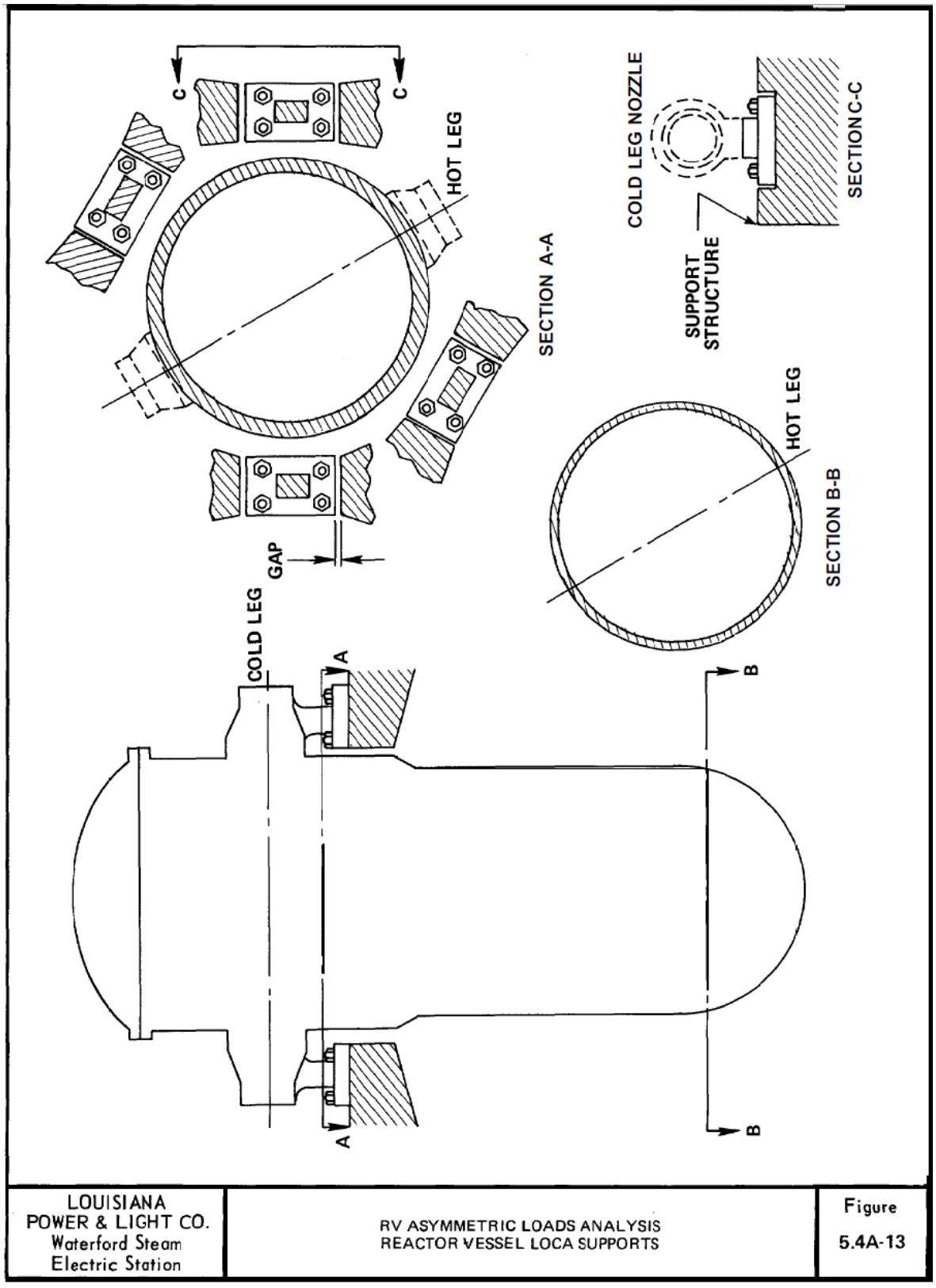

Figure D.14-3 Reactor Vessel Support Configuration at Waterford Unit 3 (UFSAR, [164])

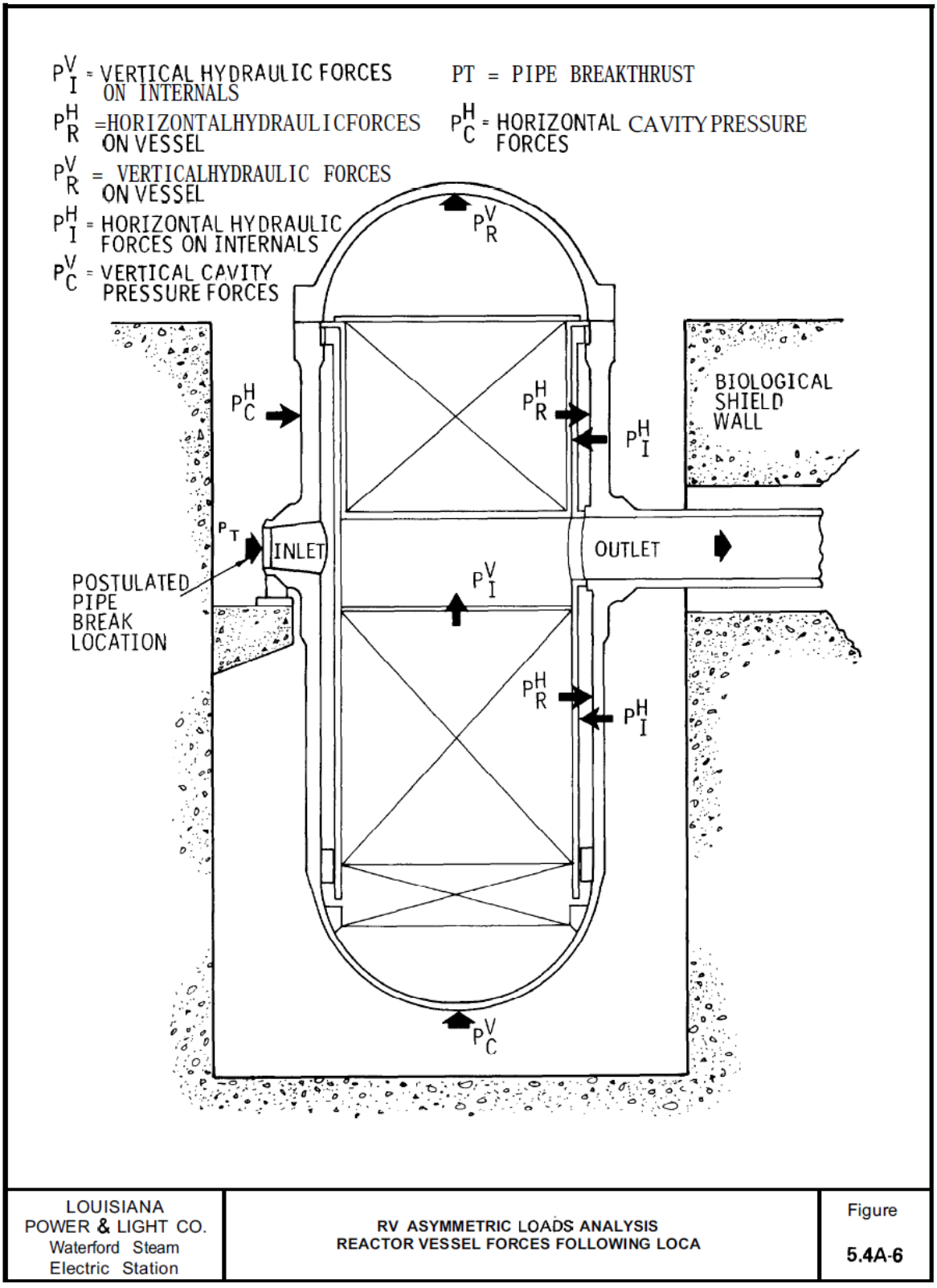

Figure D.14-4 Another View of the Reactor Vessel Support Configuration at Waterford Unit 3 (UFSAR, [164])

NRC FORM 335
(12-2010)
NRCMD 3.7

U.S. NUCLEAR REGULATORY COMMISSION

BIBLIOGRAPHIC DATA SHEET

(See instructions on the reverse)

1. REPORT NUMBER
(Assigned by NRC, Add Vol., Supp., Rev., and Addendum Numbers, if any.)

NUREG/CR-7280

2. TITLE AND SUBTITLE

Review of Radiation-Induced Concrete Degradation and Potential Implications for Structures Exposed to High, Long-Term Radiation Levels in Nuclear Power Plants

3. DATE REPORT PUBLISHED

MONTH	YEAR
July	2021

4. FIN OR GRANT NUMBER

NRC-HQ-60-16-D-0002

5. AUTHOR(S)

B. Biwer, D. Ma, Y. Xi, Y. Jing

6. TYPE OF REPORT

Technical

7. PERIOD COVERED (Inclusive Dates)

8. PERFORMING ORGANIZATION - NAME AND ADDRESS (If NRC, provide Division, Office or Region, U. S. Nuclear Regulatory Commission, and mailing address; if contractor, provide name and mailing address.)

Environmental Science Division
Argonne National Laboratory
9700 South Cass Avenue
Argonne, IL 60439

Department of Civil, Environmental and Architectural Engineering
University of Colorado
Boulder, CO 80309-0428

9. SPONSORING ORGANIZATION - NAME AND ADDRESS (If NRC, type "Same as above", if contractor, provide NRC Division, Office or Region, U. S. Nuclear Regulatory Commission, and mailing address.)

Division of Engineering
Office of Nuclear Regulatory Research
U.S. Nuclear Regulatory Commission
Washington, DC 20555-0001

10. SUPPLEMENTARY NOTES

M. Sircar, NRC Technical Lead and Contracting Officer's Representative

11. ABSTRACT (200 words or less)

Irradiation of reactor pressure vessel (RPV) concrete support structures emerged as the highest research priority among issues identified that are low-knowledge but high significance for concrete and concrete degradation related to the long-term operation of nuclear power plant (NPP) structures. The present report reviews the state of knowledge related to radiation-induced degradation, estimated radiation levels, a limited survey of reactor support structures, and important design criteria. The review indicates that all operating PWRs have the potential to generate neutron fluence levels in the reactor cavity that could result in concrete degradation before 80 years of operation, unlike BWRs which are expected to experience lower radiation levels. However, the extent of any potential degradation of concrete RPV supports cannot be quantified in a general manner because plant-specific, detailed design information of the RPV supports is necessary, radiation levels at plant-specific support locations are largely unknown, and the effect and extent of nuclear irradiation on LWR concrete supports is not well understood. Furthermore, there are a few NPPs that are operating under off-normal conditions that are monitored as part of their aging management programs. Thus, the impact of nuclear radiation on critical concrete support structures should be considered on a case-by-case basis as part of a Subsequent License Renewal application.

12. KEY WORDS/DESCRIPTORS (List words or phrases that will assist researchers in locating the report.)

Radiation damage
Radiation level
Light-water reactor
Concrete support
Concrete degradation
Subsequent license renewal

13. AVAILABILITY STATEMENT

unlimited

14. SECURITY CLASSIFICATION

(This Page)
unclassified

(This Report)
unclassified

15. NUMBER OF PAGES

16. PRICE

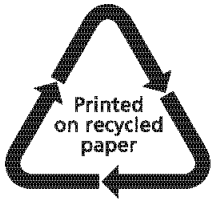

Federal Recycling Program

UNITED STATES
NUCLEAR REGULATORY COMMISSION
WASHINGTON, DC 20555-0001

OFFICIAL BUSINESS

NUREG/CR-7280

Review of Radiation-Induced Concrete Degradation and Potential Implications for Structures Exposed to High, Long-Term Radiation Levels in Nuclear Power Plants (Draft)

July 2021